AIM

Advanced Industrial Materials (AIM) Program
Office of Industrial Technologies
Energy Efficiency and Renewable Energy
U.S. Department of Energy (DOE)

Advanced Industrial Materials (AIM) Program

Annual Progress Report

FY 1996

Date Published: April 1997

ORNL/TM-13399

Advanced Industrial Materials (AIM) Program
Office of Industrial Technologies
Energy Efficiency and Renewable Energy
U.S. Department of Energy (DOE)

Advanced Industrial Materials (AIM) Program

Annual Progress Report

FY 1996

Date Published: April 1997

Coordinated by Peter Angelini
Compiled by LSD\BEIA\Information Management Technology Group
Oak Ridge National Laboratory

Prepared by the
Oak Ridge National Laboratory
Oak Ridge, Tennessee 37831
managed by Lockheed Martin Energy Research Corp.
for the U.S. Department of Energy
under Contract No. DE-AC05-96OR22464

TABLE OF CONTENTS

ADVANCED CERAMICS AND COMPOSITES (Continued)

POLYMERS AND BIOBASED MATERIALS

NEW MATERIALS AND PROCESSES

NEW MATERIALS AND PROCESSES (Continued)

INTRODUCTION

The Advanced Industrial Materials (AIM) Program
Office of Industrial Technologies
Fiscal Year 1995

C. A. Sorrell, Program Manager

In many ways, the Advanced Industrial Materials (AIM) Program underwent a major transformation in Fiscal Year 1995 and these changes have continued to the present. When the Program was established in 1990 as the Advanced Industrial Concepts (AIC) Materials Program, the mission was to conduct applied research and development to bring materials and processing technologies from the knowledge derived from basic research to the maturity required for the end use sectors for commercialization. In 1995, the Office of Industrial Technologies (OIT) made radical changes in structure and procedures. All technology development was directed toward the seven "Vision Industries" that use about 80% of industrial energy and generated about 90% of industrial wastes. These are:

- Aluminum
- Chemical
- Forest Products
- Glass
- Metal Casting
- Refineries
- Steel

OIT is working with these industries, through appropriate organizations, to develop Visions of the desired condition of each industry some 20 or 25 years in the future and then to prepare Road Maps and Implementation Plans to enable them to reach their goals.

Recently, we began working with the forging, heat treating, welding and carbon products industries, which are cross-cutting industries to the seven. Each industry has decided to go through the process to develop a vision, road map, and implementation plan and OIT is working on ways to integrate them into the Industries of the Future, even though there will not be specific budget lines for them. We are pleased to have a part in this effort.

The mission of AIM has, therefore, changed to "Support development and commercialization of new or improved materials to improve productivity, product quality, and energy efficiency in the major process industries." Though AIM remains essentially a National Laboratory Program, it is necessary that each project have industrial partners, including suppliers to, and customers of, the seven industries. Now, well into FY 1996, the transition is nearly complete and the AIM Program remains healthy and productive, thanks to the superb investigators and Laboratory Program Managers.

We were fortunate to have the foresight to begin the transition in 1993 when, at the suggestion of the AIM Guidance and Evaluation Board, we began to develop assessments of materials needs and opportunities, beginning with the pulp and paper industry, following with the glass industry. We are now engaged in assessments of the metal casting and chemical industries. These assessments identified real needs of these industries and we have been able to follow through with several new projects. In FY 1996, we can honestly say that every project addresses a need identified by one or more of the seven industries. The challenge to retain the cross-cutting benefits of materials not only remains, but is even more important now than before the changes in OIT. All seven industries understandably have identified materials as important, particularly for high temperature strength, corrosion resistance, and wear resistance, and there are many common aspects to these industry needs that can best be addressed by a true cross-cutting materials program.

The same can be said of combustion, catalysts, separations, and sensors and controls, which also require materials development. Major advances in commercialization of new materials were made in 1995 and continue into 1996, particularly in iron and nickel aluminides and molybdenum disilicide, which are being tested in production environments of all seven industries, where they are proving to have remarkable high temperature fatigue resistance, strength, and corrosion resistance. Principal investigators for all the other projects are making excellent progress in the same direction. So far, we have been able to continue support for some of the more basic aspects of materials development that are required for applications engineering and development of new applications. This will become increasingly more difficult as budgets decrease and more funding is earmarked for specific industries, with rapid commercialization or near term problem solving as the major emphases.

This Annual Report for FY 1996 contains the technical summaries of some very remarkable work by the best materials scientists and engineers in the world. It is hoped that this introduction places that work in the proper context and adequately describes the challenges facing AIM over the next few years. Congratulations from the Program Manager to those who have actually done real work and made him look good.

ADVANCED METALS
AND
COMPOSITES

ADVANCED ORDERED INTERMETALLIC ALLOY DEVELOPMENT

C.T. Liu, P.J. Maziasz and D.S. Easton

Metals and Ceramics Division
Oak Ridge National Laboratory
P.O. Box 2008, Oak Ridge, TN 37831

INTRODUCTION

The need for high-strength, high-temperature, and light-weight materials for structural applications has generated a great deal of interest in ordered intermetallic alloys, particularly in γ-based titanium aluminides. γ-based TiAl alloys offer an attractive mix of low density (~4g/cm^3), good creep resistance, and high-temperature strength and oxidation resistance. For rotating or high-speed components. TiAl also has a high damping coefficient which minimizes vibrations and noise. These alloys generally contain two phases. α_2 (DO_{19} structure) and γ ($L1_0$), at temperatures below 1120^{0}C, the euticoid temperature. The mechanical properties of TiAl-based alloys are sensitive to both alloy compositions and microstructure. Depending on heat-treatment and thermomechanical processing, microstructures with near equiaxed γ, a duplex structure (a mix of the γ and α_2 phases) can be developed in TiAl alloys containing 45 to 50 at. % Al. The major concern for structural use of TiAl alloys is their low ductility and poor fracture resistance at ambient temperatures. The purpose of this project is to improve the fracture toughness of TiAl-based alloys by controlling alloy conposition, microstructure and thermomechanical treatment. This work is expected to lead to the development of TiAl alloys with significantly improved fracture toughness and tensile ductility for structural use.

TECHNICAL PROGRESS - FY 1996

1. Alloy Preparation and Microstructural Features

Table 1 lists the alloy compositions and hot extrusion conditions for the TiAl alloys used in this study. The base composition of Ti-47Al-2Cr-2Nb (at. %) was modified with additions of 0.15B and 0.2W. Boron and tungsten were added for refining the lamellar structure and improving its stability. Tungsten was also reported to have the beneficial effect of enhancing high-temperature properties. The five alloys containing 46-48 at. % Al were prepared by arc melting and drop casting into a copper mold, using high-purity charge materials. The alloy ingots were then canned in Mo billets and hot extruded at T_1 and T_2, where $T_2>T_1>T_\alpha$ ($T_\alpha \approx 1320$°C for Ti-47 Al-2Cr-2Nb alloy).

Alloy No.	Alloy Composition (at. %)	Hot Extrusion Temperature *
TIA-20	Ti-47Al-2Cr-2Nb-0.15B	T_1
TIA-21	Ti-47Al-2Cr-1.8Nb-0.2W-0.15B	T_1, T_2
TIA-23	Ti-46Al-2Cr-2Nb-0.15B	T_2
TIA-24	Ti-48Al-2Cr-2Nb-0.15B	T_2
TIA-25	Ti-46Al-2Cr-1.8Nb-0.2W-0.15B	T_2

* $T_2 > T_1 > T_\alpha$

Table 1. Nominal Alloy Composition and Hot Extrusion Conditions

All the alloys were successfully hot extruded above T_α at T_1 and T_2 without difficulty. The hot extrusion above T_α resulted in lamellar structures with extremely fine colony sizes (22-33 μm). The hot extrusion at T, produced hear fully lamellar structures, with some equiaxed and elongated γ grains existing along colony boundaries. On the other hand, the hot extrusion at T_2 resulted in a much smaller amount of γ grains at those boundaries. Figure 1 shows a close to fully lamellar structure produced by hot extrusion of TIA-23 at T_2. This alloy was also stress-relieved for 2 h at 900°C (after extrusion), which caused no change in optical microstructure. In order to vary grain size and lamellar spacings, the hot extruded alloys were heat treated close to T_α for 2 h. As shown in Fig 2, the heat treatment at 1320°C ($\approx T_\alpha$) caused no significant change in grain size, but the heat treatment at 1350°C resulted in a sharp increase. The variation in grain size by heat treatment of TIA-20, -21. -21-2. And -25 is given in Table 2.

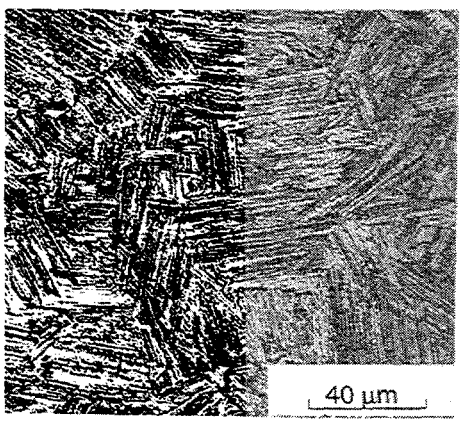

Fig. 1. TIA-23 hot extruded at T_2 and heat treated for 2 h at 900°C

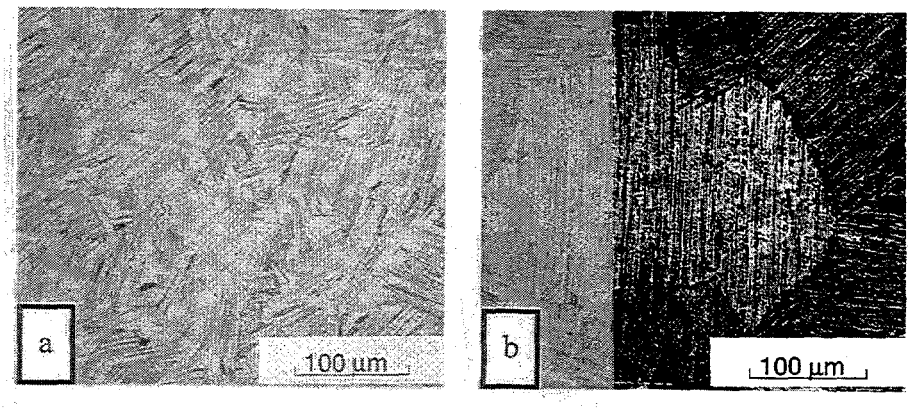

Fig. 2. TIA-20 hot extruded at T_1, (a) heat treated for 2 h at 1320°C and (b) heat treated for 2 h at 1350°C

Microstructural features in TIA-20 and -21 extruded at T_1 and TIA-21-2 and TIA-25 extruded at T_2 were examined by TEM after stress relieved for 2 h at 900°C. The lamellar spacings were carefully measured, and their results are summarized in Table 2. The average interlamellar spacing, measured to include both γ and α_2 platelets, varies from 105 to 440 nm. with the finest spacing for TIA-25 hot extruded at T_2. Because of the fine interlamellar spacing in the as-extruded materials, the ratio of γ to α_2 platelets is close to 1:1, indicating only a few γ/γ boundaries. Figure 3 compares the lamellar structures in TIA-21 hot extruded at T_1 and T_2. The extrusion at T_1 resulted in about 10-20% volume fraction of equiaxed and elongated γ in intercolony grain regions, whereas the extrusion at T_2 resulted in less than 10% intercolony γ structures. This comparison suggests that, during the hot extrusion, the temperature of the extrusion billets (which were preheated to T_1) may have dropped to below T_α, resulting in the formation of γ along the α grain boundaries.

Alloy/HT	Compositions (at. %)	Interlamellar Spacing (nm)	γ-Platelet Width (nm)	Grain Size (μm)
	Hot-Extruded at T_1			
TIA-20	47 Al-2Cr-2Nb-0.15B			
2h/900° C		225	95-870	
2h/1320° C		440	160-1250	33
2h/1350° C				182
TIA-21	47 Al-2Cr-1.8Nb-0.2W-0.15B			
2h/900° C		160	74-635	
2h/1320° C		300	290-1100	31
2h/1350° C				150
	Hot-Extruded at T_2			
TIA-21-2	47 Al-2Cr-1.8Nb-0.2W-0.15B			
2h/900° C		141	40-750	25
2h/1320° C				35
2h/1350° C				99
TIA-25	46 Al-2Cr-1.8Nb-0.2W-0.15B			
2h/900° C		105	21-520	26
2h/1320° C				135
2h/1350° C				148

Table 2. Quantitative Lamellar Microstructural Data on Hot Extruded and Heat Treated TiAl Alloys

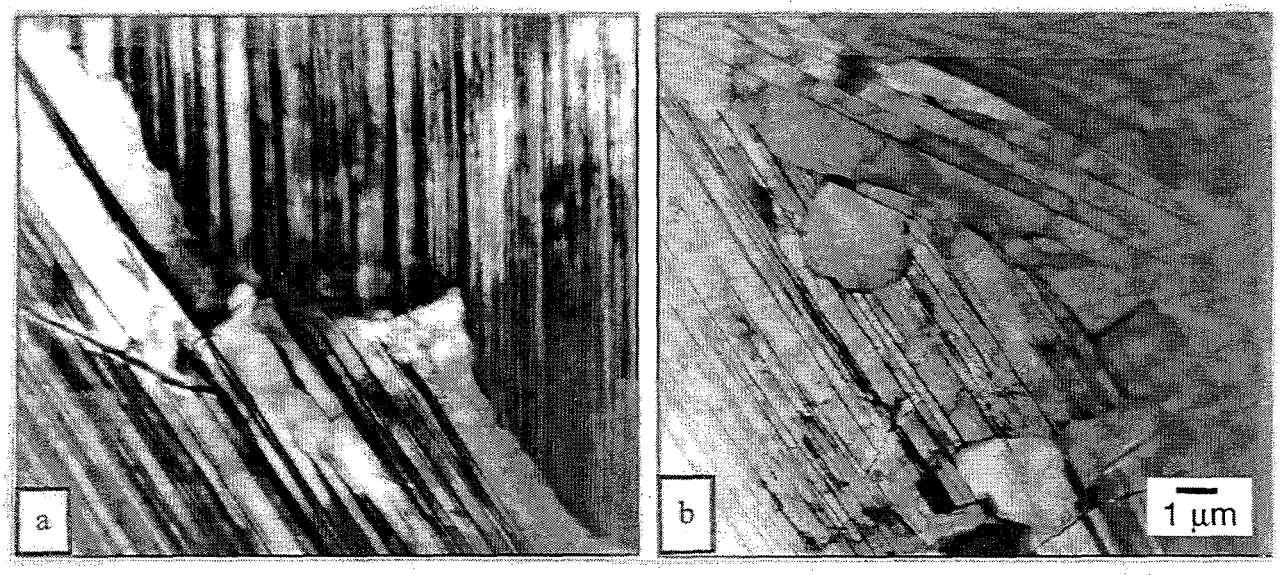

Fig. 3. Effect of hot extrusion temperature on intercolony structure in TIA-21
(a) extruded at T_2 (b) extruded at T_1

2. Tensile Properties

The tensile properties of these TiAl alloys were determined at room temperature, 300, 600, 800 and 1000°C in air. Figure 4 compares the tensile properties of TIA-25 (developed at ORNL) with the advanced two-phase TiAl alloy, K-5 (Ti-46.5A1-2.1Cr-3Nb-0.2W, at. %), developed recently. The comparison indicates that TIA-25 with a ultra-fine lamellar structure is much stronger and more ductile than K5. The superior tensile properties of TIA-25 are due to a combination of the fine colony size and interlamellar spacing produced by hot extrusion.

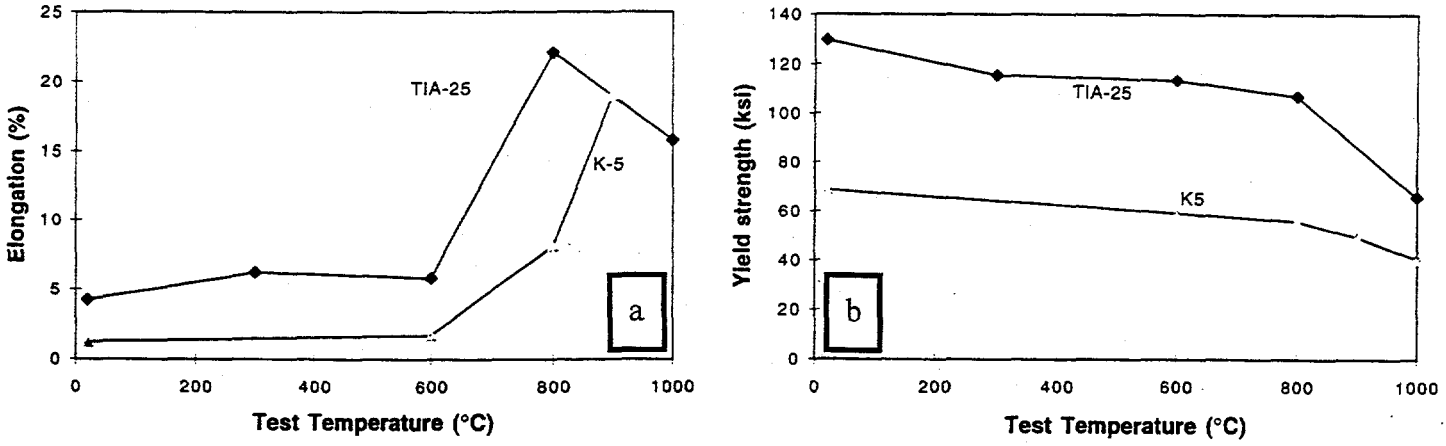

Fig. 4. Comparison of tensile properties of TIA-25 developed at ORNL with the advanced alloy K5 (Ti-46.5Al-2.1Cr-3Nb-0.2W, at. %)

3. Structure/Property Correlation

In order to identify a key parameter, the tensile elongation at various temperatures are plotted against grain size (d). Figures 5 (a) and (b) show the plot of the room-temperature tensile elongation as functions of d and $d^{-1/2}$, respectively. As indicated in Fig. 5(b), a linear relationship holds reasonably well between tensile ductility and $d^{-1/2}$. This relationship had been observed for quasi-brittle materials, based on a consideration of the propagation of cracks with an average length that is the same as the grain size. Note that such a relationship does not hold for the ductility at elevated temperatres, such as 800°C.

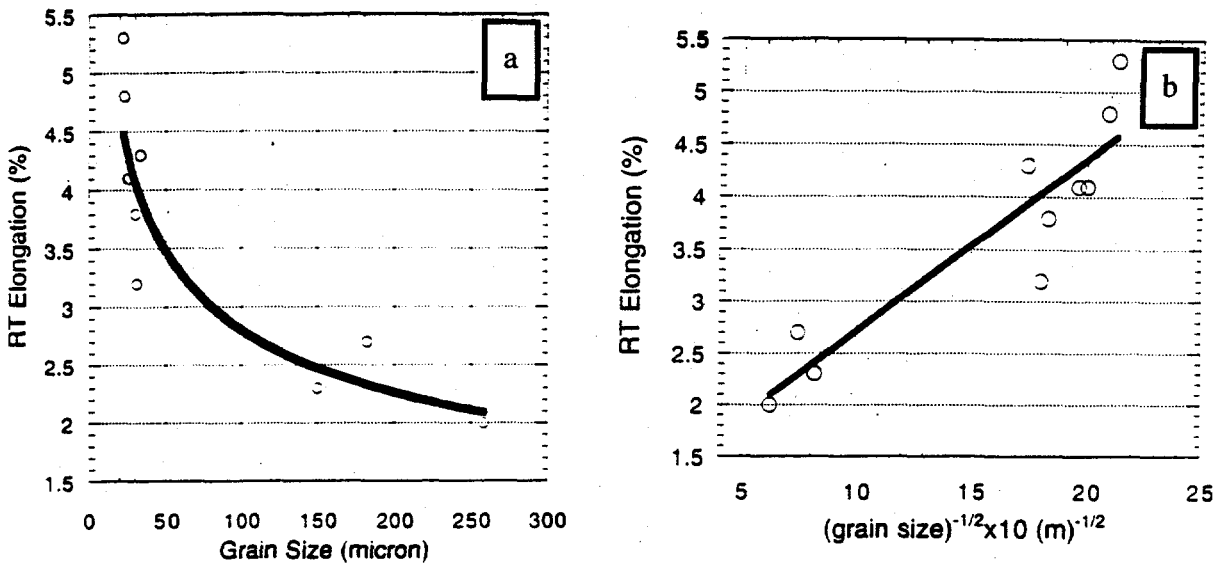

Fig. 5. Plot of room-temperature tensile elongation as a function of (a) grain size (d) and (b) $d^{-1/2}$

4. Conclusion

The study of microstructures and tensile properties of two-phase TiAl with lamellar structures based on Ti-47 Al-2Cr-2Nb leads to the following important conclusions:

1. The interlamellar spacing and grain size in the TiAl alloys with lamellar structures can be controlled by hot extrusion at temperature above T_α and subsequent heat treatment around T_α.

2. The tensile ductility around 5% and strength close to 900 Mpa at room temperature are obtained for the TiAl alloys with ultra-fine lamellar structures (grain size < 35 μm, and interlamellar spacing o.1 μm).

3. A Hall-Petch relationship exists between room-temperature tensile elongation and grain size is the key parameter in controlling the ductility at room temperature. Sych a relationship, however, does not hold for the elongation at elevated temperatures, such as 800°C.

MILESTONES DURING FY 1996

Milestone "Development of structure and property correlation for structural use of TiAl alloys" will be continued in FY 1997. The summary of the progress made in FY 1996 is given below.

The objective of this study is identify key microstructural parameters controlling the mechanical properties of two-phase γ-TiAl alloys with lamellar structures. TiAl alloys with the base composition of Ti-47Al-2Cr-2Nb (at. %) were prepared by arc melting and drop casting, followed by hot extrusion at temperatures above the α-transus temperature, T_α. The hot extruded materials were then heat treated at various temperatures above and below T_α in order to control microstructural features in these lamellar structures. The mechanical properties of these alloys were determined by tensile testing at temperatures to 1000°C. The tensile elongation at room temperature is strongly dependent on grain size, showing an increase in ductility with decreasing grain size. The strength at room and elevated temperatures is sensitive to interlamellar spacing, showing an increase in strength with decreasing lamellar spacing. The Hall-Petch relationship holds reasonable well for the tensile elongation at room temperature. Tensile elongations of about 5% and yield strengths around 900 MPa are achieved by controlling both colony size and interlamellar spacing. The TiAl alloys with controlled lamellar structures produced at ORNL are much superior to advanced TiAl alloys developed recently.

PUBLICATIONS

Journals

1. P.J. Maziasz, R.V. Ramanujan, C.T. Liu and J.L. Wright, "Effect of B and W Alloying Additions on the Formation and Stability of Lamellar Structures in Two-Phase γ-TiAl *Intermetallics,* 1997 (in press).

2. C.T. Liu, J.H. Schneibel, P.J. Maziasz, J.L. Wright and D.S. Easton, "Tensile Properties and Fracture Toughness of TiAl Alloys with Controlled Microstructures," *Intermetallics* **4**, pp. 429-440, 1996.

3. R.V. Ramanujan, P.J. Maziasz and C.T. Liu, "The Thermal Stability of the Macrostructure of γ-based Titanium aluminides," *Acta Metallurgica* **44**, pp. 2611-42, 1996.

4. C.G. McKamey, S.H. Whang and C.T. Liu, "Microstructural characterization of a γ-TiAl-Ni Alloy Produced by Rapid Solidification Techniques," *Scr. Metall.* **32**, p. 383, 1995.

5. C.T. Liu and J.A. Horton, "Effect of Refractory Alloying Additions on Mechanical Properties of Near-Stoichiometric NiAl," *Mat. Sci. And Eng.,* **A192/1963,** pp. 170-78.

6. J.A. Horton, C.T. Liu and E.P. George, "Shape Memory Properties of a Two-Phase NiAl Plus Fe Alloy," *J. Mat. Sci. And Eng.,* **A192/193,** pp. 873-880, 1995.

Other Publications

1. C.T. Liu and J.O. Stiegler, "Aluminides-Nickel," pp. 1752-60 in *Encyclopedia of Advanced Materials,* ed. M.C. Flemings, Pergamon Press, 1994.

HONORS AND AWARDS

1. C.T. Liu was appointed to NRC Panel on AFOSR Materials Science Proposal Reviews, national Research Council (NRC), 1996.

2. C.T. Liu and P.J. Maziasz received an ORNL R&D Accomplishment Award for a breakthrough in alloy design of TiAl alloys, May 1996.

PATENTS/DISCLOSURES

None

LICENSES

We started to work on TiAl alloy development in September 1994, and no license agreements have been developed with industries as of yet. Pratt & Whitney, General Electric, Howmet, and Rolls-Royce of America are interested in the ORNL work on alloy development of NiAl. We had various contacts with these companies for possible joint work on the TiAl development.

INDUSTRIAL INPUT and TECHNOLOGY TRANSFER

Based on our contact with Howmet, Pratt and Whitney, Rolls-Royce of America and other companies, one major concern for structural use of TiAl alloys is its poor tensile ductility and fracture toughness at ambient temperatures; in particular, after extensive service at elevated temperatures. This project has been formulated based on the input from the industries. P. Angelini and C.T. Liu visited Howmet Corporation to discuss technical corporation and technology transfer with Dr. Neil Paton, Vice President, and his research staff on November 9, 1995. C.T. Liu gave a seminar on "Development of NiAl and TiAl Alloys for Structural Applications" during the visit. C.T. Liu and P.J. Maziasz also discussed technology transfer with a representative from Cummins Engine Company.

ESTIMATED ENERGY SAVING

The development of high-temperature, light-weight intermetallic alloys based on γ TiAl will lead to improvement in performance (in terms of thermal efficiency, durability, etc.) of heat engines and energy conversion systems, resulting in energy savings.

DEVELOPMENT OF WELDABLE, CORROSION-RESISTANT IRON-ALUMINIDE (FeA1) ALLOYS

P.J. Maziasz, G.M. Goodwin, X.L. Wang, and D.J. Alexander

Metals and Ceramics Division
Oak Ridge National Laboratory
P.O. Box 2008, Oak Ridge, TN 37831

INTRODUCTION

A boron-microalloyed FeAl alloy (Fe-36Ai-0.2Mo-0.05Zr-0.13C, at. %, with 100-400 appm B) with improved weldability and mechanical properties was developed in FY 1994. A new scale-up and industry technology development phase for this work began in FY 1995, pursuing two parallel paths. One path was developing monolithic FeAl component and application technology, and the other was developing coating/cladding technology for alloy steels, stainless steels and other Fe-Cr-Ni alloys. In FY 1995, it was found that cast FeAl alloys had good strength at 700-750^{0}C, and some (2.5%) ductility in air at room-temperature. Hot-extruded FeAl with refined grain size was found to have ductility and to also have good impact-toughness at room-temperature. Further, it was discovered that powder-metallurgy (P/M) FeAl, consolidated by direct hot-extrusion at 950-1000^{0}C to have an ultra fine-grained microstructure, had the highest ductility, strength and impact-toughness ever seen in such intermetallic alloys.

TECHNICAL PROGRESS - FY 1996

1. Industry Testing and Corrosion Resistance

Previous work at ORNL has demonstrated that FeAl alloys are oxidation resistant to >1200^{0}C, sulfidation resistant at 800-900^{0}C and above, and resistant to corrosion in molten oxidizing nitrate salts at 650^{0}C and molten aluminum at 775-800°C. Most commercial steels or Fe-Cr-Ni heat/corrosion-resistant alloys do not have such resistance. In FY 1995, Rocketdyne/Rockwell International (Energy Technology Engineering Center (ETEC) found that as-cast FeAl was very resistant to molten sodium nitrate/cardonate salts at 900^{0}C. This year, testing by INCO (G. Smith) showed that bare metal and preoxidized as-cast FeAl was very resistant to carburization at 1000 and 1100^{0}C Fig. 1). The INCO carburizing gaseous environments simulated industrial steam/methane reformer and ethylene pyrolysis environments.

Various kinds of FeAl specimens have been sent to different industries or universities to expand the scope of the FeAl corrosion testing. Cast specimens were sent to Babcock & Wilcox (S. Cung) for exposure to oxidizing, sulfidizing and other aggressive corrosion environments at 800°C and above. As-cast, and hot-extruded I/M and P/M FeAl specimens were sent to the Corrosion and Protection Center at the University of Manchester in the U.K. (Prof. F.H. Stott) for oxidation, oxidation/sulfidation, and erosion/sulfidation testing. Testing is almost complete for wear/erosion testing of as-cast and P/M FeAl in molten aluminum at 625-650°C by Trixomat, Inc. (Dr. R. Decker). FeAl weld-overlays using Cr-free wires manufactured by Stoody Co. have also been made

on plain carbon and stainless steel substrates for testing in black-liquor recovery boilers for the pulp-and-paper industry.

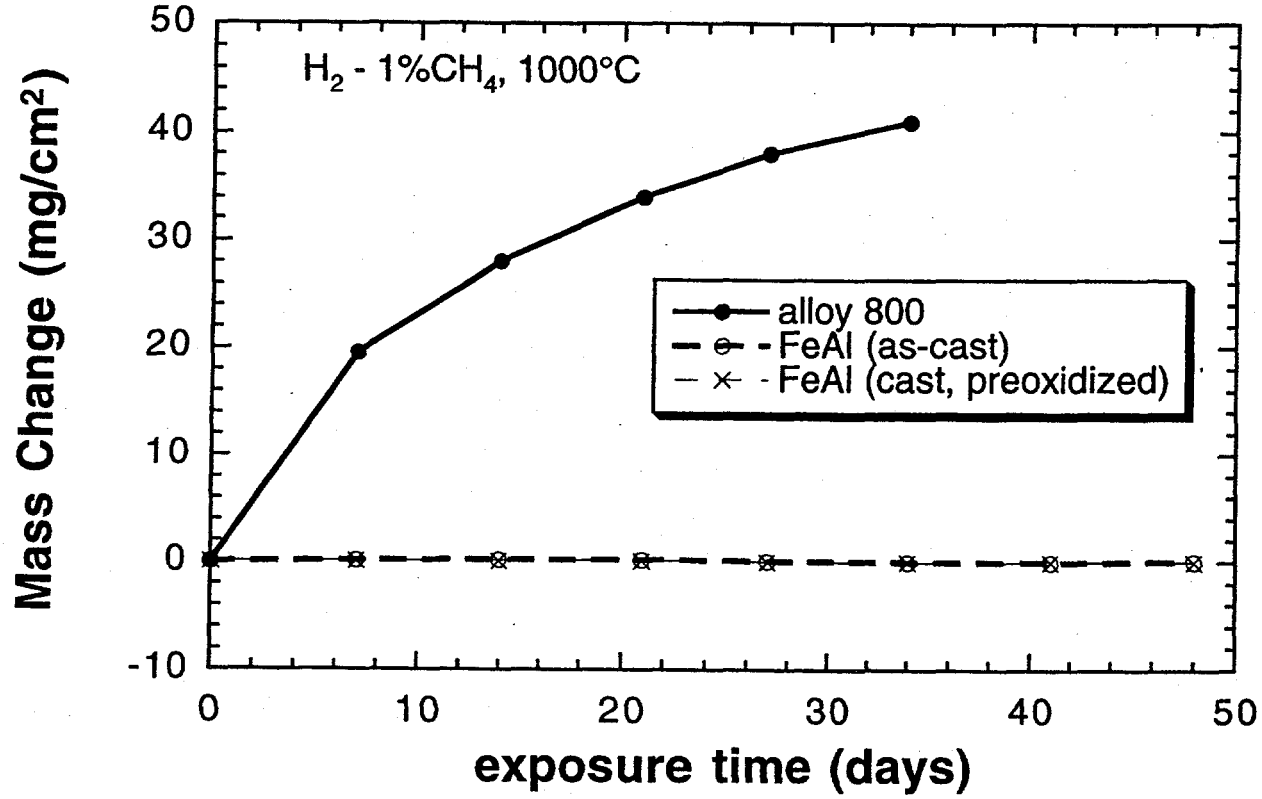

Fig. 1 Carburization testing of cast FeAl (FA-385M21 and FA-386M2 alloys, with and without preoxidation, at 1000°C in an atmosphere simulating ethylene pyrolysis.

2. FeAl Fabrication Technology

Previous FeAl weld-overlay tests involved aspiration-cast wire produced by Haynes International and others for shielded-metal-arc (SMA) and gas-tungsten-arc (GTA) welding processes. International and others. Compositions and results are summarized in Table 1. These results indicated that weld wires whose compositions approached the near-optimum FA-385 composition produced good crack-free weld overlays on steels ranging from 2 1/4Cr-lMo to 9Cr-MoVNb to type 304L austenitic stainless steel.

Automated GTA and gas-metal-arc (GMA) commercial weld-overlay processing requires continuously coiled, small diameter weld wire. Stoody Company was able to produce 1.6 mm diam. solid-and powder-cored Fe-Al weld wire with compositions formulated to produce FeAl weld deposits with near optimum Fe-36-39 at. % Al Compositions, with (Stoody I) and without (Stoody II) Cr (Table 2). Crack-free FeAl weld-overlay test pads have been produced on 2 1/4 Cr-1Mo and type 310 steels using the standard 350°C preheat and 750°C post-weld heat-treatment. Lower Al

wires (Stoody III and IV) were also obtained. The Stoody II wires have been used to produce FeAl weld-overlays on plain carbon steel and 400 series ferritic stainless steel for testing in pulp-and-paper industry black inquor recovery boilers.

Wire and description		Composition (wt.%) Al	Cr	Nb	Ti	Mo	Zr	C	B	Comments
ORNL Weldable FeAl Alloy Reference Materials										
FA-385		21.1				0.42	0.1	0.03		
FA-385M1		21.1				0.42	0.1	0.03	0.0025	
FA-385M2		21.1				0.42	0.1	0.03	0.005	
FA-385M3		21.1	2.3			0.42	0.1	0.03		
FA-385M4		21.1		1.0		0.42	0.1	0.03		
Haynes Wires, aspiration-cast, 0.125 in. diam.										
I-01,	aim	30	5	0.5	0.5	0.25	0.2	0.1		
	actual	31.2	3.3	0.5	0.7	0.3	0.2	0.12	0.007	
	weld-deposit	21.2	2.9	0.4	0.4	0.5	0.2	0.13	0.007	no cracks
(1 layer, 2¼Cr-1Mo)										
I-02,	aim	30	5	0.5	0.5	0.25	0.2	0.1	0.0025	
	actual	31.3	3.2	0.5	0.7	0.3	0.2	0.12	0.009	
	weld-deposit	26.8	3.2	0.4	0.5	0.4	0.2	0.12	0.012	
(2 layers, 2¼Cr-1Mo)										
I-03,	aim	30	5	0.5	0.5	0.25	0.2	0.1	0.005	
	actual	31.5	3.5	0.5	0.6	0.3	0.2	0.11	0.017	
	weld-deposit	26.2	3.2	0.4	0.4	0.4	0.2	0.11	0.015	2nd layer cracked
(2 layers, 2¼Cr-1Mo)										
Haynes Wires, aspiration-cast, 0.156 in. diam										
III-01	aim	30	7	0.6	0.5	0.25	0.2	0.1		
	actual									
	weld-deposit									no cracks
(1 layer, 2¼Cr-1Mo steel)										
III-02	aim	30				0.4	0.1	0.03		FA-385 repeat
	actual									
	weld-deposit									no cracks
(1 layer, 2¼Cr-1Mo steel)										
Haynes Wires, aspiration-cast, 0.156 in. in diam.										
IV-01	aim	25	7			0.4	0.1	0.03	0.005	
	weld-deposit									no cracks
(1 layer, 2¼Cr-1Mo, 9Cr-1MoNbV, and 304L steels)										

Table 1. Compositions of Development FeAl Cast Rod or Coiled Wire Filler-Metals

Wire and description	Composition (wt.%) Al	Cr	Nb	Ti	Mo	Zr	C	B	Comments
ORNL Weldable FeAl Alloy Reference Materials									
FA-385	21.1				0.42	0.1	0.03		
FA-385M1	21.1				0.42	0.1	0.03	0.0025	
FA-385M2	21.1				0.42	0.1	0.03	0.005	
FA-385M3	21.1	2.3			0.42	0.1	0.03		
FA-385M4	21.1		1.0		0.42	0.1	0.03		
Stoody Coiled Wire, Al-core, Fe-sheath, 0.0625 in. in diam.									
I aim weld-wire	20	7			0.25	0.25	0.1		
actual, weld-wire	21.8	7.3			n.a.	0.4	0.06		
actual, clad-deposit (automated GMA, $2^1/_4$Cr-1Mo steel, 1 in. thick)	12.6	6.0			0.44	0.2	0.08		single, no crack
actual, clad-deposit (manual GTA, type 310 stainless steel, 0.5 in. thick)	15.3	12.7			0.04	0.22	0.05		single, no crack
II aim weld-wire		20				0.25	0.25	0.1	
actual, weld-wire	21.5				n.a.	0.25	0.08		
III aim weld-wire	12				0.25	0.25	0.1		(ordered and received)
IV aim weld-wire	26				0.25	0.25	0.1		(ordered and received)

Table 2. Compositions of Developmental FeAl Cast Filler-Metals

Finally, welding studies on monolitic FeAl components and thicker material have begun. Efforts to weld FeAl centifugally-cast (FA-385M2) tubes using filler wire were unsuccessfully due to cold-cracking without preheat and post-weld-treatment. Subsequent microstructural examination also revealed micro-cracks in the as-cast materials. To test the hypothesis that cold-cracking and welding difficulties are related to the ductility and resistance to moisture-induced cracking of the material in ambient air, autogenuous automated GTA welds were made on hot-extruded I/M and P/M FeAl materials with much higher ductility and significantly refined grain sizes. In both cases, good crack-free welds were made on material with no preheat or post-weld heat-treatment (Fig. 2). This represents a major break-through for welding/weldability of FeAl alloys, and systematic mapping of weldability as a function of alloy composition, processing-induced microstructure and ductility will be continued next year.

Monolithic FeAl is being examined and machined into component shapes in wither the as-cast or hot extruded I/M or P/M condition. Hot-extruded I/M FeAl has sufficient ductility (10%) to allow significant deformation in air (Fig. 3), something previously almost impossible for hot-rolled sheet. Secondary hot-processing (ie. rolling or forging) of I/M and P/M materials will be explored next year.

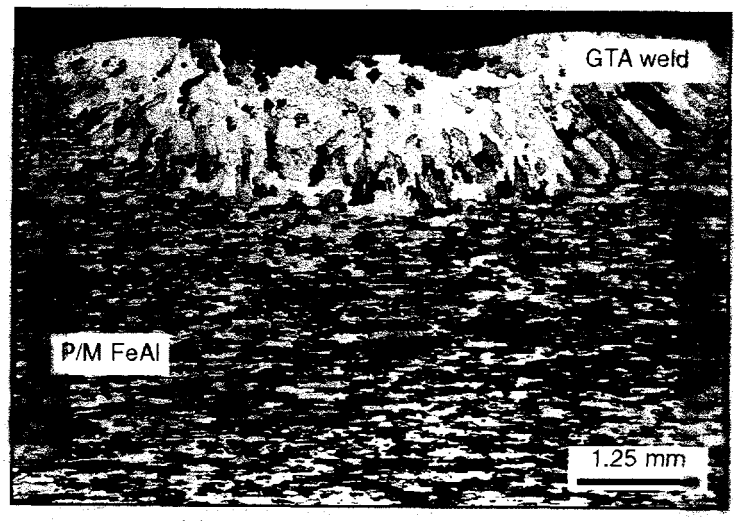

Fig. 2. Crack-free GTA autogenous weld made on P/M FeAl (FA-385) consolidated by direct hot-extrusion at 1000 °C without any preheat or post-weld heat-treatment.

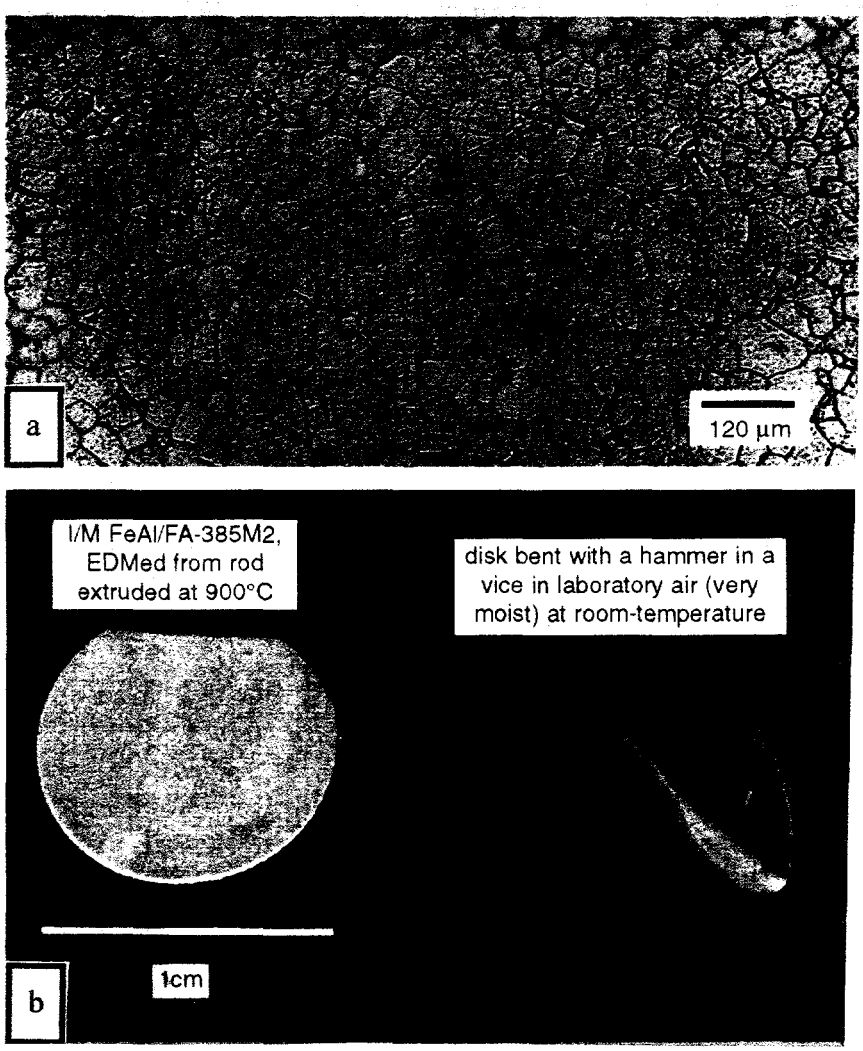

Fig. 3. I/M FeAl (FA-385M2) hot-extruded to produce (a) a refined grain size and high ductility in air (10%), and (b) a material that can be significantly deformed in air without cracking.

3. Mechanical Properties of I/M and P/M FeAl.

Mechanical properties of monolithic FeAl alloys have been examined as functions of alloy compositions and processing-induced microstructures. Emphasis has been on as-cast and hot-extruded I/M materials, with some work on P/M FeAl alloys consolidated by direct hot-extrusion. Alloy compositional effects have focussed only on minor variations and combinations of B, C, and Zr added to the FA-385/ FA-385M2 base alloys from previous work, as shown in Table 3. Boron additions are found to enhance room-temperature tensile ductility and make the fracture mode more ductile for all facrication conditions. Refining the grain size by hot-extruding I/M or P/M FeAl boost the room-temperature ductility in air, and gives the material good levels of Charpy impact toughness, something previously unachievable for FeAl or other iron-aluminide alloys. Charpy impact energies range from 25 to 105 J absorbed energy for such materials (Fig. 4). P/M FeAl extruded at 950 and 1000°C with 2-5 μm grain size also shows ductile-dimple transgranular fracture within prior power particles in air at room temperature. Such behavior has never to our knowledge been observed before in FeAl, and represents a major break-through for the effects of processing-induced microstructures on mechanical properties for this class of ordered intermetallic alloys.

	Composition (wt.%)								
Alloy	Al	Cr	Nb	Ti	Mo	Zr	C	B	Heats
FA-385M2	21.1				0.42	0.1	0.03	0.005	16238
FA-385M21	21.1				0.42	0.1	0.03	0.010	16239
									16400
									16402
									16346
FA-386M1	21.1				0.42	0.15	0.07	0.005	16240
FA-386M2	22.1				0.42	0.15	0.07	0.005	16241
									16399
									16401
									16345

Table 3. Compositions of New, Larger Heats of Cast FeAl Alloys

Previous work on as-cast FeAl alloys with B micro-alloying additions showed that they had about 400 Mpa yield strength (YS) up to about 700-750°C due to fine dispersions of ZrC precipitates (Fig. 5). Heat-treatments of 1h at 1200°C also either preserve or enhance high temperature strength and creep-resistance. New heats of FeAl alloys with 36-38 at. % Al and more C and Zr to enhance the precipitation of ZrC (Table 3) have been cast and tensile tested at room-temperature. They have 3-4% total elongation in air at room temperature and >500 MPa YS after heat-treatment at 1200-1250°C. Microstructural examination, elevated temperature tensile and creep-rupture testing, and room-temperature Charpy impact testing will be completed on these new cast FeAl alloys next year.

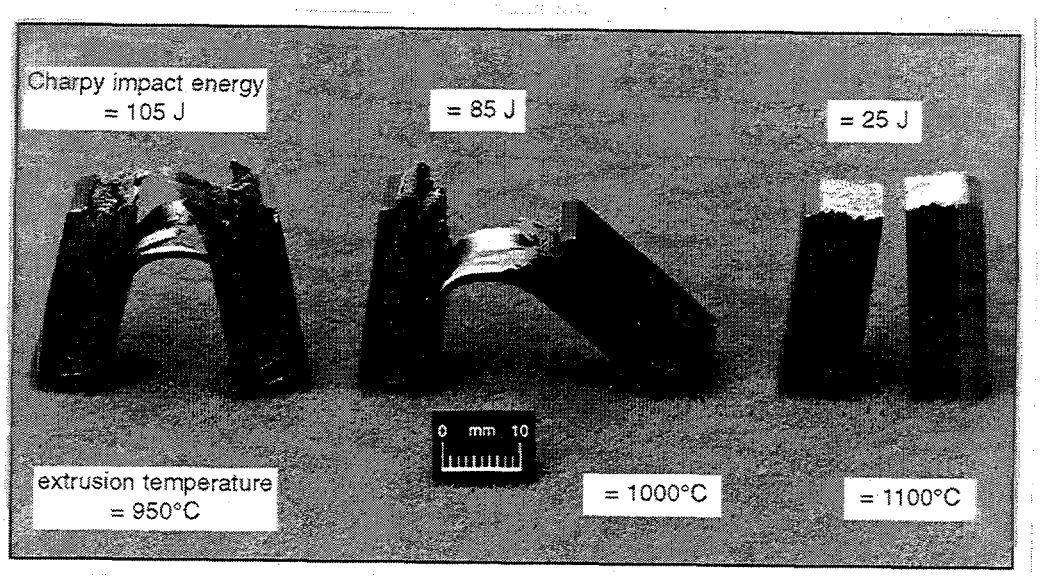

Fig. 4. Fractured Charpy impact speciments of P/M FeAl (FA-385) consolidated by direct hot-extrusion at 950-1100°C. Alloys with the highest toughness have ultrafine grained microstructures (2-5 μm) and a jagged, more ductile fracture mode.

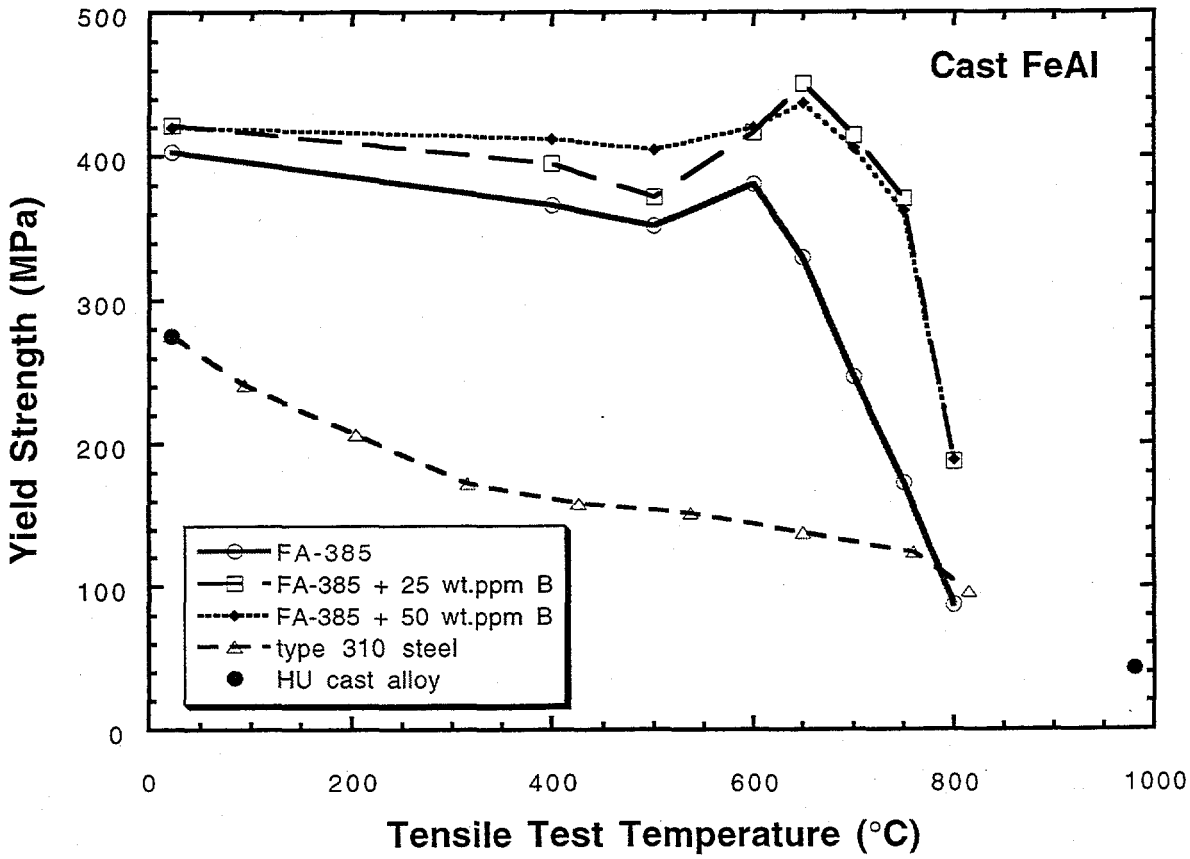

Fig. 5. Plot of yield strength (YS) versus tensile test temperature for cast FeAl alloys with and without boron doping. Data for type 310 austenitic stainless steel and cast HU stainless alloy are included for comparison.

4. Residual Stress Measurements in FeAl Weld-Overlays

ORNL has unique neutron diffraction capabilities and methods at the High Flux Isotope Reactor (HFIR), and that facility is being used to measure residual strain/stress distributions in FeAl weld-overlays on 2 1/4 Cr-1Mo steel. This work, together with finite-element modeling (FEM) of elastic-plastic response of the FeAl weld-overlay and post-weld heat-treatment process is being done to support optimizing those weld-overlay processing parameters which are required in order to eliminate cold-cracking. Previous studies have shown compressive stresses in the steel substrate underneath the FeAl weld-overlay, and high tensile residual stresses in the FeAl weld-deposit itself, close in value to the YS. The post-weld heat-treatment of 1h at 750°C relieves some of the stresses developed after welding, and indeed, specimens without the post-weld heat-treatment showed 300-750 Mpa tensile stresses in the FeAl weld-overlay deposit. Such data suggess that the FeAl alloy composition and microstructure in the weld-deposit must enable that material to be strong, ductile and resistant to moisture-induced embriddlement for such weld-overlays to resist cold-cracking.

This year, new FeAl weld-overlays were made on 3 in. Outer diam. plain-carbon steel tubes and on 2 1/4 Cr-1Mo steel plate using Stoody II and IV wires. Materials wre preheated to 350°C, but no post-weld heat treatment was used. The Stoody II FeAl weld-overlay on the steel tube was crack-free. The Stoody IV FeAl weld-deposits on the steel plate were crack-free, but similar FeAl weld-deposits made on the same substrate with the Stoody II wires did contain cracks.

Neutron diffaction measurements of residual strain were made for the single pass Stoody II FeAl weld-deposits made on the steel tubes, and data are shown in Fig. 6. Strains in the steel tube underneath the FeAl weld-overlay were compressive in both the radial and axial directions. Limited data was collected for hoop strain evaluation, but some preliminary observations can be made. The axial strain data for the steel as a function of angular position from the weld center line (Fig. 6a) clearly shows a peak in tensile strain in the hear-affected-zone (HAZ). The strain peak has a flat top or actually dips at the weld center line. The hoop strain component shows a similar feature (Fig. 6b). Together, these details of the data suggest that the FeAl weld metal on the top of the steel may actually have yielded and strained plastically during cooling. The 2-dimensional plot of radial strain at a depth of 0.1 in. into the steel is shown in Fig. 7. At any given angular position, the radidal strain was quite uniform along the tube axis. Strain data and analysis on this tube speciman, and on a 5-pass flat plate specimen will continue next year. FEM work also continues.

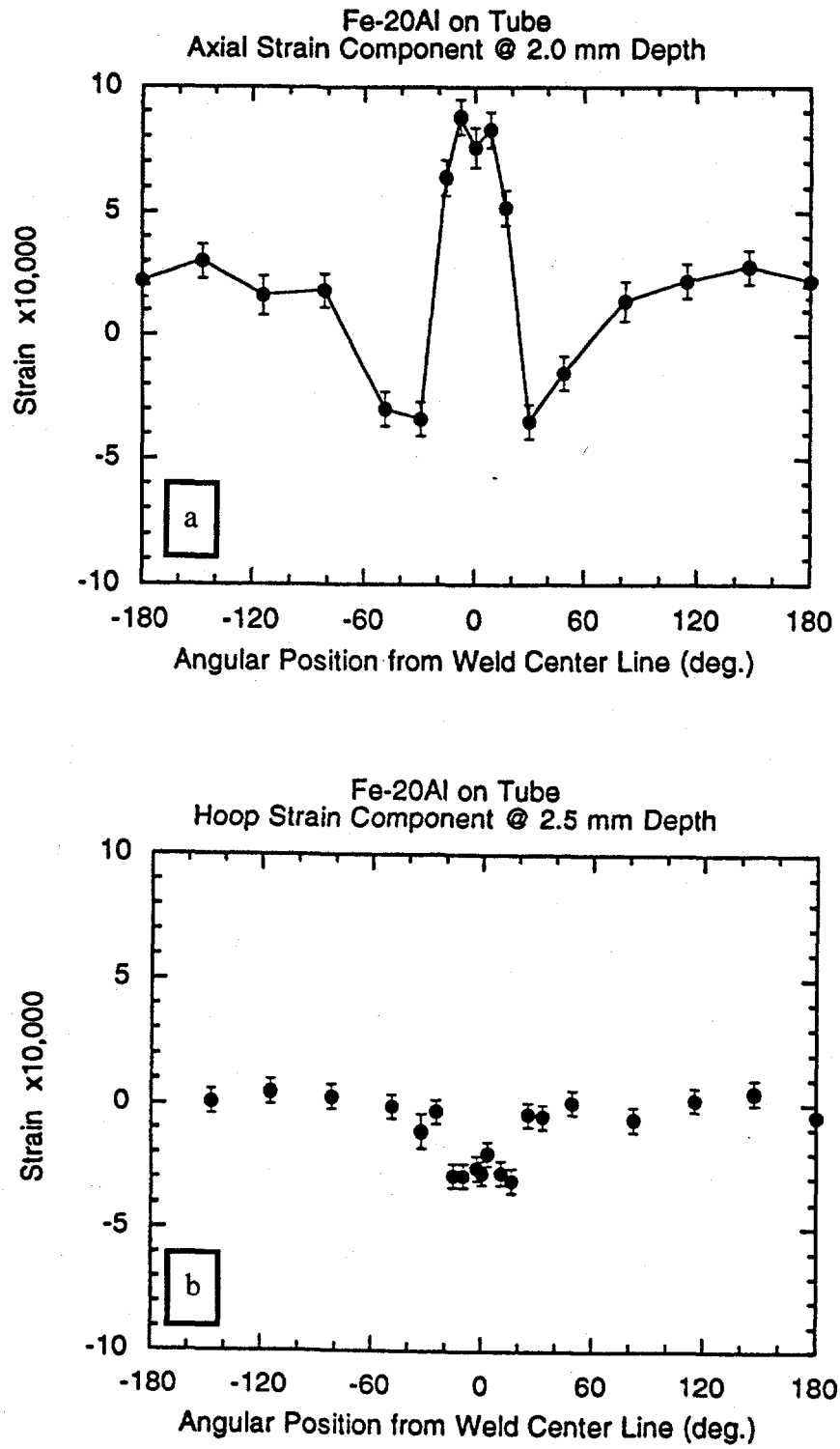

Fig. 6. Plot of strain components measured in plain carbon steel tube with a FeAl weld overlay deposit above, measured as a function of angular position using neutron diffraction. (a) axial strain and (b) hoop strain.

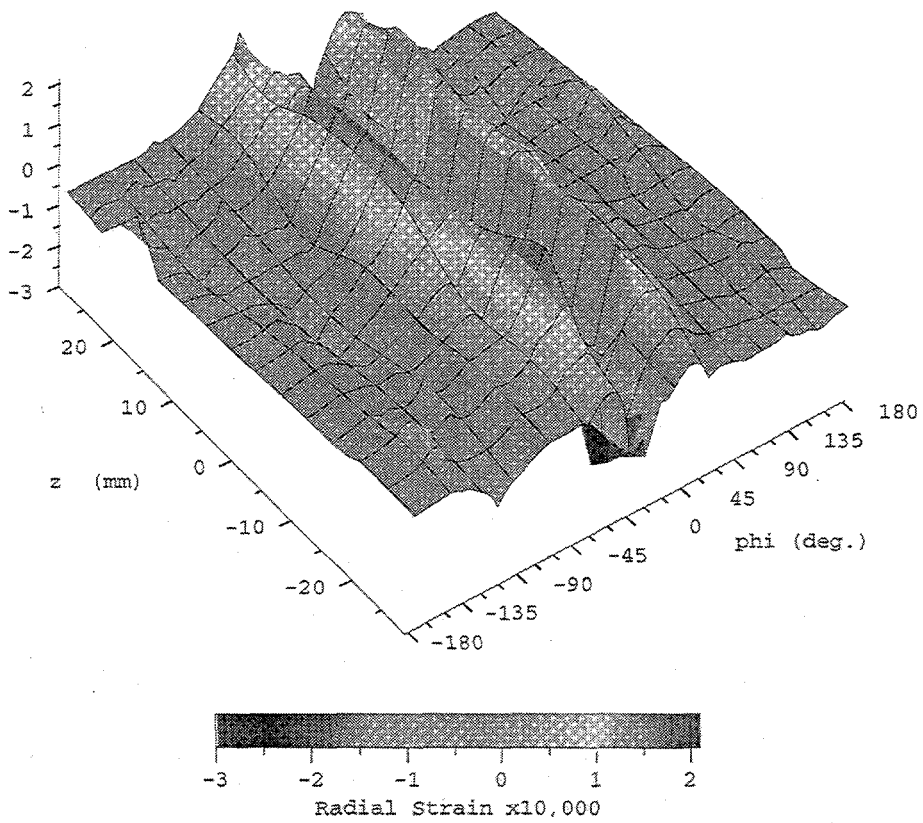

Fig. 7. Radial strain distribution at a depth of 0.1 in. from the interface of a FeAl weld overlay on a plain carbon steel tube.

MILESTONES

For this task, the milestone was "Completle effects of industrial variables and scale-up on properties on FeAl. Provide monolithic FeAl and FeAl weld-overlays on steel to industry for corrosion/properties testing relevant to new applications for FeAl; prepare draft publication, August 1996." This milestone was met with the first draft of the manuscript "High Strength, Ductility and Impact-Toughness at Room-Temperature in Hot-Extruded I/M and P/M FeAl Alloys," by P.J. Maziasz, D.J. Alexander and J.L. Wright for submission to *Intermetallics* Journal.

PUBLICATIONS

Journals

1. P.J. Maziasz, D.J. Alexander, and J.L. Wright, "High Strength, Ductility and Impact-Toughness at Room Temperature in Hot-Extruded FeAl Alloys," paper submitted to *Intermetallics* November, 1996 (in review).

Other Publications

1. X.L. Wang, S. Spooner, C.r. Hubbard, P.J. Maziasz, G.M. Goodwin, Z. Feng and T. Zacharia, "Residudal Stress Distributions in FeAl Weld Overlays on Steel," in High-Temperature Ordered Intermetallic Alloys, VI, Part 1, Matls. Res. Soc. Symp. Proc. Vol. 288, eds. J.A. Horton, et al, MRS, Pittsburg, PA (1995) pp. 109-114.

2. P.F. Tortorelli, J.H. Goodwin and M. Howell, High-Temperature Coatings I, TMS, Warrendale, PA (1995).

3. P.J. Maziasz, C.T. Liu, and G.M. Goodwin, "Overview of the Development of FeAl Intermerallic Alloys," in Heat-Resistant Materials II, eds, K. Natesan, P. Ganesan, and G. Lai, ASM-International, materials park, OH (1995) pp. 555-566.

4. P.F. Tortorelli, G.M. Goodwin, M. Howell and J.H. DeVan, "Weld-Overlay Iron-Aluminide Coatings for Use in High-Temperature Oxidizing/Sulfidizing Environments." In Heat-Resistant Materials II, eds. K. Natesan, P. Ganesan, and G. Lai, ASM-International, Materials Park, OH (1995) pp. 585-590.

5. Z. Feng, X.L. Wang, S. Spooner, G.M. Goodwin, P.J. Maziasz, C.R. Hubbard and T. Zacharia, "A Finite Element Model for Residual Stress in Repair Welds," in Proc. Welding-Induced Residual Stresses in Pressure Vessels and Piping, held at the 1996 ASME PVP Conf. July 21-26, 1996 in Montreal, Canada.

6. P.J. Maziasz, D.J. Alexander, J.L. Wright and V.K. Sikka, "High Strength, Ductility and Toughness in New P/M FeAl Intermetalic Alloys," Advances in Powder Metallurgy & Particulate Materials - 1996, Vol. 4, Metal Powder Industries Federation, Princeton, NJ (1996), pp. 15-41-15-54.

PRESENTATIONS

Oral Presentations

1. P.J. Maziasz, C.T. Liu and G.M. Goodwin, "Overview of the Development of FeAi Intermetallic Alloys," presented at the 2nd International Conference on Heat-Resistant Materials II, held 11-14, September, 1995 in Gatlinburg, TN, co-sponsored by ASM-International and NACE-International.

2. P.F. Tortorelli, G.M. Goodwin, M. Howell and J.H. DeVan, "Weld-Overlay Iron-Aluminide Coatings for Using in High-Temperature Oxidizing/Sulfidizing Environments," presented at the 2nd International Conference on Heat-Resistant Mamterials II, held 11-14, September, 1995 in Gatlinburg, TN, co-sponsored by ASM-International and NACE-International.

3. P.J. Maziasz and G.M. Goodwin, "Effects of Alloying Additions on the Weldability of FeAl," presented at the Internat. Symp. Interstitial and Substitutional Solute Effects in Intermetallics, held during the 1995 TMS Fall Meetings/ASM-International Materials Week, Cleveland, OH October 29 - November 2, 1995.

4. P.J. Maziasz, "Effects of Alloying Additions on the High-Temperature Strength of FeAl," presented at the Symp. Strengthening and Toughening Mechanism in High-Temperature Materials, held during the 1995 TMS Fall Meetings/ASM-International Materials Week, Cleveland, OH October 29 - November 2, 1995.

5. P.J. Maziasz, V.K. Sikka, S. Viswanathan, D.J. Alexander and J.L. Wright, "Processing for Improved Mechanical Properties of FeAl," presented at the Symposium on Intermetallic Compounds held during the '95 Annual JIM/TMS Meeting in Honolulu, HA, December 13-15, 1995.

6. P.J. Masiasz, D.J. Alexander, J.L. Wright and V.K. Sikka, "Processing/Microstructure Control for High Strength, Ductility and Toughness at Room-Temperature in P/M FeAl," invited talk presented at the Symposium on Physical Chemistry of High Temperature Composites and Intermetallics, held during the 1996 Annual TMS Meeting, in Anaheim, CA . February 4-8, 1996.

7. P.J. Maziasz, D.J. Alexander, J.L. Wright and V.K. Sikka, "High Strength, Ductility and Toughness in New P/M FeAl Intermetallic Alloys," invited talk presented at Sessions on P/M Structure/Properties Relationships at $PM^2TEC'96$ World Congress, held June 16-21, 1996 in Washington, D.C., sponsored by ASMI-International.

8. P.J. Maziasz, "Using Extreme Processing-Induced Microstructures to Radically Improve the Mechanical Properties of Advanced Intermetallic Alloys (B2-FeAl and γTiAl)" Invited Graduate Seminar presented at the Department of Materials Science and engineering, University of Tennessee - Knoxville, October 1, 1996.

HONORS AND AWARDS

Lockheed Martin Energy Research Corporation chose to submit this work for a R&D Award in March, 1996.

A Poster, "Processing/Microstructure for High Ductility, Strength and Toughness in P/M FeAl Intermetallic Alloys," was awarded First Plalce in Electron Microscopy and the overall Grand Prize for the Metallography contest at $PM^2TEC'96$ World Congress, held June 16-21, 1996 in Washington, D.C., sponsored by APMI-International.

PATENTS/DISCLOSURES

1. C.T. Liu, C.G. McKamey, P.F. Tortorelli and S.A. David, "Corrosion Resistance Iron Aluminides Exhibiting Improved Mechanical Properties and Corrosion Resistance," U.S. Patent No. 5,320,802, granted June 14, 1994.

2. P.J. Maziasz, G.M. Goodwin and C.T. Liu, "High-Temperature Corrosion-Resistant Iron-Aluminide (FeAl) Alloys Exhibition Improved Weldability," U.D. Patent No. 5,545,373, granted August 13, 1996.

LICENSES

None. However, preliminary discussions have begun with United Defense and several other companies interested in FeAl.

INDUSTRIAL INPUT and TECHNOLOGY TRANSFER

A CRADA with Devasco International, Inc. of Houston, TX for development of shielded-metal-arc (SMA) FeAl (FA-385) electrodes was completed in October, 1995.

Work to develop aspiration cast FeAl filler-metal weld-wires was completed in 1995. Work brgan in 1995 with Stoody Company (Bowling Green, KY) to develop small-diameter coiled Fe-Al solid- and powder-core weld wire for continuous, automated gas-tungsten-arc (GTA) and gas-metal-arc (GMA) weld-overlay applications, and will continue next year.

Commercial spherical, nitrogen-atomized FeAl powders (400 lb melt, 250 lb yield) were produced by Ametek Specialty Powder Division (Eighty-Four, PA) in 1995, and the initial tensile and impact properties of P/M FeAl consolidated by direct hot-extrusion were excellent. Discussions are under way with other powder producers to make water-atomized FeAl powders, examine various consolidation methods, and explore applications as replacements for austenitic and ferritic stainless steels. FeAl powders can be used to make hot-gas clean-up filters, and P/M FeAl can also be processed into sheet or thin foil for various applications.

FeAl pipes (800 lb heat) were centrifugally cast by Alloy Engineering and Casting (Champaign, IL), similar to those used for radiant-heating tube applications. Such tubes can be centrifugally cast onto other steels or stainless steels and co-extruded to produce piping for chemical or petro-chemical processing applications that require oxidation, sulfidation or carburization resistance.

Rocketdyne-Rockwell International (Conoga Park, CA) tested cast FeAl in molten sodium nitrate/carbonate salts at 900°C and found them to be much more resistant than alloy 600 coupons in 1995. Application would be vessel liner in waste remediation.

In 1995-96 a new series of industrial tests began. Thixomat Inc. (Ann Arbor, MI) is evaluating FeAl for wear-erosion in molten aluminum for semi-solid injection-molding applications. Babcock & Wilcox (S. Cung) has FeAl to test for oxidation and sulifidation resistance, as do the University of

Manchester (Prof. F.H. Stott) and INCO Alloys International (G. Smith) INCO testing has found that cast FeAl has outstanding carburization resistance. Testing is in progress with other OIT Vision Industries, including forging, aluminium processing and forest products industries for corrosion resistance of monolithic or weld-overlay FeAl.

ESTIMATED ENERGY SAVINGS

Energy savings accrue from the Exo-Melt™ processing of FeAl compared to conventional processing (50%) and the savings in energy and material from replacing steels, stainless steels or Fe-Cr-Ni alloys with longer-lasting "super" corrosion-resistant FeAl to reduce or prevent metal wastage. Benefits for reduced metal wear of FeAl may also be realized. FeAl is also a Cr- and Ni-free substitute for heat/corrosion resistant steels and alloys for applications with such environmental and toxicity requirements.

MATERIALS FOR THE PULP AND PAPER INDUSTRY

SECTION 1: DEVELOPMENT OF MATERIALS FOR BLACK LIQUOR RECOVERY BOILERS

J.R. Keiser, C.R. Hubbard, P.J. Maziasz, E.A. Payzant, S.J. Pawel, R.W. Swindeman, B. Taljat, R.L. Thomas, X.L. Wang, and T. Zacharia

Metals and Ceramics Division
Oak Ridge National Laboratory
P.O. Box 2008
Oak Ridge, TN 37831

D.L. Singbeil and R. Prescott

Pulp and Paper Research Institute of Canada
3800 Wesbrook Mall
Vancouver, BC, Canada V6S 2L9

J. Empie

Institute of Paper Science and Technology
500 10th Street, N.W.
Atlanta, GA 30318

INTRODUCTION

Black liquor recovery boilers are essential components of kraft pulp and paper mills because they are a critical element of the system used to recover the pulping chemicals required in the kraft pulping process. In addition, the steam produced in these boilers is used to generate a significant portion of the electrical power used in the mill. Recovery boilers require the largest capital investment of any individual component of a paper mill, and these boilers are a major source of material problems in a mill. The walls and floors of these boilers are constructed of tube panels that circulate high pressure water. Molten salts (smelt) accumulate on the floor of recovery boilers, and leakage of water into the boiler can result in a violent explosion when the leaked water instantly vaporizes upon contacting the molten smelt. Tube leaks, often leading to such explosions, have occurred with some regularity in the paper industry.

Because corrosion of the conventionally-used carbon steel tubing was found to be excessive in the lower section of recovery boilers, use of stainless steel/carbon steel co-extruded tubing was adopted for boiler walls to lessen corrosion and reduce the likelihood of smelt/water explosions. Eventually, this co-extruded or composite (as it is known in the industry) tubing was selected for use as a portion or all of the floor of recovery boilers, particularly those operating at pressures >6.2 MPa (900 psi), because of the corrosion problems encountered in carbon steel floor tubes.

However, cracking into, or through, the stainless steel outer layer of this composite tubing has been encountered. Almost without exception in sloped-floor boilers, cracks have first been seen in wall tubes that form the openings for removal of the molten salts (smelt spout openings). Subsequently, cracks have been found in floor tubes themselves in both sloped-floor and flat-floor types of boilers.

Since neither the cause of the cracking nor an effective solution has been identified, this program was established to develop a thorough understanding of the degradation that occurs in the composite tubing used for walls and floors. This is being accomplished through a program that includes collection and review of technical reports, examination of unexposed and cracked tubes from boiler floors, collection and analysis of smelt samples, collection and tabulation of temperature data, measurement of residual stresses in as-produced, as-formed, and exposed composite tubing, computer modeling to predict residual stresses under operating conditions, and operation of laboratory tests to study corrosion, stress corrosion cracking, and thermal fatigue. From this work it is anticipated that alternate materials or operating procedures will be identified, and these will be tested in recovery boilers.

TECHNICAL PROGRESS - FY 1996

1. Composition of Information on Composite Tube Cracking

The review of known public domain and company confidential reports pertaining to cracking of co-extruded tubes in kraft recovery boilers was completed and the final draft presented to the Advisory Committee (Ref. 1). Key findings from this report are summarized below:

- Based on the information collected, it is likely that all 304L/SA-210 co-extruded tubes exposed to the smelt bed in a kraft recovery boiler are susceptible to cracking in service.

- No strong mitigating factors have been discovered which might exclude these tubes in a boiler from cracking. Some circumstantial evidence exists which suggests that a deep smelt bed or a thick refractory cover over the boiler floor might offer a degree of protection.

- Most of the cracking which has been found in floor and wall tubes exposed to the smelt bed has been confined to the outer stainless steel layer. Penetration of the cracks across the stainless steel/carbon steel interface is rare, and almost always occurs near highly restrained welds at spout and air port openings. Three instances of cracking into the carbon steel core of floor tubes have been reported.

- A thorough review of both private and public domain documents pertaining to cracking of co-extruded tubes in recovery boilers floors was unable to positively identify a failure mechanism. Some cracks, particularly at port openings are most likely due to thermal fatigue.

- The mechanism of cracking for the majority of cracks is unknown, but appears to be a form of environmentally assisted cracking (EAC).

- Insufficient information exists to select a material combination for co-extruded tubes which will guarantee crack-free service over the predicted lifetime of the boiler. Laboratory testing and accumulated service history for co-extruded tubes made from Alloy 825 indicate that an improvement in tube life over 304L can be expected, but cracking of these tubes has already been reported.

2. Examination of Unexposed and Exposed Composite Tubing

2.1 Characterization of composite tubes at four stages of fabrication

A consistent feature on most cracked composite tubing is the tendency for cracks in the stainless steel layer to turn as they approach the stainless steel/carbon steel interface and continue in the stainless steel parallel to the interface. Previous examinations of the interfacial area of composite tubes from both major manufacturers have shown that there is a carbon depleted region in the carbon steel and a carbide-rich area in the stainless steel. It is not clear that the carbide-rich region in the stainless steel has an effect on crack behavior, but it is clear that cracks do move preferentially through the harder, more brittle, carbide-rich region in the stainless steel. In order to determine when in the manufacturing process this redistribution of carbon occurs, tube sections were collected by Sandvik at four stages of the composite tube manufacturing process.

Four tube samples were collected and sent to ORNL for examination. These samples were taken after the initial extrusion, after cold reduction to final size, after annealing, and after straightening. Samples from each tube section were examined metallographically, and hardness measurements were made from the stainless steel across the stainless steel/carbon steel interface and into the carbon steel. Hardness measurements were also made in an axial direction along the outer surface of the straightened sample.

The results of hardness measurements across the interface of each sample, which are shown in Fig. 1, indicate that precipitation of carbides in the stainless steel occurred during the annealing treatment. An increase in hardness, primarily in the stainless steel, resulted from the straightening operation. These observations were confirmed by the microstructural studies.

Hardness measurements on the surface of the straightened tube were made to determine if there was a variation in hardness that could be associated with the helical advance of the tube through the straightening device. As can be seen in Fig. 2, there is some periodicity to the hardness measured on the surface of the tube. It might be expected that this variation in properties might also be seen as a variation in residual stresses as measured by X-ray diffraction. In fact, the reported measurements of residual stresses show a significant variation around the circumference of the tube which is most likely an indication of the periodicity in the hardening caused by the straightening process.

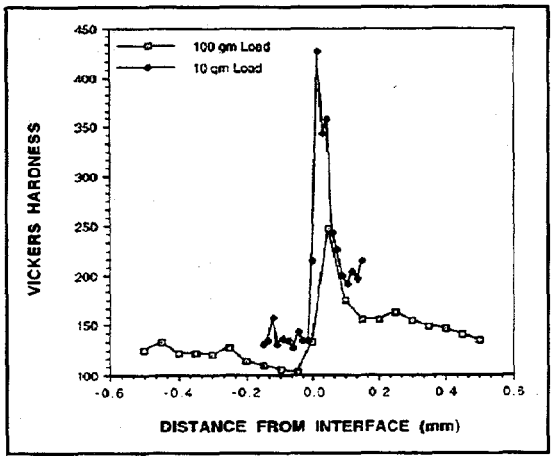

Fig. 1. Microhardness in the vicinity of the 304L stainless steel/SA210 carbon steel interface for a sample collected after the annealing operation of the composite tube fabrication process.

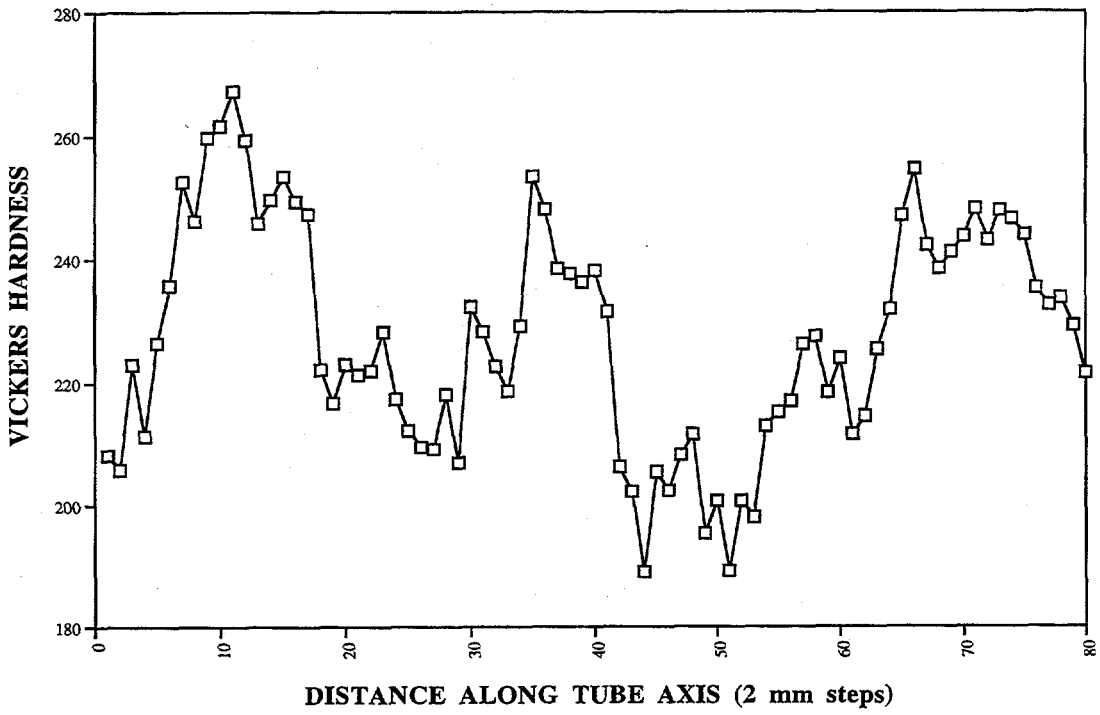

Fig. 2. Microhardness measured on the outer surface parallel to the tube axis of an as-fabricated 304L/SA210 coextruded tube.

2.2 Examination of cracked tubing after recovery boiler exposure

Examinations were performed on a significant number of cracked tubes that had been removed from North American and European recovery boilers. Tubes with circumferential and/or craze cracks were examined, and the cracking patterns observed were typical of what has been seen in

previous examinations. An example of the subsurface pattern of a tube with craze cracking is shown in Fig. 3. This cracking is relatively shallow, has little branching, and the sides of the cracks match very well in many areas. An example of extensive membrane cracking is shown in Fig. 4. Most of these cracks advance to the interface where they turn and proceed parallel to the interface or they end in a corrosion pit in the carbon steel.

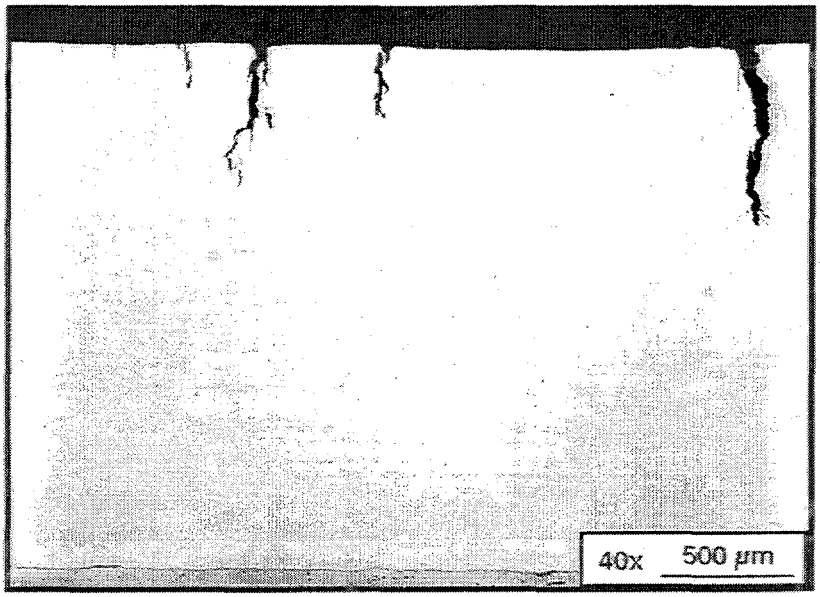

Fig. 3. Cross section through craze cracking found in 304L/SA210 composite tube exposed in a North American recovery boiler.

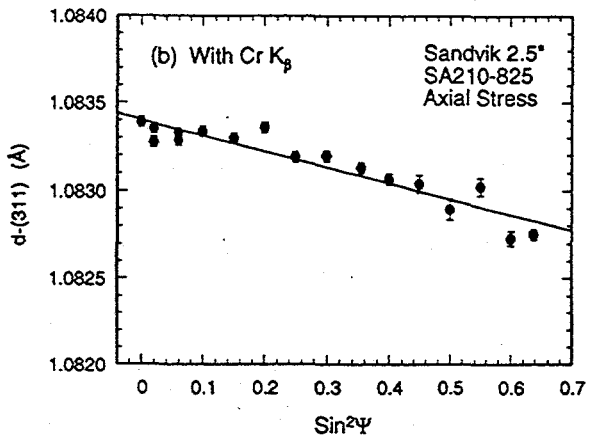

Fig. 4. D-$\sin_2\psi$ plot obtained using the fcc (311) reflection and CR K_β radiation. The close to linear relationship allows accurate determination of the slope, from which the residual stress is derived.

From the examination of a large number of cracked composite tubes, the following observations can be made.

1) Near the outer surface, most longer cracks in the stainless steel layer are fairly wide, transgranular, and have little or no branching;

2) these longer cracks often display more branching a significant distance into the stainless steel layer;
3) short cracks can sometimes be found originating at the surface and these cracks are narrow and transgranular with some branching;
4) longer cracks end at (or before) the interface, or they turn and proceed in the stainless steel parallel to the interface;
5) corrosion pits are often found growing into the carbon steel when a crack ends at the interface; and
6) a few cases of intergranular attack of the carbon steel have been found.

2.3 Transmission electron microscopy examination of samples

There are several possible cracking mechanisms that could be operative on composite tubes in black liquor recovery boilers, and it has been quite difficult to positively determine which mechanism(s) are causing the cracking of composite floor tubes. However, it is known that metallic samples that have been subjected to cyclic stresses develop a dislocation structure typified by "cells" along with relatively large and extended stacking faults and fine dislocation loops. In order to detect these features, very high magnification ($\geq$10,000X) microscopy is needed. Consequently, transmission electron microscopy has been used to examine several samples taken from cracked composite tubes.

Samples were taken from two positions in the stainless steel layer of the composite tubes; one sample was taken from approximately the middle of the layer and one was taken from as close to the surface as possible (within 0.1 mm). Samples from an unexposed composite tube and from a 304L thermal fatigue sample were also examined.

Although these studies have not been completed, the initial data indicate that the samples taken from the 304L layer of a cracked composite tube have many features similar to the thermal fatigue control microstructure. The density of the characteristic dislocation structures is not as dense in the exposed sample as in the control, but the features do suggest that the exposed sample has been subjected to thermal cycling.

3. Measurement of Residual Stresses in Unexposed and Exposed Tubing

Since the beginning of this research program, one of the goals of the residual stress task has been to provide information to help identify the mechanism of cracking experienced in composite tubes subjected to kraft recovery boiler service conditions. Microstructural and other evidence suggests that stress corrosion cracking and thermal fatigue are the most likely explanations for the observed cracking. In either case, the residual stress state in the clad layer plays an important role in that tensile residual stresses at the surface could facilitate crack initiation, whereas tensile residual stresses below the surface layers assist the propagation of cracks. If, however, the surface is under a compressive residual stress, stress corrosion cracking is considered unlikely.

3.1 Surface residual stresses in exposed tubes

To determine the surface residual stresses in composite tubes, a special X-ray diffraction technique had to be developed because of the characteristic texture present in the clad layer, which resulted in an oscillating d-sin$^2\Psi$ relationship and hence poor experimental precision (40-50 MPa) when measurements were made with the conventional Cr K_α radiation and the fcc (220) reflection [$2\Theta \approx 128°$]. To improve the experimental precision, attempts were made to measure the fcc (311) reflection using the Cr K_β radiation [$2\Theta \approx 148.5°$]. The results indicate that the (311) pole exhibited a much weaker texture (<1.5:1) and hence, the measured d-sin$^2\Psi$ relationship was quite linear (Fig. 4). This method gives an experimental precision of $\pm$10-20 MPa and was employed for all subsequent X-ray measurements.

The X-ray stress data revealed that the hoop and axial residual stress state at the surface can be highly non-uniform, as illustrated by Fig. 5. For some of the tubes, a sign change in residual stress values was observed along the circumference. Similar degrees of stress variations were also observed along the axial direction. Neutron diffraction results confirmed that stress variations along the circumference existed at all depths in the clad layer. A likely cause of the observed stress variability is the straightening process that the tube manufacturer applied to these composite tubes after annealing at 920°C.

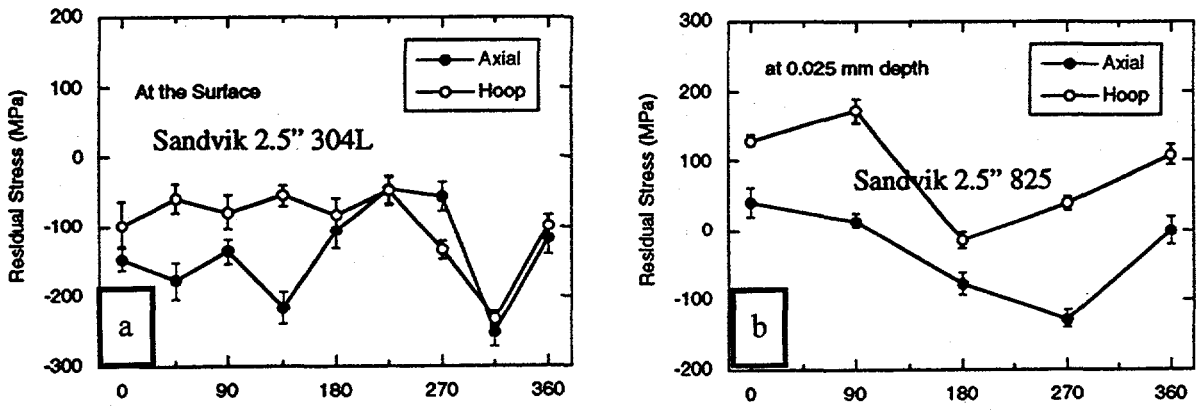

Fig. 5. Surface residual stress data as a function of the position along the circumference in four as-manufactured Sandvik composite tubes.

Despite the variation in stress values, to within the experimental precision, it is clear that for 2½ in. OD 304L tubes the axial and hoop stresses in the surface layers are compressive. For 3 in. OD 304L tubes the measured residual stresses show greater variability, tensile at some locations and compressive at others. It is well known that stress corrosion cracking cannot take place if the material never experiences tensile stresses at the surface. To determine if exposure in a recovery boiler might have affected the residual stresses in composite tubes, tube panels were removed from operating mills and analyzed with X-ray or neutron diffraction. One of the panels was made of Sandvik 2½ in. 304L composite tubes. A two-tube section was torch- and saw-cut from the panel and X-ray diffraction was used to determine the surface residual stresses on both sides of the

sub-panel. To determine the through-thickness stress profile, a single-tube section was saw-cut from a panel made of Sandvik 3 in. 304L composite tubes and measured with neutron diffraction.

Figure 6 shows the surface residual stresses obtained by X-ray diffraction [with fcc (311) reflection and the Cr K_β radiation] at the surface of the two-tube sub-panel. Clearly, the fire side (side of exposure) exhibits a different residual stress state than the cold side (opposite side) after exposure. For both axial and hoop stress components, the fire side crown is highly tensile with a maximum of 250 MPa, while the cold side crown is compressive and less than -150 MPa. Also, it can be seen that the measurement technique developed for as-manufactured composite tubes worked well here, as evidenced by the small error bars associated with individual data points.

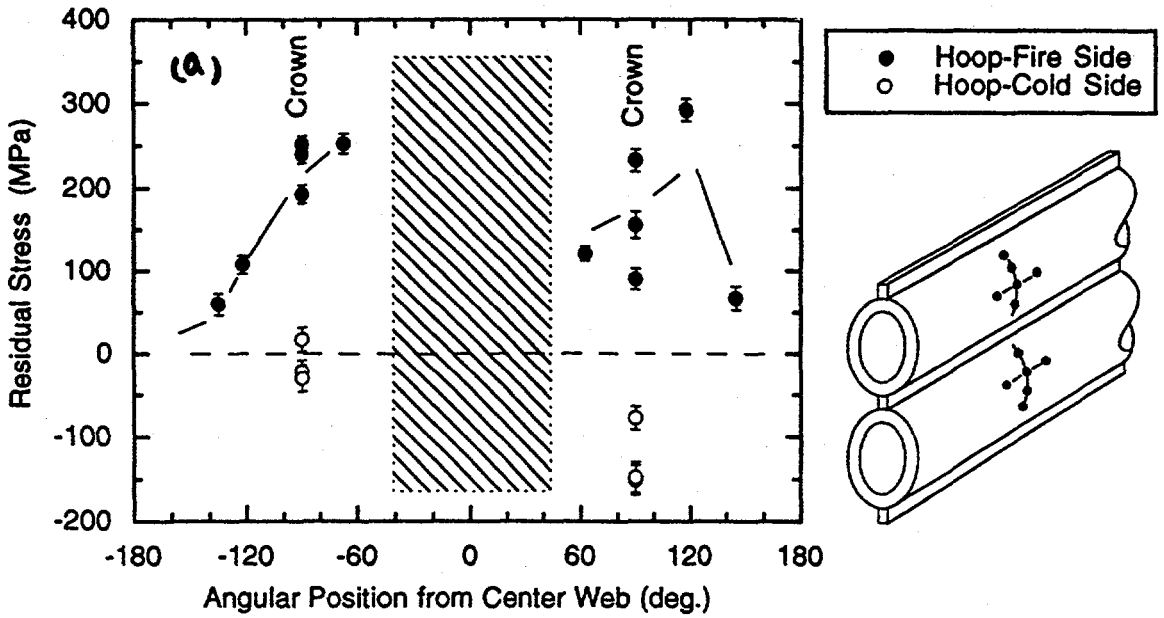

Fig. 6. Surface residual stress data in an exposed two-tube sub-panel. The experimental data were obtained with the Cr K_β radiation and the fcc (311) reflection. The shaded area close to the weld was not accessible with X-ray.

The through-thickness stress profile determined by neutron diffraction is shown in Fig. 7. Again, the fire side exhibits higher tensile residual stresses than the cold side. The maximum tensile stress is also 250 MPa, consistent with the surface stress data obtained by X-ray diffraction on the two-tube sub-panel.

These experimental results indicate that after being put into service, e.g., exposure to recovery boiler operation, the residual stresses in the composite tubes have become tensile on the side of exposure (fire side), which creates one of the necessary conditions for stress corrosion cracking to occur. The marked difference in residual stress magnitudes between the fire and cold sides of the tubes shows that the tensile residual stress on the fire side is due to exposure, rather than fabrication of the panels.

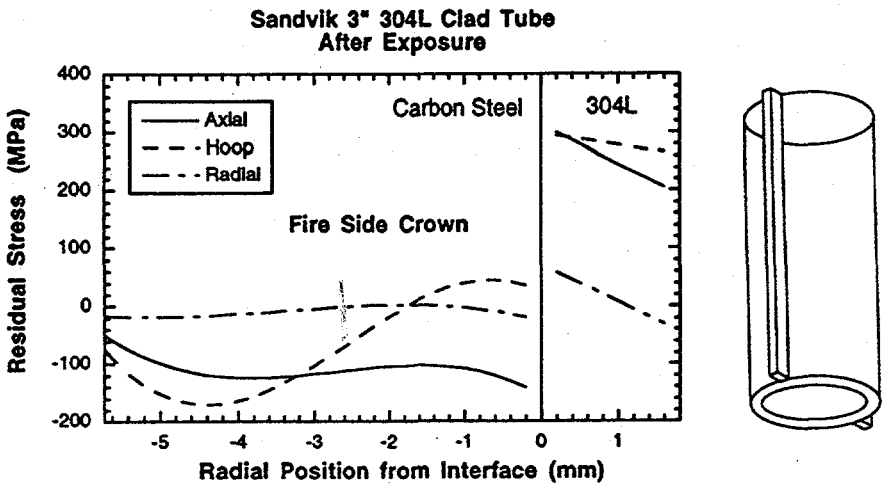

Fig. 7. Through-thickness residual stress profile in an exposed tube determined by neutron diffraction. Residual stresses in the carbon steel on the cold side can not yet be evaluated, since the hoop strain component has not been determined.

3.2 Residual stresses in tubes with weld overlay

Because of the cracking problems experienced by co-extruded composite tubes, there has been growing interest in an alternative manufacturing technology, where the corrosion resistant layer is applied to the carbon steel tube by welding. Limited experience to date with boilers containing tubes covered with a repair weld shows less frequent occurrence of cracking. Figure 8 shows a section of a spiral weld overlay tube made by continuous weld deposition.

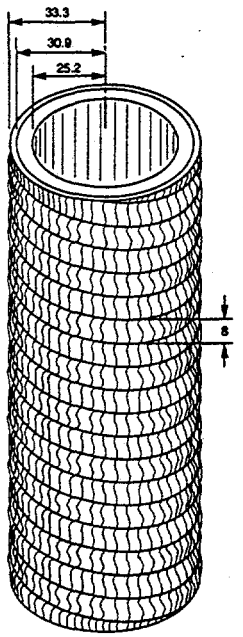

Fig. 8. Schematic of the weld overlay tube specimen.

Neutron diffraction was used to determine the through-thickness residual stress profile and results are shown in Fig. 9. Tensile stress regions were found not only in the weld metal but also in the heat-affected zone in the carbon steel. The maximum tensile stress was located in the weld overlay layer and amounted to 360 MPa, about 75% of the 0.2% yield strength of the weld metal. The tensile residual stresses in the overlay layer make weld overlay tubes vulnerable for both stress corrosion and thermal fatigue cracking. However, after heat treating at 900°C for 20 min., additional neutron diffraction measurements revealed that these welding residual stresses vanished. The experimentally determined residual stress profile was compared with the results of a finite element analysis conducted in parallel with the neutron diffraction work. Overall, the modeling results are in satisfactory agreement with the experimental data, although the hoop strain (stress) seems to have been overestimated by the finite element model.

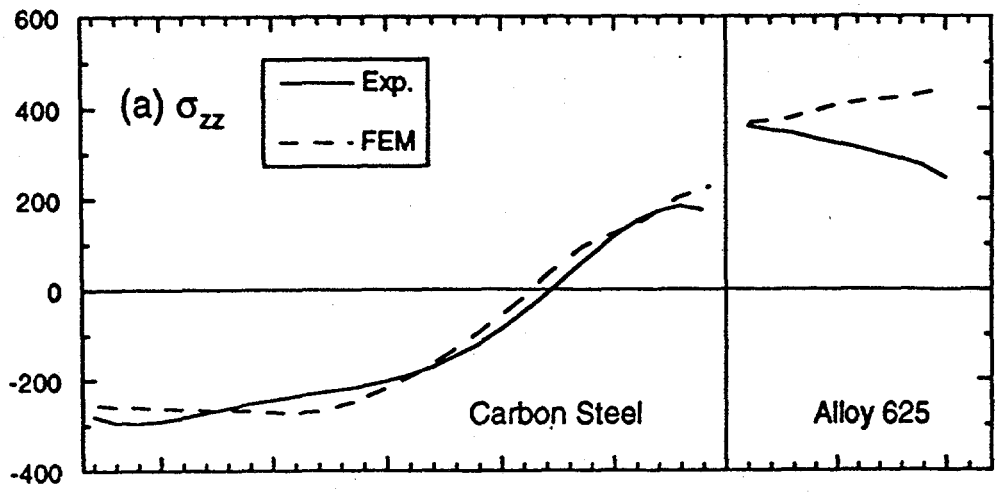

Fig. 9. Residual stresses in a weld overlay tube. The dashed lines are calculations from a finite element analysis.

Next year, measurements will be made on an as-welded composite tube panel to determine the residual stresses as a result of welding. To study the effect of exposure, an as-manufactured composite tube will be subjected to thermal conditions similar to that in an operating mill and the residual stresses determined at the end of each cycle using neutron diffraction. The experimental data will also serve to validate the finite element model currently being developed and provide guidance to improve the model. In addition, on-site X-ray measurements will be conducted using the technique developed above.

4. Modeling of Residual Stresses

The results of earlier analyses showed that there is a possibility for developing tensile stresses at the tube fireside surface at the presence of lateral constraints during operation. Soon it became clear that the boiler construction allows free thermal expansion of boiler floor and walls, which means there are no global constraints on the floor. Analyzing different thermal loading scenarios we learned that there are other potential loading cases which would presumably cause local constraints on the floor tubes and so tensile stresses at the tube surface. A local temperature nonuniformity (hot-spot) is a feasible in-operation loading condition which would cause that sort

of stress distribution. In order to analyze stresses in the case of nonuniform temperature loading of the floor, a 3D model was developed. Several modifications were made to the initially established 3D model in terms of computational accuracy. The model was used to perform various analyses throughout the year, from initial steady state cases to more complex transient analyses including various in-service and manufacturing effects.

To support the thermal transient analysis with the 3D model a thorough thermal analysis was made for a system including the floor tube, the smelt layer, and the fluid inside the tube. Another study was performed to determine the residual stress state in a tube with a spiral weld overlay tube for two different overlay materials.

4.1 Thermal analysis of the smelt-tube-fluid system

A finite element model for thermal analysis of the smelt-tube-fluid system was developed to thoroughly determine the temperature distribution in the circumferential and radial direction of the tube at regular operation and during temperature excursions. The analyzed composite tube is SA210/SS304L with SS312 weld material. A sensitivity analysis, under the conditions shown in Table 1, was performed to study the effects of smelt thickness (0.5, 1, 3, and 6 in.), extent of steam blanketing (0, 90, and 180°), and smelt properties (thermal conductivity, specific heat) on the tube temperature and the heat flux to the fluid during normal operation (steady state case). Since the smelt composition depends on various factors it may not be easy to determine the exact values of physical properties. Therefore, a reasonable range for each smelt property; i.e. maximum and minimum possible values for specific heat and thermal conductivity as functions of temperature, were specified.

No:	Name	Smelt thermal conductivity, k [W/mK]	Smelt specific heat, c [J/gK]	Smelt thickness [mm]	Steam blanket coverage [^{0}]	Tube-fluid convection, h [W/m^{2}K]
1	MP1	0.5	0.75	25.4 (1.0")	0	56780
2	MP2/ST2/SB1	5.0	1.25	25.4 (1.0")	0	56780
3	CNV	5.0	1.25	25.4 (1.0")	0	5678
4	ST1	5.0	1.25	12.7 (0.5")	0	56780
5	ST3	5.0	1.25	76.2 (3.0")	0	56780
6	ST4	5.0	1.25	152.4 (6.0")	0	56780
7	SB2	5.0	1.25	25.4 (1.0")	90	56780/567.8
8	SB3	5.0	1.25	25.4 (1.0")	180	56780/567.8

Table 1. Sensitivity analysis parameters.

The results of the sensitivity study show a significant effect of steam blanketing on the tube temperature. Heat flux to the fluid depends on the smelt thermal conductivity and thickness of the smelt layer.

A typical temperature excursion, measured by a thermocouple (TC) positioned on the crown of the tube, was taken into account to simulate the hot spot (HS) appearance (transient analysis). It was assumed that the temperature measured by the TC corresponds to the smelt temperature at 3 mm from the tube surface, which is therefore higher than the tube surface temperature. The tube surface temperature was calculated by an assumption that only the smelt above the tube crown is melted, and by controlling the temperature at the TC location. A typical temperature excursion measured by the TC is presented in Fig. 10.

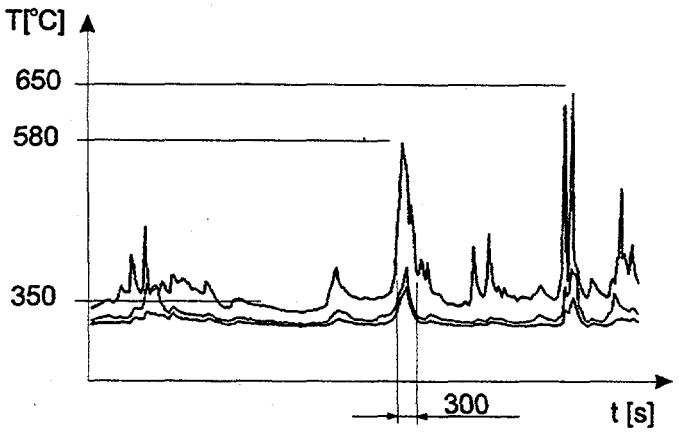

Fig. 10. A typical temperature excursion measured by a floor thermocouple.

4.2 Analysis of stress state due to floor temperature nonuniformity

Analysis with the 3D model has gone through several stages. Initially the model was used to analyze the steady state thermal cases, with only the in-service loading applied (specified constant temperature at the fireside surface; internal pressurization). The model was used to study different cases with the emphasis on different types of hot spots and different material configurations. The analysis showed that the fireside tube surface might experience tensile stresses under certain hot-spot conditions (temperatures: fireside 343°C, inside 287°C, fireside HS 550°C, inside HS 500°C; see Fig. 11). Later on, the manufacturing residual stresses (combined extrusion and welding) were remapped from the simple cross-sectional 2D model, which was used to perform the tube-web welding analysis and to combine the calculated stress field with the residual stresses from extrusion measured by Neutron Diffraction (ND). After completion of the 2D thermal analysis the temperature results (the actual surface temperature in the circumferential direction) were used to modify the assumption of constant surface temperature of the 3D model. This also satisfied the conditions to initiate the transient analysis with the 3D model.

Shell finite elements (thick shell formulation) with the composite material formulation were used to built the model. In addition, the 3D solid elements were used to model the welds joining the tubes and membranes. The model needed to be large enough relative to the hot spot dimensions so the hot spot effect diminishes within the model and the infinity assumption could be considered.

Therefore, the model length of 70 in. and the width of 11 tubes was used in the analysis (see Fig. 12). The FE model was built with the assumption of dual geometric symmetry. This enables the actual FE mesh to be only a quarter of the actually analyzed geometry. This saves computational time or allows a detailed FE mesh with more shell (through thickness) section points.

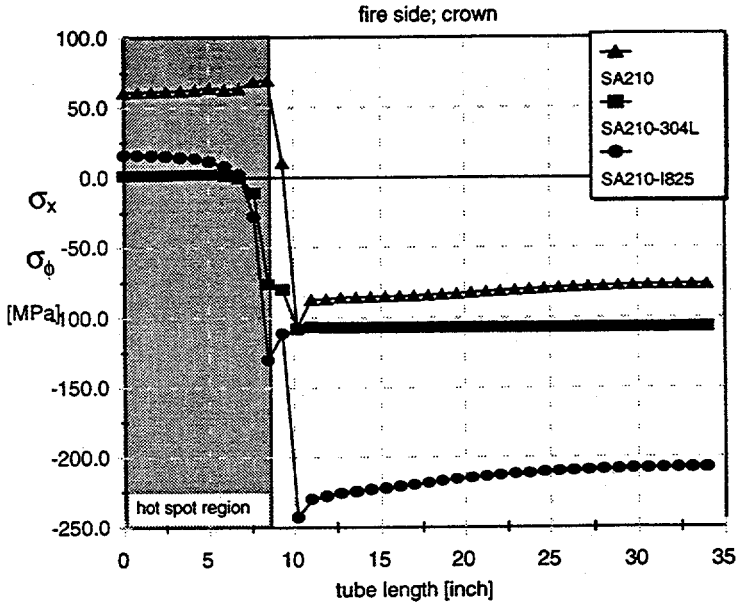

Fig. 11. Hoop stresses at the fireside crown surface along the tube length during a temperature excursion (i.e., hot spot) for an SA210/SS304L composite tube, and an SA210/Alloy 825 composite tube. Only the in-service loading is shown; residual stresses are not considered.

4.3 Incorporating manufacturing residual stresses to the 3D model

A new model of the tube-weld-web cross section with the actual-scanned geometry was built. Residual stresses from extrusion measured by ND were applied and balanced. Welding simulation was performed such that the weld on one side was made first, the tube was cooled to the room temperature, and then the weld on the other side was made. The movement of the web in the Y direction (X is the tube to tube direction, perpendicular to the tube axis; Y is perpendicular to X; and Z is the axial direction) is constrained during welding. The analysis was performed for SS304L and Alloy 825 tube overlay materials.

Stresses were determined at both surfaces and at an additional four points through the tube thickness at 17 circumferential locations. Since the composite shell elements used in the 3D model have six through thickness points, the stress values were interpolated in the circumferential direction only. Only two stress components (hoop and axial) were remapped, because there are no radial and shear (radial-hoop) stress components available with shell elements. Stresses were also evaluated at two locations along the web, one close to the tube and another at the web center. The values at other locations were simply determined by interpolation. Four Cartesian stress components (σ_{xx}, σ_{yy}, σ_{zz}, σ_{xy}) were determined for each weld at one central location, which represents the average stress value throughout the weld.

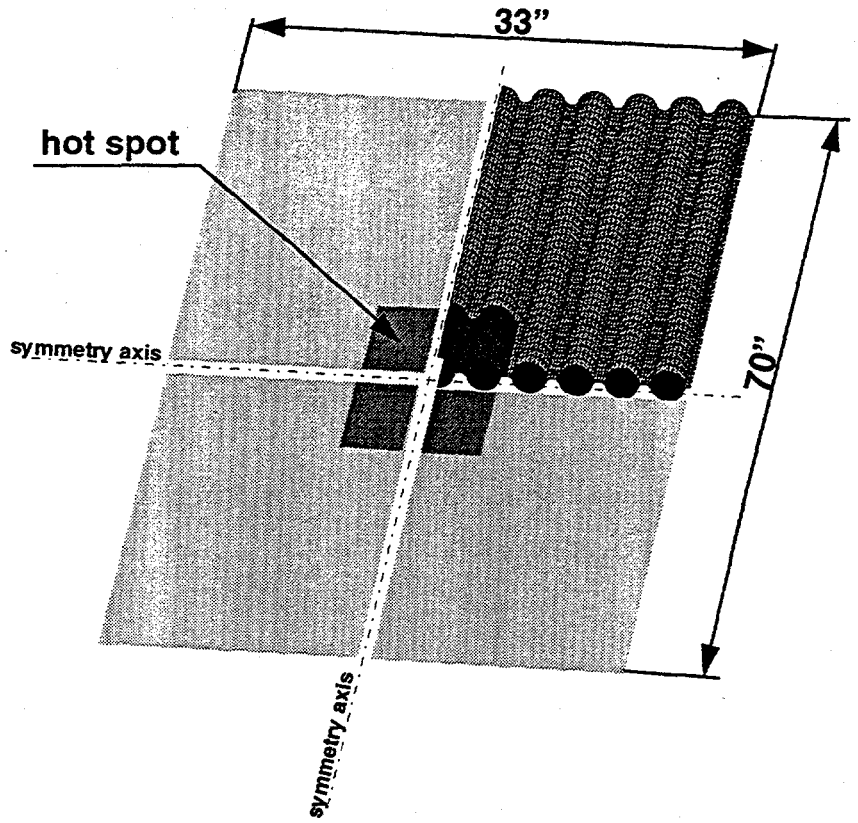

Fig. 12. Three dimensional finite element model of a composite tube panel with a hot spot.

An analysis was performed under the same in-service conditions as previous analyses in order to evaluate the effect of manufacturing residual stresses on the tube in-service stress state. The comparison shows that the manufacturing residual stresses tend to elevate the tensile stresses within the HS location at the fireside tube surface (see Fig. 13).

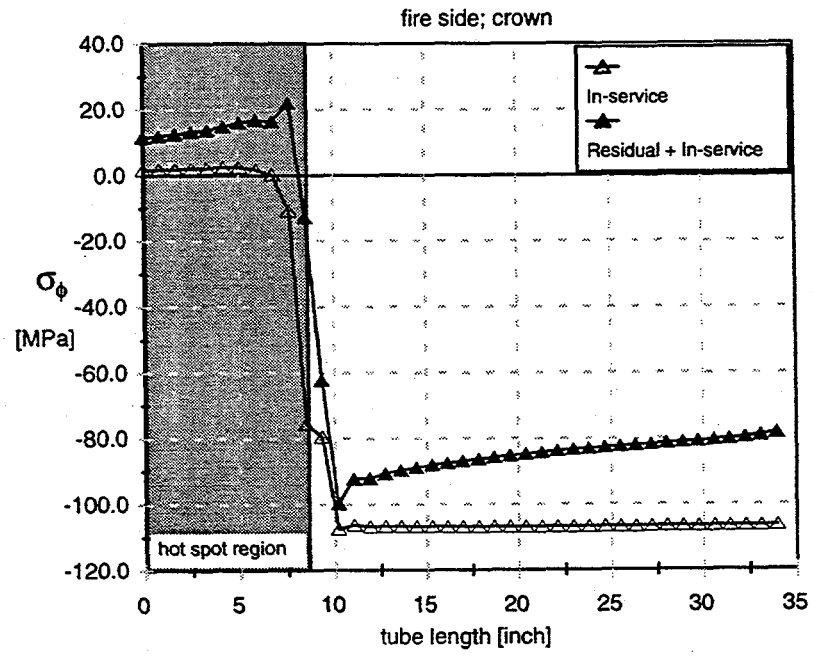

Fig. 13. Manufacturing residual stress effect on hoop stresses at the fireside crown surface along the tube length during the HS for SA210/SS304L composite tube.

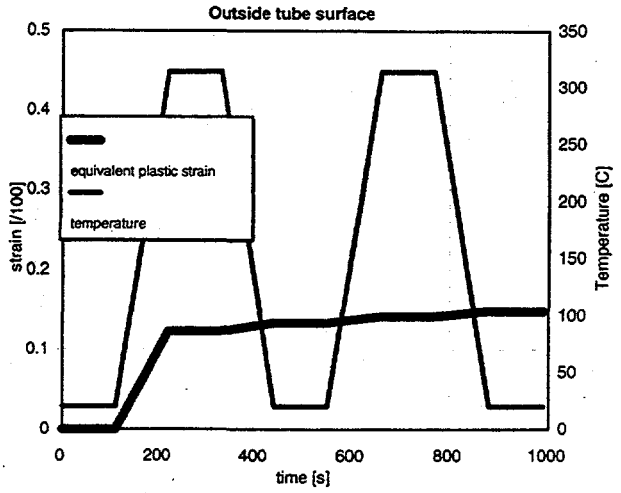

Fig. 14. Temperature and equivalent plastic strain for case 1.

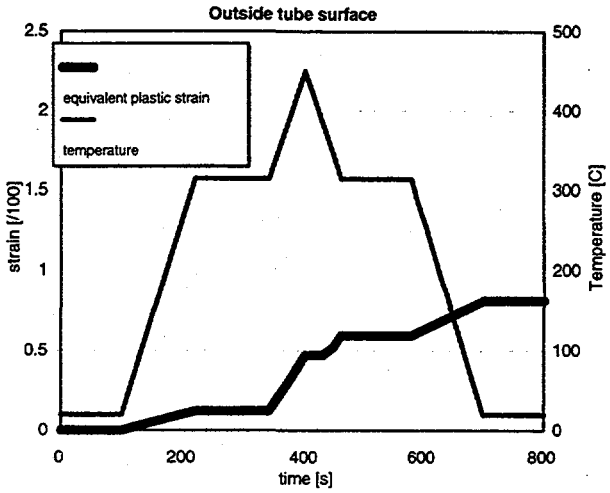

Fig. 15. Temperature and equivalent plastic strain for case 2.

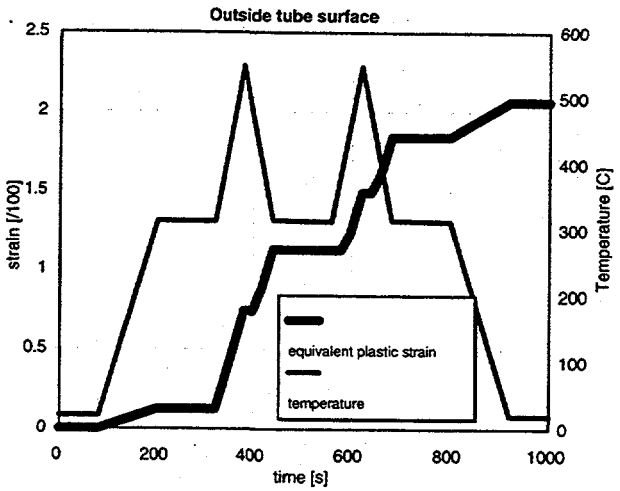

Fig. 16. Temperature and equivalent plastic strain for case 3.

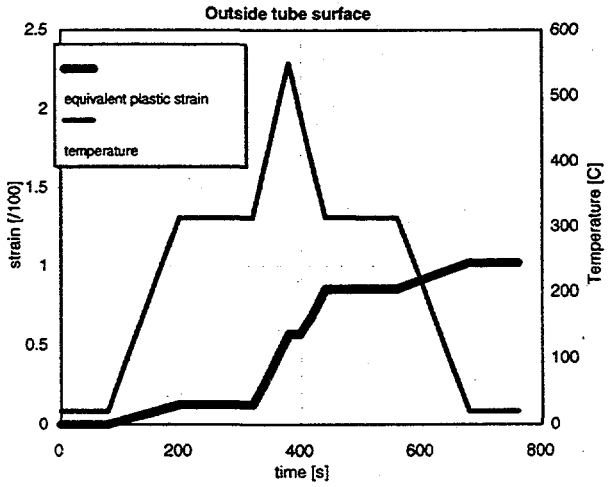

Fig. 17. Temperature and equivalent plastic strain for case 4.

The results of case 4 show that a higher tube temperature, which is due to steam blanketing, causes a pronounced effect of lateral constraint and thus larger deformation and yielding of the carbon steel. The presence of steam blanketing allows higher temperatures at the inside tube surface, which means a lower temperature gradient through the tube thickness. The constraints provided by adjacent tubes cause small tensile hoop stresses at the fireside surface during temperature excursion. Stresses at the 304L overlay are tensile after the temperature excursion and remain tensile during operation. Stresses in this case are lower due to a smaller temperature gradient through the tube thickness.

4.5 Weld overlay analysis

The simulation of the welding process was performed to determine the residual stress state in a spiral overlay tube. This welding process consists of two layers applied in a circumferential

direction. The first layer is made by the automated Gas-Metal-Arc-Welding (GMAW) process with added filler material and the second layer by the Gas-Tungsten-Arc-Welding (GTAW) automated process without the filler metal. The tube is water cooled during welding, and no preheat is applied. The first weld layer is made with a single electrode [diameter 1.14 mm (0.045 in.)] with the step-over of 9.53 mm (3/8 in.), which means the electrode weaving technique is used to achieve the desired weld width. The tube material is SA210 carbon steel, and Alloy 625 and SS309 are the weld materials.

The analysis is uncoupled and is performed in two steps, thermal and mechanical. Because the welds are made in a circumferential direction, an axisymmetric model can be considered. This considerably simplifies the modeling effort, but requires acceptance of some assumptions, which mainly address the effect of thermal processes on the observed section while the electrode travels around the tube. The overall length of the tube model is 500 mm, which is approximately 9 times the length of the weld overlay.

To model the welding arc, a moving heat source of Gaussian shape was applied. The speed of the heat source when it travels across the observed point is equal to the actual electrode travel speed. Six welding passes were simulated in order to obtain a weld of sufficient width and to get an uniform region of residual stresses, which is not affected by the start and end effect of the welding process. After the first layer is finished, the tube is cooled to room temperature, and then the second weld layer is started. After the last (sixth) pass of the second layer is made, the tube is again cooled to room temperature.

To verify the simulation, the residual strains of the SA210 tube with the circumferential weld overlay made of Alloy 625 were measured by the ND technique. The comparison of three elastic strain components (axial, hoop, and radial) was made, and a good agreement is obtained (see Fig. 18). Figures show the strain magnitude along the radial cross section at two different locations (section lines). Section line 1 intersects the tube between the third and the fourth weld pass and section line 2 intersects it in the middle of the fourth pass.

The axial, hoop, and radial residual stresses for the Alloy 625 weld overlay are presented in Fig. 19. The stress pattern for the SS309 weld is very similar except the stress magnitude in the overlay is lower due to the lower strength of 309 stainless steel. The Von Mises stress at the carbon steel interface, at certain weld locations, is below the yield strength. At the same time the plastic deformation is very high at these points. This indicates that substantial plastic yielding occurs during the welding process. In fact, the whole weld region (weld and part of the tube) experiences high yielding. The equivalent plastic strain is higher than 10%.

In the weld overlay, tangential and axial stresses are well above the yield stress. Radial and shear stress components are not significant. The inner surface of the tube experiences high tangential and axial compressive stresses.

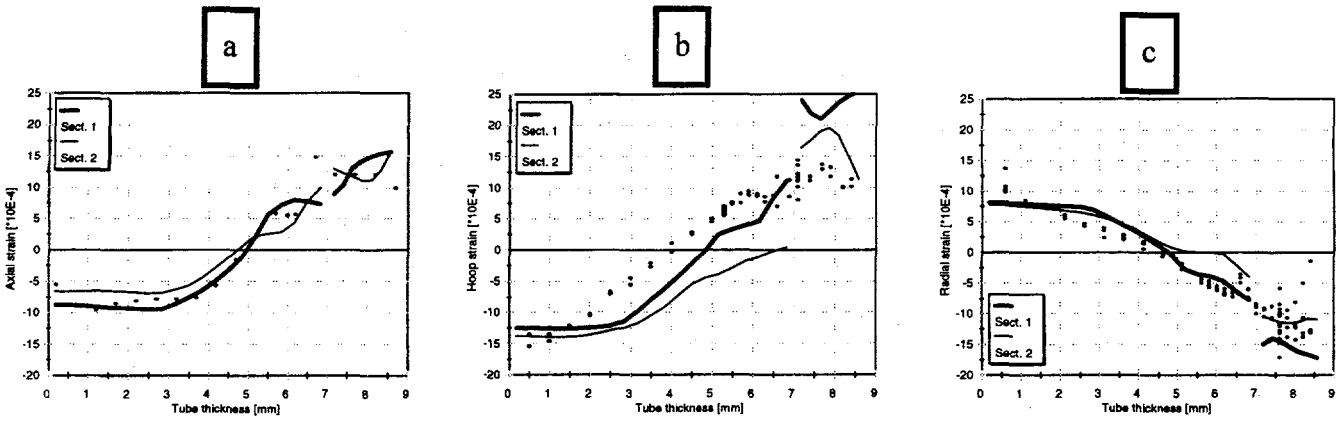

Fig. 18. Comparison of elastic strain components (axial, hoop, radial) measured by neutron diffraction (dots) and calculated by the finite element method (lines) for an Alloy 625 weld overlay on a carbon steel tube.

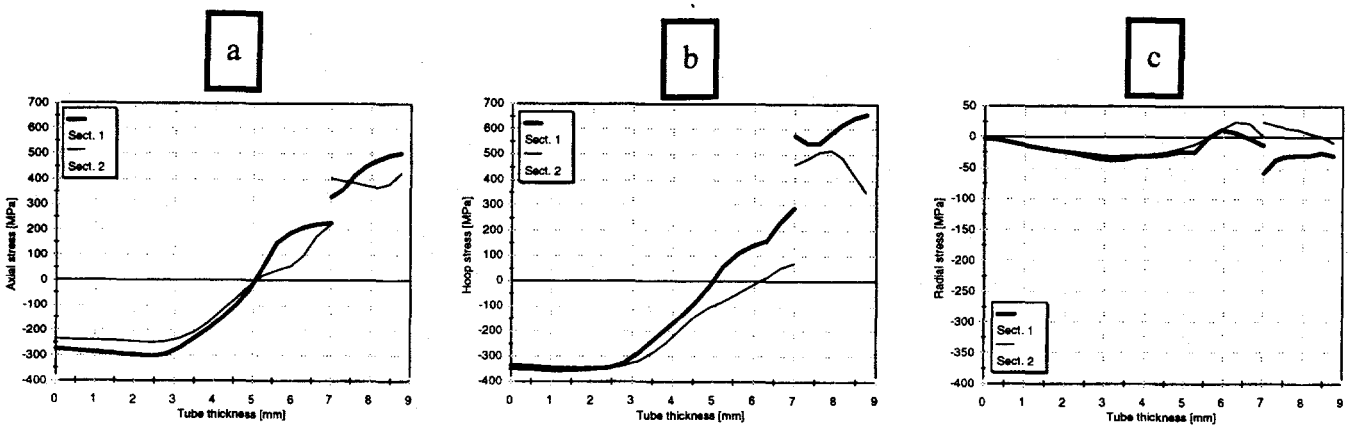

Fig. 19. Residual stress distribution along the radial cross section for an Alloy 625 weld overlay on a carbon steel tube.

4.6 Future work

During the next year, the current 3D model will be refined, and transient analyses will be made for different material combinations. The residual stress state after panel assembly will be calculated assuming weld overlay tubes are used, then the effect of thermal transients on this panel will be calculated.

5. Smelt Corrosion Studies

One consideration in the selection of an alternate material for the outer, corrosion-resistant, layer of composite tubing is the material's resistance to corrosion by molten smelt. Ideally, molten smelt does not contact the composite tubes, but there is strong evidence that smelt does make contact with floor tubes and, especially, smelt spout opening tubes. Consequently, the resistance of alternate materials to corrosion by molten smelt is important to know. In addition, there have been reports from Ahlstrom Corporation (Ref. 2) that the smelt in contact with the floor tubes

contains polysulfides and has a much lower melting point than "typical" smelt. To address the issue of the corrosion resistance of potential cladding materials, corrosion tests of the alternate materials were done using a typical smelt as well as a smelt that contained higher than normal amounts of sulfur and potassium that were introduced as potassium polysulfides. Corrosion rates were determined electrochemically using a custom built polarization cell.

These tests revealed that all the materials tested had corrosion rates greater than 12.7 mm/yr (0.5 in./yr). In the typical smelt, alloy 825 and 304L stainless steel had the lowest rates while several iron-base high-chromium alloys had the greatest resistance to corrosion by the potassium and sulfur-rich smelt mixture.

6. Stress Corrosion Testing

Laboratory tests to identify environments which might cause SCC of 304L stainless steel in kraft recovery boiler service were carried out using U-bend specimens made from 3 mm thick strips with dimensions 92 mm long by 9 mm wide, in accordance with the standard method described in ASTM designation G30-90. For these preliminary tests, simple mixtures were made from the solid constituent salts and placed into either a carbon steel or ceramic crucible and the U-bend specimen was then embedded into the salt mixture. In the case of Na_2S, the salt added was the nona-hydrated version, although all calculations for the proportion added were based on the non-hydrated salt. No rigorous attempts were made to homogenize the mixtures prior to heating. The test crucibles were placed into a furnace, and brought rapidly to the test temperature. Unless otherwise stated, the test temperature in each case exceeded the expected melting point of the salt mixture.

The first tests were carried out in a simulated smelt composed of Na_2CO_3, Na_2S, Na_2SO_4 and NaCl. No cracks were detected after exposures up to 65 hours at 550-650°C.

The second series of tests was carried out in mixtures of NaOH and Na_2S at 350°C. Cracking took place in 17-hour tests when the salt mixtures contained 10%, 25%, 50% and 75% Na_2S. Cracking also occurred with 50% Na_2S at 300 and 250°C. No cracking was observed in molten NaOH at 350°C, which suggests that Na_2S is a necessary agent for SCC. Na_2S by itself also did not cause cracking at 350°C, but at this temperature no liquid phase is present. By reducing the temperature to 160°C (the boiling point of $Na_2S{\cdot}9H_20$) it proved possible to induce cracking in one test specimen, although further tests at 150-160°C could not reproduce this cracking.

In order to make the composition of the test environment more typical of a recovery boiler smelt, 50% Na_2CO_3 was added to the Na_2S. Cracking was produced by slowly heating a specimen to 250°C (12h ramp, 36h soak). In a following experiment, it was found that cracking could be accelerated by repeatedly dripping water onto a 50/50 Na_2S/Na_2CO_3 mixture at 200°C, and it was concluded that the cracking takes place near the boiling point of $Na_2S{\cdot}9H_20$. The same procedure was used to initiate small cracks in Alloy 825; however, this material shows significantly greater resistance than 304L. A similar test using a carbon steel U-bend produced no evidence of cracking.

In many of the tests where cracking occurred, one or more cracks nearly penetrated through the thickness of the U-bend. Due to the many different experimental procedures employed in these preliminary tests, a direct comparison of crack penetration rates across the range of tests is not possible, but there is a clear indication that crack velocities can be extremely rapid. The most intriguing results were those obtained in the aqueous solutions of Na_2S and Na_2CO_3 at temperatures below 200°C. These conditions approximate those expected during the cool-down and heat-up periods to which the boiler is subjected when it is removed from service for water washing or maintenance.

Preliminary testing has identified an environment which is likely to cause SCC of 304L co-extruded tubes in recovery boilers. Further testing will be conducted in this and similar environments using specimen geometries which offer more control over crack initiation and propagation than U-bends. In a separate effort, data on tube temperatures and wash water composition will be collected from boilers during shut-downs and start-ups, and these will be used to modify the test environments to correspond more closely to actual conditions.

7. Thermal Fatigue Studies of Composite Tubes

The activity on thermal fatigue of composite tubes involves a review of thermal/mechanical fatigue in composite tube materials, the compilation and production of the physical and mechanical properties needed for the modeling, the isothermal and thermal/mechanical fatigue of tubes, and the determination of cracking patterns for various thermal/mechanical loadings. Materials of concern include carbon steel (equivalent to SA-210, Gr A-1), 304L stainless steel, Fe-Cr-Ni alloy 825, nickel-base alloy 625, 309L stainless steel filler metal, and 312 stainless steel filler metal.

7.1 Review of thermal/mechanical fatigue in composite tube materials

A review, completed during 1995 (ref. 3), reached nine conclusions that bear on the experimental and analytical work:
(1) the physical and mechanical properties were needed for 309L and 312 stainless steel filler metals;
(2) tensile curves were needed for very-fine-grained 304L stainless steel;
(3) exploratory fatigue data to 600°C were needed for very-fine-grained 304L stainless steel, 309L deposited filler metal, 312 stainless steel deposited filler metal, alloy 625, and alloy 825;
(4) the isothermal fatigue curves constructed following the procedures of ASTM E606 were required;
(5) exploratory thermal-mechanical fatigue data were needed for alloy 825, alloy 625, 312 stainless steel and 309L stainless steel;
(6) fatigue damage under multiaxial strains should be evaluated using the equivalent strain approach recommended in the ASME Code Section III;
(7) fatigue crack growth testing was not required;
(8) the constitutive equations recommended in DOE RDT F9-5T (ref. 4) were suitable for use in elastic plastic analysis of composite tubes; and
(9) thermal fatigue testing of tubing was needed to confirm the validity of the analysis methods.

In this reporting period, the physical properties were determined for 309 stainless steel and 312 stainless steel in the weld-deposited condition. Properties included the thermal expansion, specific heat, and thermal diffusivity. The 312 stainless steel, containing as much as 40% ferrite, exhibited characteristics typical of ferritic steel. The characteristics included a lower thermal expansion and a detectable Curie point in the specific heat versus temperature trend.

Exploratory tensile tests were performed on weld-deposited 309 and 312 stainless steels. Figures 20 and 21 compare the tensile yield and ultimate strengths of the weld metals with wrought metal properties. The 309 stainless steel weld metal was found to possess higher yield strength and lower tensile strength than the wrought metal whose properties have been used in the modeling studies. The 312 stainless steel weld metal was found to have a yield strength similar to that assumed in the modeling efforts.

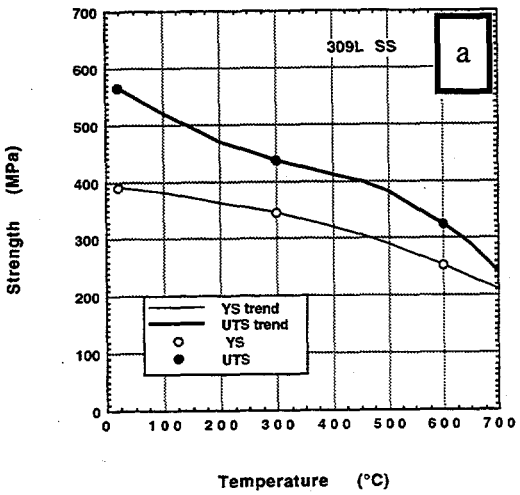

Fig. 20. Yield and ultimate strengths for type 309L stainless steel wrought and weld metal.

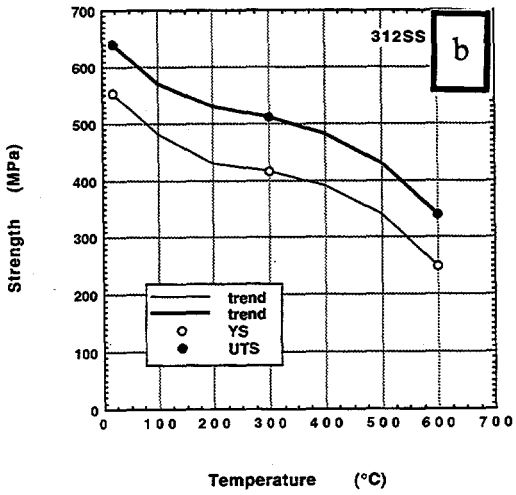

Fig. 21. Yield and ultimate strength for Type 312 stainless steel weld metal.

7.2 Mechanical Properties of Fine-Grained 304L Stainless Steel

Tensile yield curves for very-fine-grained 304L stainless steel were produced for the temperature range of room to 600°C. These stress versus strain curves to 2% strain have been reproduced in Fig. 22. Important to the analysis of inelastic behavior were the observations that the yield strength of the annealed material was well-defined, the yield decreased monotonically with increasing temperature, and the rate of work-hardening was independent of temperature. These observations confirmed the behavioral trends specified for 304H stainless steels and embodied in the constitutive equations recommended in DOE RDT F9-5T for inelastic analysis.

Isothermal and restrained thermal-cycling experiments were performed on very-fine-grained type 304L stainless steel to examine hardening behavior and cracking patterns. The yield curves during the first quarter-cycle of isothermal cyclic tests were identical to the tensile yield behavior shown in Fig. 23, but the well-known Bauschinger effect dominated cyclic behavior from the first load

reversal onward. Here, the small-strain offset yield exhibited kinematic behavior, and the yield strength upon reversal of loading was less (in absolute value) than the flow stress at the time of stress reversal. Cycle-to-cycle work hardening continued for isothermal tests at 316 and 600°C (600 and 1112°F).

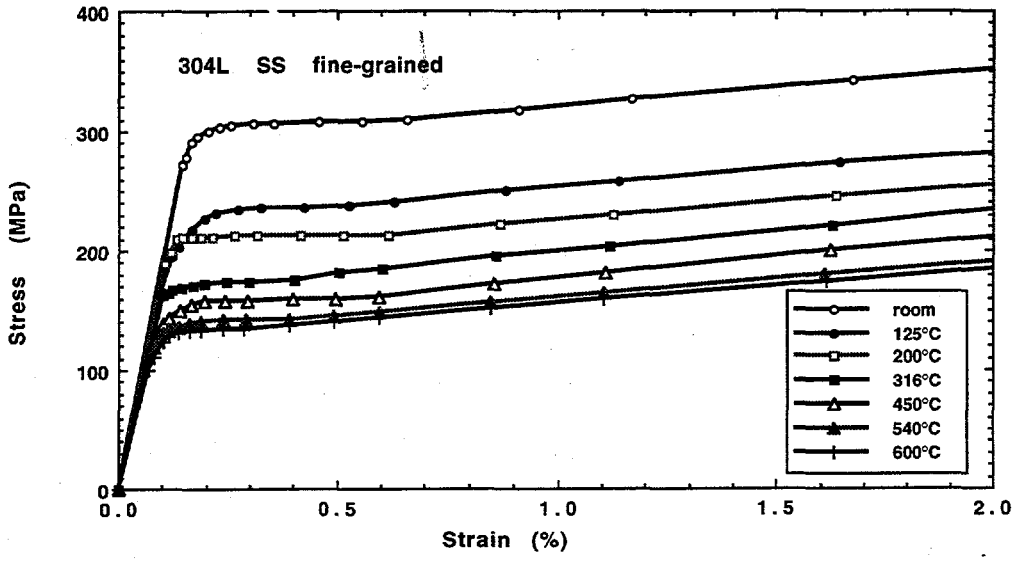

Fig. 22. Stress versus strain for fine-grained 304L stainless steel.

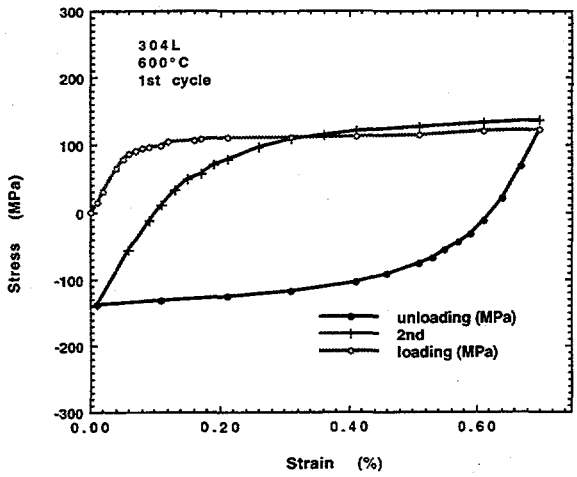

Fig. 23. Stress versus strain during the first cycle on an isothermal test at 600°C.

The first quarter-cycle of restrained thermal cycling produced a curve that was similar to the isothermal tests. The yield strength was well-defined, and the combination work hardening plus the temperature-dependent decrease in flow stress produced a flat tensile flow curve. Upon reversal from heating to cooling, the Bauschinger effect was observed. Cycle-to-cycle hardening was observed. It was found that hardening was greater under thermal cycling conditions than under isothermal cycling.

7.3 Cracking patterns and microstructure in fatigue

Since the review report showed that the fatigue damage rate in 304L stainless steel increases with increasing temperature and time at the peak temperature, it was speculated that a few hundred cycles in which the cladding surface reached 600°C could produce significant damage if the time at 600°C lasted a few tenths of an hour during each cycle. The accumulated time at the high temperature would not exceed one hundred hours. There would be no metallurgical deterioration of the pearlite in the carbon steel which would remain cooler than 600°C and be exposed for less than 100 hours. To explore this possiblity, two types of experiments were undertaken. In the first, composite tube specimens were aged at 545°C (1013°F) and 478°C (892°F), then examined metallographically. Results for specimens aged at 545°C (1013°F) are shown in Fig. 24. A clear indication of high- temperature exposure was observed at the 304L/carbon steel interface. Carbide precipitates formed at the interface after a few hours and carbide precipitates in the 304L stainless steel could be observed after 18 hours. No such precipitates were found in service exposed tubes.

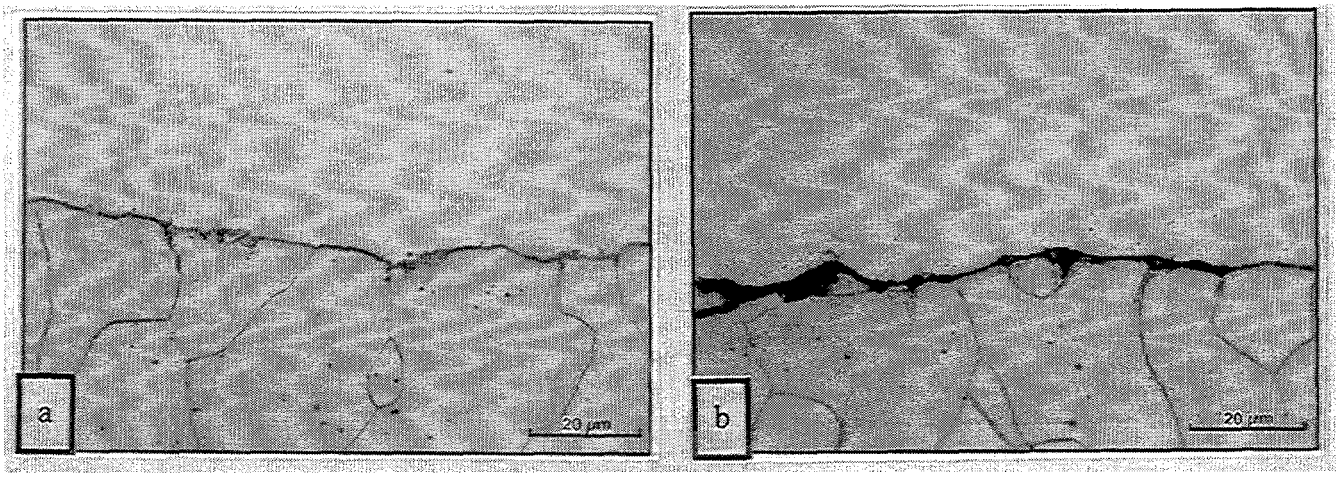

Fig. 24. Microstructure of the interface on a composite tube: a) as-received tube showing an interface nearly free of precipitates and no carbides in the stainless steel; b) aged tube (19 hours at 545°C) showing carbides on the interface and in the stainless steel.

Hold-time fatigue tests at 600°C will be undertaken on 304L stainless steel to produce fatigue cracking patterns for comparison to cladding crack patterns. Photomicrographs of the cracking are shown in Fig. 25. Similar to the composite tubes, all cracks in the stainless steel were transgranular. Also, the cracks exhibited branching. However, the branching in fatigued specimens was not as extensive as observed in the composite tubes.

7.4 Composite tube and panel testing

The radiant lamp heating system to be used for thermal-cycling of composite tubes and panels was installed. Check-out testing was completed with a single lamp heating set-up in preparation for planned studies.

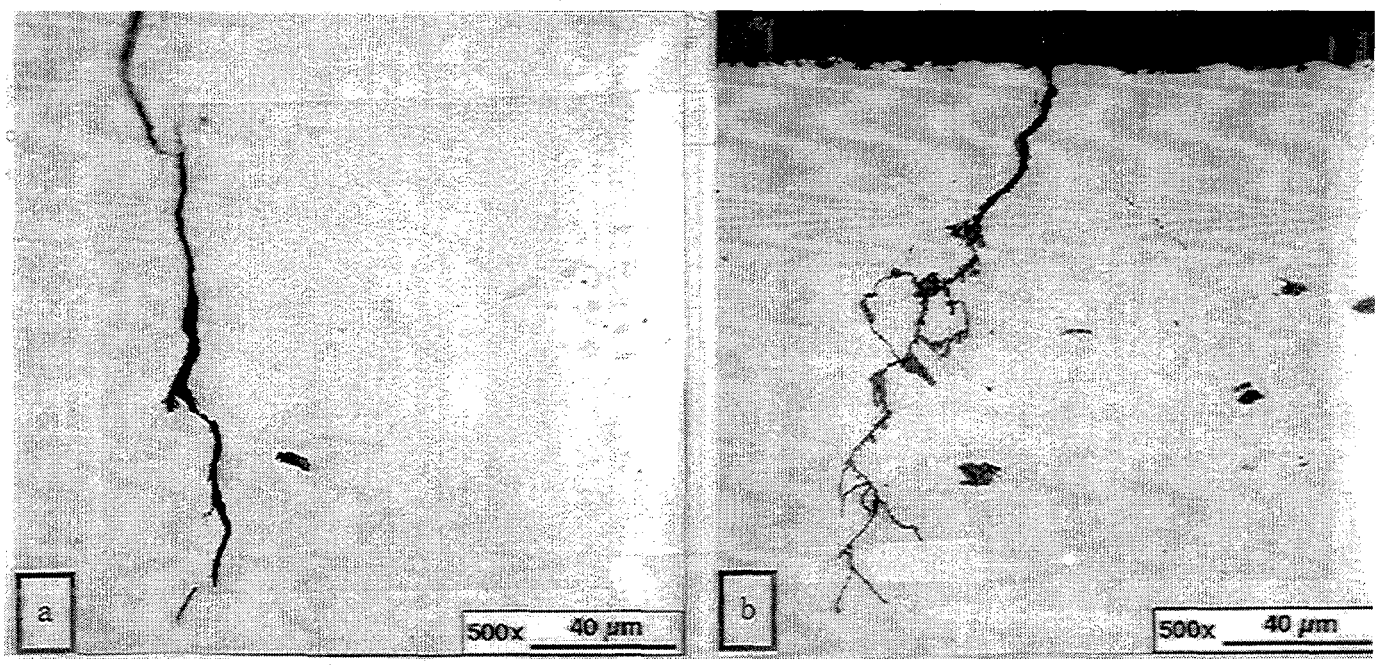

Fig. 25. Fatigue cracking patterns in 304L stainless steel produced by 730 cycles near 1% strain range and 600°C: a) material annealed at 925°C; b) material cold worked 50% by rolling.

References:

1. D.L. Singbeil, R. Prescott, J.R. Keiser, and R.W. Swindeman, Composite Tube Cracking in Kraft Recovery Boilers, Oak Ridge National Laboratory Draft TM-Report (August 1996).

2. J.R. Keiser, ORNL Foreign Trip Report, ORNL/FTR-5619, October 31, 1995.

3. R.W. Swindeman, A Review of Thermal/Mechanical Fatigue in Composite Tube Materials, Oak Ridge National Laboratory Draft TM-Report (August 1996).

4. RDT Standard F9-5T, *Guidelines and Procedures for Design of Nuclear System Components at Elevated Temperature* (September 1974).

SECTION 2: CORROSION AND FAILURE ANALYSIS STUDIES IN SUPPORT OF THE PULP AND PAPER INDUSTRY

J.R. Keiser, S.J. Pawel, R.W. Swindeman and H.F. Longmire

Metals and Ceramics Division
Oak Ridge National Laboratory
P.O. Box 2008
Oak Ridge, TN 37831

INTRODUCTION

Technical support is being provided to various pulp and paper companies and related industries to help determine the cause of material degradation problems and to identify alternate materials to prevent such degradation. During the past year, examinations have included parts from several sootblowers, two failed economizer tubes, and inspection of a continuous digester. The results of the analyses and inspections were communicated to the plant operators, and, in some cases, recommendations were made.

TECHNICAL PROGRESS - FY 1996

Examination of Sootblower Nozzles

Several sootblower nozzles that experienced cracking were examined to characterize the nature of the cracking and to determine the cause and a means to prevent cracking of other nozzles in the future. The tip of one of the nozzles examined apparently had small pieces fall off, and there was considerable cracking on the side of the nozzle in an area between the steam outlets (see Fig. 26). Metallographic samples were prepared from both the side and the tip of this nozzle, and examination of the sample from the side of the nozzle showed that the cracking was totally intergranular in nature, as shown in Fig. 27, and almost all of the cracks originated on the outside surface of the nozzle.

Since intergranular attack is frequently associated with a sensitized microstructure, a sample was electrolytically etched with oxalic acid to check for evidence of sensitization. This test showed that the sample had chromium carbide precipitates along the grain boundaries causing the sample to be sensitized and thus vulnerable to grain boundary attack. In order to determine if polythionic acid might be the cause of this cracking, an electron microprobe examination was conducted on two samples to determine if sulfur were present in the grain boundaries. The examination showed significant oxygen but very little sulfur present in the grain boundaries.

Ni_3Al TECHNOLOGY TRANSFER

V. K. Sikka, S. Viswanathan, M. L. Santella, R. W. Swindeman and G.A. Aramayo*

Metals and Ceramics Division
*Engineering Division
Oak Ridge National Laboratory
P. O. Box 2008
Oak Ridge, Tennessee 37831

INTRODUCTION

Ductile Ni_3Al and Ni_3Al-based alloys have been identified for a range of applications. These applications require the use of material in a variety of product forms such as sheet, plate, bar, wire, tubing, piping, and castings. Although significant progress has been made in the melting, casting, and near-net-shape forming of nickel aluminides, some issues still remain. These include the need for: (1) high-strength castable composition for many applications that have been identified; (2) castability (mold type, fluidity, hot-shortness, porosity, etc.; (3) weld reparability of castings; and (4) workability of cast or powder metallurgy product to sheet, bar, and wire.

The four issues listed above can be "show stoppers" for the commercial application of nickel aluminides. This report describes the work completed to address some of these issues during FY 1996.

TECHNICAL PROGRESS - FY 1996

Summary

Major accomplishments have occurred during this year and are briefly described below.

1. The cast compositions were licensed to United Defense LP for commercial production.
2. The Exo-Melt™ process for air melting of Ni3Al-based alloys was transferred to United Defense LP (Anniston, Alabama), Alloy Engineering & Casting Company (Champaign, Illinois), and Sandusky International (Sandusky, Ohio).
3. Castings of the cast alloy IC-221M were installed or continued to operate under commercial conditions at Delphi Saginaw (Saginaw, Michigan), Bethlehem Steel (Chesterton, Indiana), United Defense LP, The Timken Company (Canton, Ohio), and Chevron (Richmond, California).
4. Two new rolls were cast at Sandusky International.
5. Base-metal composition of cast alloy IC-221M was modified for weldability.
6. Weld design and procedures were developed for butt welds in rings of large-diameter pipe.
7. Weld process was also developed for a dissimilar metal weld between ring of nickel aluminide and alloy 800 H.
8. Test material was supplied to many potential users for evaluation under their operating conditions.

9. Foundries were assisted with development of on-line chemical analysis standards. Nearly 100,000 lb of the Ni_3Al-based alloy IC-221M were cast under production conditions.
10. Strong efforts continued for technology transfer of Ni_3Al-based alloys.

1. High-Strength Castable Compositions. Start 10/95 End 9/96

The Ni_3Al-based compositions compete strongly with commercially available nickel-and iron-based alloys. The chemical compositions of Ni_3Al-based alloys and commercial alloys are shown in Table 1. The density and melting point of the Ni_3Al-based alloys are compared with the competitive alloys in Table 2. Similar comparisons for thermal expansion, thermal conductivity and modules are presented in Tables 3 and 4. The comparative yield strength of Ni_3Al-based alloys with commercial alloys is shown in Fig. 1. The physical properties and yield strength data can be used to calculate the thermal stress resistance factor R' for all competitive alloys:

(1)

$$R' = k\,(ys)(1-\upsilon)/\alpha\,E$$

where

k = thermal conductivity,
ys = yield strength,
υ = Poisson's ratio,
α = thermal expansion coefficient,
E = modules.

By assuming Poisson's ratio value of 0.3 for all alloys and using values of various properties from Tables 3 and 4 and Fig. 1, the calculated values of R' are summarized in Table 5. Data in this table show that the cast Ni_3Al-based alloy IC-221M has a factor of three better thermal stress resistance than the competitive alloys.

The factor of three improvement in thermal resistance adds to other attributes of Ni_3Al-based alloys of oxidation resistance, carburization resistance, chlorine resistance, and high-temperature strength. These attributes make Ni_3Al-based cast alloy IC-221M suitable for the following applications:

1. Trays and fixtures for carburizing furnaces.
2. Trays and fixtures for oxidizing heat-treating furnaces.
3. Grate bars and tips for calcination furnaces.
4. Hot-forging and extrusion dies.
5. Furnace support structures for steel manufacturing.
6. Tube hangers for oil industry applications.
7. Transfer rolls for steel applications.
8. Radiant burner tubes for heating and controlling furnace temperature.
9. Roll guides for furnace applications.
10. Mixing spokes for ceramic slurries.
11. Nuts and bolts for corrosive environment applications at high temperatures.

Element	Alloy, weight percent								
	IC-50[a]	IC-396M[b]	IC-221M[c]	Haynes 214[d]	HU[e]	Alloy 800[d]	MORE 1	MORE 2	SUPERTHERM[f]
Al	11.3	7.98	8.0	4.5	–	0.4	–	0.75-1.50	–
Cr	–	7.72	7.7	16.0	18.0	21.0	25.0-28.0	32.0-34.0	26.0
Mo	–	3.02	1.43	–	–	–	–	–	–
Zr	0.6	0.85	1.7	–	–	–	–	–	–
B	0.02	0.005	0.008	–	–	–	–	–	–
C	–	–	–	0.03	0.55	0.05	0.40-0.50	0.15-0.25	0.5
Fe	–	–	–	3	42.45	45.5	–	–	16.2
Ti	–	–	–	–	–	0.4	–	–	–
Ni	88.08	80.42	81.1	76.35	39.0	32.5	35.0-38.0	48.0-52.0	35.0
Si	–	–	–	0.1	–	–	–	–	1.6
Y	–	–	–	0.02	–	–	–	–	–
W	–	–	–	–	–	–	1.25-2.00	15.0-17.0	5.0
Co	–	–	–	–	–	–	–	–	15.0
Mn	–	–	–	–	–	–	–	–	0.70

[a]Cold workable.
[b]Castable alloy for static applications (some microporosity).
[c]Castable alloy for dynamic application (minimum microporosity).
[d]Wrought alloy.
[e]Cast alloy.
[f]SUPERTHERM is a registered trademark of Abex Corporation.

Table 1. Chemical composition of Ni_3Al-based alloys and commercially available competing alloys

Alloy	Density		Melting temperature	
	lb/in.^{3}	g/cm^3	°F	°C
IC-221M	0.284	7.86	2140[a] to 2467	1171[a] to 1353
IC-218LZr	0.281	7.77	2529[b]	1387
IC-50	0.275	7.60	2543	1395
Alloy 800	0.287	7.94	2475 to 2525	1357 to 1385
HU	0.290	8.02	2450	1343
SUPERTHERM™	0.297	8.22	–	–

[a]Eutectic temperature.
[b]No eutectic formation.

Table 2. Density and melting point of Ni_3Al-based alloys as compared to commercial alloys.

Most of the applications of Ni_3A1-based alloys fit into vision industry categories such as: (1) casting, (2) heat treating, (3) steel, (4) petroleum products, and (5) chemical.

The Exo-Melt™ process details were transferred to United Defense LP, Alloy Engineering and Casting Company, and Sandusky International. Using the Exo-Melt™ process, each of the companies has melt and cast components for commercial applications. The component operating experience under commercial conditions is listed below for each application.

Transfer Rolls at Bethlehem Steel Corporation - Two transfer rolls have been operating at Bethlehem Steel Corporation for over two years and three months. The roll operation is so great that Bethlehem Steel is actively pursuing the installation of 30 additional rolls in their furnace during 1997. A ring from the currently used roll material has been received at the Oak Ridge National Laboratory (ORNL) to determine the cause(s) for blister formation. This analysis is currently in progress.

Heat-treating Trays and Fixtures at Delphi Saginaw - Two carburizing furnace assemblies have been operating in the pusher furnace at Delphi Saginaw since January 1996. One assembly is operating in the as-cast condition, and the other one in then preoxidized condition. At the time of this writing, both assemblies will be removed from the furnace for photographing and dimensional change measurement in January 1997 after one year of operation.

Five sets of batch furnace trays were prepared and shipped to Delphi Saginaw. One of the sets consisted of one each as-cast and preoxidized trays of IC-221M. Two sets consisted of as-cast IC-221M with HT trays supplied by Delphi Saginaw. Two additional sets consisted of preoxidized IC-221M with HT trays. All of the five sets are expected to go into service in batch furnaces at Delphi Saginaw during the early part if 1997.

Temperature (°C)	Alloy					
	IC-221M		HU		SUPERTHERM™	
	Mean coefficient of expansion (10^{-6}/°C)[a]	Thermal conductivity (w/m·k)	Mean coefficient of expansion (10^{-6}/°C)[b]	Thermal conductivity (w/m·k)	Mean coefficient of expansion (10^{-6}/°C)	Thermal conductivity (w/m·k)
100	12.77	11.9	17.28[b]	4.04	18.36[c]	4.10
200	13.08	13.9		4.62		4.73
300	13.40	15.2		5.08		5.26
400	13.72	16.7		5.54		5.78
500	14.01	18.0		5.95		6.35
600	14.33	20.3		6.58		6.93
700	14.72	23.0		7.16		7.51
800	15.17	25.2		7.62		8.09
900	15.78	27.5[d]		8.32		8.66
1000	16.57	30.2[d]		8.95		9.12

[a]Room temperature to specified temperature.
[b]Room temperature to 982°C.
[c]Room temperature to 1204°C.
[d]Extrapolated from data up to 800°C.

Table 3. Thermal expansion and thermal conductivity of cast IC-221M and cast competitive alloys

Temperature (°C)	Young's Modulus (GPa)					
	Alloy					
	IC-221M[a]	IC-218LZr[a]	IC-50[a]	Alloy 800	HU	SUPERTHERM™
20	200.0	225.0	203.5	196.5	186.2	178.5
150	195.0	223.0	198.0	188.0	–	*b*
300	184.0	218.0	–	178.3	–	*b*
500	163.0	206.5	178.0	171.6	–	*b*
700	157.0	193.5	162.5	150.1	–	133.8
900	139.0	–	136.0	*b*	–	112.4
1100	114.0	170.0	127.0	*b*	–	89.6

[a]Determined by Dynamic method.
[b]Data not available.

Table 4. Elastic modulus of Ni3Al-based alloys and competitive alloys

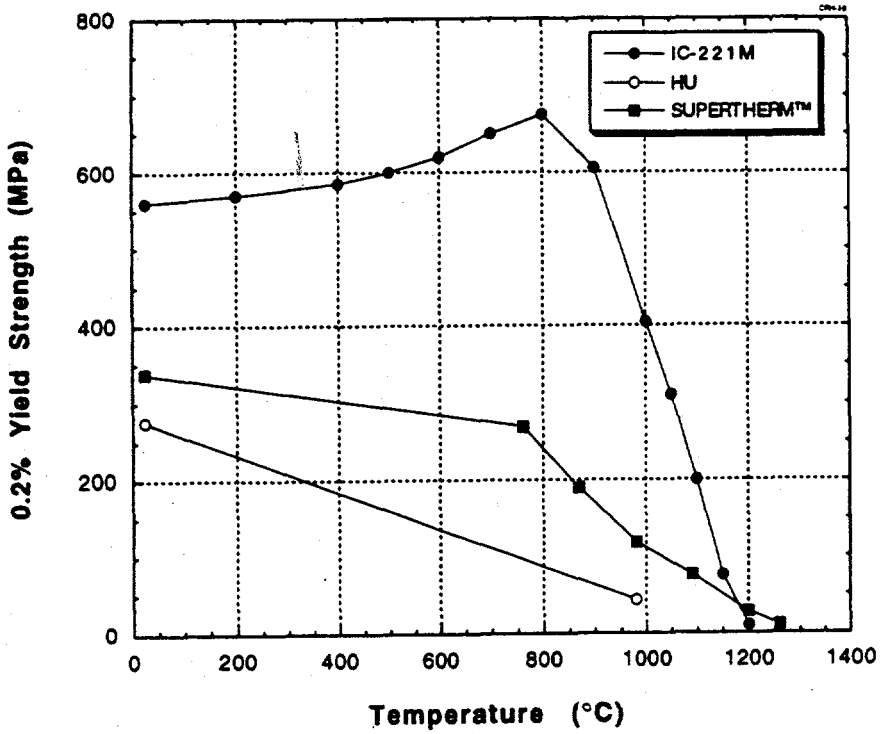

Fig. 1. Comparative yield strength of Ni_3Al-based alloys with commercial alloys.

Alloy	Thermal stress resistance factor R' (w/m)
IC-221M	4034
HU	1208
SUPERTHERM™	1246

Table 5. Calculated values of thermal stress resistance factor for IC-221M and competitive alloys HU and SUPERTHERM™.

Heat-treating Trays at The Timken Company - The heat-treating trays of IC-221M have been operating in the pit carburizing furnace at The Timken company as of March 1, 1996. As of the end of September 1996, the IC-221M trays are operating without any obvious change.

Heat-treating Trays at United Defense LP - The heat-treating of IC-221M have been operating in the air heat-treating furnace at United Defense LP for nearly one year. During the same period, the currently used HU alloy trays have already been replaced twice.

Forging Dies at United Defense LP - A forging die of IC-221M has been in operation for nearly one year. The die has already been used for forging 100,000 components. This performance is nearly ten times that of the current die material, which is discarded after 10,000 forged components.

A second die set with extremely complex parts operated for 7500 parts as opposed to only 1500 parts for the conventional die. Although this die had to be taken out of service because of crack development, it still operated five times longer than that of the current die material.

2. Castability of Nickel Aluminides, Start 10/95, End 9/96

Work under this task deals with optimizing the melting process, composition control, and modeling of solidification behavior. Significant progress continued in the following areas:

Exo-Melt™ Progress - This process has become a standard melting process at United Defense LP, Sandusky International, and Alloy Engineering & Casting Company. Effort is now extending to using the process for melting the revert stock, which continues to build up as more and more nickel-aluminide components are produced.

On-line chemical analysis is an essential part of being able to produce IC-221M of correct composition. This is absolutely important for melts produced by using the revert stock. ORNL provided a large number of standards to all three producers to develop online capability. These capabilities now exist at United Defense LP, Alloy Engineering & Casting Company, and Sandusky International.

Sensitivity Analysis of thermophysical Properties - Thermophysical properties for IC-221M had been previously determined at the facilities of the High Temperature Materials Laboratory at ORNL.

During this reporting period, a procedure was developed to determine the density by high-temperature dilatometry. A dual push-rod differential dilatometer equipped with a thermally isolated linear displacement transducer was used to accurately measure displacement as a function of temperature. For density measurements, the dilatometer was operated in a single push-rod configuration outfitted with a special precision ground alumina tube and end caps which contained the alloy sample during melting (see Fig. 2). The alloy specimen was then heated to 1500°C and cooled to below its solidification temperature (1160°C). The change in length was measured and multiplied by the cross-sectional area of the specimen to determine the volume change during solidification, after compensating for the thermal expansion of the specimen container and the system. The density was calculated over this temperature range from the mass and volume of the

specimen. Table 6 lists the nominal composition of the alloy. Table 7 lists the measured density as a function of temperature for IC-221M alloy. Figure 3 shows the variation of density with temperature for IC-221M alloy.

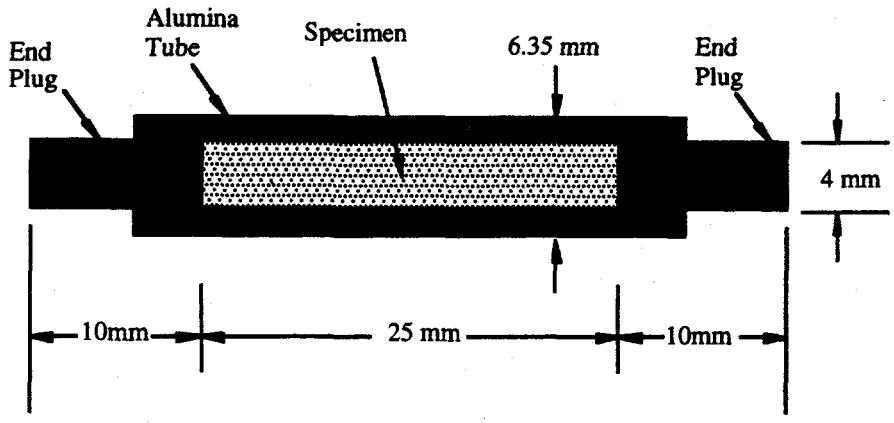

Fig. 2. Schematic of modified push-rod arrangement used for density measurement by dilatometry.

Element	Weight percent
Ni	81.15
Al	7.98
Cr	7.74
Mo	1.43
Zr	1.70
B	0.008

Table 6. Nominal composition of IC-221M alloy

Temperature (°C)	Density (g/cc)
0.0	7.825
400.0	7.725
800.0	7.575
1000.0	7.475
1160.0	7.370 - Solidus
1300.0	7.225
1325.0	7.200
1350.0	7.100
1366.4	6.950 - Liquidus
1700.0	6.760

Table 7. Measured values of density for IC-221M alloy.

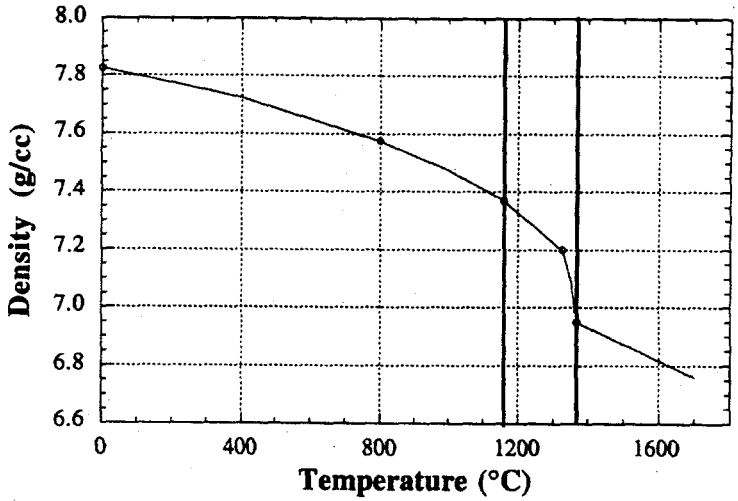

Fig. 3. Measured variation of density of IC-221M alloy with temperature.

Although accurate thermophysical properties are important for obtaining accurate results, the use of temperature-dependent thermophysical properties imposes a penalty in terms of computing time, since additional computational or even nonlinearity is introduced into the problem. Consequently, it is useful to estimate the sensitivity of the calculated temperatures on the various thermophysical properties. Accordingly, results obtained using temperature-dependent properties were compared to results obtained when constant properties were used.

Table 8 lists the various conditions investigated. The column on the left side lists the conditions for the control simulation using temperature-dependent properties, comprising a single run. The column on the right lists the various conditions investigated for constant properties, comprising multiple runs. The effect of doubling the mesh size (course mesh spacing) on the calculated temperatures was also included, as there is often a tendency to use large mesh sizes in industry in an effort to limit the size of the problem. For each condition listed, all the other parameters were maintained the same as the control simulation.

It is clear from Figs. 4 and 5 that some thermophysical properties have a more drastic effect on the simulation than others. However, in general, the use of constant properties introduces significant than others. However, in general, the use of constant properties introduces significant errors in the calculation. The largest deviation was obtained when the room-temperature value of specific heat capacity of the metal was used instead of temperature-dependent properties. This effect may well be alloy-dependent, and in the present case be due to the fact that the specific heat capacity of IC-21M alloy at the solidus temperature is double that at room temperature. If constant metal properties must be used, a value corresponding to that at the solidus temperature introduces the smallest errors, since the temperature range of interest for solidification problems is near the solidus temperature and above. Interestingly, values that are usually known with the least amount of certainty, such as the density of the alloy and thermophysical properties of the sand, contribute to large errors. The use of a coarse mesh spacing also introduces significant errors. It is also well known that another

Control simulation	Sensitivity study
$K = f(T)$	$K = K_{RT}$ or K_{TS}
$\rho = f(T)$	$\rho = \rho_{RT}$ or ρ_{TS}
$C_p = f(T)$	$C_p = C_{P,RT}$ or $C_{P,TS}$
$K_{SAND} = f(T)$	$K_{SAND} = K_{SAND,RT}$
$C_{P,SAND} = f(T)$	$C_{P,SAND} = C_{P,SAND,RT}$
Mesh spacing fine	Mesh spacing coarse

K = Thermal conductivity.
ρ = Density.
C_p = Specific heat.
RT = Room-temperature value.
TS = Solidus-temperature value.

Table 8. Variations in thermophysical properties considered in sensitivity study.

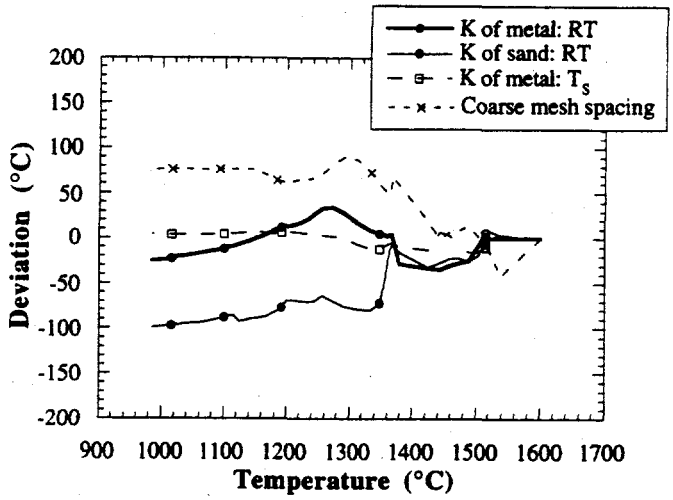

Fig. 4. Deviation for thermocouple 1 between the control simulation and sensitivity study when constant value of thermal conductivity is assumed for the metal or sand or when a coarse mesh spacing is used.

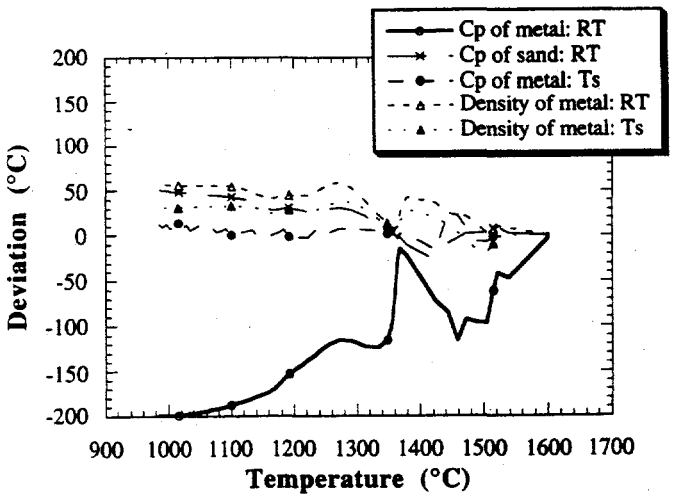

Fig. 5. Deviation for thermocouple 1 between the control simulation and sensitivity study when a constant value of density or specific heat capacity is assumed for the metal or sand.

property that is not well defined, the value of the mold-metal interface heat transfer coefficient, has a large effect on the calculated results. The results strongly reinforce the importance of the use of accurate, temperature-dependent thermophysical properties.

Modeling of Centrifugal Casting - Another potential large-scale application of the nickel aluminide alloy is for transfer rolls for reheating furnaces in the steel industry. The rolls are centrifugally cast and welded to statically cast trunions. The build-up of oxidation or other corrosion products on the surface of the rolls causes the surface of the steel ingot in contact with the rolls to be scoured, resulting in a reduction in yield, since the damaged material must be ground off prior to further processing. The nickel-aluminide alloy has the potential to eliminate the formation of these corrosion products on the roll surface due to its superior oxidation resistance. However, the formation of oxide films in the molten alloy coupled with the severe turbulence produced during centrifugal casting could potentially give rise to large-scale defects in the casting, impairing both structural integrity and weldability. The modeling of the centrifugal casting process may be used to evaluate the impact of process parameters during centrifugal casting, in particular the rotational speed and pouring rate, on the likelihood of defect formation.

Figure 6 shows the dimensions of a test centrifugal casting used to illustrate the application of modeling to optimize the centrifugal casting process. The casting is 61 cm long and has an outside diameter of 20 cm. Metal enters the cavity through a 2.5-cm diam inlet at one end attached to a pouring cup (not shown). A rotational speed of 1000 rpm is used. Mold filling is modeled for two pouring conditions, corresponding to an inlet velocity of 1 m/s (10 cm metal head in the pouring cup) and 2 m/s (20 cm metal head in the pouring cup).

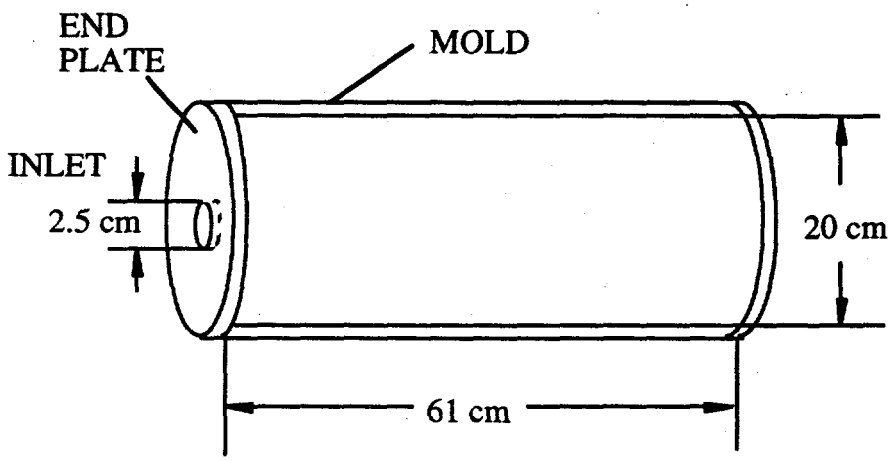

Fig. 6. Test configuration used to illustrate filling behavior in centrifugal casting.

Figure 7 shows the results of a filling simulation for an inlet metal velocity of 1 m/s. Metal initially enters the cavity in a stream but is quickly forced to the mold edges by the centrifugal forces and proceeds to fill the cavity progressively from the inlet as intended. Figure 8 shows the results of a filling simulation for an inlet velocity of 2 m/s. In this case, the initial momentum experienced by the metal is so large that the stream is broken up before being captured by the centrifugal forces. The broken up segments of the stream are splattered onto the mold surface, where they would be entrained into the incoming metal. However, the metal that is splattered to the mold surface is also likely to solidify. If the solidified portions are not remelted by the incoming metal, they are likely to form defects. In addition, splattered portions of metal are also likely to spread out as thin layers

and possibly oxidize, further serving as sources of defects in the casting. Figure 8 © also indicates that the force of the incoming metal causes the mold to be first filled away from the inlet rather than progressively from the inlet, further giving rise to the possibility that defects or oxide films may be trapped in the casting instead of being pushed to the end of the casting, where they may be cropped off if necessary.

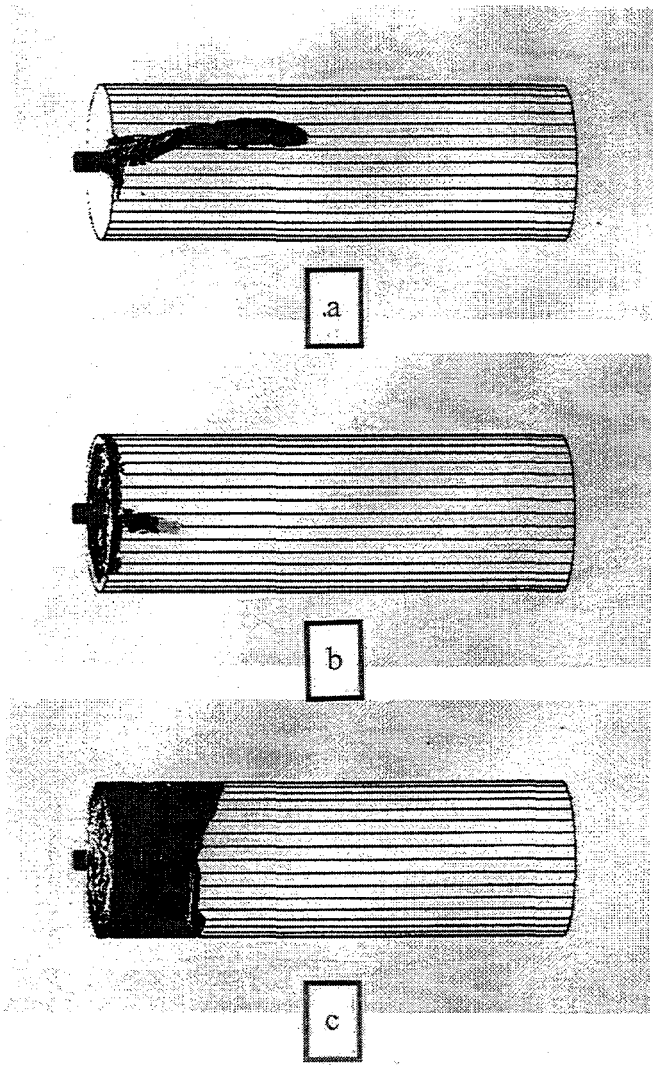

Fig. 7. Filling behavior during centrifugal casting at: (*a*) 0.36 s, (*b*) 0.47 s, and (*c*) 0.53 s from the start of pour, for an inlet velocity of 1 m/s.

The above analysis clearly indicates how the choice of pouring conditions in the form of the design of the pouring spout could affect casting quality in centrifugal casting. Importantly, the effects illustrated by the simulation occur at very short times, typically within 0.5's from the start of pour, making them very difficult to be observed by experiment or by foundry personnel. Consequently, trial and error methods of eliminating defects caused by pouring conditions could be very difficult.

Also, such defects could be periodic and depend on the personnel pouring the casting, or even vary from pour to pour for the same personnel pouring and casting, or even very from pour to pour for the same personnel. Similar analyses could be conducted for other process parameters such as the rotational speed, pouring cup size, and pouring temperature.

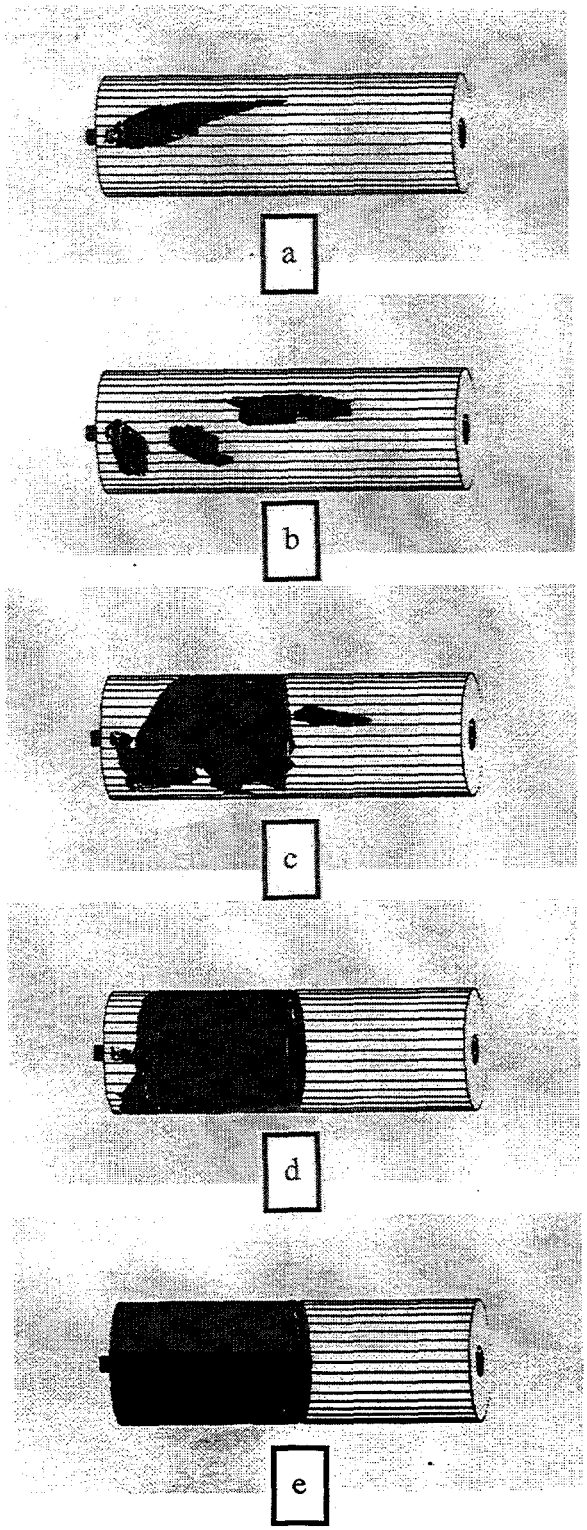

Fig. 8. Filling simulation during centrifugal casting: (*a*) 0.22 s, (*b*) 0.37 s, (*c*) 0.39 s, (*d*) 0.43 s from the start of pour, for an inlet velocity of 2 m/s.

The importance of the availability of accurate thermophysical properties is illustrated by comparing the sensitivity of the computed cooling curves to changes in thermophysical properties. The analysis indicates that if constant thermophysical properties are used in solidification simulation, the values at the solidus temperature are likely to provide the greatest accuracy; in particular, the analysis indicates that significant errors may be incurred by the use of constant room-temperature properties. The modeling of centrifugal casting of rolls indicates that changes in the height of metal in the pouring cup can significantly affect casting quality. Moreover, the conditions that affect casting quality occur at very short times, making them difficult to be observed during normal foundry operation. The use of casting simulation is shown to be a useful tool in defect control and the optimization of the centrifugal casting process.

3. Weld reparability of casting, Start 10/95, End 9/96

Efforts continued in the areas of: (a) evaluating the mechanical properties of welds, (b) assessing the effects of ingot composition on weld-induced cracking, and © developing procedures for welding IC-221M castings.

a. Mechanical Properties of Welds. As previously reported, stress-rupture testing was done on specimens made from welds of 95-mm-OD centrifugally cast IC-221M pipe using both the IC-221LA and IC-221W filler metals. These weldment specimens were oriented across the welds so that both base metal and weld deposit were contained in their gage lengths. As shown in Fig. 9, the rupture life of the weldment specimens was somewhat less than that of the base metal. However, rupture life compares very favorably with those of other high-strength nickel-based alloys such as Haynes 214, Inconel 617, and Inconel 618. Data for these alloys, as well as for several other IC-221M weldments, are included in Fig. 9.

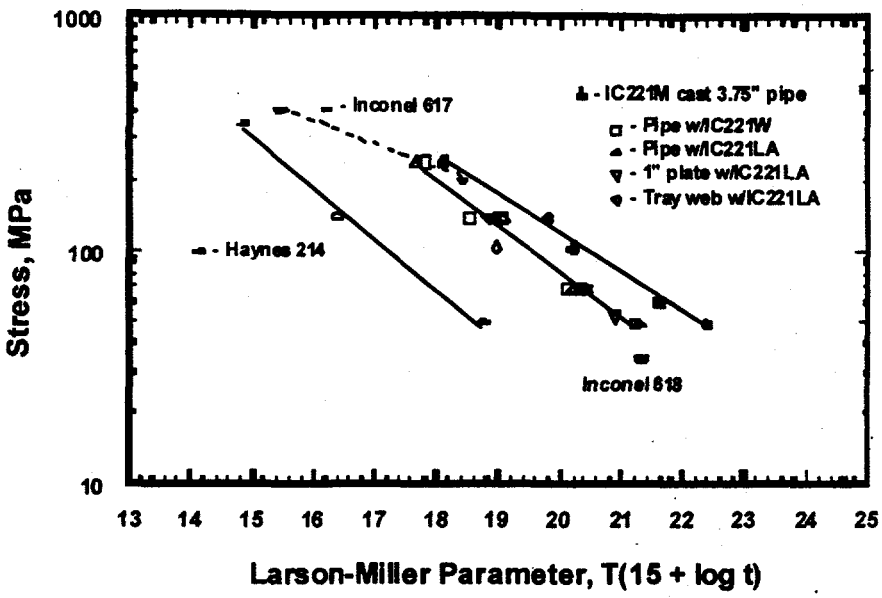

Fig. 9. Larson-Miller plot of stress-rupture test results of IC-221M weldments. Data for Haynes 214, Inconel 617, and Inconel 618 weldments are shown for comparison.

b. Effects of Ingot Composition on Weld Cracking. Based on a large number of welding trials, it became apparent that control of IC-221M ingot composition beyond the major alloying elements of Al, Cr, Mo, Ni, Zr, and B was required to produce castings with acceptable weldability. To address this issue, a series of 15 ingots was made in which elements such as, B, C, S, Si, and Fe, which are reasonably expected to occur in commercially processed IC-221M alloys were intentionally added in controlled amounts. The ingots were air-melted and cast into 100 x 150 x 25-mm permanent molds. The plates were prepared with a single-vee bevel and clamped in a rigid fixture for welding. All weld deposits were made under identical conditions using the same IC-221LA filler metal. The cracking response of these weldments was then used to set limits on the secondary chemical elements. When coupled with existing data, the result of this experiment was a more detailed specification of the IC-221M chemical composition: Ni-(7.5 to 8.5)Al-(7.5 to 8.5)Cr-(1.3 to 1.8)Mo-(1.7 to 2.2)Zr-(0.02 max)B-(0.15 max)/c-(0.01 max)S-(0.2 max)Si-(0.3 max) Fe, weight percent. Maintaining the IC-221M chemical composition within these ranges is expected to improve both castability and weldability.

c. Welding Procedure Development. Two procedures were developed for making circumferential welds on centrifugally cast roll shells (355.6 mm OD by 22.2 mm wall) produced by Sandusky International. Both procedures were used to produce full penetration welds on the IC-221M castings using IC-221LA filler metal and gas tungsten arc welding. The preferred procedure consisted of machining away a thickness of about 9.5 mm of material from the inside diameter of the centrifugally cast roll shell rings to remove accumulated casting defects. The remaining thickness of about 12.5mm was prepared with a single J-groove edge preparation. Two rings, so prepared, were then set up with a 3.2-mm root gap opening and a type 304 stainless steel backing ring. A root welding bead was then manually deposited with 1.6-mm-diam metal-power-cored welding wire. The circumferential weld was then completed using 3.2-mm-diam welding wire. Fourteen weld beads were used to complete this weldment, which is shown in Fig. 10.

Selected specimens, tested at 800°C/241 Mpa or 1000°C/48 Mpa, of both filler metal types were also examined by optical metallography. This confirmed that failures occurred in the weld deposits for both IC-221LA and IC-221W. The failure mode also appeared to be independent of test conditions.

The overall stress-rupture behavior of the IC-221M weldments is typical of what is often observed for similar testing of a wide variety of structural alloys (i.e. weldment rupture life is usually less than that of base metal), and the weld deposit is a preferred failure site.

4. Workability of Cast or Powder Metallurgy Product to Sheet, Bar, and Wire, Start 10/95, End 9/96

This task is looking at the production of wrought product through both powder metallurgy and near-net-shape methods. Since castings have turned out to be the major application, this task has gotten less attention. More work is expected in this area during FY 1997.

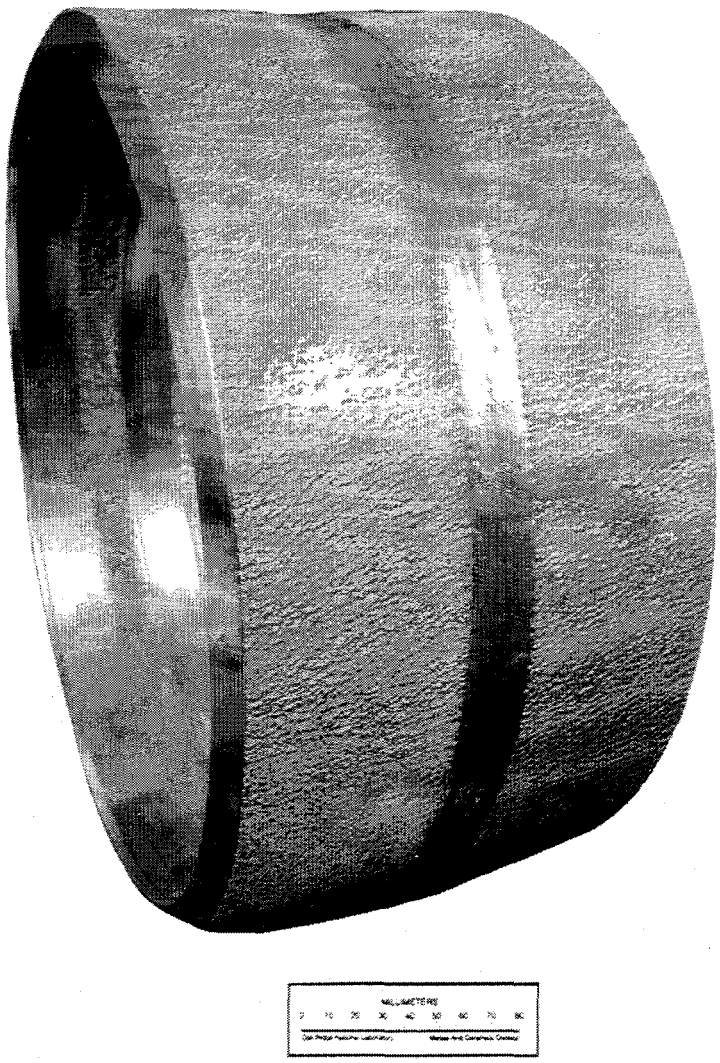

Fig. 10. Photograph of centrifugally cast rings of IC-221M welded together using IC-221LA filler metal and gas tungsten arc welding.

5. Technology Transfer Activities, Start 10/95, End 9/96

The purpose of this task is to undertake activities that will promote the transfer of nickel-aluminide technology to industry. These activities include visiting potential producers and users of materials and describing the technology in detail, training industry personnel either at ORNL or at the industrial facilities, providing data package, and holding technology transfer meetings at ORNL. As a result of these activities, several additional applications have been identified for these materials.

Significant technology transfer has occurred through the following companies:

United Defense LP - Have become a licensee with substantial effort in the area of marketing and production of nickel aluminide. They are also using the alloy for trays and dies.

Sandusky International - Is currently negotiating for a license for centrifugal cast rolls.

Alloy Engineering & Casting Company - I considering a license.

The Timken Company - Is testing the trays.

FMC Corporation - The parent company of United Defense LP is testing the alloy for grate bar and pallet tips for phosphate calcination furnace.

Jeffrey Chain - Has requested for trays and furnace hearths of nickel aluminide.

E. I. DuPont de Nemours & Company - Is testing the sample material for corrosion properties.

Bethlehem Steel Corporation - Is testing the rolls in heat-treating furnace.

PCC Airfoils, Inc. - Is testing the trays for firing of investment molds.

Trinity Forge - Is testing nickel aluminide a punch during forging process.

Waukesha Cherry-Burrell - Is testing nickel aluminide a punch during forging process.

Chevron - Is evaluating nickel aluminide as tube hangers.

Delphi Saginaw - Is evaluating pusher and batch furnace fixtures in carburizing atmosphere.

Visits were made to alloy Engineering & Casting Company, Sandusky International, United Defense LP, Delphi Saginaw, Jeffrey Chain, Trinity Forge, Duraloy Technologies, Inc., and Bethlehem Steel Corporation.

PUBLICATIONS

N. S. Stoloff and V. K. Sikka, *Physical Metallurgy and Processing of Intermetallics* (Chapman & Hall: New York, December, 1995).

V. K. Sikka, "Processing of Intermerallic Aluminides," pp. 561-604 in *Physical Metallurgy and Processing of Intermetallic Compounds,* ed. N. S. Stoloff and V. K. Sikka (Van Nostrand Reinhold: New York, 1996).

S. C. Deevi and V. K. Sikka, "Nickel and Iron Aluminides: An Overview on Properties, Processing and Applications," *Intermetallics*, **4**, 357-375 (1996).

J. E. Orth and V. K. Sikka. "High Temperature Performance of Nickel aluminide Coatings for Furnace Fixtures and Components," *Heat Treating,* 47-53 (1996).

S. C. Deevi and V. K. Sikka, "Exo-Melt™ Process for Melting and Casting Intermetallics," *Intermetallics,* in press, 1997.

V. K. Sikka and S. C. Deevi, Exo-Melt™ Process for Intermetallic Powders," to be published in proceedings of PM²TEC'96 World congress on Powder Metallurgy and Particulate Materials, Washington, D. C., June 18, 1996.

S. C. Deevi, R. D. Seals, V. K. Sikka, and C. J. Swindeman, "Application of Reaction Synthesis Principlels to Thermal Spray Coatings of Intermetallics," *J. Materials Science,* in press, 1997.

S. C. Deevi, V. K. Sikka, C. J. Swindeman and R. D. Seals, "Application of Reaction Synthesis Principles to Thermal Spray Coating," *J. Materials Science,* **32**, in press, 1997.

S. C. Deevi, V. K. Sikka, C. J. Swindeman and R. D. Seals, "Reactive Spraying of Nickel Aluminide Coatings," *J. Thermal Spray Technology,* in press, 1997.

V. K. Sikka, S. C. Deevi and J. E. Orth," Exo-Melt™ Process for Commercialization of Nickel Aluminides," *Progress in Materials Science,* in press, 1997.

PRESENTATIONS

V. K. Sikka, "Commercicalization of Nickel and Iron Aluminides," Int. Symp. on Nickel and Iron Aluminides: Processing, Properties, and Applications, ASM-TMS Materials Week'96 Cincinnati, Ohio, ASM International Materials Park, Ohio, October 9, 1996.

S. C. Deevi and V. K. Sikka, "Reaction Synthesis and Densification of Ni_3Al and Its Composites," Fall Meeting of Minerals, Merals amd Materials Society on Physical Metallurgy and Materials, Cleveland, Ohio, November 1, 1995.

V. K. Sikka, "New Class of Advanced Materials," High Tech. Materials Center Mini Symp., Richmond, Virginia, November 17, 1995.

V. K. Sikka, S. C. Deevi and J. E. Orth, "Exo-Melt™ Process for Commercialization of Nickel Aluminides," Fall annual Meeting of Joint Inst. of Metals on Advanced Materials and Technology for the 21st Century, JIM '95, Honolulu, December 14, 1995.

S. C. Deevi, V. K. Sikka and C. T. Liu, "Processing, Properties, and Applications of Nickel and Iron Aluminides," Conference on Perspectives in Materials Science, Bangalore, India, December 19, 1995.

V. K. Sikka, "Exo-Melt™ Process for Casting of Aluminides," Department of Met. And Mater. Eng. personnel, University of Alabama, Tuscaloosa, Alabama, February 29, 1996.

S. C. Deevi, r. D. Seals, V. K. Sikka and C. J. Swindeman, "Aplication of Reaction Synthesis Principles to Thermal Spray Coatings of Intermetallics," PM^{2}TEC'96 World Congress on Powder Metallurgy and Particulate Materials, Washington, D. C., June 18, 1996, Metal Powder Indistries Federation.

V. K. Sikka and S. C. Deevi, "Exo-Melt™ Process for Intermetallic Powders," PM^{2}TEC'96 World Congress on Powder Metallurgy and Particulate Materials, Washington, D.C., June 20, 1996, Metal Powder Industires Federation.

S. C. Deevi and V. K. Sikka, "Technology and Application of Intermetallics," ASM International (Richmond Chapter) Meeting, Richmond, Virginia, October 5, 1995.

S. C. Deevi and V. K. Sikka, "Technology and Applications of Nickel Aluminides," Materials Week'96, Cleveland, Ohio, November 1, 1996.

HONORS AND AWARDS

Renew America's special Recognition, the U. S. Department of Energy 1996 National Awards for Energy Efficiency and Renewable Energy, honoring *Exo-Melt™ Process for Melting Nickel Aluminides, Oak Ridge National Laboratory* for its outstanding contributions in promoting an environmentally sustainable energy future, October, 1996.

PATENTS/DISCLOSURES

"Intermetallic Alloy Welding Wires and Method for Fabricating the Same," M. L. Santella and V. K. Sikka, U. S. Patent No. 5,525,779, June 11, 1996.

"Weldable Nickel Aluminide," M. L. Santella and V. K. Sikka, ESID-0224, elected for application.

"Method of Aluminizing Metal Alloys by Weld Overlay Using Aluminum and Aluminum Alloy Wire," M. L. Santella, V. K. Sikka, and S. Viswanathan, invention disclosure submitted to patent counsel.

LICENSES

In addition to United Defense LP, serious licensing agreements are under way with Sandusky International and Alloy Engineering & Casting Company.

INDUSTRIAL INPUT AND TECHNOLOGY TRANSFER

Delphi Saginaw - A purchase request for 63 pusher furnace assemblies of nickel-aluminide alloy IC-221M was placed with Alloy Engineering & Casting company. This purchase is cost-shared with ORNL. The completed assemblies will be shipped to Delphi Saginaw by the end of December 1996 and will go into application by the end of January 1997.

Bethlehem Steel Corporation - Based on the evaluation of two furnace rolls of nickel aluminide during the visit in August 1996, they had started planning for installing 30 rolls. The final procurement decision is expected in December 1996.

Chevron - After six months of successful experience with IC-221M hangers, Chevron has indicated expansion of hangers and other applications during 1997.

COST INFORMATION

None

COST SHARING

The Cooperative Research and Development Agreement (CRADA) partners continue to provide in-kind cost shares. Substantial cost contributions were made by United Defense LP.

SYNTHESIS AND DESIGN OF SILICIDE INTERMETALLIC MATERIALS

J.J. Petrovic, R.G. Castro, D.P. Butt, Y. Park, K.J. Hollis, A. Bartlett, H.H. Kung

Los Alamos National Laboratory
Los Alamos, New Mexico 87545

INTRODUCTION

The overall objective of this program is to develop structural silicide-based materials with optimum combinations of elevated temperature strength/creep resistance, low temperature fracture toughness, and high temperature oxidation and corrosion resistance for applications of importance to the U.S. processing industry. A further objective is to develop silicide-based prototype industrial components. The ultimate aim of the program is to work with industry to transfer the structural silicide materials technology to the private sector in order to promote international competitiveness in the area of advanced high temperature materials and important applications in major energy-intensive U.S. processing industries.

The program presently has a number of developing industrial connections, including a CRADA with Schuller International Inc. targeted at the area of $MoSi_2$-based high temperature materials and components for fiberglass melting and processing applications. We are also developing an interaction with the Institute of Gas Technology (IGT) to develop silicides for high temperature radiant gas burner applications, for the glass and other industries. Current experimental emphasis is on the development and characterization of $MoSi_2$-Si_3N_4 and $MoSi_2$-SiC composites, the plasma spraying of $MoSi_2$-based materials, and the joining of $MoSi_2$ materials to metals.

TECHNICAL PROGRESS - FY 1996

1. CRADA with Schuller International

CRADA No. LA95C10271-A001 "Advanced High Temperature Materials for Glass Applications" with Schuller International Inc. was formally executed on 19 March 1996. This is a three-year CRADA targeted at the area of $MoSi_2$-based high temperature materials and components for fiberglass melting and processing applications. On 30 January 1996, a CRADA kick-off meeting was held at Schuller Mountain Technical Center, Littleton, Colorado. Attendees of this meeting included: Los Alamos National Laboratory - Richard Castro, John Petrovic, Darryl Butt, Andy Bartlett, Kendall Hollis; Schuller International - Walter Johnson, Ted Michelson, Bob Vernetti, Foster Harding, Chris Reed. A review of the Joint Work Statement (JWS) was completed during this kick-off meeting and individual responsibilities were assigned for Phase I Tasks.

Schuller CRADA activities have been reported in the January-March 1996 and April-June 1996 Quarterly Progress Reports, submitted to Dr. Charles A. Sorrell at DOE/AIM. All of the Schuller

CRADA activities are considered to be Proprietary Information by Schuller International, and the Quarterly Reports have been marked as such. The Proprietary Information Schuller CRADA activities for the quarterly period July-September 1996 have been submitted as a separate progress report to Dr. Sorrell. None of the Schuller CRADA activities can be included in this Annual Report, due to their Proprietary Information nature.

2. Plasma Spraying of $MoSi_2$ Materials

Three plasma spray processing conditions were selected to evaluate the effect of processing condition on final plasma spray coating composition. Three sets of plasma spray parameters were chosen to give: high temperature and high velocity; medium temperature and medium velocity; low temperature and low velocity. The plasma spray helium flow and the current were varied to change the particle temperatures and velocities.

Silicon loss occurs during the spray deposition process as evidenced by an increase in Mo_5Si_3 from the starting $MoSi_2$ powder to the $MoSi_2$ coatings. Mo_5Si_3 content was calculated to be 4-8% in the plasma sprayed coatings, and 0.6% in the starting powder by quantitative x-ray analysis. The samples sprayed under the low spray conditions showed the highest Mo_5Si_3 content. The Mo_5Si_3 particles were observed to be in the 1-4 μm range by SEM backscattered electron analysis. The trends observed can be explained by the trajectory of the small $MoSi_2$ particles, which penetrate to hotter parts of the plasma plume in the low conditions, due to lower impulse from the plasma. It is likely that the amount of Mo_5Si_3 in the $MoSi_2$ coatings can be decreased. One way of accomplishing this would be to eliminate the fine $MoSi_2$ particles from the feed powder. Another way would be to more carefully match the powder injection gas flow to the plasma condition to insure large particle penetration into the hot part of the plasma, but prevent small particle penetration.

3. Mechanical Properties of $MoSi_2$ Materials

Impression Creep Testing

Impression creep tests were performed on air-plasma-sprayed (APS) consolidated Exotherm $MoSi_2$-Si_3N_4 powder. There was a definite creep rate dependence on temperature, but little dependence on applied stress. The activation energy for creep in the samples was calculated to be 374 kJ/mole. The activation energy for the same powder in hot pressed form was measured to be 336 kJ/mole. The stress exponent was difficult to determine for the APS consolidated samples but appeared to be less than 1. The stress exponent for the same powder in hot pressed form was measured to be 4.4. The creep rates for the hot pressed samples were lower under all testing conditions than the creep rates for the APS samples.

Residual Stresses in Plasma Sprayed $MoSi_2$ Tubes

Residual stresses in plasma sprayed $MoSi_2$ tubes were measured by x-ray microdiffraction. A phenomenological model was proposed to explain these residual stresses, which is based on mechanical equilibrium considerations were solidifying constrained material on a substrate. Stresses are based on elastic calculations as layers are incrementally added to the substrate. The model

indicates that the compressive to tensile stress profile in a net-shape tube results from evolving force balances when adding layers of material. Cooling of the sample during plasma spraying results in reduced residual stresses in the final piece. However, the overall residual stress field for a homogeneous piece can never be eliminated due to equilibrium requirements when solidifying a constrained layer onto the surface. Thermal expansion differences between the substrate and coating can significantly alter the stress state during spraying, but will not change the final stress state upon substrate removal. This is important when noting that cracking of the plasma sprayed tubes can occur both during the spray process, or after during post-spray handling.

Joining of $MoSi_2$ Materials

Efforts have been directed at joining $MoSi_2$ to 316L stainless steel. Robust $MoSi_2$-316L joints were made using Nb and Ni interlayers. Four-point bend fracture tests demonstrated that failure occurred in the $MoSi_2$ rather than along the joint interface. These results indicate that it is possible to make strong joints, but that some residual stress is present in the $MoSi_2$ due to the large thermal expansion mismatch between $MoSi_2$ and stainless steel.

Studies were also performed on $MoSi_2$-Al-$MoSi_2$ joints. Al is a low melting temperature braze that readily wets $MoSi_2$, due to the formation of a $Mo_5Si_3Al_x$ reaction product. Lower temperature joints were successfully made at 730 °C. There was $Mo_5Si_3Al_x$ formation at the joint interface, as well as the presence of a possible SiO_2 phase.

4. Impression Creep Measurements

Further measurements of the creep of the $MoSi_2$/SiC and $MoSi_2/Si_3N_4$ hot pressed samples made from composite powders from Exotherm were performed. These measurements allowed the refining of the values calculated for the activation energy and the stress exponent dependence of the creep rate. The revised value of the activation energy for the $MoSi_2$/SiC samples is 329.0 kJ/mole while the revised value for $MoSi_2/Si_3N_4$ is 335.9 kJ/mole. The revised value for the stress exponent for the $MoSi_2$/SiC samples is 4.34 while the revised value for the $MoSi_2/Si_3N_4$ is 6.07.

For comparison to the creep rates of $MoSi_2$ components fabricated at LANL, $MoSi_2$ heating elements produced by Kanthal were tested to determine their impression creep rates. The creep rates are shown in Figure 1. From the data available at this time it is difficult to determine the stress exponent for creep rate dependence. However, the activation energy for loads of 259.8 MPa and 320.9 MPa were determined to be 417.1 kJ/mole and 488.1 kJ/mole respectively.

Data collection for impression creep testing will continue into the next quarter. Several of the tested samples have been mounted and polished and will be investigated by optical microscopy to help determine the mechanisms responsible for creep in the various samples.

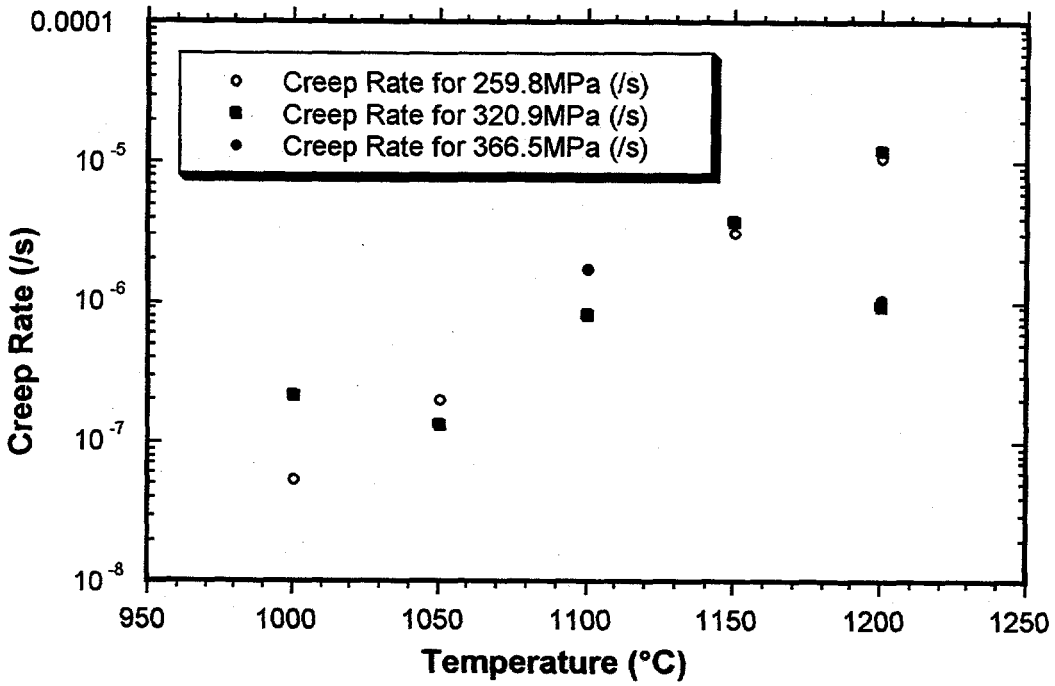

Fig. 1. Impression creep rates for Kanthal heating element.

Modeling of Residual Stress in Net-Shape Tubes

Modeling work has recently incorporated finite element modeling (FEM) techniques to understand the relative contributions of material and spray properties on the final stress state of a free standing tube. This elastic model follows the rationale of previously reported analytic models, but is able to easily incorporate the effects of N-layers of added material, and as well can account for temperature gradients developing in the piece during spraying.

Stresses are assumed to arise from four contributions:
1) Quenching stresses, which result from the constrained solidification of molten droplets on a substrate.
2) Thermal gradient/workpiece heating stresses. These occur when the workpiece and coating heat up during the spray process. FEM easily accounts for this effect with each incremental addition of material.
3) Cool down stresses. Thermal expansion mismatch and temperature gradients within the full sized piece will give significant stresses when cooling down to room temperature.
4) Substrate removal stresses. Substrate removal will significantly affect the final stress state; this is necessary to compare the model with previously reported x-ray results that were for free-standing pieces.

The FEM model required inputs of mechanical and thermal material properties. These were estimated by various test methods, and from literature values. Boundary conditions included heat flux, emissivity, and a convective coefficient. These were estimated from literature values. Material was added in increments of 100 μm; quenching stresses were imposed at each increment, and varied from 25 to 150 MPa. A transient heat transfer analysis was run for 30 s increments, based on the approximate buildup rate of the net-shape piece. Results from the transient analysis were used to

estimate the stresses #2 and #3 of above. Stresses #1, 2 and 3 were then summed, and the substrate removal stress was obtained from this summation.

Previously reported results showed that a tensile to compressive gradient of the hoop stress existed, as measured from the outer to inner radius of the free standing tube. Cracking of these tubes- sprayed under higher power conditions- led to a residual opening, as shown in Figure 2, consistent with the measured stress profile. However, under reduced power spray conditions, cracking of the rings led to a *negative* residual opening of the ring, as shown schematically in Figure 3; this contraction of the ring upon cracking suggests a stress gradient of opposite sign to that measured in the rings sprayed under higher power. One intent of the model, then, was to understand how a change in spray conditions and concomitant material properties allowed for an apparent reversal in the residual stress field in the tube.

Figures 4a,b,c show some preliminary results of the FE modeling. In Figure 4a, the effects of varying the quenching stress are presented. Other researchers have measured quenching stresses ranging from 5 to 150 MPa. Accurate values are not yet known for this system. Figure 4b shows the effect of the thermal gradient stresses. Modeling was done in which the thermal conductivity of the coating was varied by an order of magnitude. This affected the cool down stresses - also shown in Figure 4b- because of the large thermal gradient that developed, but didn't significantly change the stresses generated during heating because of a relatively constant heat flux flowing in the sample.

Figure 4c shows the total stresses in a free standing piece under different conditions. Reduction in the quenching stress or the thermal gradient stress will reduce the total stress in the piece. However, none of the generated stress states will result in the reverse gradient suggested by Figure 3; continuing investigations are studying the effect of out of plane shearing stresses and their effect on final stress state.

5. RF Joining of $MoSi_2$

$MoSi_2$ has been successfully joined to itself using thin Al interlayers, as described in previous reports. RF techniques are being investigated in order to facilitate bonding under very short time cycles, and with minimum specimen heating. To that end, $MoSi_2$ was successfully bonded to itself using RF heating in a 2 minute bonding cycle. Figure 5 plots the temperature of the $MoSi_2$ as a function of time; this initial experimental setup was such that the temperature of the silicide controlled the output of the RF coil (because of the current impossibility of monitoring the temperature of the Al foil). After only 30 s at a soak temperature of 700°C, the $MoSi_2$ was successfully bonded to another piece of $MoSi_2$. A similar experiment was attempted in which the silicide was heated to only 600°C, under identical ramp rates and soak times. This bond was unsuccessful, however; the very thin Al foil did not allow for RF coupling with the foil at the frequency used. Apparently, then, the initial joint was successful owing to conductive heating of the Al foil by the coupled $MoSi_2$. Future work will investigate frequency and geometry effects on bonding, in order to obtain a successful joint without excessive heating of the materials to be joined.

Fig. 2. Indented $MoSi_2$ net-shape ring, sprayed under high power. Residual opening implies tensile to compressive hoop stress, going from outer to inner radius.

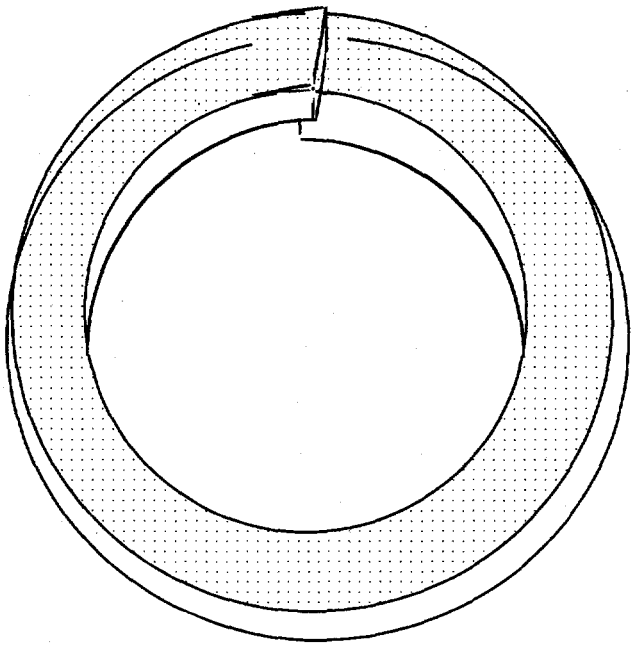

Fig. 3. Schematic of indented $MoSi_2$ net-shape ring, sprayed under low power conditions. Residual closure of ring implies a reversed stress field to that of Figure 2.

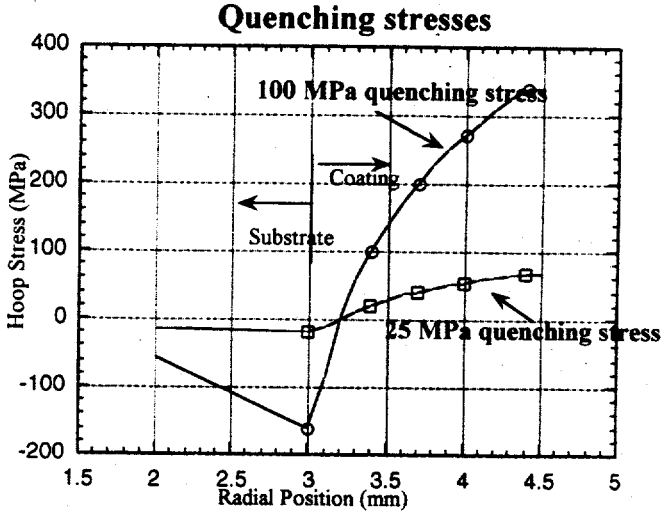

Fig. 4a. FEM results of quenching stress in net-shape tubes.

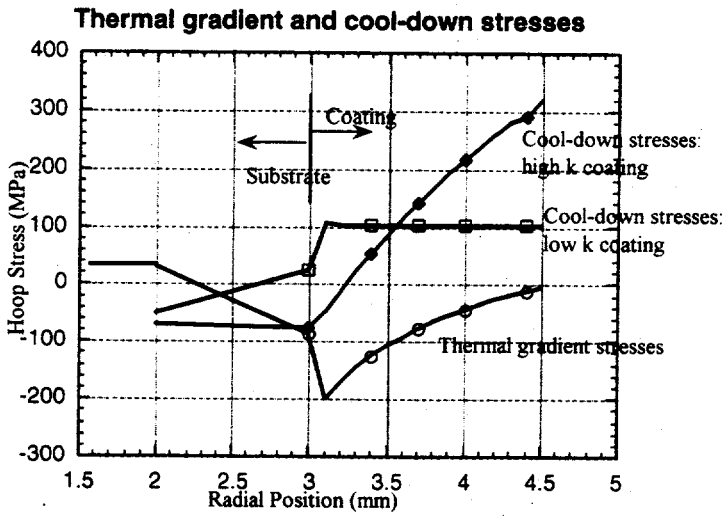

Fig. 4b. FEM results of temperature gradient effects in net-shape tubes.

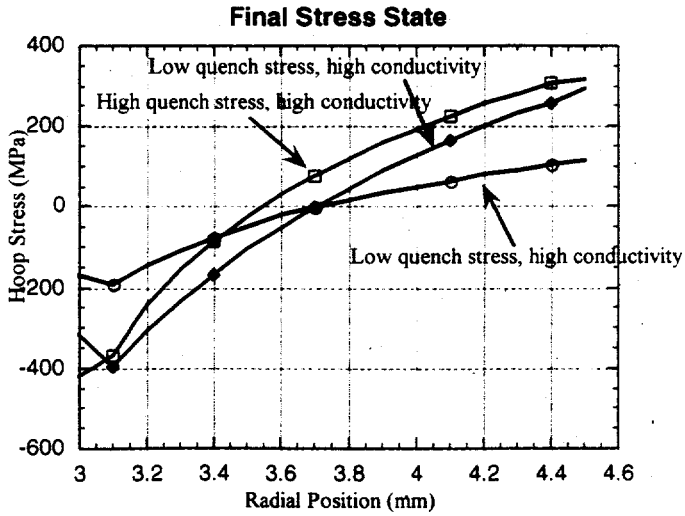

Fig. 4c. FEM results of final stress state in net-shape tubes.

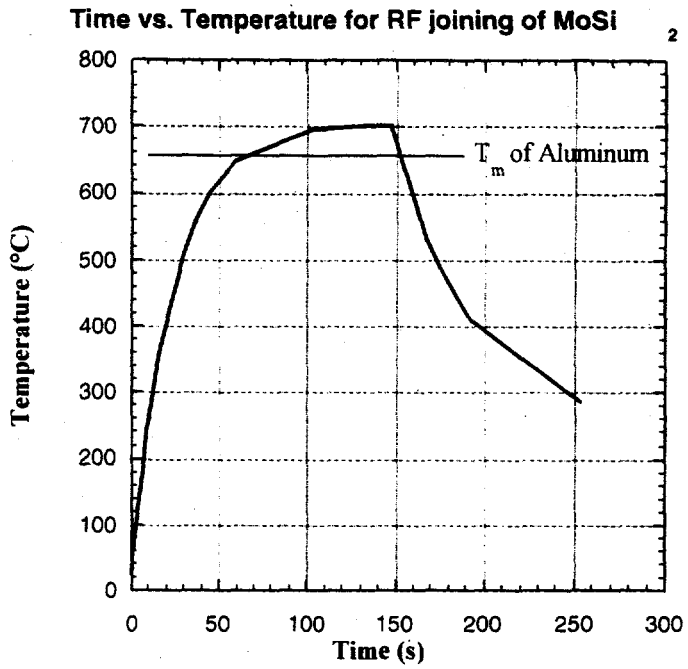

Fig. 5. Plot of temperature ramp employed in RF joining of $MoSi_2$.

6. Self-Joining of $MoSi_2$ Using Al Braze

In an effort to develop techniques for joining $MoSi_2$ to itself, an Al braze was investigated as a candidate for partial transient liquid phase joining method. Transmission electron microscopy (TEM) was carried out to characterize the interfacial reactions occurred near the Al/$MoSi_2$ interfaces. Figure 6 shows a cross-sectional view of the interface between the Al braze and $MoSi_2$. This sample has been joined at 730 C for 60 min in air. Selected area diffraction (SAD) patterns taken from the Al region show that the materials have the f.c.c. structure, and with the lattice parameter close to pure Al. This is consistent with the EDS results showing Al to be the only major peak in this region. A thin layer of Si ($\sim 0.3\ \mu m$) was found to be present immediately adjacent to the Al region, as was shown by both EDS and SAD. In regions next to Si, EDS spectrum revealed the diffusion of Al into the $MoSi_2$ matrix. Small crystallites with an average grain size of 50 nm formed near the interface. These ternary Mo-Si-Al grains have the structure of a metastable form of $MoSi_2$, the C40 phase. The stabilization of the C40-$MoSi_2$ with Al alloying addition has been demonstrated previously [1,2]. An addition of up to 12 at% of Al into the stable $C11_b$-$MoSi_2$ was reported to cause the stabilization of the C40 phase, and the Al was believed to substitute for Si in the new C40 phase. This also explains the presence of the Si layer between the Al and the ternary C40 region. The Al diffuses into $MoSi_2$ to replace Si, and under a displacive reaction, Si was forced out towards the Al side and formed a thin layer of pure Si. A systematic study is underway to further characterize the interfacial reaction with the aim of quantifying the Al stabilization of C40 $MoSi_2$ and the C40-$C11_b$ phase transformation.

References

A. Costa e Silva and M.J. Kaufman, Sripta Met. Vol. 29, p. 1141 (1993).
D.E. Alman and R.D. Govier, Scripta Met. Vol. 34, p. 1287 (1996).

7. Characterization of Combustion-Synthesized $MoSi_2$-Mullite Powders

In this quarter, transmission electron microscopy (TEM) characterization of the $MoSi_2$-Mullite composite powders has been performed. The main objective is to provide a baseline of information on the structure, chemistry, grain size, and phase distribution of the powders. The information will be used as guidelines along with x-ray diffraction data to evaluate the composite powders as starting materials for the plasma spray forming of $MoSi_2$-Mullite composites. The powders were combustion synthesized and supplied by Exotherm Corp.. The as-received powders were supported on ultrathin amorphous carbon film deposited on fine Cu mesh grids. TEM characterization was performed on a Philips CM30 and a JEOL 3000F high resolution TEM, operating at 300kV.

Figure 7 shows a low magnification TEM micrograph of an agglomerated particles with a nominal composition of Mullite-46v/o $MoSi_2$. The background material with the light contrast is Mullite, while $MoSi_2$ grains (darker contrast) decorate the surface of the agglomerates. A higher magnification view of a smaller (less agglomerated) particle was shown in Figure 8. It can be seen that the two phases are well dispersed. The distribution of $MoSi_2$ was reasonably uniform and the volume fraction was estimated to be ~ 40%. The Mullite grains were often seen with faceted side surfaces and the average grain size is ~ 500nm. $MoSi_2$ has a finer average grain size of ~ 200nm. Figure 9 shows a clean interface between a $MoSi_2$ grain (in <331> orientation) and a Mullite grain showing the{210} lattice fringes. In summary, TEM results show that the two phases are nicely inter-dispersed in the combustion-synthesized composite powders, which will provide a good starting base for either hot-pressing or plasma spray forming of $MoSi_2$-Mullite composites.

8. Electrochemical Measurements in Molten Glass

This quarter, significant time was spent setting up an apparatus for doing electrochemical impedance spectroscopy in molten glass. The objective is to use this apparatus to rapidly evaluate the corrosion rates of materials. This quarter preliminary studies were completed to characterize the electrochemistry of molten (and solidified) glass in the temperature range 30-1200°C. These data are summarized in Figures 10 and 11. These studies have demonstrated that the apparatus works. Also, because of the very low solution resistance of the glass we are confident that it is possible to measure the corrosion rates of $MoSi_2$ by impedance spectroscopy. Other investigators have attempted to measure corrosion rates of $MoSi_2$ using electrochemical methods. However, critical evaluation of their work has lead us to conclude that their techniques were flawed due in part to the way their samples were mounted in solution. As a consequence, we spent significant time this quarter developing improved ways to mount $MoSi_2$ specimens for electrochemical testing. We hope to have a viable mounting technique developed in the next month.

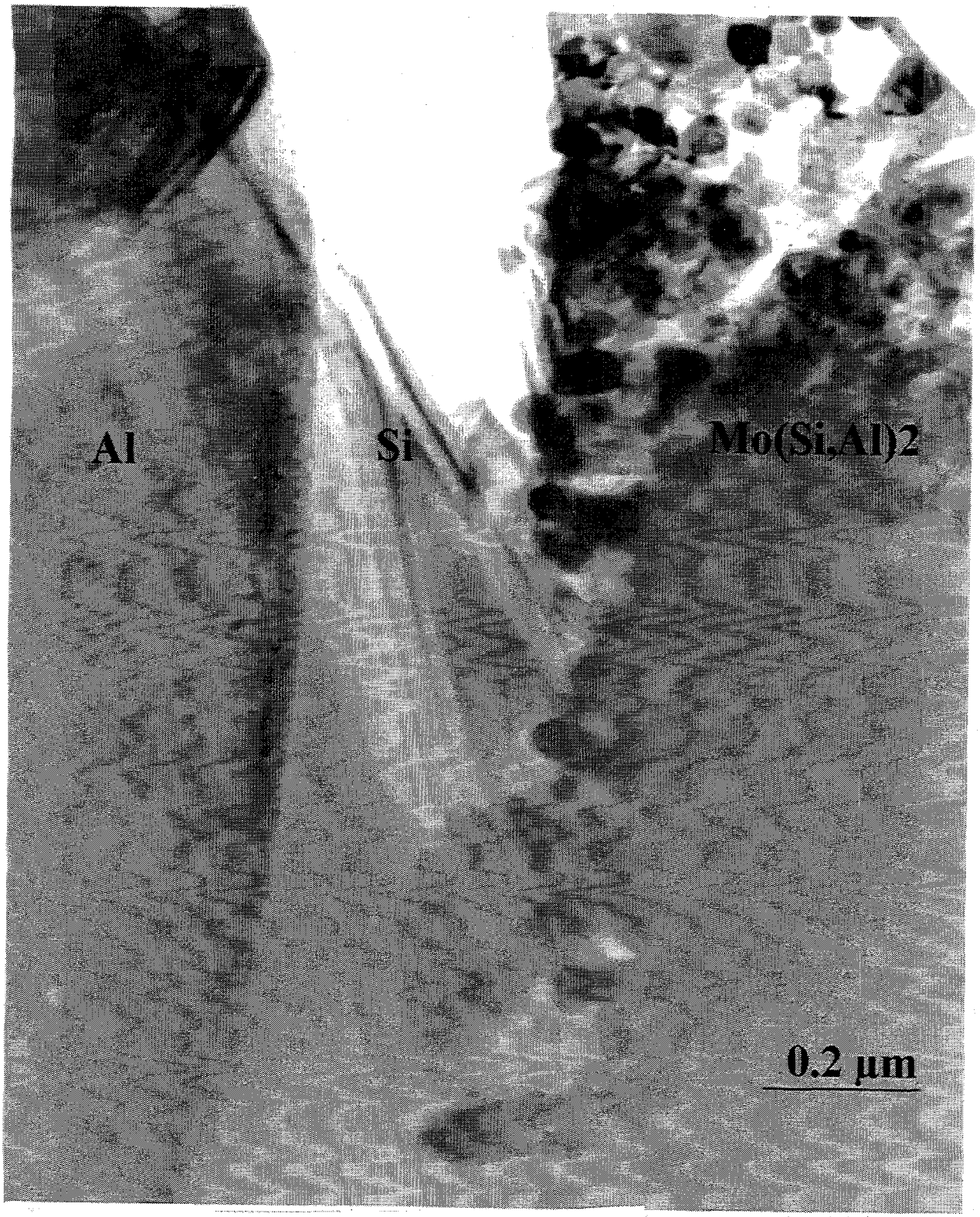

Fig. 6. TEM micrograph of an Al/$MoSi_2$ joining interface.

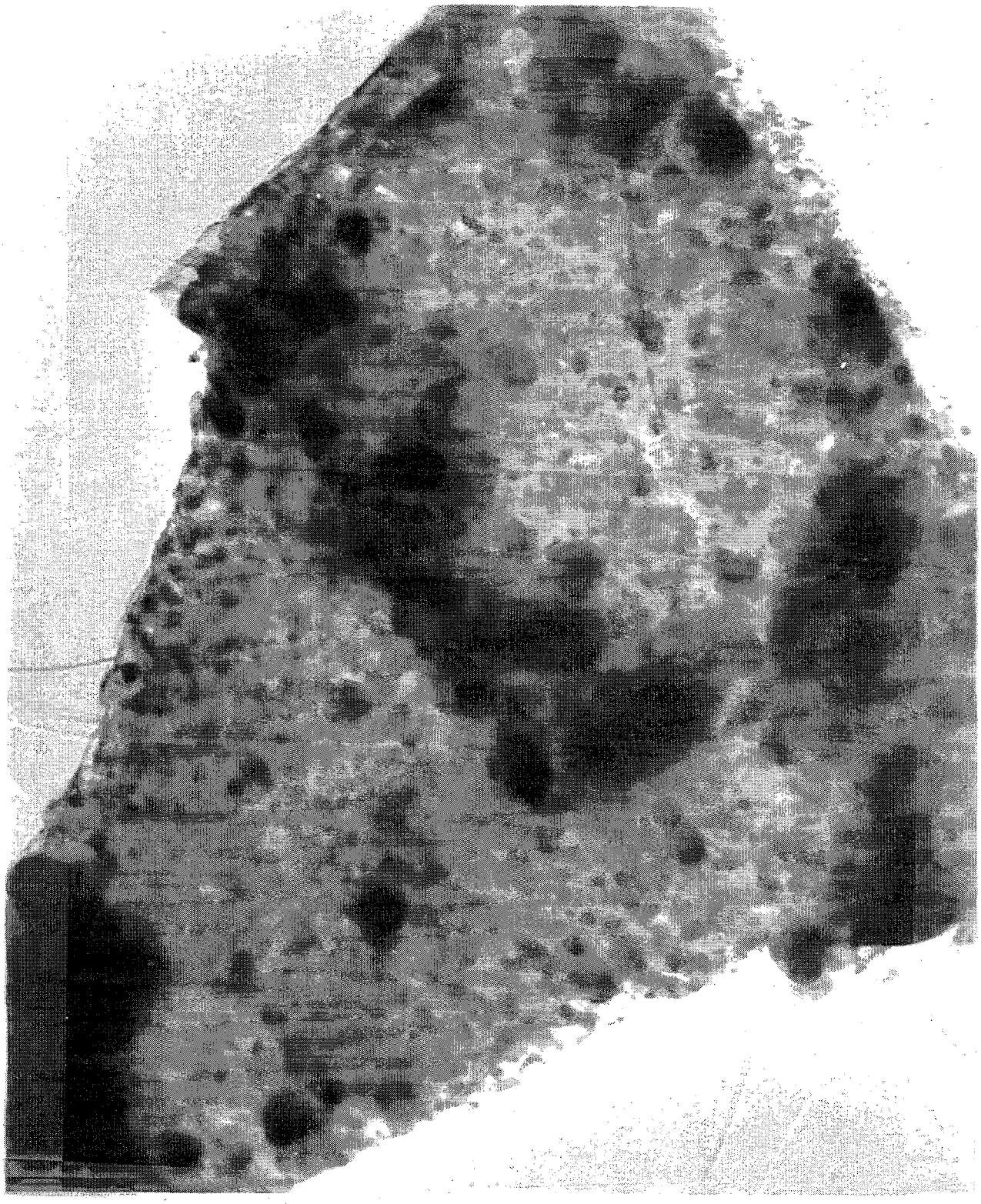

Fig. 7. TEM micrograph of an agglomerated $MoSi_2$-Mullite particle by combustion synthesis.

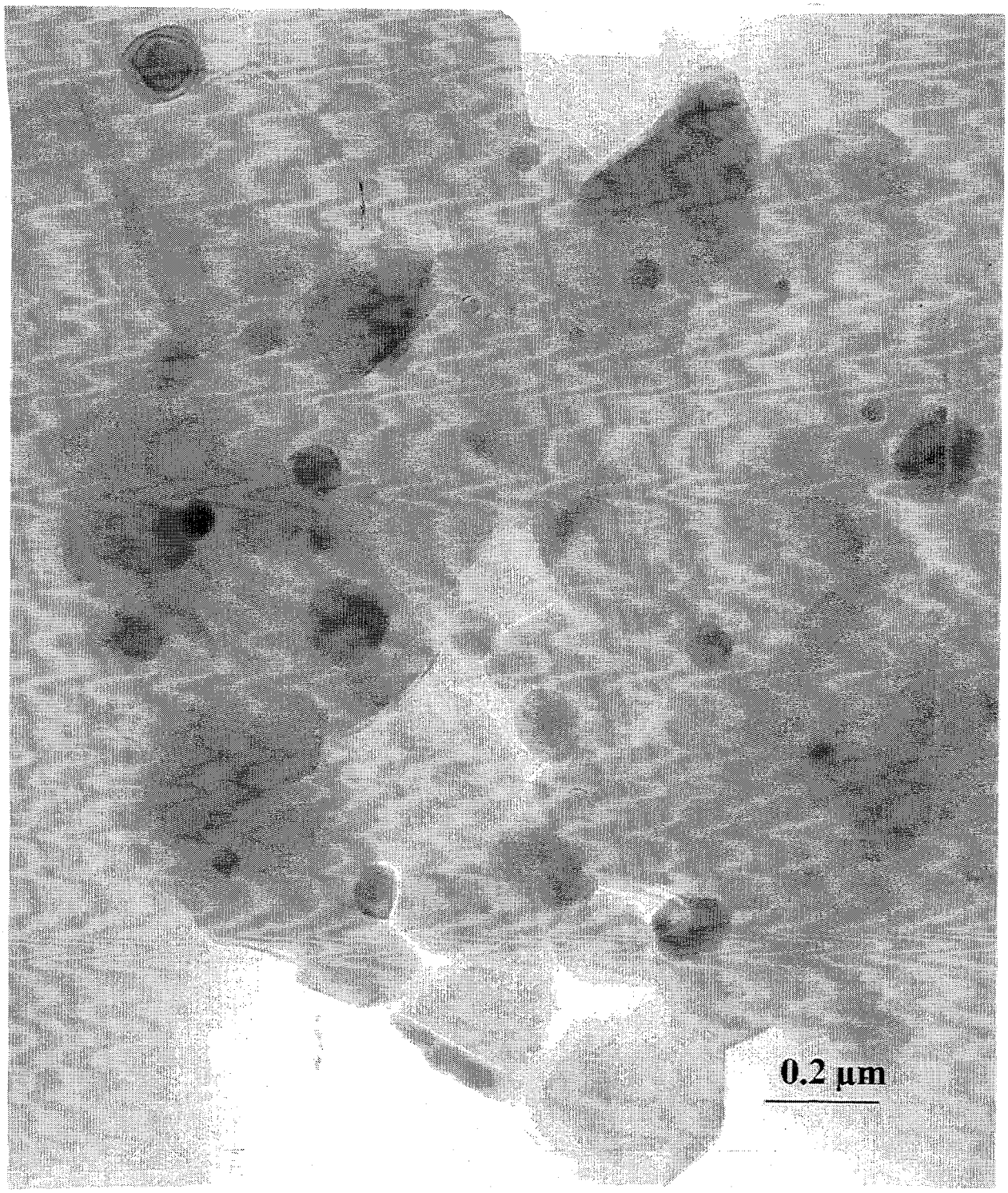

Fig. 8. TEM micrograph of a $MoSi_2$-Mullite particle. The light contrast grains are Mullite and the darker contrast grains are $MoSi_2$.

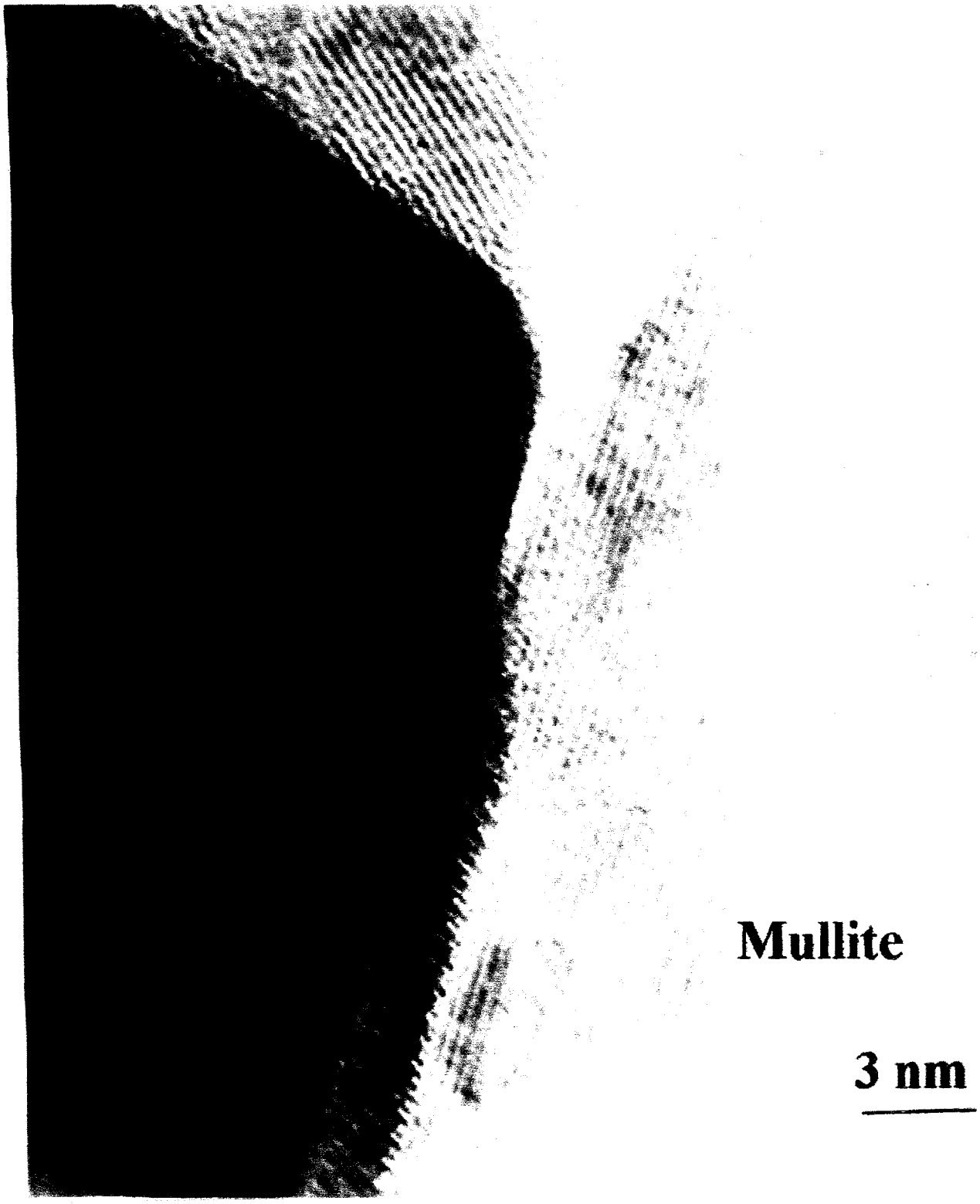

Fig. 9. High resolution TEM micrograph of a MoSi2/Mullite interface.

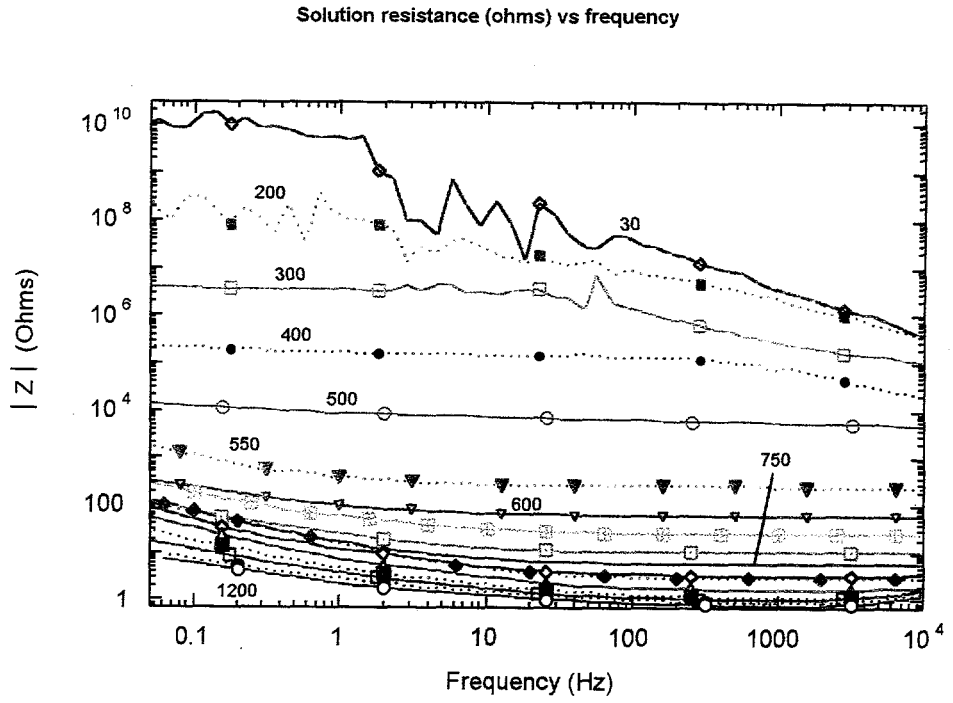

Fig. 10. Bode magnitude plot of the frequency response of glass melt from 30-1200 °C.

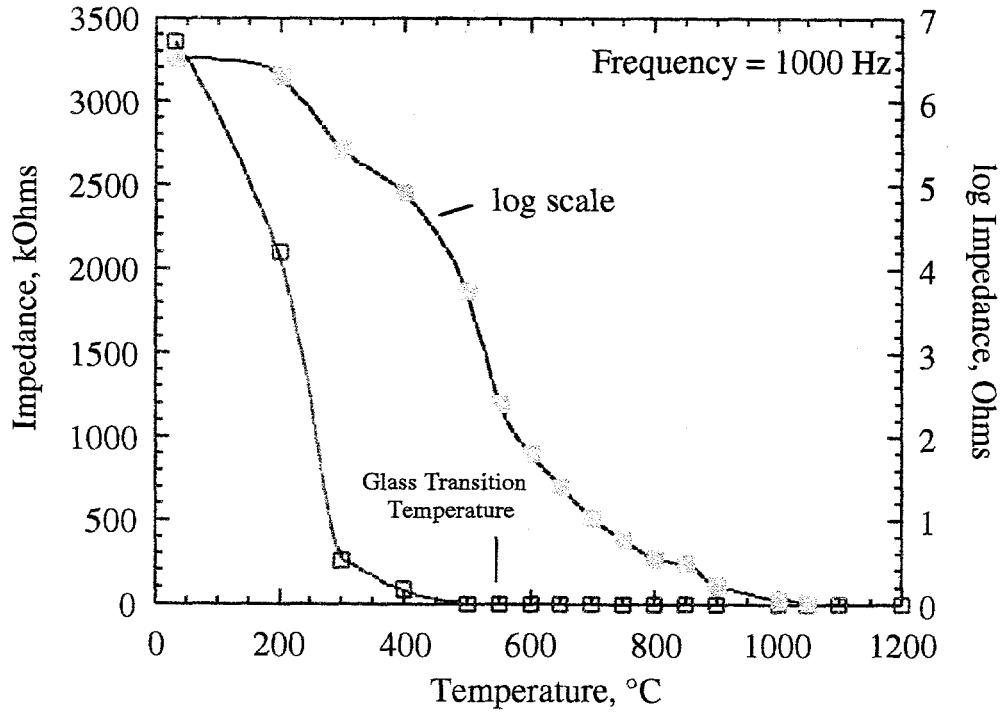

Fig. 11. Glass resistance as a function of temperature measured by electrochemical impedance spectroscopy. Values of impedance were obtained at 100 Hz.

PUBLICATIONS

Journals

H. Kung, R.G. Castro, A.H. Bartlett and J.J. Petrovic, "The Structure of Plasma Sprayed $MoSi_2$ - Al_2O_3 Microlaminate Tubes," *Scripta Metall. Mater.*, 32, 179 (1995).

A.H. Bartlett, R.G. Castro, D.P. Butt, H. Kung, J.J. Petrovic, and Z. Zurecki,"Plasma-Sprayed $MoSi_2$-Al_2O_3 Laminate Composite Tubes as Lances in Pyrometallurgical Operations," *Industrial Heating, J. of Thermal. Tech.*, 63, 33 (1996).

J.J. Petrovic, H. Kung and M.I. Pena,"Fabrication and Microstructures Of $MoSi_2$ Reinforced-Si_3N_4 Matrix Composites," *Journal of American Ceramic Society* (1996).

H. Kung, Y-C. Lu, A.H. Bartlett, R.G. Castro, and J.J. Petrovic,"Structural Characterization of Combustion Synthesized $MoSi_2$-Si_3N_4 Composite Powders and Plasma Sprayed $MoSi_2$-Si_3N_4 Composites," submitted to *Journal of Materials Research* (1996).

J.J. Petrovic, M.I. Pena, I.E. Reimanis, M.S. Sandlin, S. Conzone, and H. Kung,"Mechanical Behavior Of $MoSi_2$ Reinforced-Si_3N_4 Matrix Composites," submitted to *Journal of American Ceramic Society* (1996).

D. P. Butt, D. A. Korzekwa, S. A. Maloy, H. Kung, and J. J. Petrovic, "Impression Creep Behavior of SiC Particle-$MoSi_2$ Composites," *J. Mater. Res.*, **11** [6], 1528-1536 (1996).

D. P. Butt, D. Albert, and T. Taylor, "Kinetics of Thermal Oxidation of Silicon Nitride Powders," *J. Am. Ceram. Soc.*, **79** [11] 1996, in print.

R. U. Vaidya, A. H. Bartlett, H. H. Kung, and D. P. Butt, "Joining of $MoSi_2$ to Itself and Reactions with Aluminum Interlayers," submitted to *J. Mater. Sci.*, 1996.

S. D. Conzone, A. Bartlett, and D. P. Butt, "Joining $MoSi_2$ to 316L Stainless Steel," submitted *to J. Mater. Sci.*, 1996.

R. U. Vaidya, A. H. Bartlett, S. D. Conzone, and D. P. Butt, "Joining $MoSi_2$ to 316L Stainless Steel," in *Ceramic Transactions, Ceramic Joining and Interfaces*, Ed. I. Reimanis, American Ceramic Society, Westerville, OH, 1996, in print.

"Elevated Temperature Mechanical Properties of $MoSi_2/Si_3N_4$, $MoSi_2$/SiC Composites Produced by Self-Propagating High Temperature Synthesis", A.H. Bartlett, R.G. Castro, submitted to the *Journal of Materials Science*.

"High Temperature Deformation and Damage of Plasma-Sprayed Layered $MoSi_2/Al_2O_3$ Beams", A.H. Bartlett and R.G. Castro, submitted to *Acta Materialia*.

Other Publications

R.U. Vaidya, A.H. Bartlett, S.D. Conzone, D.P. Butt,"Investigations into the Joining of $MoSi_2$ to 316L Stainless Steel," Proceedings of the 98th Annual Meeting of the American Ceramic Society, Ceramic Joining Symposium (1996).

A.H. Bartlett, R.G. Castro, K.J. Hollis,"Residual Stress in Net-Shape Plasma Sprayed Tubes: Measurement, Modeling and Modification," Proceedings of the 9th National Thermal Spray Conference, 1996.

K.J. Hollis, A.H. Bartlett, R.G. Castro, R.A. Neiser, "Investigation of the Silicon Loss in APS $MoSi_2$ Under Typical Spray Conditions," *Thermal Spray: Practical Solutions for Engineering Problems*, C.C. Berndt (Ed.), ASM International, Materials Park, OH, pp. 429-437.

PRESENTATIONS

Invited Presentations

J.J. Petrovic, M.I. Pena, M.S. Sandlin, H.H. Kung, "Silicon Nitride-Molybdenum Disilicide Composites," Symposium on Covalent Ceramics, Fall 1996 MRS Meeting, Boston, Massachusetts.

A.H. Bartlett, "$MoSi_2$ and $MoSi_2$ Composites: Microstructures, Mechanical Properties, and Residual Stress," Colorado School of Mines, April 1996.

Other Presentations

A.H. Bartlett, "Residual Stress Generation during Net-Shape Plasma Spray Forming: Characterization and Modeling," 98th Annual American Ceramic Society Meeting, April 1996, Indianapolis, Indiana.

A.H. Bartlett, "Residual Stress in Net-Shape Plasma Sprayed Tubes: Measurement, Modeling and Modification," 8th Annual NTSC Meeting, October 1996.

K.J. Hollis, A.H. Bartlett, R.G. Castro, R.A. Neiser, "Investigation of the Silicon Loss in APS $MoSi_2$ Under Typical Spray Conditions," 9th National Thermal Spray Conference, October 1996.

HONORS AND AWARDS

R.G. Castro and J.J. Petrovic, Los Alamos National Laboratory Technology Transfer Recognition Award, October 1995.

J.J. Petrovic inducted as a Fellow of ASM International, for "Pioneering Contributions to the Science and Technology of Advanced Structural Silicides and Ceramics," October 1995.

INDUSTRIAL INPUT AND TECHNOLOGY TRANSFER

Institute of Gas Technology (IGT) - On 21 November 1995, representatives of the Institute of Gas Technology (IGT) visited the Los Alamos National Laboratory, to begin discussions of potential interactions. On August 23, 1996 a visit was made to IGT to discuss potential collaborative research on the use on $MoSi_2$-based composites for heat treating furnace applications. Discussions focused specifically on the use of $MoSi_2$ composites for high temperature composite radiant tubes and for applications in low-inertia furnaces for heat-treating and drying. Attending the meeting were Richard Castro from LANL and Pete Angelini from ORNL. Representatives from IGT were Dr. Hamid A. Abbasi, Dr. Mark J. Khinkis and Mr Lawrence Fedder. A follow-up meeting is being planned to identify specific components which could be fabricated at LANL and tested at IGT's industrial heat treating test facility.

Exotherm Corporation - On 5 December 1995, a meeting was held with the Exotherm Corporation to discuss Los Alamos results on the plasma sprayed and hot pressed $MoSi_2$-Si_3N_4 powders which were produced by the self-propagating high temperature synthesis (SHS) process developed by Exotherm. Discussions focused on optimizing the SHS process for producing optimum powder feedstock for both plasma spraying and conventional powder consolidation processes. Investigations to reduce agglomerated Si_3N_4 particles in $MoSi_2$, and to improve the retention of Si_3N_4 in $MoSi_2$ during the SHS process will continue jointly between LANL and Exotherm.

Evaluations of new and improved Exotherm $MoSi_2$-Si_3N_4 powders are being conducted by LANL. These powders include composite powders of $MoSi_2$-Al_2O_3, $MoSi_2$-Mullite, and Mo_5Si_3 with boron.

Materials Resource Inc. - On 5 December 1995, a meeting was held with Dr. Ronald Smith of Materials Resource Inc. (a small business involved in the spray-forming of unique materials for high temperature applications), to discuss a Phase I STTR research proposal for developing spray-formed $MoSi_2$ fuel burners for applications in the U.S. glass industry. Discussions focused on potential licensing of current LANL/DOE patents on $MoSi_2$ and $MoSi_2$ composites which could be applied by spray-forming technology.

A.P. Green Industries, Inc. - A proprietary information agreement was signed with A.P. Green Industries, to investigate and develop a method of production of insulating refractory aggregate by energy intensive methods such as plasma and flame spraying. This aggregate will be used as a raw material in refractory products such as insulating castables, insulating brick, and insulating plastics. LANL has performed preliminary investigations on the feasibility of using plasma spraying on insulating refractory aggregate supplied by A.P. Green.

Finkel and Sons - On August 21-22, 1996 a visit was made to Finkel and Sons Forging in Chicago to discuss with members of the Forging Industry Vision Team their materials needs for the future. This visit was done as part of a DOE assessment to help develop and assist the Forging Industry in formulating their vision plan for the future. Presentations were given by a number of forging representatives which included: Finkel & Sons Co., Eaton Corp, Ladish Co., Inc. United Defense/FMC and Erie Press Systems. National Laboratory representatives were present to answer questions and provide information on technology which may be available within the National

Laboratory's to assist the forging industry. Some of the issues which were discussed included the use of new materials with improved compositions, properties and formability which could be used in the forging process and in primary forming equipment.

UNIFORM-DROPLET SPRAY FORMING

Craig A. Blue and Vinod K. Sikka

Metals and Cerarnics Division
Oak Ridge National Laboratory
P.O. Box 2008
Oak Ridge, Tennessee 37831 -6083

with
Jung-Hoon Chun
Laboratory of Manufacturing and Productivity
Massachusetts Institute of Technology
77 Massachusetts Avenue
Cambridge, Massachusetts 02139

and
Teiichi Ando
Department of Mechanical Engineering
Tufts University
Medford, Massachusetts 02155

INTRODUCTION

The uniform-droplet process is a new method of liquid-metal atomization that results in single droplets that can be used to produce mono-size powders or sprayed-on to substrates to produce near-net shapes with tailored microstructure The mono-sized powder-production capability of the uniform-droplet process also has the potential of permitting engineered powder blends to produce components of controlled porosity. Metal and alloy powders are commercially produced by at least three different methods: gas atomization, water atomization, and rotating disk. All three methods produce powders of a broad range in size with a very small yield of fine powders with single-sized droplets that can be used to produce mono-size powders or sprayed-on substrates to produce near-net shapes with tailored microstructures. The economical analysis has shown the process to have the potential of reducing capital cost by 50% and operating cost by 37.5% when applied to powder making. For the spray-forming process, a 25% savings is expected in both the capital and operating costs. The project is jointly carried out at Massachusetts Institute of Technology (MIT), Tuffs University, and Oak Ridge National Laboratory (ORNL). Preliminary interactions with both finished parts and powder producers have shown a strong interest in the uniform-droplet process. Systematic studies are being conducted to optimize the process parameters, understand the solidification of droplets and spray deposits, and develop a uniform-droplet-system (UDS) apparatus appropriate for processing engineering alloys.

OAK RIDGE NATIONAL LABORATORY

TECHNICAL PROGRESS - FY 1996

Summary

The uniform-droplet program requires that three droplet heating systems, one for low-temperature metals (Tm< 400°C), one for medium-temperature metals (Tm 400 to 1250°C), and one for high-temperature metals (Tm 1250 to 1650°C) be assembled. The fabrication of the low-temperature system provided a basis for the design of the mediumtemperature unit. The apparatus consists of a vacuum chamber, melt furnace for the crucible, melt-temperature-control system, pressure-control system, melt-vibration system, droplet-charging assembly, jet-monitoring system, and supporting structures.

Construction of the low-temperature UDS at ORNL is completed. Over 80 runs have been completed to date, and further tailoring of this system is ongoing. The tailoring of the system includes elimination of orifice clogging and large-diameter uniform-droplet formation (> 750 Em). The large-diameter work was accomplished in line with the possible development of a new additional funding source.

Low-Temperature System Results

All of the initial experimentation with the low-temperature system utilized tin as the material of choice. The operating parameters for the experiment included: 300+°C melt temperature, 103-kPa crucible/chamber pressure difference, 10-kHz perturbation frequency, 100-m orifice diameter, and a dc charge plate voltage of 400 V. Sizedistribution data revealed an average diameter of 1681lm and a standard deviation of 2 1lm. As can be seen by the scanning electron micrographs and the size-distribution data, the produced powder is very uniform.

Medium-Temperature System

The medium-temperature apparatus has been completely assembled, and testing is under way. This system will allow for the fabrication of uniform droplet of materials with melting points as high as 1250°C. Also, this system was designed for higher volume melts (15 to 20 lb/materials dependent). Therefore, this system will aid in the development of the UDS for industrial practices. Also, a drop tower has been erected in order to solidify larger-diameter droplets and is shown in Fig. 1.

Substantial increases in spray temperature have been accomplished in this quarter. Both aluminum, copper-phosphorus, and copper materials have been successfully sprayed. Figure 2 shows the micrograph of sprayed aluminum material.

Initial results for the aluminum and bronze spraying are extremely encouraging. Microstructural analysis of the sprayed aluminum and size-distribution analysis are being accomplished. The initial problem encountered when spraying high-temperature materials included charging of the droplets, but this has been resolved; analysis of these powders will be forth coming in the first quarter of FY 1997.

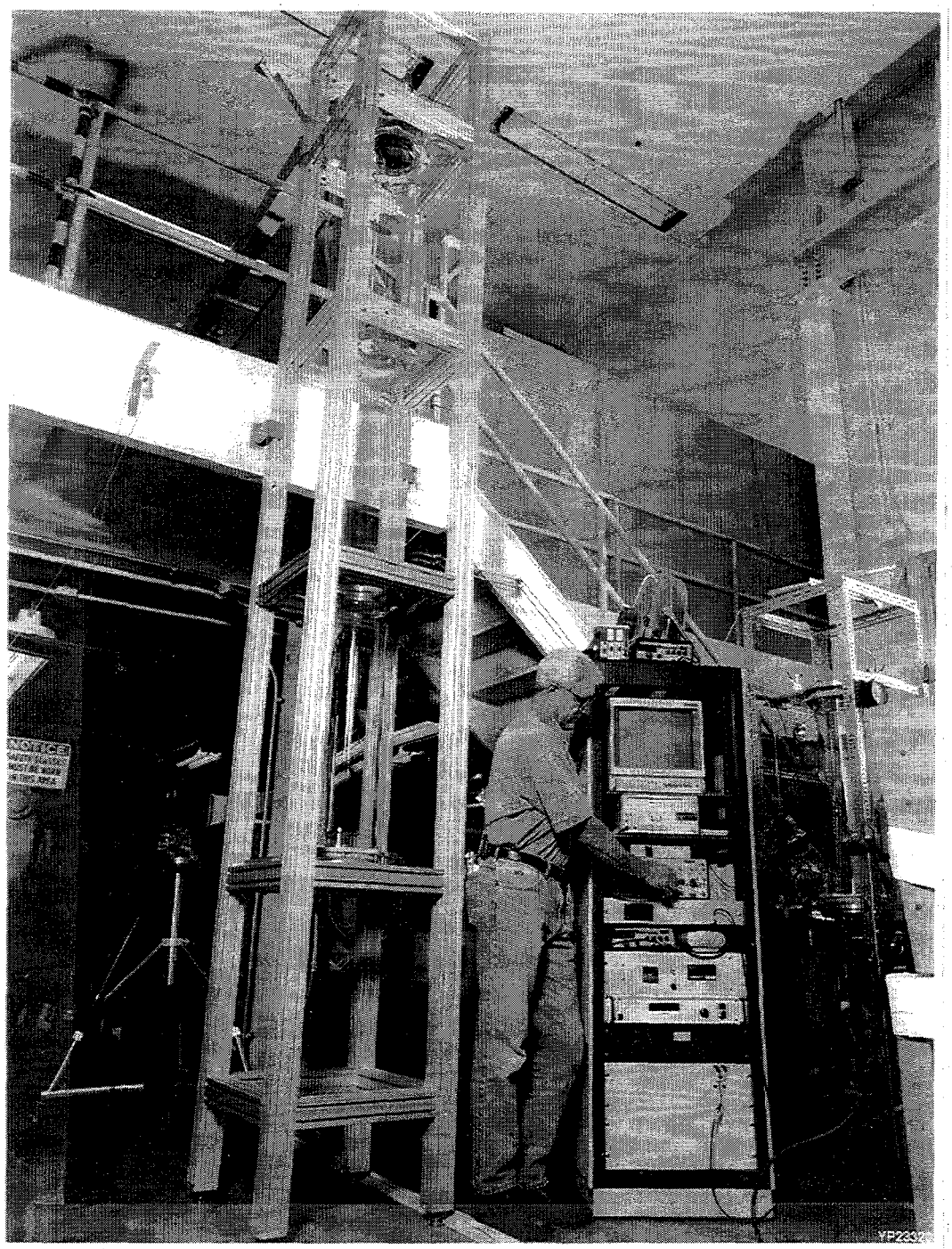

Fig. 1. Uniform-droplet system at the Oak Ridge National Laboratory for solidifying larger droplets.

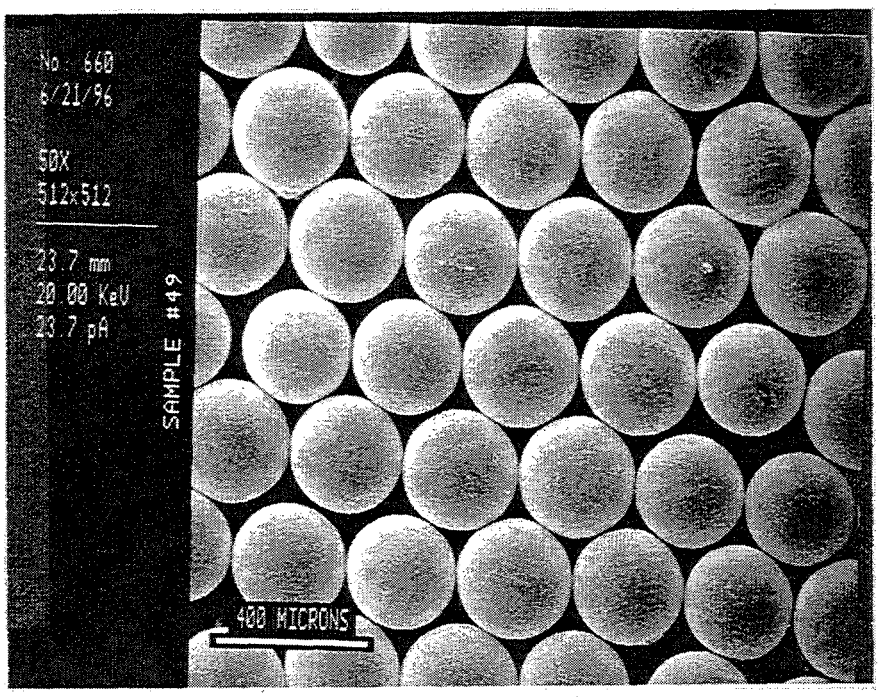

Fig. 2. Scanning electron micrograph of uniform aluminum-powder droplets produced by the Oak Ridge National Laboratory uniform-droplet spray-forming experimental facility.

MASSACHUSETTS INSTITUTE OF TECHNOLOGY*

Optimization of Process Parameters for the Development of the Uniform-Droplet Spray Process

Technical Progress (FY 1996)

In this second year of research, we have made continuous progress towards developing UDS processes for industrial applications. We have built on our knowledge gained in the previous year to better understand how process parameters affect the final spray-formed deposit microstructure. One of our goals is to apply the UDS process to near-net-shape spray forming with engineering alloys such as aluminum and bronze. Another objective is to establish an on-line, closed-loop control system to monitor and adjust the droplet-size distribution during spray forming. Further details regarding progress on this year's tasks are outlined below.

*Personnel at M1T are Prof. Jung-Hoon Chun, Principal Investigator, and two M.S. students, Jean-Pei Cherng and Ho-Young Kim.

Task 1. Study of the Impact Behavior of Uniform Droplets

(1) Droplet Solidification and Its Effect on Deposit Microstructure

Microstructure evolution in the UDS process can be divided into three stages: droplet solidification in-flight; droplet impact; and postimpact evolution. Droplet thermal states, characterized by the degree of undercooking in undercooked droplets or by the liquid fraction and morphology of solids in partially solidified droplets, can have a great influence on droplet-impact behavior and postimpact microstructure evolution. A numerical simulation model that predicts the thermal state of a droplet in which no undercooking occurs during flight was developed. This model was validated by measuring the liquid fraction of 288-m droplets of Zn-20 wt % Sn alloy at different flight distances (see item 1 in PUBLICATIONS section). Experimental work also concluded that as droplet size decreases, the population of undercooled droplets, degree of undercooking, and tendency to nucleate internally all increase.

(2) Droplet-Impact Behavior

Droplet-impact behavior affects how splats coalesce and bond with the deposit to produce the final deposit microstructure. Droplet consolidation will also determine the surface porosity and geometric conformity to substrate shapes. Microsensors are being developed and tested to measure the transient-spreading behavior of a droplet. The sensor design is based on very fine electrical-resistance networks mounted on a substrate. Initially, the circuit has infinite resistance, but the networks become connected as a droplet impacts and spreads on the sensor surface. Thus, the transient change in electrical resistance of the total circuit can be correlated with the growth area of the spreading droplets.

Preliminary tests with a pure tin droplet deposited on different sensor materials (i.e., aluminum, polycrystalline silicon, copper, and gold) showed that high-electrical resistivity, good electrical contact, and good wetting with the splats are required. Therefore, gold, a material least likely to oxidize, has been selected for the sensor material. We have had success in capturing the transient spreading signal of a pure tin droplet deposited manually on a gold sensor in the atmospheric condition. The next steps are to deposit a droplet with the UDS process onto a sensor within the inert-gas environment and capture its transient-spreading signal. Because the UDS process allows for precise control of the droplet's size, velocity, and thermal state upon impact, the dynamics of droplet spreading can be studied systematically

Task 2. Applications to Engineering Alloys and Processes

(1) Characterization of the Aluminum Droplet Spray

Preliminary attempts made last year to spray uniform droplets of aluminum with a 100-1lm orifice produced erratic, jumpy-stream behavior and unstable break-up. This problem was attributed to the oxidation of the molten aluminum. It was hypothesized that the stream flow was disrupted by oxide inclusions that formed in the melt and on the surface of the stream as it exited from the orifice. Persistent clogging of the orifice even with ceramic filters led to the spraying of aluminum with a

to decrease the level of oxygen in the chamber. The gas-purification system now consists of a molecular sieve and desicator for trapping H20 and a sponge titanium furnace heated to about 800°C to remove H20 and °2 from the gas in the spray chamber. The oxygen content in the chamber was reduced by nearly two orders of magnitude by these means. As a result, uniform break-up of an aluminum alloy was achieved with 150 and 200-1lm orifices. The larger orifice diameter not only stabilizes the stream of molten aluminum but also increases the mass flux of the spray, which was measured to be about 0.25 g/s for a 150-m orifice. Currently, experiments are being conducted to characterize the aluminum spray by measuring the droplet-thermal states as a function of flight distance. The droplet-thermal state can then be used as an input parameter to produce fine-equiaxed-deposit microstructure Future work involves adding multiple orifices to the UDS apparatus to increase throughput capability for the fabrication of aluminum sheet.

(2) Production of Uniform Solder Balls

The work done concerning the use of the UDS apparatus to produce uniform solder balls has focused on improving geometric accuracy (i.e., mean size, size distribution, and sphericity). It has been proved that the ball diameter is determined by the driving frequency, jet velocity, and orifice diameter (see item 2 in PUBLICATIONS section). Therefore, our efforts are first centered on controlling and monitoring these parameters. The jet of molten metal is forced to break up into droplets by perturbations generated from a stack of piezoelectric crystals. It was observed that noise variation in the electric signal sent to the crystals has a significant effect on the output of the crystals. Hence, an in-situ monitoring device for the output of the vibration system has been developed. Through this device, we can ensure that constant frequency and vibration amplitude are maintained during a production run despite noise or signal variations. Future work will address how to control the effect of driving pressure on jet velocity. The overall goal is to achieve closed-loop control of the UDS process by monitoring the output and correlating it to the inputs.

TUFTS UNIVERSITY*

Process-Structure Relationship in the Uniform-Droplet Spray Process Objective

The objective of the work at Tufts University is to characterize the solidification and microstructural evolution in the UDS process through experimentation and modeling, with the eventual goal of developing novel microstructures by the UDS process in a controlled manner. The first year of the study is focused on the solidification of the traveling uniform droplets, although the solidification and microstructural evolution in the spray deposit are also to be investigated.

*Personnel at Tufts are Prof. Teiichi Ando, Principal Investigator, Rajesh Shingavi, Alfred DiVenuti, and Charles Tuffile (three M.S. students), Tina Notosoehardjo and Mona Masghati (two B.S. students), and Prof. Anil Saigal, who participates in the project through advising the students. Partial support for Shingavi, DiVenuti, and Tuffile is provided through this grant from the Advanced Industrial Materials (AIM) Program of the U.S. Department of Energy.

Technical Progress (FY 1996)

Summary

Our tasks in the proposed work at Tufts University are comprised of three elements to achieve the eventual goal of developing UDS processes for industrial applications. These include: (1) fundamentals of the UDS process, (2) applications to engineering alloys and processes, and (3) apparatus modifications.

Task 1. Study of the Nonequilibrium Solidification of Traveling Droplets

The in-flight thermal state of traveling uniform droplets is the single most important parameter that affects the microstructure of the material produced by the UDS process, whether it is in the powder or deposit form. A nonadiabatic calorimetric method and an apparatus have been developed to measure droplet-enthalpy values over a range of flight distances. Preliminary results with a Sn-5% Pb alloy showed good agreement between experimentally determined droplet-enthalpy values and theoretical values calculated with a model we are developing. Figure 3 shows the nonadiabatic calorimeter.

Modeling of the in-flight solidification of the traveling uniform droplets has been progressed with the particular objective of accounting for the large, prior undercoolings encountered in the UDS process. We have derived a set of expressions for the solidification in a highly undercooked droplet of a binary alloy. These equations are being solved simultaneously with an iterative technique for the dendrite growth velocity, tip radius, and interfacial solute concentrations for high undercoolings. So far, we have solved them for the case of a straight solidus and a liquidus for a tin-5 wt % lead alloy. The results of preliminary calculations were presented at the 1996 Advanced Industrial Materials Annual Meeting held in Oak Ridge, Tennessee last June.

Tasks 2 and 3. Applications to Engineering Alloys and System Modifications

In order to extend the capabilities of the UDS process to aluminum and other engineering alloys, a high-temperature UDS apparatus has been designed, and the construction of this unit is in progress. The unit consists of five subsystems: (1) crucibleheater assembly, (2) melt-vibration assembly, (3) high-temperature insulation package, (4) heat exchanger, and (5) droplet-charging system. The first of these subsystems consists of a flanged 710 graphite crucible and a molybdenum band heater rated to 1600°C.

A UDS deposition chamber has been designed to expand the range of materials processing capabilities to encompass the manufacture of metaValloy strips and controlledmicrostructure deposits. An aluminum chamber measuring approximately 2 ft cube has been designed to vacuum pressures below 100 mtorr. A controlled substrate deposition system has been designed consisting of two linear-motion control tables powered by dc stepper motors. Motor velocity and position are determined by optical encoders, and control is implemented using an MCBasic motion control package and cascaded single-axis servo controllers. The substrate temperature can be controlled by water circulation or arrays of thermoelectric cooling modules.

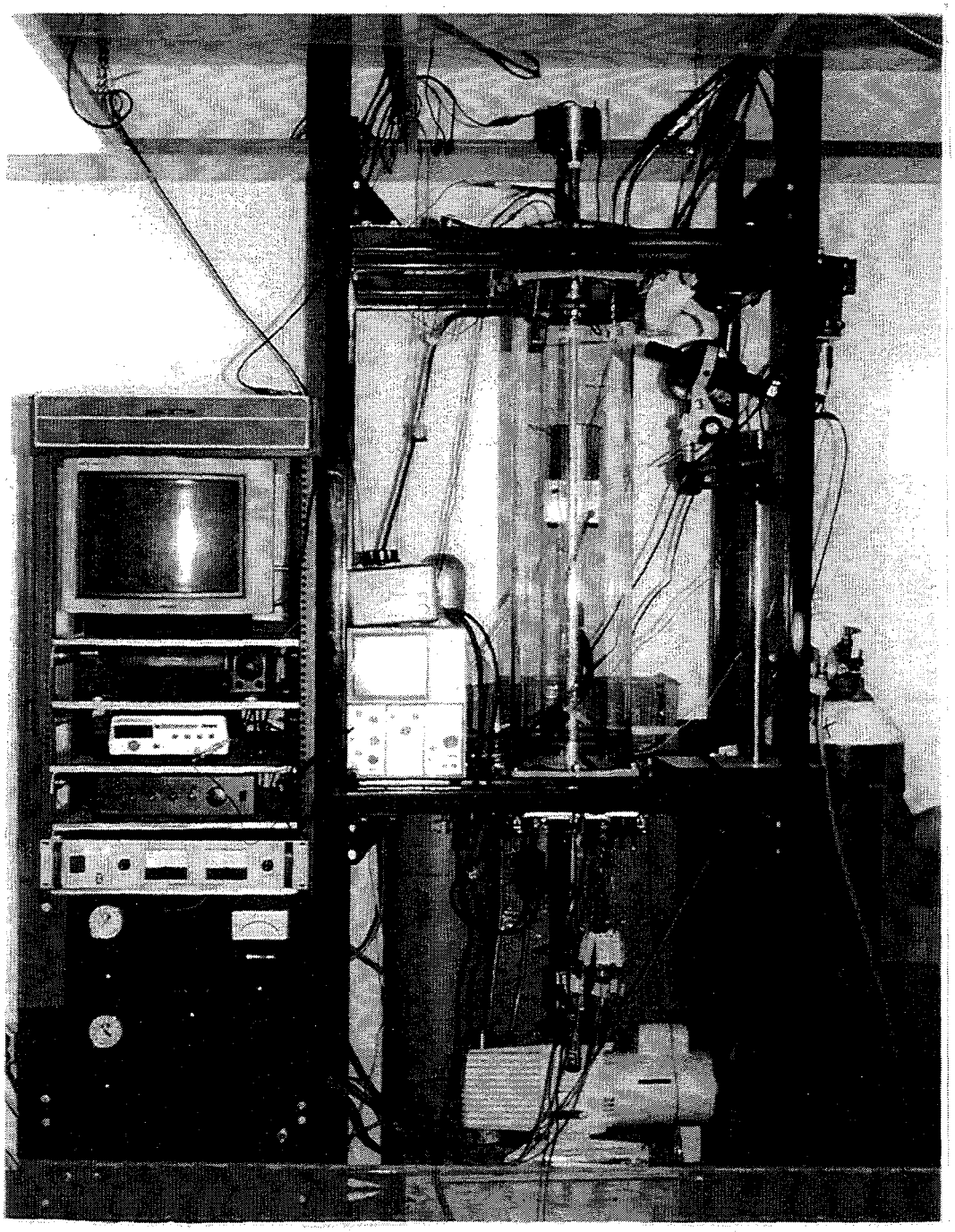

Fig. 3. Nonadiabatic calorimetric apparatus located at Tufts University, Medford, Massachusetts.

PUBLICATIONS

1. C.-A. Chen, "Droplet Solidification and Its Effect on Deposit Microstructure in the Uniform Droplet Spray Process," PhD Thesis, Department of Mechanical Engineering, Massachusetts Institute of Technology, 1996.

2. P. Yim, "The Role of Surface Oxidation in the Break-Up of Laminar Liquid Metal Jets," Ph.D. Thesis, Department of Mechanical Engineering, Massachusetts Institute of Technology, 1996.

INTERACTION WITH INDUSTRY

The Droplet-Based Manufacturing Research Program Meeting was held on June 28, 1996, at MIT to foster collaboration with industry and review current progress. The attendees from industry are listed below.

Mr. Richard Aubin, Manager of Rapid Manufacturing, United Technology Research Center.
Ms. Sara Dillich, Program Manager, Advanced Industrial Concept Division, U . S . Department of Energy.
Mr. Richard Foulke, President, Ultra Clean International Corp. Mr. Frank Haas, Senior Engineer, Aeroquip Corporation;
Mr. Hoang Hoang, Motorola.
Mr. Ken Johnson, National Center for Manufacturing Sciences.
Mr. James Ingram, President, Micro Engineering (on-site visit to ORNL for one week). Mr. Cord Ohlenbusch, Senior Engineer, Ultra Clean International Corp.
Dr. John Pien, Technical Specialist, Alcoa Aluminum Company.
Dr. Atul Sudhalkar, Associate Engineer, Aeroquip Corporation.
Prof. Ampere Tseng, Adv. Manufacturing Processing Laboratory, Arizona State University.
Mr. Krishna Patel, ACuPowder International, has utilized bronze powder produced at ORNL and was extremely pleased. This company is interested in technology transfer.
Mr. Frank Rauch, FMC Chemical Products Group, visited ORNL and is presently looking to transfer the technology for lithium.
Dr. James F. Ingram, Micro Engineering, visited ORNL for one week to observe the UDS process.

PRESENTATIONS

None.

HONORS AND AWARDS

None.

PATENTS/DISCLOSURES

None.

LICENSES

None.

ADVANCED CERAMICS
AND
COMPOSITES

ADVANCED METHODS FOR PROCESSING CERAMICS

W.B. Carter

School of Materials Science and Engineering
Georgia Institute of Technology
Atlanta, GA 30332-0245

INTRODUCTION

Combustion chemical vapor deposition (combustion CVD) is being developed for the deposition of high temperature oxide coatings. The process is being evaluated as an alternative to more capital intensive conventional coating processes. The thrusts during this reporting period were the development of the combustion CVD process for depositing lanthanum monazite, the determination of the influence of aerosol size on coating morphology, the incorporation of combustion CVD coatings into thermal barrier coatings (TBCs) and related oxidation research, and continued work on the deposition of zirconia-yttria coatings.

TECHNICAL PROGRESS - FY 1996

1. $LaPO_4$ Coatings

Lanthanum monazite ($LaPO_4$) has been identified as a possible weak phase material for use in alumina-alumina continuous fiber ceramic composites (CFCCs). Coatings of weak phase material on the reinforcement fibers serve to toughen such composites by causing crack deflection along the fiber-matrix interface.

Lanthanum monazite was successfully deposited onto single crystal sapphire (Al_2O_3) substrates via liquid fuel combustion CVD. Table 1 lists the process parameters that produced the best results. As displayed in the table, a mixture of toluene and ethanol was used as the solvent. Ethanol was required to dissolve the lanthanum nitrate hexahydrate, which would not dissolve substantially in toluene. The use of toluene was necessitated by the need to reach higher deposition temperatures than could be obtained using ethanol alone. Triphenylphosphine dissolves in both liquids.

2. Aerosol Size Effects

The effects of aerosol droplet size, solution concentration, precursor volatility, and deposition temperature on the surface morphology of ceria (CeO_2) combustion CVD coatings were investigated by G.W. Book and reported in his Ph.D. thesis (graduation summer 1996). Ceria coatings were deposited onto single crystal alumina substrates via combustion chemical vapor deposition using toluene as a solvent and Tetrakis(2,2,6,6-tetramethyl-3,5-haptanedionato)cerium [Ce-$(TMHD)_4$] and Ce (III) 2-ethylhexanoate [Ce-EH] as precursors. Depositions were made using aerosols of three droplet size distributions and the resulting film morphologies quantified. An oscillating capillary nebulizer (OCN) was used to control the aerosol droplet size distribution. Characteristic features of the film morphologies include faceted grains attached to the substrate and polycrystalline particle

clusters. Larger aerosols, higher precursor concentrations, and use of the lower vapor pressure precursor Ce-EH promote the formation of clusters. Vapor phase deposition is favored by the use of smaller aerosols, lower precursor concentrations, and use of the higher vapor pressure precursor Ce-$(TMHD)_4$.

The clusters apparently result from processes in the flame involving the larger aerosol droplets. It is believed that heterogeneous nucleation and growth (vapor phase deposition) are responsible for the larger faceted grains observed in some coatings. Clusters appear to grow by a vapor phase growth process after being deposited. A simple phenomenological model was developed that relates the size distribution of clusters on the coatings to the aerosol size distribution and precursor concentration. The model assumes that a cluster forms in the flame when the product of the cube of an aerosol droplet's diameter and the precursor concentration exceeds a critical value, which depends on reagent and deposition temperature. Deposited clusters grow due to vapor deposition.

Solvent	80% Toluene, 20% Ethanol
Reagents	Triphenylphosphine Lanthanum Nitrate Hexahydrate
P:La Stoichiometry	4:1
Molarity (mol/liter)	0.001
Solution Flow Rate (ml/min)	4
Oxidizer	Oxygen
Oxidizer Flow Rate (l/min)	6.2
Deposition Temperature (°C)	1100
Sample Stage Temperature (°C)	550
Substrate	Polished, A-axis Sapphire
Pilot Flame Fuel	Natural Gas

Table 1. Optimized Process Parameters for theCombustion CVD Deposition of $LaPO_4$ Coatings

For a given reagent and deposition temperature, the size distribution of clusters in a film can be approximated by:

$$f\,(d_{cluster}) \propto v * \int_{\tau=0}^{\tau=t} [\mathrm{K}(d_{cluster} - 2G\tau)]^3 u[\mathrm{K}(d_{cluster} - 2G\tau) - d^*_{drop}]\xi[\mathrm{K}(d_{cluster} - 2G\tau)]d\tau$$

where

$f\,(d_{cluster})$ is the cluster size distribution on the film in number of clusters with diameters between $d_{cluster}$ and $d_{cluster} + \Delta\, d_{cluster}$,
$d_{cluster}$ is the cluster diameter,
v is the velocity of the fluid as it exits the OCN,
t is the deposition time in seconds,

K is the proportionality constant relating the initial diameter of a cluster to the diameter of the aerosol droplet from which it formed,
$u[x]$ is the unit step function ($u[x] = 0, x < 0$; $u[x] = 1, x > 0$),
d^*_{drop} is the diameter of the smallest aerosol droplet capable of producing a cluster and is a function of c, as discussed above ($d^{*3}_{drop}c = (d^3_{drop}c)^*$),
G is the deposition rate in μm/hr and is proportional to the volume of aerosol in droplets with diameters less than d^*_{drop}, and
$\xi(d)$ is the aerosol size distribution in number of droplets with diameters between d and $d + \Delta d$ emitted per unit time.

3. Thermal Barrier Coatings/Oxidation Protection

Combustion CVD coatings were incorporated into thermal barrier coatings and subjected to furnace cycle testing. Either ceria or theta alumina was deposited via combustion CVD directly onto NiCrAlY bond coated single crystal N5 substrates. Some of the alumina coated specimens were then vacuum annealed for four hours at 1080°C. Afterwards, all specimens were air plasma sprayed with 8 wt. % yttria stabilized zirconia. Control and modified TBC specimens were furnace cycle tested in air to 1093°C. Table 2 displays the results. Detailed microstructural characterization of the failed TBCs is being conducted.

Thermogravimetric analysis at 800, 900, 1000, and 1100°C was used to evaluate the oxidation protection provided Ni-20Cr substrates by combustion CVD alumina coatings. The decrease in the oxidation rate at all temperatures was attributed to both a decrease in the amount of NiO formed and a Cr_2O_3 scale that thickened more slowly with the alumina present. These results are consistent with aluminum serving as a reactive element in the system.

Interlayer Material	Average Cycles to Failure
Control (no interlayer)	1118
Ceria	745
Alumina	1111
Alumina (vacuum annealed)	1825

Table 2. Furnace Cycle Lifetimes of Combustion CVD Modified TBCs

4. Zirconia-Yttria Coatings

The effects of solution concentration on zirconia/yttria coatings produced by liquid fuel combustion CVD were reported by S. Godfrey in her M.S. thesis (graduation winter 1996). Precursors of zirconium and yttrium 2-ethylhexanoate dissolved in toluene were used to deposit coatings of various stoichiometries. A simple right angle pneumatic nebulizer (perfume sprayer type) fed with oxygen was used to atomize the solution, which was combusted with the help of a propane pilot flame. Solutions containing total precursor concentrations (Zr + Y cations) of 0.02 molar and 0.005

molar were investigated by varying the Y:Zr cation stoichiometry and maintaining all other deposition conditions constant. Substrates were A-axis oriented sapphire (alumina). Table 3 lists the deposition conditions.

Electron diffraction patterns indicated that solutions containing 2.5 and 7.5 mol % yttrium 2-ethylhexanoate (bal. Zr 2-ethylhexanoate) using the larger precursor concentration produced coatings with a higher yttria content than did those deposited using the lower concentration. Energy dispersive spectroscopy (EDS) data taken in the transmission electron microscope supported these results. These observations have not been explained.

Solvent	Toluene
Precursors	Zr & Y 2-ethylhexanoates
Y:Zr solution molar ratios	0.025, 0.05, 0.075
Total cation concentration (mol/l)*	0.005 & 0.02
Solution flow rate (ml/s)	0.11
Oxygen flow rate (ml/s)	~50
Substrates	A-axis sapphire (~0.05x1x1 cm)
Deposition temperature(°C)**	1300 ± 100

* Concentration of Y+Zr in solution.

** As indicated by a thermocouple occasionally placed near the front surface of the substrate during deposition.

Table 3. Process Parameters for Depositing Zirconia-Yttria

MILESTONES

AIM Program FY 1996 Milestone - Deposition of lanthanum phosphate via combustion chemical vapor deposition. This milestone was satisfied by:

"Deposition of (La)-Monazite by Combustion Chemical Vapor Deposition" reported by J.L. Satterwhite, T.A. Polley, and W.B. Carter at the 1996 International Conference on Metallurgical Coatings and Thin Films, San Diego, CA, 25 April 1996.

PUBLICATIONS

Other Publications

1. S. Godfrey, "Concentration and Composition Effects in Combustion Chemical Vapor Deposited Yttria-Zirconia," M.S. thesis, Georgia Institute of Technology, December, 1995.

2. M.R. Hendrick, J.M. Hampikian, and W.B. Carter, "High Temperature Oxidation of an Alumina Coated Ni-Base Alloy," to be published in Elevated Temperature Coatings: Science and Technology II, eds. N.B. Dahotre and J.M. Hampikian, TMS, 1996.

3. G.W. Book, "Aerosol Size Effects in Combustion Chemical Vapor Deposition," Ph.D. thesis, Georgia Institute of Technology, July, 1996.

4. J.M. Hampikian, M.R. Hendrick and W.B. Carter, "The Effects of Alumina Coatings on the Oxidation of Ni-20Cr," to be published in Fundamental Aspects of High Temperature Corrosion - VI.

PRESENTATIONS

Oral Presentations

1. M.R. Hendrick, J.M. Hampikian, and W.B. Carter, "High Temperature Oxidation of an Alumina Coated Ni-Base Alloy," presented at the Symposium on High Temperature Coatings - II, TMS Annual Meeting, Anaheim, CA, Feb. 4-8, 1996.

2. M.R. Hendrick, J.M. Hampikian, and W.B. Carter, "High Temperature Oxidation of an Alumina Coated Ni Based Alloy", Southeastern section of the American Ceramic Society Annual Spring Meeting, March 13-15, 1996.

3. J.L. Satterwhite, T.A. Polley, and W.B. Carter, "Deposition of (La)-Monazite by Combustion Chemical Vapor Deposition," presented at the 1996 International Conference on Metallurgical Coatings and Thin Films, San Diego, CA, 25 April 1996.

4. J.M. Hampikian, M.R. Hendrick, and W.B. Carter, "The Effects of Alumina Coatings on the Oxidation of Ni-20Cr," presented the Electrochemical Society Annual Meeting, San Antonio, TX, October 6-11, 1996.

Poster Presentation

1. W.B. Carter, J.M. Hampikian, G.W. Book, M.R. Hendrick, T.A. Polley and D.W. Stollberg, "Combustion Chemical Vapor Deposited Coatings for Thermal Barrier Coating Systems," invited poster presentation at the Advanced Turbine Systems Materials Workshop, Charleston, SC, February 13-14, 1996.

HONORS AND AWARDS

None

PATENTS/DISCLOSURES

Patent pending: Andrew T. Hunt, Joe K. Cochran, and William Brent Carter, "Method for the Combustion Chemical Vapor Deposition of Films and Coatings," U.S. patent application # 08/036,554 filed 24 March 1993.

LICENSES

None

INDUSTRIAL INPUT and TECHNOLOGY TRANSFER

A concept paper was written with Allison Engine Company (AEC), and others, and submitted to the Office of Naval Research outlining a program to develop thermal barrier coatings (TBCs) incorporating thin films deposited via combustion CVD. Allison is interested in using combustion CVD coatings to modify conventional TBCs. Several combinations of combustion interlayer and overlayer coatings, and various bond coats and ceramic top coats were described. AEC would like to perform a realistic engine/rig test on coated parts in the final year of the proposed three year program.

ESTIMATED ENERGY SAVINGS

The combustion chemical vapor deposition process should reduce energy consumption by replacing conventional coating methods for certain applications. The elimination of furnace and vacuum hardware and their concomitant energy requirements should more than offset the consumption of inexpensive organic solvents and gases. Often, less expensive reagents can be used with combustion CVD than are required for conventional CVD processes. The substantially smaller capital investment anticipated for the combustion CVD process relative to conventional techniques will also entail less energy expenditure up front in equipment production. As the process is presently in the early stages of development and those applications to which it may ultimately be applied are uncertain, it is not possible to produce a quantitative estimate of potential energy savings.

CHARACTERIZATION OF THREE-WAY AUTOMOTIVE CATALYSTS

E. A. Kenik and K. L. More

Oak Ridge National Laboratory
Metals ad Ceramics Division
Oak Ridge, TN 37831-6376

W. LaBarge, R. F. Beckmeyer, J. R. Theis
Delphi Automotive Systems
Flint, MI 48556

INTRODUCTION

The CRADA between Delphi Automotive Systems (Delphi; formerly General Motors - AC Delco Systems) and Lockheed Martin Energy Research (LMER) on automotive catalysts was completed at the end of FY96, after a ten month, no-cost extension. The CRADA was aimed at improved performance and lifetime of noble metal based three-way-catalysts (TWC), which are the primary catalytic system for automotive emission control systems. While these TWC can meet the currently required emission standards, higher than optimum noble metal loadings are often required to meet lifetime requirements. In addition, more stringent emission standards will be imposed in the near future, demanding improved performance and service life from these catalysts. Understanding the changes of TWC conversion efficiency with ageing is a critical need in improving these catalysts. Initially in a fresh catalyst, the active material is often distributed on a very fine scale, approaching single atoms or small atomic clusters. As such, a wide range of analytical techniques have been employed to provide high spatial resolution characterization of the evolving state of the catalytic material.

TECHNICAL PROGRESS - FY 1996

Summary

Three technical review meetings between Delphi and LMER were held in FY96 on 9/6/95 and 8/27/96 in Oak Ridge and on 2/22/96 in Flint, MI. The work reviewed at these meetings included the characterization of the field tested (110,000 km) Tech-III monolith and the new tier of advanced catalytic materials (in both the as-prepared and engine-aged conditions). The latter monoliths were supplied by Delphi in December 1995 and work has concentrated on engine testing and characterization of these advanced catalyst formulations, which include high performance washcoats and different active metal combinations. Characterization has emphasized the application of scanning electron microscopy (SEM), electron probe microanalysis (EPMA), analytical electron microscopy (AEM), and X-ray diffraction. A poster on the CRADA goals and results was presented at the annual AIM program review meeting held in Oak Ridge on June 24-26, 1996. A final report for the CRADA, containing no proprietary or protected CRADA information, was approved by Delphi for public release and submitted before the end of FY96.

MILESTONES

1. Vehicle-Aged Monolith

The Tech-III monolith had been vehicle-aged under normal road conditions for 110,000 km (~68,300 miles). The initial engine exhibited high oil consumption and was replaced at ~15,000 miles. This problem was the probable origin of the severe sintering of the inlet washcoat, the presence of calcium both in discontinuous particles of calcium phosphate glaze (~0.5 m diameter) and generally on the washcoat surface, and may have contributed to the higher poison levels observed. Periodic FTP testing was performed during the field test indicated marginal performance relative to current U.S. standards; however, this was attributed to the less advanced engine/emission controls present on Australian vehicles. Post-ageing FTP tests performed at Delphi on an engine dynamometer of current U.S. standard configuration indicated very good conversion efficiency.

2. Advanced washcoats/poisoning

Advanced catalyst formulations have been provided by Delphi in both as-prepared and engine- aged conditions. The engine ageing was performed under conditions designed to simulate poisoning at higher engine exposures. Both single and double washcoat formulations were studied. The characterization concentrated on the evolution of the catalyst/washcoat microstructure, especially those changes associated with the deactivation and poisoning of the catalysts. Some bulk degradation of the washcoat was observed when the as-prepared and RAT specimens were compared, including cracking and some local loss of washcoat. These washcoats exhibited a heterogeneous mixture of large (5-20 m diameter) Al_2O_3 and CeO_2 aggregates with a finer mixture of these phases (down to <0.2 m diameter). Both of these coarse aggregates were comprised of fine crystallites (γ-Al_2O_3 <5 nm diameter and CeO_2 ~15 nm diameter). The CeO_2 spheres in the as-prepared washcoat were partially sintered to form the larger CeO_2 aggregates.

In addition to the Al_2O_3 and CeO_2 phases, the as-prepared washcoat exhibited the presence of both additional elements and phases. X-ray microanalysis indicated the presence of Group IIA, IIIB, and IVB elements which were distributed in different relative amounts in the Al_2O_3 and CeO_2 phases, as well as other secondary phases. Elemental mapping in the AEM was used to demonstrate the inhomogeneous distribution of elements between the different phases present on the 10-20 nm scale. The association of specific precious metals with certain washcoat phases and certain locations in the washcoat relative to the various interfaces was identified. The presence of poisons on the free surface of the washcoats were confirmed by both EPMA mapping and cross-section TEM specimens. High P levels were associated with most, if not all, of the phases present at the surface of the washcoat (including CeO_2, the IIIB oxide, and a high Al+P phase); whereas high levels of both P and Zn were generally associated with phase(s) enriched in either Ce or the IIA element.

Moderate-sized (~50 nm diameter) heavy metal clusters (HMCs) of Pd were observed in the aged single layer washcoat, primarily in association with Al_2O_3, but also with several other phases (CeO_2, the IIIB oxide, and an Al,P phase). Both essentially pure (~97 wt%) Pd and tri-metal alloy HMCs (10-110 nm diameter) were observed in the aged double layer washcoat. No association of one type of HMC with a specific washcoat layer in the crushed AEM specimens, as a result of the loss of

spatial correlation. However, analytical SEM, EMPA, and transverse section AEM studies allowed these associations to be identified. On average, the alloy HMCs were smaller than the Pd HMCs. The alloy HMCs contained about 10 wt% Pd and the Pt/Rh increased from 0.1 to 1.2 as a function of increasing HMC size.

The amorphous Al-P phase observed at the free surface of these washcoats often contained either PMCs or ceria particles. Such encapsulation of these phases would interfere with their contribution to the catalysis. Comparison to the evolution of these advanced catalyst formulations with that of the Tech-III based formulation studied earlier in the CRADA were made.

3. Future directions

The program plan developed for CRADA research was completed with the characterization of these advanced catalyst formulations under rapid poisoning conditions. The no-cost extension of the CRADA to the end of FY96 permitted these final results to be obtained. These results have been presented to Delphi.

PUBLICATIONS

Three CRADA related publications have been published. References were given in the FY95 annual report.

PRESENTATIONS

Thirteen sets of presentations have been made at periodic progress report meetings between Delphi and LMER personnel working on this CRADA. Posters have been presented at the last three AIM annual information and review meetings. A presentation of goals and results from this CRADA was made by Delphi personnel at the PNGV CRADA review meeting held on March 6-9, 1995. Two presentations on the preparation techniques developed for TEM specimens from catalytic convertor monoliths were made last year (regional American Vacuum Society meeting and annual Catalysis Society meeting). Two more presentations (one invited) were presented on these techniques in the last quarter of FY95 (Microbeam Analysis Society and Microscopy Society of America meetings).

HONORS AND AWARDS

None for CRADA at this time.

PATENT/DISCLOSURES

A patent application was submitted by Delphi in December 1995, which was based upon CRADA results and utilized microstructural characterization from the CRADA to support the application.

LICENSES

None for CRADA at this time.

INDUSTRIAL INPUT AND TECHNOLOGY TRANSFER

Joint work proceeding under CRADA No. ORNL92-0115 on "Improved Catalyst Materials and Emission Control Systems" between Delphi Automotive Systems (formerly General Motors Corporation, AC Delco Systems) and Lockheed Martin Energy Research.

COST SHARING

CRADA specifies matching levels of effort and support between Delphi and LMER.

HIGHLIGHTS

1. No-cost extension of CRADA between General Motors Corporation, AC Delco Systems and Lockheed Martin Energy Research on "Improved Catalyst Materials and Emission Control Systems," CRADA No. ORNL92-0115 approved for FY96.
2. Characterization of field tested (110,000 km) Tech-III monolith was completed and presented to CRADA participants and other interested GM parties.
3. Characterization of as-prepared and engine-aged specimens of next tier of advanced catalyst formulations selected by Delphi was completed and presented to Delphi participants at last quarterly review meeting before the end of CRADA.
4. Prepared and tested catalytic monoliths provided by Delphi during CRADA were shipped back to Delphi before the end of CRADA for recycling/disposal.
5. CRADA final report, containing no proprietary or protected CRADA information, was approved for public release by Delphi and submitted before the end of both FY96 and the CRADA.

CHEMICAL VAPOR INFILTRATION OF TiB_2 FIBROUS COMPOSITES

Theodore M. Besmann

Metals and Ceramics Division
Oak Ridge National Laboratory
P.O. Box 2008
Oak Ridge, TN 37831

INTRODUCTION

This program is designed to develop a Hall-Heroult aluminum smelting cathode with substantially improved properties. The carbon cathodes in current use require significant anode-to-cathode spacing in order to prevent shorting, causing significant electrical inefficiencies. This is due to the non-wettability of carbon by aluminum which causes instability in the cathodic aluminum pad. It is suggested that a fiber reinforced-TiB_2 matrix composite would have the requisite wettability, strength, strain-to-failure, cost, and lifetime to solve this problem. The approach selected to fabricate such a cathode material is chemical vapor infiltration (CVI). This process produces high purity matrix TiB_2 without damaging the relatively fragile fibers. The program is designed to evaluate potential fiber reinforcements, fabricate test specimens, and scale the process to provide demonstration components.

TECHNICAL PROGRESS - FY 1996

Bench-scale testing of a section of the 8x8 inch disk provided to the Alcoa Technical Center revealed excellent electrical, wetting, and aluminum production capability. Problems arose from the delamination of the composite, indicating inadequate interlaminar shear strength. To solve this problem multidimensional preforms are being investigated and were procured for fabricating scale-up samples for Alcoa.

Three different multidimensional carbon fiber preforms were acquired from commercial sources. Two were three-dimensionally woven and one is a random orientation fiber body. In addition, the Carbon and Insulating Materials Group at ORNL is prepared a multidimensional preform by slurry molding for evaluation. A low-cost, 8" x 8" x 0.3" three-dimensional weave preform produced from pitch-based fibers was infiltrated with TiB_2 and sections removed for evaluation. Infiltration was suboptimal due to the very large fiber tows. In addition, testing in molten aluminum resulted in the preform disassembling. It is believed that the lack of stability is due to the poor infiltration, and perhaps also due to apparent attack of the fibers.

The above problems were addressed on two fronts. First, the random orientation preforms that are not woven will be tested, as these avoid the problem of large tows. The preforms also have the potential for being exceptionally low cost. Second, the preforms are being treated at 2500°C to graphitize the fibers. It is expected that graphitic fibers will have a substantially better resistance

to aluminum than do ungraphitized, pitch fibers. During this period a 26% fiber content, 8"x8", slurry molded preform of chopped carbon fibers was prepared by the Carbon and Insulating Materials Group at ORNL. A first attempt to infiltrate this material failed due to the high surface density of the fibers. Titanium diboride deposited on the entrance surface of the preform preventing the infiltration of the body of the material.

Modeling efforts with the Georgia Institute of Technology have pointed toward a pulse flow method for overcoming the difficulty of proper infiltration of a rapidly depositing matrix. Resource limitations did not allow this to be tested.

An issue with the ply-layup preforms has been apparent delamination of the material seen in solidified aluminum bath. The question remains, however, whether this damage occurs in the melt, or only upon solidification of the aluminum. An experiment was designed to answer this question in which the displacement of an alumina rod resting on a section of composite in the bottom of a crucible filled with aluminum was measured as the aluminum melts. The composite did "expand" in the molten aluminum, providing evidence that the composite does not survive in a Hall-cell.

Finally, in an effort to understand the recent failures of the composite material in molten aluminum, a microprobe study of the a polished cross-section of composite was performed. The results indicated that there was a slight excess of titanium in the TiB_2, and it is hypothesized that this may be the cause of the poor stability. Boron-rich feed gas was then used to prepare another composite specimen. Microprobe analysis of this material indicated stoichiometric composition in the bulk, but remaining titanium-rich areas near the fiber surfaces.

PRESENTATIONS

1."Chemical Vapor Infiltration of Fibrous TiB_2 Composites," T. M. Besmann and J. C. McLaughlin, Advanced Industrial Materials Program Annual Meeting, Washington, DC, June 14-16, 1995.

LICENSES

Refractory Composites, Inc. has executed a non-exclusive license on the U. S. patent "Titanium Diboride Ceramic Fiber Composites for Hall-Heroult Cells," No. 4,929,328.

INDUSTRIAL INPUT and TECHNOLOGY TRANSFER

The Alcoa Technical Center has temporarily ceased small-scale sample testing, and has initiated large-scale panel testing of inert cathodes. They have indicated that they will perform small-scale sample testing for a fee.

ESTIMATED ENERGY SAVINGS

Between 10% and 18% of the power consumed in aluminum reduction (0.75 and 1.35×10^{10} kWhr/y) could be saved by the use of TiB_2 electrodes.

DEVELOPMENT OF HIGH TOUGHNESS, HIGH STRENGTH ALUMINIDE-BONDED CARBIDE CERAMICS

Paul F. Becher, Kevin P. Plucknett, Terry N. Tiegs, Joachim H. Schneibel, and Ramesh Subramanian

Metals and Ceramics Division
Oak Ridge National Laboratory
Oak Ridge, TN 37831

INTRODUCTION

Cemented carbides are widely used in applications where resistance to abrasion and wear are important, particularly in combination with high strength and stiffness. In the present case, ductile aluminides have been used as a binder phase to fabricate dense carbide cermets by either sintering of mixed powders or a melt-infiltration sintering process. The choice of an aluminide binder was based on the exceptional high temperature strength and chemical stability exhibited by these alloys. For example, TiC–based composites with a Ni_3Al binder phase exhibit improved oxidation resistance, Young's moduli > 375 GPa, high fracture strengths (> 1 GPa) that are retained to ≥ 900°C, and fracture toughness values of 10 to 15 MPa$\sqrt{m}$, identical to that measured in commercial cobalt-bonded WC with the same test method. The thermal diffusivity values at 200°C for these composites are ~ 0.070 to 0.075 cm^2/s while the thermal expansion coefficients rise with Ni_3Al content from ~ 8 to ~11 x 10^{-6}/°C over the range of 8 to 40 vol. % Ni_3Al. The oxidation and acidic corrosion resistances are quite promising as well. Finally, these materials also exhibit good electrical conductivity allowing them to be sectioned and shaped by electrical discharge machining (EDM) processes.

TECHNICAL PROGRESS – FY 1996

Summary

1. Densification by Melt-Infiltration Sintering

After heating the preforms to 1275°C and holding for 1 h, only partial infiltration of the Ni_3Al had occurred, with most retained on top of the sample. However, melt infiltration and densification reached completion when the processing temperature was raised to 1300°C, Figure 2. Further increases in the processing temperature had little effect on the density of the composites except in samples with low (<12 vol. %) Ni_3Al contents. These experiments reveal that full density can be readily achieved with Ni_3Al contents of ≥ 12 vol. % at temperatures as low as 1300°C for hold times of ≤ 1 h.

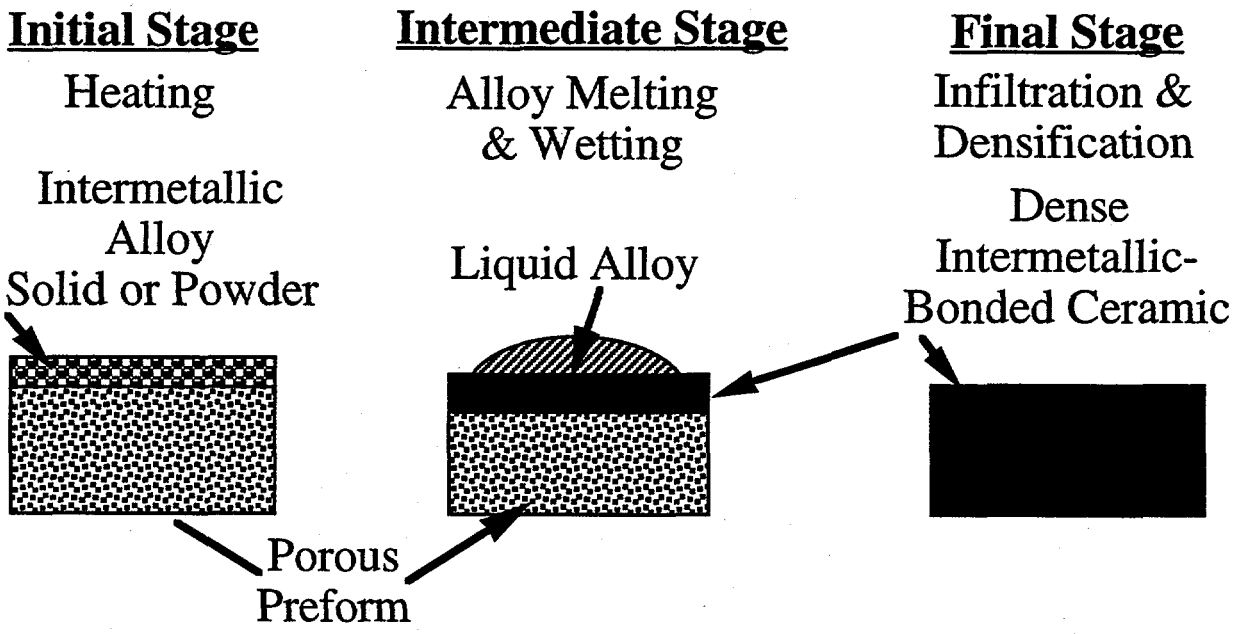

Fig. 1. Schematic representation of steps involved in the melt-infiltration sintering process.

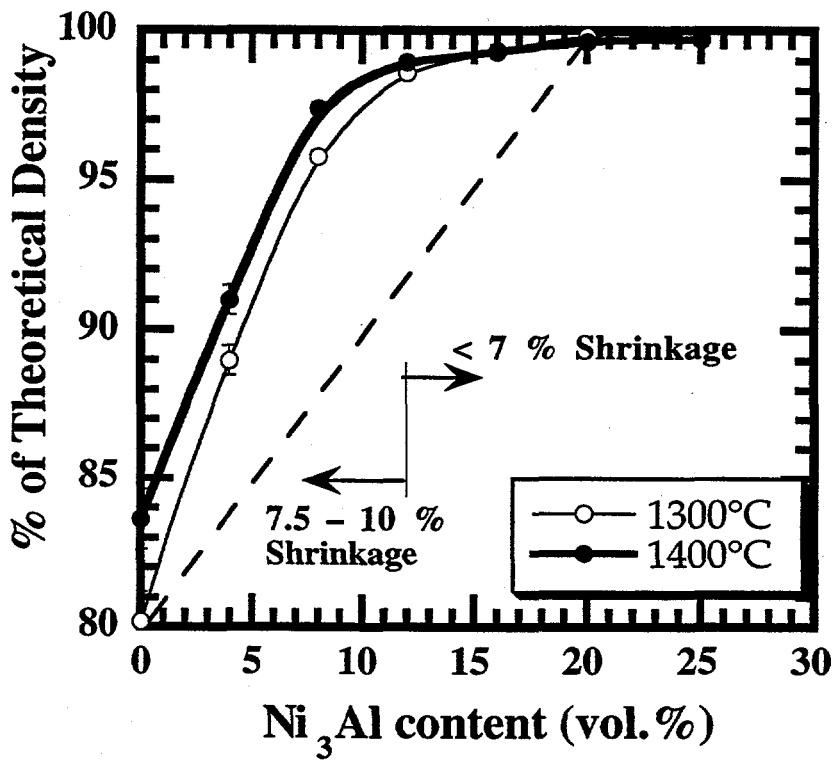

Fig. 2. Final density is as a function of Ni_3Al content at both 1300° and 1400 °C. However, an increase in density with temperature is only seen with aluminide contents < 12 vol. %.

It is possible, using the sintered density of the 'pure' TiC sintered at 1300°C (Figure 2), to estimate the final density that would be obtained if only infiltration of the TiC by a known amount of Ni_3Al occurred (i.e., there is no particle rearrangement). This is shown by the dashed line in Figure 2. This reveals that with Ni_3Al contents between ~ 5 to ~15 vol. % there would be insufficient intermetallic to totally infiltrate the whole piece if it retains its original dimensions. In addition, the measured densities are much greater than those predicted for infiltration alone. Therefore, densification must be aided by particle rearrangement within the TiC preform as the liquid intermetallic infiltrates the preform. When the infiltration process dominates the densification (by increasing either the aluminide content, ≥ 12 vol. %., or the density of the carbide preform), the linear shrinkage during the densification cycle is < 7 %, Figure 2. This approach has the benefit of near-net shape capability; thus, composites with a wide range of Ni_3Alcontents can be produced with the present technique.

2. Properties of the Composites

Thermal-Mechanical

As expected, the properties of the intermetallic-bonded carbide can be tailored by controlling the binder phase content. For example, the linear thermal expansion coefficient can be increased with Ni_3Al content, as expected from simple Rule-of-Mixtures (ROM) calculations, Figure 3. Thus one can match the expansion coefficients of other materials (e.g., metallic alloys0 whose values lie in between those of the carbide and the intermetallic.

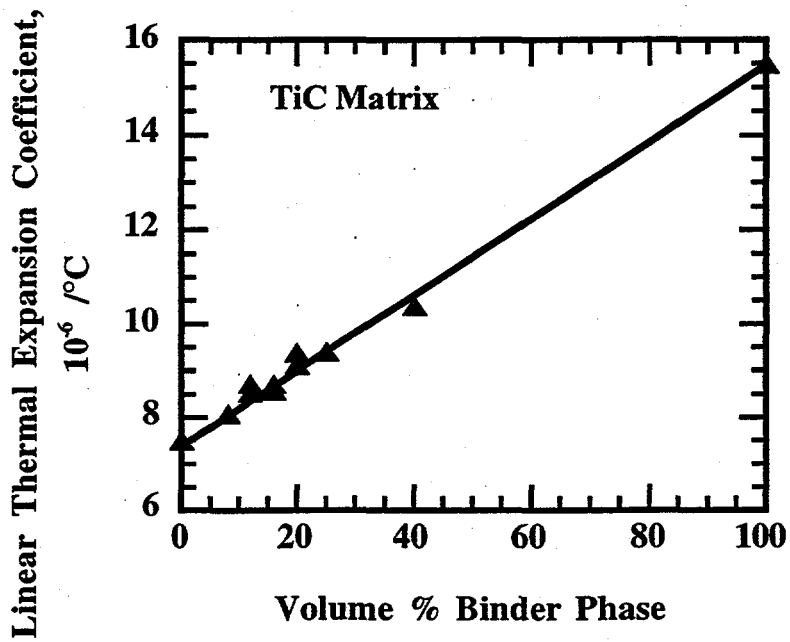

Fig. 3. Measured thermal expansion coefficients increase with Ni_3Al content; the solid line is the projection based on Rule-of-Mixtures calculations.

In the TiC-Ni_3Al composites, the Young's modulus and hardness values decrease and the density increases with aluminide content, Table 1, again consistent with ROM estimates. On the other hand, there are only slight changes in the thermal diffusivity values when the Ni_3Al content is ≤25 vol. %.

Volume % Ni_3Al	Density g/cc	Thermal Diffusivity (@ 200°C) cm^2/s	Diamond Pyramid Hardness GPa @ 1 kg	Young's Modulus GPa
0	4.94	0.0658	21	455
8	5.13	0.0703	17.2	
12	5.23		15.3	430
15	5.31			
16	5.33		16	
20	5.43	0.0755	14.6	410
25	5.55			370
40	5.92			
100	7.39	0.0343	3	185

Table 1. Thermal-Mechanical Properties of TiC-Based Composites with Nickel Aluminide (Ni_3Al) Binder Phase.

Fracture Strengths and Fracture Toughness

The room temperature fracture strengths of fully dense composites generally increase with Ni_3Al content but greater strengths are also achieved when the minimum processing temperature is used, Figure 4. The decrease in strengths with increase in processing temperature can, in part, be attributed to the increase in TiC grain size observed at the higher processing temperature. Keeping this in mind, fracture strengths of over 1 GPa are routinely obtained in samples containing > 12 vol. % Ni_3Al and processed at the lower sintering temperature.

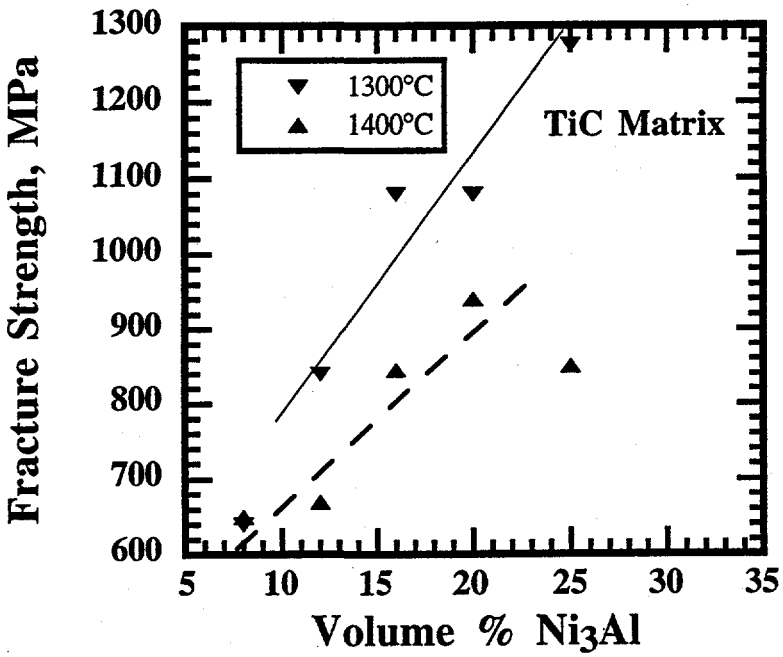

Fig. 4. Room temperature fracture strengths increae with Ni_3Al content; however, the strengths are reduced as the processing temperature is increased from 1300° to 1400 °C. While increasing the processing temperature results in decreased porosity for Ni_3Al contents < 12 vol. %, an increase in TiC grain size also occurs for all compositions.

The steady-state (or long crack) fracture toughness values are in the range of 10 to 15 MPa$\sqrt{m}$ when the Ni_3Al content is > 12 vol. %, Figure 5. In fact, the toughness values for the Ni_3Al-bonded TiC composites are comparable to those measured in our facilities for commercial cobalt-bonded WC materials.

As noted earlier, the aluminides can exhibit exceptional retention of their mechanical properties with increase in temperature. To assess the upper limit for the composites, one composition was subjected to additional testing. As seen in Table II, the TiC-20 vol. % Ni_3Al composite exhibits an increase in fracture strength (e.g., 1.1 from to 1.3 GPa with temperature up to 950°C. The temperature (950°C) for the maximum in fracture strength for the composite is well above that (~ 600°C) for the maximum in the yield (and ultimate) strength observed for the commercial Ni_3Al alloy used to fabricate the composite. Factors that could be contributing to this include changes in the composition of the intermetallic alloy during composite processing and/or the presence of the hard TiC phase and the constraint it would place on deformation within the Ni_3Al binder phase.

Oxidation and Corrosion Resistances

The weight loss in two Ni_3Al-bonded TiC composites, resulting from oxidation at 900°C for 24 hours, is compared to that of a commercial Co-bonded WC in Figure 6. Notice that increasing the Ni_3Al binder content diminishes the weight loss. The oxidation of Ni_3Al involves the formation of a stable aluminum oxide scale; thus, the incorporation of the aluminide binder offers considerable potential for oxidation protection at elevated temperatures. From the immersion tests, it is apparent that the composites are more

resistant to sulfuric acid corrosion than to nitric acid, Figure 7. The resistance to hydrochloric acid is intermediate to the other two acids with the resistance decreasing for each acidic solution with increase in temperature.

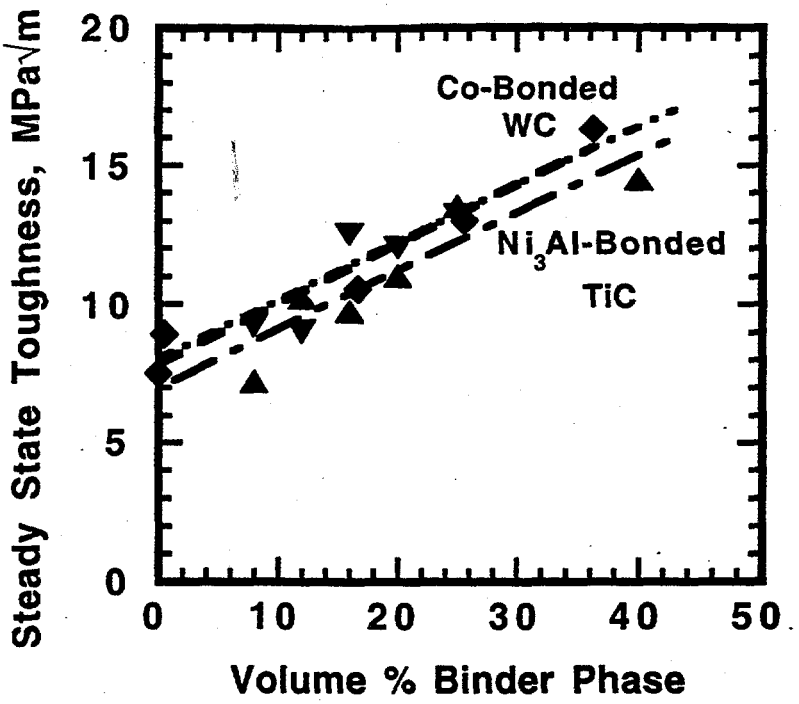

Fig. 5. Room temperature toughness values of Ni_3Al-bonded TiC composites (filled triangles) increase with binder content and are comparable to cobalt-bonded WC cermets (filled diamonds). Note that data for TiC-based composites includes samples fabricated by normal sintering and by melt-infiltrate sintering; no effect of processing route is apparent. Note that data was obtained for each material using the same precracked double cantilever beam test method.

Temperature, °C	Strength, MPa @ Stressing Rate of ~ 300 MPa/s	
22	1080	Fracture Strength
800	1235	Fracture Strength
950	1330	Fracture Strength
1025	1030	Fracture Strength
1100	690	Yield Strength
1100	540	Yield Strength @ 105 MPa/s
1100	380	Yield Strength @ 15 MPa/s

Table 2. Temperature Dependence of the Strength of a TiC-20 vol. % Ni_3Al Composite.

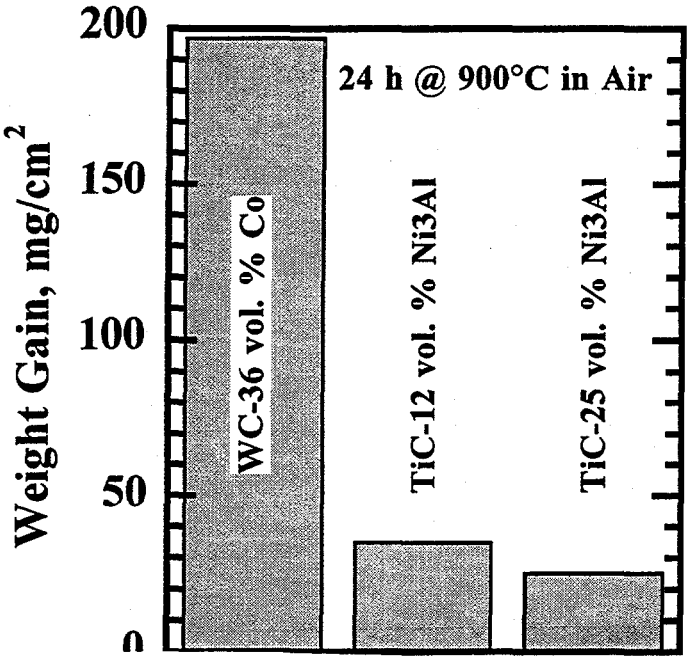

Fig. 6. Weight change associated with oxidation at 900 °C in air is reduced in the Ni_3Al-bonded TiC as compared to Co-bond WC.

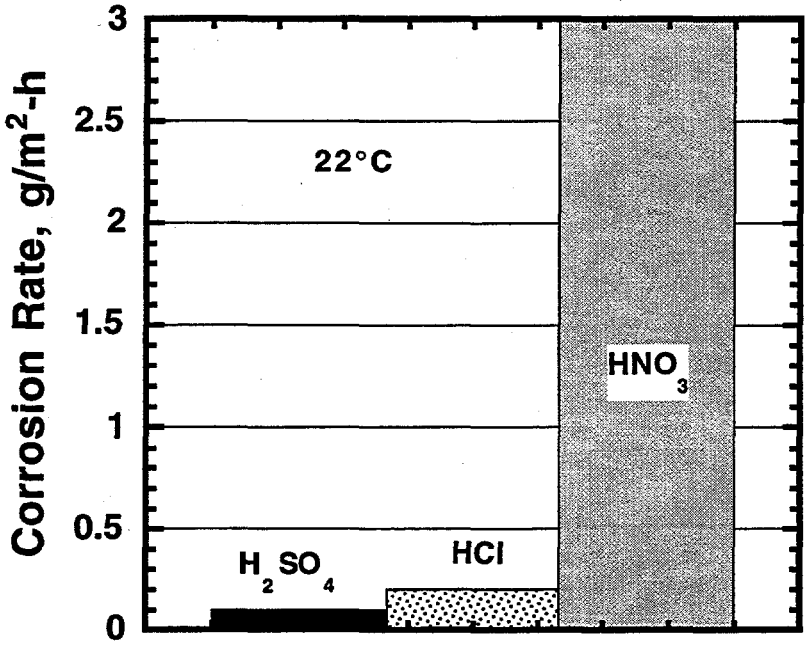

Fig. 7. Corrosion resistance of a TiC-20 vol. % Ni_3Al composite in acid solutions (1 normal concentration levels) at 22 °C varies with specific acid being most resistant to hydrochloric and sulfuric acids.

PUBLICATIONS

Journals

K. P. Plucknett, P. F. Becher, and K. B. Alexander, "In–Situ SEM Observations of Fracture Behavior of Titanium Carbide/Nickel Aluminide Composites," *J. Microscopy*, accepted.

K. P. Plucknett, P. F. Becher, T. N. Tiegs, S. B. Waters, and P. A. Menchhofer, "Ductile Intermetallic Toughened Carbide Matrix Composites," *Ceram. Eng. Sci. Proc.* accepted.

K.P. Plucknett, P.F. Becher, and S.B. Waters, "Flexure Strength Behavior of Melt-infiltration Processed TiC/Ni_3Al Composites," submitted to *J. Am. Ceram. Soc.*

K.P. Plucknett, P.F. Becher and R. Subramanian, "Melt-infiltration Processing of TiC/Ni_3Al Composites," submitted to *J. Mater. Res.*

P. F. Becher and K. P. Plucknett, "Properties of Ni_3Al-Bonded TiC," *J. Eur. Ceram. Soc.*, submitted.

J. H. Schneibel, C. A. Carmichael, E. D. Specht, and R. Subramanian, "Liquid-Phase Sintered Iron Aluminide-Ceramic Composites," *Intermetallics*, in press.

R. Subramanian and J. H. Schneibel, "Intermetallic Bonded WC-Based Cermets by Pressureless Melt Infiltration," Intermetallics, accepted.

T. N. Tiegs, K. B. Alexander, K. P. Plucknett, P. A. Menchhofer, P. F. Becher, and S. B. Waters, "Ceramic Composites with a Ductile Ni_3Al Binder Phase," *Mat. Sci. Eng. A*209, 243-47 (1996).

R. Subramanian, J. H. Schneibel, K. B. Alexander, and K. P. Plucknett, "Iron Aluminide–Titanium Carbide Composites by Pressureless Melt Infiltration- Microstructure and Mechanical Properties," *Scripta Mater.*, 35, 583-88 (1996).

Other Publications

K. P. Plucknett, T. N. Tiegs, K. B. Alexander, P. F. Becher, J. H. Schneibel, S. B. Waters, and P. A. Menchhofer, "Intermetallic-Bonded Ceramic Matrix Composites. " pp.511-520 in Proc. of the CIM Int. Symp. on Advanced Ceramics for Structural and Tribological Applications, T. Troczynski and H. M. Hawthorne(eds.), CIM, Montreal, Canada (1995).

J. H. Schneibel and C. A. Carmichael, "Liquid-Phase Sintering of Iron Aluminide-Bonded Ceramics," pp. 253-60 in Sintering Technology, R. M. German, G. L. Messing, and R. G. Cornwall (eds.), Marcel Dekker, New York, 1996.

T. N. Tiegs, P. A. Menchhofer, K. B. Alexander, K. P. Plucknett, P. F. Becher, S. B. Waters, and J. H. Schneibel, "Hardmetals Based on Ni_3Al as the Binder Phase," Proc. 4th Int'l Conf. on Powder Metallurgy in Aerospace, Defense and Demanding Applications, in press.

T. N. Tiegs, K. P. Plucknett, P. A. Menchhofer and P. F. Becher, "Ni_3Al-Bonded WC and TiC Hardmetals" to be published in Proc. of International Powder Metallurgy Conference, Washington, DC (1996).

T. N. Tiegs, K. P. Plucknett, P. A. Menchhofer and P. F. Becher, "Development of Ni_3Al-Bonded WC and TiC Cermets" to be published in Proc. of International Symposium on Nickel and Iron Aluminides, Cincinnati, OH (1996).

J. H. Schneibel and R. Subramanian, "Bonding of WC with an Iron Aluminide (FeAl) Intermetallic," pp. 16-167 to 16-175, in "Advances in Powder Metallurgy & Particulate Materials - 1996, Vol. 5," Proceedings of the 1996 World Congress on Powder Metallurgy & Particulate Materials, Metal Powder Industries Federation, Princeton, New Jersey.

R. Subramanian, J. H. Schneibel, and K. B. Alexander, Iron Aluminide-Titanitum Carbide Composites - Microstructure and Mechanical Properties, pp. 16-159-16-165, in "Advances in Powder Metallurgy & Particulate Materials - 1996, Vol. 5," Proceedings of the 1996 World Congress on Powder Metallurgy & Particulate Materials, Metal Powder Industries Federation, Princeton, New Jersey.

PRESENTATIONS

K. P. Plucknett and P. F. Becher, "*In-situ* SEM observation of fracture behavior of titanium carbide/nickel aluminide composites," International Electron Microscopy Symposium, Oxford, England.

T. N. Tiegs, "Ceramic Composites With A Ductile Ni_3Al Binder Phase," American Ceramic Society Pacific Coast Meeting, Seattle, WA (November 1995).

T. N. Tiegs, "Development of Ni_3Al-Bonded WC and TiC Cermets," International Symposium on Nickel and Iron Aluminides, Cincinnati, OH (October 1996).

T. N. Tiegs, "Ni_3Al-Bonded WC and TiC Hardmetals," International Powder Metallurgy Conference, Washington, DC, June 1996.

T. N. Tiegs,"Ceramic Composites With A Ductile Ni_3Al Binder Phase," University of Tennessee Graduate Seminar, February 1996.

P. F. Becher, K. P. Plucknett, and T. N. Tiegs, "Fracture Resistance Response of Ni_3Al-Bonded Carbide-Based Ceramets," American Ceramic Society Annual Meeting, Indianapolis, IN, April 1996.

R. Subramanian and J. H. Schneibel, "Iron Aluminide-Titanium Carbide Composites - Microstructure and Mechanical Properties," 1996 World Congress on Powder Metallurgy & Particulate Materials, June 16-21, 1996, Washington, DC.

J. H. Schneibel, "Iron and Nickel Aluminide Bonded Cermets," Sept. 17, 1996, Kennametal, Latrobe, PA.

HONORS AND AWARDS

None

LICENSES

None

INDUSTRIAL INPUT AND TECHNOLOGY TRANSFER

Composite samples have been prepared for evaluation as extrusion dies for aluminum tubing by Reynolds Metals; in wear applications by Cummins Engines; in wear/drill applications by Kennametal, Latrobe, PA; and by Thixomat for evaluation in liquid aluminum environments. A data book detailing the properties of various aluminide-bonded carbides and borides has been prepared and distributed to various interested industrial contacts.

PATENTS AND DISCLOSURES

Method to Fabricate Ceramic Composites, K. B. Alexander, T. N. Tiegs, P. F. Becher, and S. B. Waters, U. S. Patent No. 5,482,673 issued Jan. 9, 1996.

Alumina-Based Ceramic Composite, K. B. Alexander, T. N. Tiegs, P. F. Becher, and S. B. Waters, U. S. Patent No. 5,538,533 issued July 23, 1996.

Method to Fabricate Ductile Intermetallic Bonded Ceramic Composites by Sintering and Articles Resulting Therefrom, K. P. Plucknett, T. N. Tiegs, and P. F. Becher, Invention Disclosure ESID #1751X.

Metal Matrix Composites Based On Iron Aluminides and Ceramic Particles, J. H. Schneibel, Invention Disclosure ESID # 1609-X

GELCASTING POLYCRYSTALLINE ALUMINA

M.A. Janney

Metals and Ceramics Division
Oak Ridge National Laboratory
P.O. Box 2008, Oak Ridge, TN 37831

INTRODUCTION

This work is being done as part of a CRADA with Osram-Sylvania, Inc. (OSI) OSI is a major U.S. manufacturer of high-intensity lighting. Among its products is the Lumalux® line of high-pressure sodium vapor arc lamps, which are used for industrial, highway, and street lighting. The key to the performance of these lamps is the polycrystalline alumina (PCA) tube that is used to contain the plasma that is formed in the electric arc. That plasma.consists of ionized sodium, mercury, and xenon vapors. The key attributes of the PCA tubes are their transparency (95% total transmittance in the visible region), their refractoriness (inner wall temperature can reach 1400°C), and their chemical resistance (sodium and mercury vapor are extremely corrosive). The current efficiency of the lamps is very high, on the order of several hundred lumens / watt. (Compare - incandescent lamps -13 lumens/watt, fluorescent lamps -30 lumens/waft.)

Osram-Sylvania would like to explore using gelcasting to form PCA tubes for Lumalux® lamps, and eventually for metal halide lamps (known as quartz-halogen lamps). Osram-Sylvania, Inc. currently manufactures PCA tubes by isostatic pressing. This process works well for the shapes that they presently use. However, there are several types of tubes that are either difficult or impossible to make by isostatic pressing. It is the desire to make these new shapes and sizes of tubes that has prompted Osram-Sylvania's interest in gelcasting.

The purpose of the CRADA is to determine the feasibility of making PCA items having sufficient optical quality that they are useful in lighting applications using gelcasting.

TECHNICAL PROGRESS - FY 1996

Summary

Gelcasting is a process for forming ceramic and metal powders into complex shapes. It was originally developed for ceramic powders (1-5). It is a generic process that has been used to produce complex-shaped ceramic parts from over a dozen different ceramic compositions ranging from alumina-based refractories to high-performance silicon nitride. The present application is to gelcast thin-walled tubes of polycrystalline alumina (PCA) having high enough quality that they are useful in high-pressure sodium vapor arc lamps. Background information on the gelcasting process is given in another section of this Annual Report, entitled Advanced Powder Processing.

1. Results And Discussion

We have formulated slurries at 45 to 50 vol % solids using standard gelcasting formulations based on methacrylamide monomer and methylene bisacrylamide crosslinker. These slurries were made using proprietary powders supplied by OSI. Good flow behavior was achieved; viscosities were on the order of 200 cps.

The slurries were successfully cast as thin-walled tubes (0.3 inch OD, 0.020 inch wall, 2 inch long) in molds supplied by OSI. The tubes were fired using a standard schedule and produced translucent material.

We have demonstrated the importance of selecting appropriate mold release agents and mold surface finishes to achieving good parts. An extensive study of the interactions of mold release agents with mold materials and slurry was conducted. The results of that study are summarized in Table 1. Several features of mold-slurry-release agent interactions become clear after examining Table 1. First, there are some materials are not good mold materials for precision casting under any circumstances. Neither Lexan® nor Plexiglas performed well under any of the conditions studied. A thin, ungelled layer always formed at the surface of the mold. Such a layer would cause imperfections in the surface of the parts which is unacceptable. In contrast, anodized aluminum (both rough and smooth) performed well with all of the release agent except F-57. In general, anodized aluminum performed somewhat better than non-anodized aluminum. Glass also performed well with the release agents tested in this study.

It was further discovered that at least on of the mold releases adversely affected the microstructure of the fired alumina tubes. The cause was traced to a minor constituent in the mold release that contained titanium. This underscored the need to be especially careful with potential sources of contamination when dealing with opticl grade ceramic materials.

MILESTONES

Demonstrated the ability to gelcast small arc tubes of optical quality.

INDUSTRIAL INPUT AND TECHNOLOGY TRANSFER

OSI is actively pursuing applications of gelcast tubes to their product line.

MEMBRANE SYSTEMS FOR ENERGY EFFICIENT SEPARATION OF LIGHT GASES

David J. Devlin,Thomas Archuleta and Robert Barbero

Los Alamos National Laboratory
MS E549, MST-7
PO. Box 1163
Los Alamos, New Mexico 87545

Nari Calamur and Martin Carrera

Amoco Research Center
P.O Box 3011
Naperville, Illinois 60566-7011

INTRODUCTION

Ethylene and propylene are two of the largest commodity chemicals in the United States and are major building blocks for the petrochemicals industry. These olefins are separated currently by cryogenic distillation which demands extremely low temperatures and high pressures. Over 75 billion pounds of ethylene and propylene are distilled annually in the US. at an estimated energy requirement of 400 trillion BTU's. Non-domestic olefin producers are rapidly constructing state-of-the-art plants. These energy-efficient plants are competing with an aging United States olefins industry in which 75% of the olefins producers are practicing technology that is over twenty years old. New separation opportunities are therefore needed to continually reduce energy consumption and remain competitive. Amoco has been a leader in incorporating new separation technology into its olefins facilities and has been aggressively pursuing non-cryogenic alternatives to light gas separations. The largest area for energy reduction is the cryogenic isolation of the product hydrocarbons from the reaction by-products, methane and hydrogen. This separation requires temperatures as low as -150°F and pressures exceeding 450 psig. This CRADA will focus on developing a capillary condensation process to separate olefinic mixtures from light gas byproducts at temperatures that approach ambient conditions and at pressures less than 250 psig; this technology breakthrough will result in substantial energy savings. The key technical hurdle in the development of this novel separation concept is the precise control of the pore structure of membrane materials. These materials must contain specially-shaped channels in the 20-40A range to provide the driving force necessary to remove the condensed hydrocarbon products. In this project, Amoco is the technology end-user and provides the commercialization opportunity and engineering support. LANL provides the material development expertise that is critical for achieving the desired product separation.

TECHNICAL PROGRESS - FY 1996

1. Materials Synthesis

The development of thin films with controlled pore size in the nanometer range is an objective of this program. The separations approach is based on the capillary condensation of hydrocarbons in 1 to 5 nm pores. Figure 1 illustrates one version of the concept.

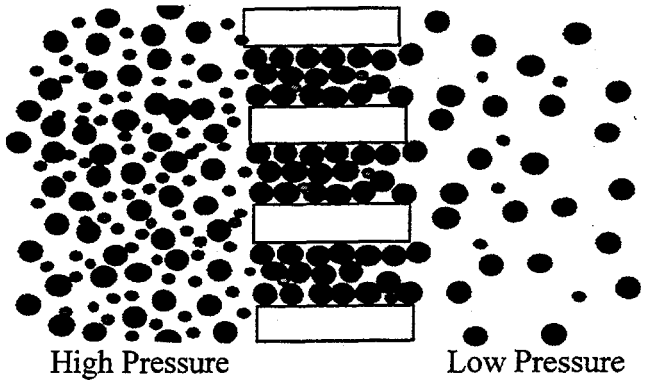

Fig. 1. Illustration of capillary condensation of hydrocarbons in a porous substrate.

In this approach a feed consisting of hydrocarbon and hydrogen gas pass over the high pressure side of the membrane. Preferential condensation of the hydrocarbon in the pores occurs blocking them with hydrocarbon and restricting flow of hydrogen. The hydrocarbon is evaporated on the low pressure side leaving a hydrogen rich feed. The actual operating conditions will depend on the pore size, geometry and membrane permeability.

Thin film deposition by evaporation and sputter techniques often result in porous microstructures. This is problem which effects thin film properties such as electrical conductivity and represents a limitation to these techniques when applied to complex geometric structures. However for the development of porous structures this problem can be used to our advantage. The microstructures typically consist of columnar grains separated by porous regions. These structures are dependent on a number of parameters such as substrate temperature, deposition rate , ambient atmosphere, angle of incidence, and energy of depositing flux. Porous structures are generally observed for conditions where the surface mobility of depositing atoms is limited. It is found in many examples that the direction of columnar growth is related to the angle of incidence according to the relationship known as the tangent rule:

$$\tan(\beta)=1/2\tan(\alpha) \qquad (1)$$

Where α is the angle between the surface normal and the direction of the vapor flux and β is the angle between the surface normal and growth direction, figure 2. While this exact relation does not always hold, it is universally found that the angle β is less then α and the effect is a consequence of a process known as "self shadowing "(1-3).

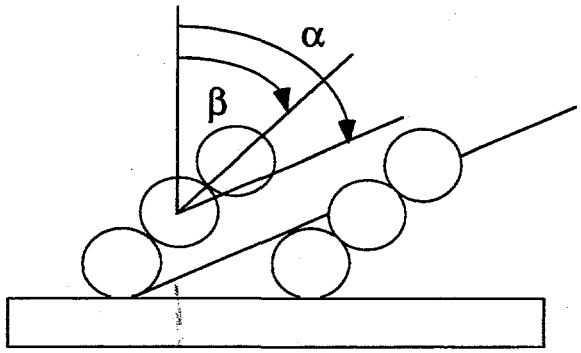

Fig. 2. Self shadowing of vapor flow during oblique angle deposition. α is the angle of the incoming beam and β is the direction of columnar grain growth.

This occurs when deposited atoms exposed to the incoming vapor flux shield the substrate or unoccupied sites form direct impingement. When the surface mobility is low such that rearrangement to fill the shielded sites is not possible, columnar grains form.

The dimensions of the pore in simplistic terms is dependent on the incident angle and size of the shadowing adatom, cluster or nuclei. Crystallographic effects can also be important in defining the grain structure. Substrate temperature and therefore mobility will effect nuclei size and rearrangement. Also the energy and distribution of the atomic flux, and degree of thermalization of the beam is important. For carbon materials sputter deposited at room temperature the surface mobility is low. Sputtering at an oblique angle is expected to produce a columnar structure.

The substrate used for the deposition of the carbon films was an anodized alumina filter made up of straight pores with uniform dimensions. Filters available from Whatman contain channels 200 nm in diameter and 60 microns in length with a 0.02 micron diameter membrane layer approximately 100 nm thick on one side. The pore size distribution is uniform, and the pores as shown in figure 3 are straight.

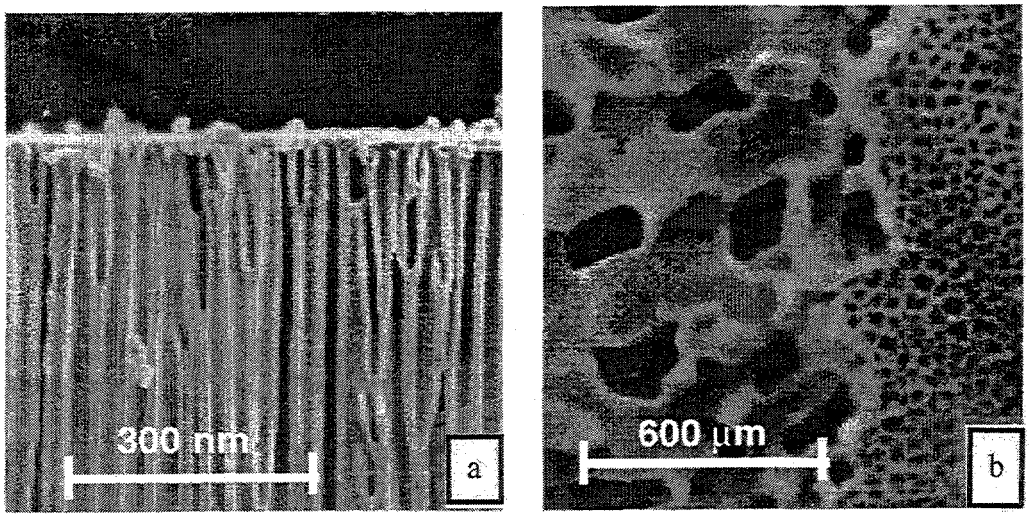

Fig. 3. Microstructure of anodized alumina filters used as substrates in this work. Fig. 3a is a cross section showing the straight 200 nm diameter pores; Fig. 3b is a top view showing both the 200 nm and 20 nm pores.

The fine pore side of the filter provides a suitable substrate for the deposition of carbon films with a 4 to 5 nm pore dimension. Films were deposited with a 10 cm. diameter RF powered magnetron sputter gun in a high vacuum system . The arrangement is illustrated in figure 4.

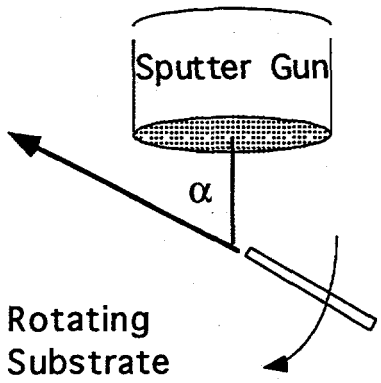

Fig. 4. Illustration of the oblique angle deposition arrangement used in this study.

Substrates were set at an angle with respect to the gun and rotated. Rotation of the stage improved uniformity and altered the microstructure. Typical sputter conditions were argon pressures of 0.1 to 0.3 Pa and RF power of 90 watts. Deposition rates were on the order of 100 nm/hr and angle of incidence varied from 0 to 85° . Coated and uncoated filters are shown in figure 5.

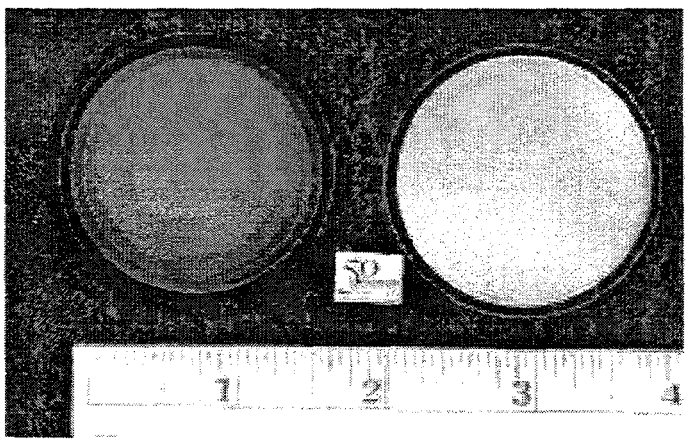

Fig. 5. Coated and uncoated filters. Carbon deposited at an angle of 85° and rotated.

Samples were prepared for TEM by ion milling, and the microstructure of oblique angle and normal incidence sputter films, with and without substrate rotation were examined.

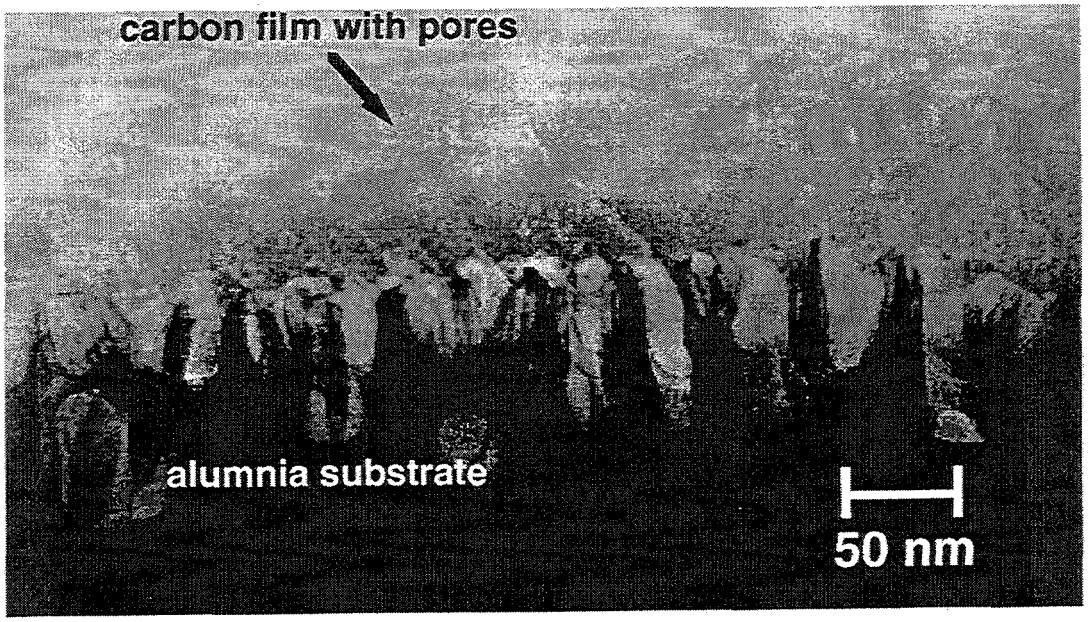

Fig. 6. TEM micrograph of a sputtered film inclined at an angle of 85° to gun.

Figure 6 is a TEM micrograph of a sputtered film inclined at angle of 85° to gun. The film clearly shows the presence of columnar grains tilted in the direction of the incoming atomic flux. The pore size between grains can be estimated at 5 nm. Figure 7 shows the effect of rotating the substrate during deposition at an angle of 85°. Again columnar grains are formed with a pore size on the order of 5 nanometers, however the grains are now oriented normal to the substrate surface. In addition, the rotation leads to a uniform deposition across the substrate.

As a check against the possibility that the film structure and pore size is an artifact of the substrate surface and not due to the oblique deposition angle, samples were also prepared at normal incidence. The micrograph of figure 8 shows one such sample prepared under identical conditions as the 85° sample with rotation but at normal incidence. No porosity is evident in the carbon film.

Permeability measurements were used as a means of verifying the pores observed in the TEM micrographs were continuous and roughly 5 nm in diameter. Coated and uncoated filters were examined in the apparatus illustrated in figure 9. The membranes were mounted between two o-rings in stainless steel flange.

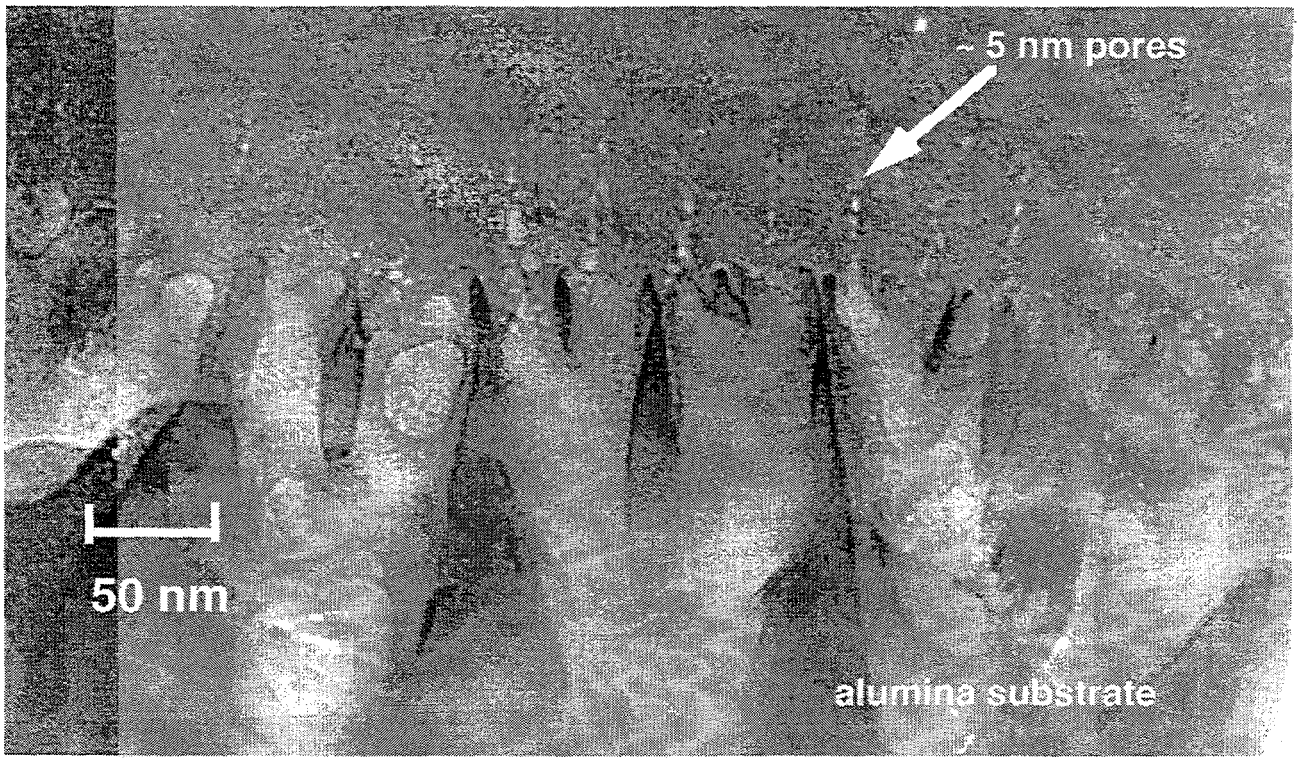

Fig. 7. TEM micrograph showing the effect of rotating the substrate during deposition at an angle of 85°.

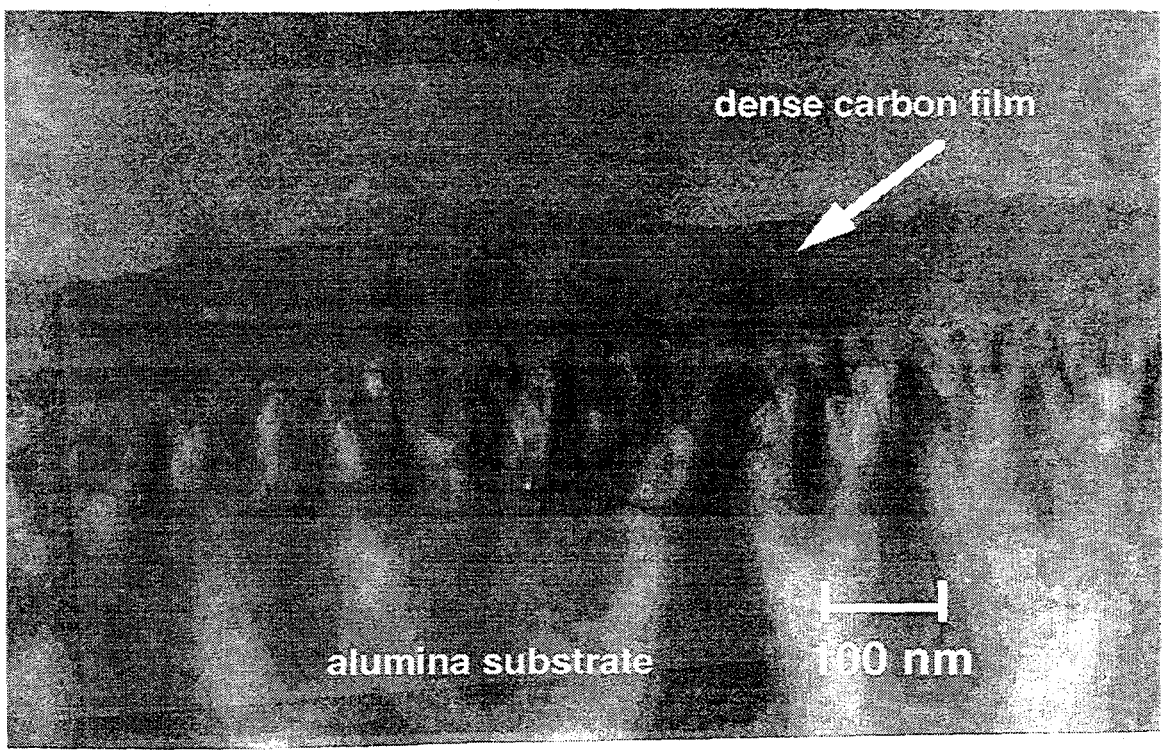

Fig. 8. TEM micrograph of a carbon film deposited while rotating with the vapor flux normal to the substrate surface.

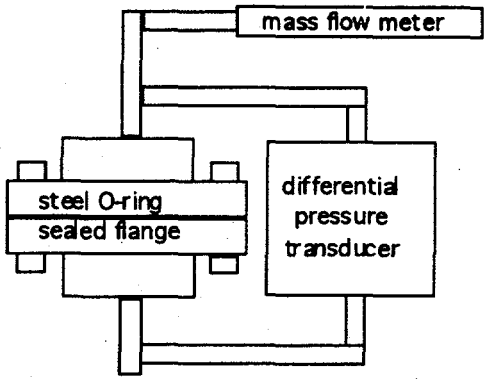

Fig. 9. Illustration of apparatus used to measure permeability of hydrogen through the coated and uncoated filters.

A differential capacitance pressure gauge was used to monitor the pressure drop across the membrane. The gas flow was set and measured with a mass flow meter. The results were analyzed by the following relation for Knudsen flow through a cylinder.

2

Q is the total flow
r is the pore radius
N(r) is the pore size distribution
ΔP is the pressure drop across the membrane.
δ is the film thickness.

$$Q=N(r)\left[\frac{32\pi}{MRT}\right]^{1/2} r^3 \frac{\Delta P}{\delta}$$

Figure 10 shows the results of measurements on an uncoated membrane and two coated membranes. The coating thicknesses were estimated at 100 and 150 nm based on deposition rates Both coatings were sputtered at 85° and rotated. The flow through the uncoated filters is restricted by the large 200 nm pores as opposed to the smaller 20 nm film due to the greater thickness, 60 μm and lower pore density.

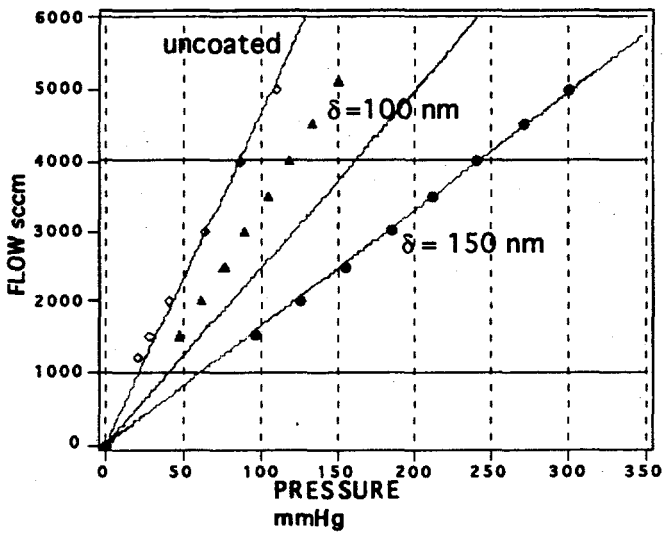

Fig. 10. Hydrogen flow through the uncoated filter, 100 nm thick and 150 nm thick carbon films. Solid lines are calculated based on equation 2.

Calculations for the uncoated membrane were based on the 200 nm diameter pores 60 μm length. Pore density was estimated from SEM micrographs. Good agreement was obtained using the Knudsen flow in cylindrical pore model. Figure X compares the experimental and calculated values. Calculations for the 100 and 150 nm thick sputtered carbon films, assuming a 4.5 nm pore diameter are also shown in fig X along with the experimental values. Assuming a 4.5 nm pore diameter good agreement is obtained for the 150 nm thick carbon coating. For the 100 nm thick carbon coating the measured flow is higher then predicted. This could be attributed errors in the estimated film thickness and uniformity, a higher then 4.5 nm average pore diameter, incomplete coverage or pin holes in the thinner coating. The overall results do support the conclusion that the pores in the carbon are continuous channels on the order of 5 nm in diameter.

The results demonstrate the potential for using oblique angle deposition techniques to develop porous thin films with controlled pore size. The is not restricted to carbon but in principle can be applied to any material. The geometry and shape of the pore can be varied by altering the angle of incidence. A number of samples have been prepared for separation testing and delivered to Amoco's Olefin R& D group. A test apparatus is being developed for evaluation of the membranes by the capillary condensation method described earlier. Future efforts will involve optimizing this technique. This will include microstructural simulations using SIMBAD ™thin film process simulator from Alberta Microelectronics center. This code performs simulations of the vapor flux transport including the angular distribution for planar magnetron sputter guns. The film growth simulation is a 2-D Monte Carlo simulation incorporating vapor flux shadowing and surface diffusion. These simulations will be used along with experimental results to predict and further refine the development of porous microstructures in carbon and other material films.

REFERENCES

Dirks A.G. and H.J Leamy, "Columnar Microstructures in Vapor Deposited Thin Films," *Thin Solid Films*, **47**, 219-233 (1977).

Muller K.H. "Dependence of thin film microstructure on deposition rate by means of computer simulation," *J Appl. Phys.* **58**(7),1, 2573,(1985).

Messier R., A.P. Giri, R.A. Roy" Revised structure zone model for thin film physical structure," *Vac Sci. Technol. A,* **2**, 2, 500, (1984).

MILESTONES

A method for developing carbon pores for capillary condensation of hydrocarbons has been devised. The use of oblique angle sputter techniques to develop thin films with controlled pore size has been demonstrated. A CRADA entitled " Membrane Systems for Energy Efficient Separation of Light Gases" is in place with Amoco.

PUBLICATIONS

R.P. Currier, D.J. Devlin and J. Morziski, "Dynamics of Chemical Vapor Infiltration in Carbon Fiber Bundles," *J. Adv. Mater.*, **27**(4), 13-24 (1996).

D.J. Devlin, J. Cowie and D. Carrol, "Carbon Based Prosthetic Devices," *Proceedings of International Mechanical Engineering Congress. Advances in Bioengineering* , **31**, (1995).

D.J. Devlin, R.S Barbero, K.N. Siebein, "Radio Frequency Assisted Chemical Vapor Infiltration," *Proc. of the 13th International Conference on Chemical Vapor Deposition*, (1996).

PRESENTATIONS

(Related to earlier work on RF and Microwave Assisted CVI)

D.J. Devlin, R.S. Barbero, K.N. Siebien, "Chemical Vapor Infiltration," Advanced Industrial Materials Program Annual Review, Washington D.C., June 95.

D. J. Devlin, J. Cowie, D Carrol, "Carbon Based Prosthetic Devices," American Society of Mechanical Engineers, Annual Winter Meeting, November 1995.

D.J. Devlin, R.S Barbero, K.N. Siebein, "Radio Frequency Assisted Chemical Vapor Infiltration," 13th International Conference on Chemical Vapor Deposition, April 1996.

INDUSTRIAL INPUT and TECHNOLOGY TRANSFER

This effort will continue in '97 as a joint research effort with Amoco's Olefins R&D group. Amoco will develop characterization capabilities and design criteria for the membrane systems. With their guidance we will develop the materials and processing for the fabrication of these membranes. Amoco's goal is a materials system capable of scaling for use in a pilot plant system.

COST SHARING

Amoco will coat share with in kind funds and capital investment exceeding the present DOE allocation.

ESTIMATED ENERGY SAVINGS

Initial economic analyses have shown that the commercialization of this novel separation concept could result in an energy reduction potential of 5 trillion BTUs per year for an olefins complex: this corresponds to a potential annual savings of nearly $8 million.

PROCESS SIMULATION FOR ADVANCED COMPOSITES PRODUCTION

M. D. Allendorf, S. M. Ferko, S. Griffiths, A. McDaniel, R. Nilson,
T. H. Osterheld[†], M. T. Schulberg[*], N. Yang and D. R. Hardesty

Sandia National Laboratories
Livermore, California 94551-0969

INTRODUCTION

The objective of this project is to improve the efficiency and lower the cost of chemical vapor deposition (CVD) processes used to manufacture of advanced ceramics by providing the physical and chemical understanding necessary to optimize and control these processes. Project deliverables include: numerical process models; databases of thermodynamic and kinetic information related to the deposition process; and process sensors and software algorithms that can be used for process control. Target manufacturing techniques include CVD fiber coating technologies (used to deposit interfacial coatings on continuous fiber ceramic preforms), chemical vapor infiltration, thin-film deposition processes used in the glass industry, and coating techniques used to deposit wear-, abrasion-, and corrosion-resistant coatings for use in the pulp and paper, metals processing, and aluminum industries.

Experimental measurements are performed under realistic processing conditions to obtain gas-phase concentrations, precursor decomposition kinetics, and deposition rates, using a high-temperature flow reactor (HTFR) equipped with mass spectrometric and laser diagnostics. In addition, advanced characterization methods such as high-resolution transmission electron microscopy and energy-dispersion spectroscopy are used to characterize the microstructure and composition of reactor deposits. Computational tools developed through extensive research in the combustion field are employed to simulate the chemically reacting flows present in typical industrial reactors.

Currently, this project includes two industrial collaborations. First, joint work with DuPont Lanxide Composites (DLC; Newark, DE) is directed toward development of a process model for simulating, optimizing, scaling, and controlling boron nitride (BN) fiber coating processes using in the manufacturing of fiber-reinforced composites. Second, research performed in collaboration with Libbey-Owens-Ford Co. (LOF; a major manufacturer of float glass located in Toledo, OH) is directed toward development of new CVD methods for depositing coatings on glass. Work with LOF is performed under a CRADA (see discussion below under "Industrial Input and Technology Transfer").

[†] Current address: Applied Materials Inc., Santa Clara, CA 95054
[*] Current address: Varian Associates, Palo Alto, CA 94304

TECHNICAL PROGRESS - FY 1996

Task 1. Characterization of reactor deposition chemistry.
Task 2. Simulation of reactor fluid dynamics and mass transport; process control algorithms.
Task 3. Implementation of strategies for process design, optimization, and operation.
Task 4. Development of process control sensors.

Summary

Experiments and modeling investigations were conducted, leading to the development of a verified model simulating the formation of BN coatings on ceramic-fiber preforms. Experiments in a high-temperature flow reactor provided quantitative measurements of the rate of reaction between the BN precursors boron trichloride and ammonia. These data were used in the formulation of a computer model that includes all relevant transport processes as well as gas-phase and surface chemistry. The model predicts BN deposition rates as a function of reactor temperature, pressure, reactant concentration, and preform geometry. Model predictions were compared with measured deposition rates and are found to be in good agreement. The flow-reactor experiments also provided insight into potential strategies for developing process control sensors.

MILESTONES

Task 1. Characterization of reactor deposition chemistry

In FY96 we conducted extensive experiments designed to probe the chemical reactions responsible for the formation of boron nitride (BN) coatings. The primary objective of this investigation is to provide kinetic data needed to develop quantitative process models. The results can also be used to suggest strategies for on-line process control. Results of the kinetics experiments are summarized below; those relevant to process control are described under Task 4.

Kinetics of BN deposition. The overall chemical reaction describing the formation of BN from the reactants boron trichloride (BCl_3) and ammonia (NH_3) in a CVD reactor is:

$$BCl_3(g) + NH_3(g) \rightarrow BN(solid) + 3HCl \qquad (1)$$

Equation (1) is a "global" reaction that hides the fact that a series of homogeneous (i.e., gas-phase) and heterogeneous (i.e., surface) reactions occur that convert the gas-phase reactants into solid product. It is suspected, for example, that the reactants BCl_3 and NH_3 can react in the gas phase to form new species that may be the actual precursors to BN formation:

$$BCl_3 + NH_3 \xrightarrow{k} Cl_2BNH_2 + HCl \qquad (2)$$

To probe reactions such as this requires the use of sophisticated experimental techniques that can detect minute quantities of gas-phase species as a function of variables relevant to the CVD process, namely, gas residence time, temperature, pressure, and reactant concentration. To accomplish this, we upgraded an existing high-temperature flow reactor (HTFR) (constructed previously with funding

from the AIM Program) to obtain increased sensitivity and experimental flexibility. The current configuration of the HTFR is shown in Figure 1.

The new HTFR configuration provides two major improvements to the previous design. First, the reactor orientation was changed from vertical to horizontal so that the reactor interior is more accessible. The new design provides maximum flexibility for maintenance, insertion of substrates, cleaning, and mass-spectrometer alignment. An additional advantage over the vertical orientation is that reactor tubes can be easily interchanged, allowing different materials to be used and more frequent cleaning. The second major improvement is the implementation of direct molecular-beam sampling of the reactor gases. Rather than sampling reactor gases through a quartz probe, a small portion of the gas is expanded through a nozzle containing a 125-μm orifice. The expansion of the gases from the reactor into the nozzle chamber, which operates at a much lower pressure (10^{-5} torr vs 1-250 torr in the furnace section), forms a molecular beam in which there are no intermolecular collisions. Thus, gas-phase reactions following sampling are completely quenched, eliminating the ambiguity associated with sampling probes operating at higher pressures. The sensitivity of this system is as much as two orders of magnitude better than the previous design; species with concentrations as low as 1 ppm at 10 torr can be detected.

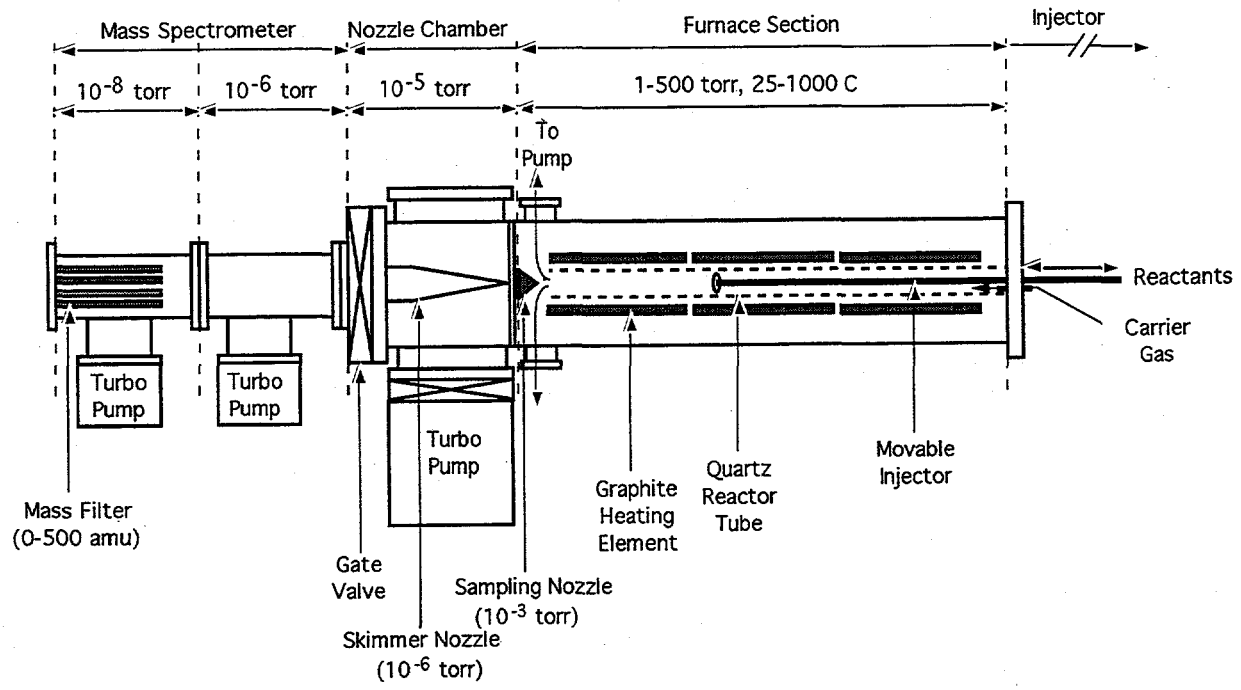

Fig. 1. Schematic of upgraded high-temperature flow-reactor.

The new HTFR configuration was used to measure the rate of Reaction 2. Previous experiments and modeling suggest that Cl_2BNH_2 is the primary gas-phase species reacting with the substrate and also predict the existence of several other boron- and nitrogen-containing compounds. With the

improved sensitivity of the mass spectrometer, it is now possible to make accurate measurements of the rate of this, as yet, uncharacterized reaction, using low initial concentrations of BCl_3 and NH_3 to minimize interference from secondary reactions that may occur simultaneously with Reaction 2.

The reaction was conducted in a graphite-foil-lined quartz tube with an internal diameter of 6.4 cm. The temperature of the reactor tube was maintained at its setpoint with an accuracy of ± 2 K over a heated length of 50 cm. Chemical residence times ranging from 0 to 2000 ms were varied by translating the point of BCl_3 injection and by varying the gas flow rates, reactor temperature, and pressure. Typical experimental conditions were as follows: He or N_2 carrier gas flows of 1280-2000 sccm, reactor temperatures from 670-920 K, reactor pressures of 10, 15, 25, and 50 torr, NH_3 concentrations between 0.08×10^{-8} and 1.7×10^{-8} mol cm^{-3}, and BCl_3 concentrations ranging from 0.3×10^{-9} to 3.0×10^{-9} mol cm^{-3}. All experiments were conducted in excess ammonia, making the rate of BCl_3 loss a pseudo first-order process.

In the presence of excess ammonia, the rate of BCl_3 loss in Reaction 2 is governed by the following expression:

$$\dot{r} = \frac{d\,[BCl_3]}{dt} = -k_{obs}[BCl_3], \tag{3}$$

where k_{obs} (s^{-1}) is the apparent first-order rate constant which, in the ideal (plug-flow) case, is the product of the bimolecular rate constant (k) and the ammonia concentration. Upon integration from an initial state (0) (chosen to be sufficiently far downstream from the point of reactant injection that mixing can be assumed to be complete), and substituting for time (t) the residence time of the gases in the HTFR ( ) (calculated using the plug-flow approximation to determine the gas velocity), the rate of reactant loss becomes

$$\ln \frac{[BCl_3]}{[BCl_3]_0} = -k_{obs}(\tau - \tau_0). \tag{4}$$

It is evident from Equation 4 that the observed rate constant can be obtained from the slope of a log-linear plot of concentration and relative residence time.

The experiments conducted in the HTFR only approximate the plug-flow conditions expressed in Equations 3 and 4. In reality, the spatial dependence of the BCl_3 concentration in the reactor tube is a complex function of fluid dynamics, reactant transport, and chemical reaction, whose effects on the reactant decay result in a single loss term (k_{obs}). The extraction of the true bimolecular rate constant governing Reaction 2 involves solving the single-species Navier-Stokes equations under the simplifications of Poiseuille flow. Although not trivial, it is possible to separate the effects of transport from those of chemical reaction to obtain k from the observed decay of BCl_3 .

Illustrated in Figure 2 is the ln-linear decay of boron trichloride as a function of gas residence time for a reactor temperature of 720 K, a reactor pressure of 10 torr, and an ammonia concentration of

2.0×10^{-9} mol cm^{-3}. The symbols represent BCl_3 concentrations measured by the mass spectrometer, while the solid line is the best least-squares fit. The linear behavior of the decay curve over all residence times indicates that the experiment satisfies the criteria for pseudo-first-order kinetics. To extract the desired bimolecular rate constant and its associated Arrhenius parameters, experiments are performed at various ammonia concentrations and reactor temperatures. Figure 3 shows the observed first-order rate constant, which is obtained by calculating the slopes of lines similar to those in Figure 2, as a function of the ammonia concentration for various reactor temperatures at a pressure of 10 torr.

The observed rates depicted in Figure 3 must be corrected for the effects of viscous (Poiseuille) flow in the reactor, which can introduce significant errors in bimolecular rate constants extracted by using Equation 4. Various methods exist for determining this correction, most of which involve solving a two dimensional transport equation. In this report all measured first-order constants have been corrected according the method developed by R.L. Brown (*Journal of Research of the National Bureau of Standards*, 1978), assuming no heterogeneous losses of boron trichloride. While this method is commonly used to correct flow-tube data for the effects of Poiseuille flow, we are currently developing a more general approach that makes use of sophisticated numerical models for predicting boundary-layer flow in tubes.

Figure 4 is a plot of the natural log of the rate constant (k) for Reaction 2 as a function of inverse temperature at a reactor pressure of 10 torr. The data behave in a typical Arrhenius fashion and are plotted in this way to extract the kinetic parameters for the reaction. The experimentally determined activation energy is 7790 ± 160 cal mol^{-1} K^{-1}, the pre-exponential factor is $2.65 \pm 0.30 \times 10^{11}$ cm^3 mol^{-1} s^{-1}. All values are reported at the 95% confidence interval. This result confirms experimental results obtained in FY95 indicating that Reaction 2 is fast on the time scale of CVD processes used in fiber-coating.

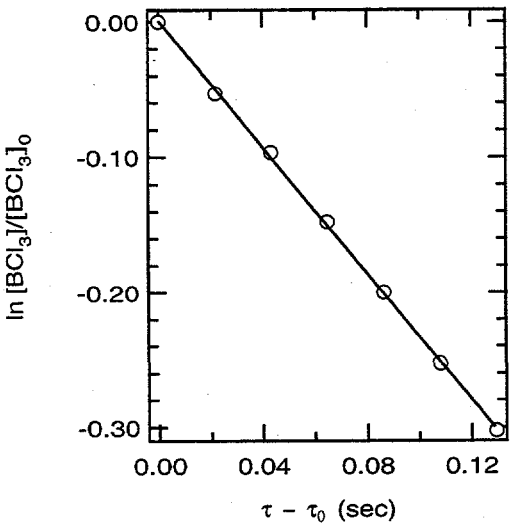

Fig.2. Ratio of the BCl3 signal to the initial-state Bcl3 signal as a function of relative residence time. Symbols are data points, solid line is a least squares fit to the data.

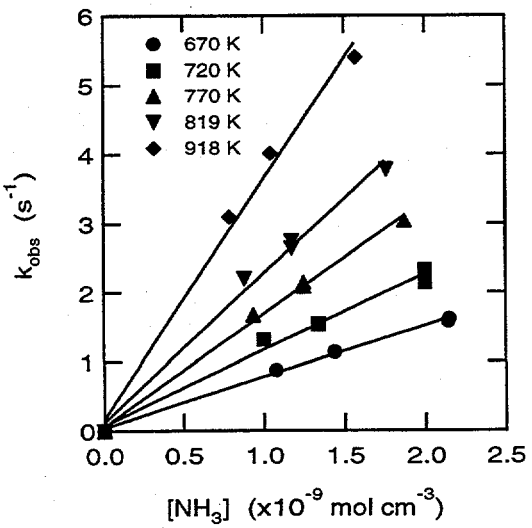

Fig. 3. Observed first-order rate constant as a function of ammonia concentration for various reactor temperatures. Symbols are data points, solid lines are least squares fits to the data.

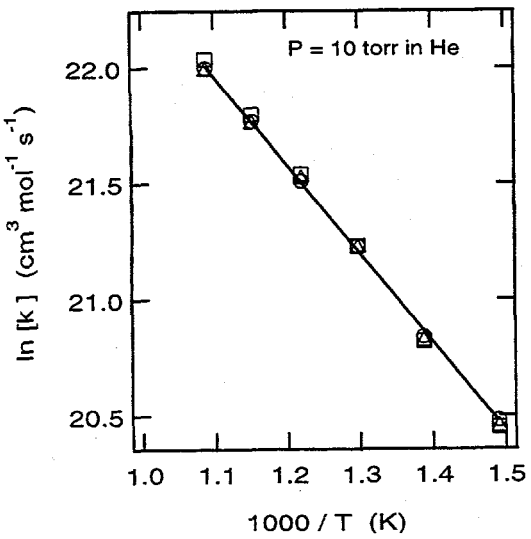

Fig. 4. Natural log of the bimolecular rate constant as a function of inverse temperature. Symbols are data points, solid line is least squares fit to data.

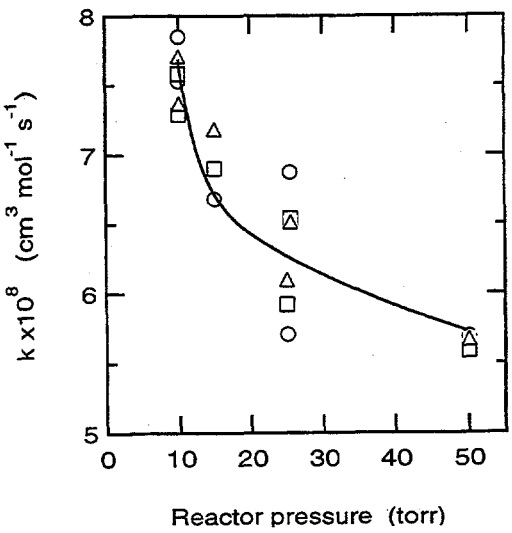

Fig. 5. Bimolecular rate constant as a function of reactor pressure at 670 K. Symbols are data points, solid curve illustrates the pressure trend.

The measured rate for Reaction 2 is considerably faster than what we predicted in FY95 using *ab initio* quantum chemistry methods. It is conceivable that a fast process with the same overall result as Reaction 2 could occur heterogeneously, i.e., on the HTFR walls, instead of in the gas phase. If this were so, one would expect changes in pressure and reactant diffusion constants, which change the rate at which reactant is transported to the walls, to affect the measured rate constant. Figure 5 shows that, indeed, the rate constant at 670 K decreases as the reactor pressure increases. This observation is not an unambiguous indication that wall reactions are occurring, however. The existence of radial concentration gradients caused by Poiseuille flow or third-body effects on the reaction rate could also produce this result. It is important to determine the relative contributions of homogeneous and heterogeneous processes to Reaction 2, since the accuracy of model predictions depends on a correct determination of the deposition mechanism. Thus, future work will involve HTFR experiments coupled with detailed modeling designed to distinguish between the gas-phase and surface components of Reaction 2.

Task 2. Simulation of reactor fluid dynamics and mass transport

This year we extended a model developed in previous work supported by Sematech to the problem of depositing interfacial coatings on ceramic-fiber preforms. In this earlier work, we derived a rigorous perturbation expansion describing the spatial distribution of the reactive deposition precursor through the preform thickness. This new series solution accounts for all relevant transport processes, including both diffusive and convective transport, as well as both ordinary and Knudsen diffusion. Solutions for the reactive species fraction and fluid speed were carried to second order in the Thiele modulus. Although the original motivation for developing this model was to optimize furnace pressures and temperatures for wafer processing in the semiconductor manufacturing industry, the results are directly applicable to fiber-coating processes such as those used by DLC.

To validate the model, we obtained rectangular samples of boron-nitride-coated fiber preforms from DLC. These samples were analyzed using scanning electron microscopy to determine BN coating thicknesses as a function of location within the preform. An example of these measurements is shown in Figure 6. Comparison of model predictions with the measured thickness profiles provides a fairly rigorous test of the fiber-coating model. In general, measured coating thicknesses are in excellent agreement with those predicted by the model. With the increased confidence in the validity of the model, it is now possible to recommend strategies for optimizing the DLC process. Results of the model/experiment comparison are summarized below and in Figures 7-10.

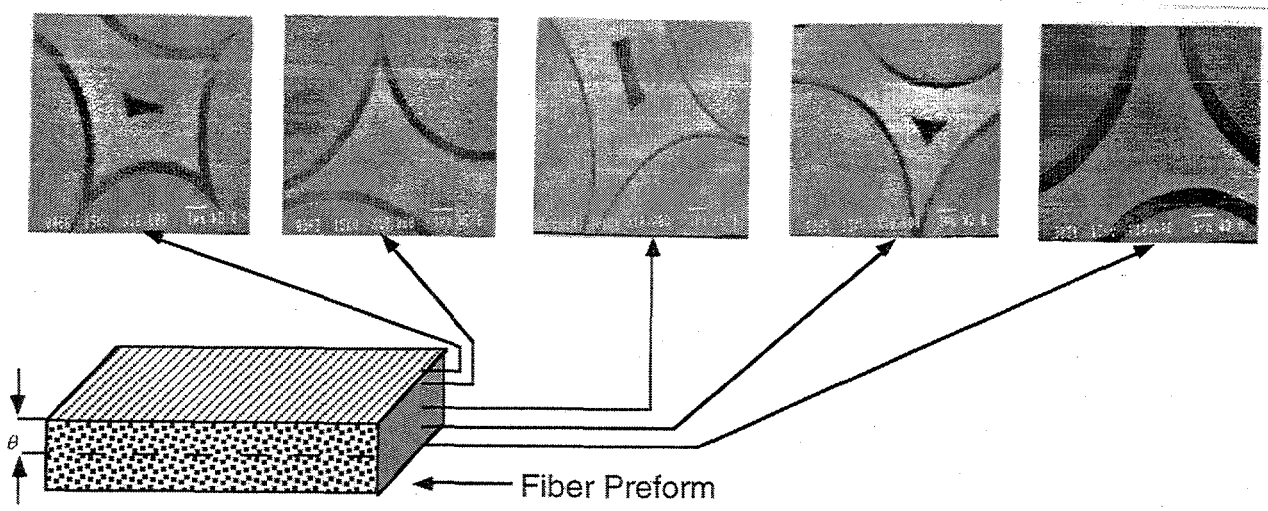

Fig. 6. Schematic illustrating how BN thickness profiles were measured on coated ceramic-fiber preforms using scanning electron microscopy. Each image corresponds to a particular location within the preform, as shown by the arrows. Gases infiltrate the preform, which is at high temperature, forming BN upon contacting fiber surfaces. In each image, portions of fiber are seen as partial circles, with dark bands of BN indicating the fiber coating. θ is the non-dimensional distance from the center of the preform to the edge.

- Predicted BN coating thickness profiles agree very well with measured thicknesses. An example of this is shown in Figure 7. In this figure, the position on the (non-dimensional) x axis varies from the center of the coated preform (x = 0) to the outside edge (x = 1). Each data point corresponds to an average of several measurements. Both the shape and the magnitude of the thickness profile are well reproduced. Similar agreement is found for data obtained in two different furnaces (varying in size by a factor of 2) and for factors of 2 variation in pressure, reactant flow rates, preform thickness, and clamping-plate porosity. Deposition rates obtained over a range of temperatures also agreed with model predictions.
- Processing conditions currently in use by DLC are nearly optimal for achieving the maximum deposition rate on the preform centerline. This is shown in Figure 8, which displays the edge, center, and mean deposition-rate profiles vs. relative temperature (where 0 = current operating condition). The figure shows that the centerline deposition rate exhibits a maximum at a temperature 30-50 °C lower than the current operating conditions, suggesting that faster deposition with slightly improved uniformity should be achievable by lowering the deposition temperature. The temperature cannot be lowered much more than this, however; although the model predicts that the uniformity would improve, it also indicates there would be a substantial reduction in the deposition rate. The maximum center-line deposition rate occurs for a uniformity of about 0.25 (determined from the ratio of the center-to-edge deposition rates).

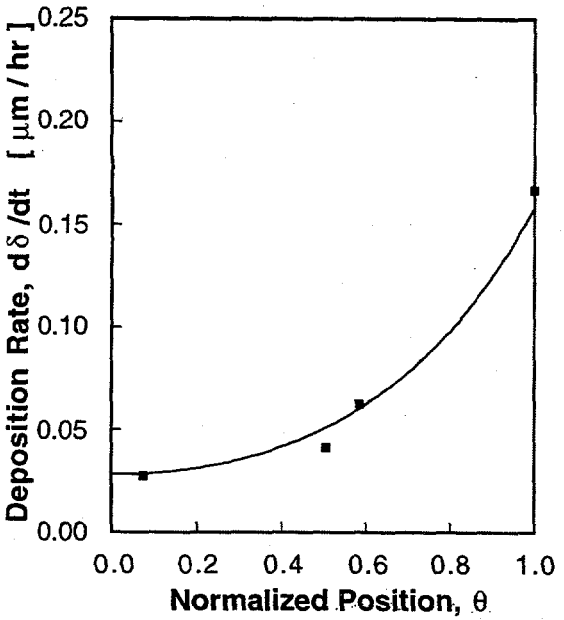

Fig. 7. Deposition rate as a function of normalized position within the part. θ of zero corresponds to the center of the part, while θ=1 corresponds to the outside surface of the part. Points represent the average of several thickness measurements; the curve is the model prediction.

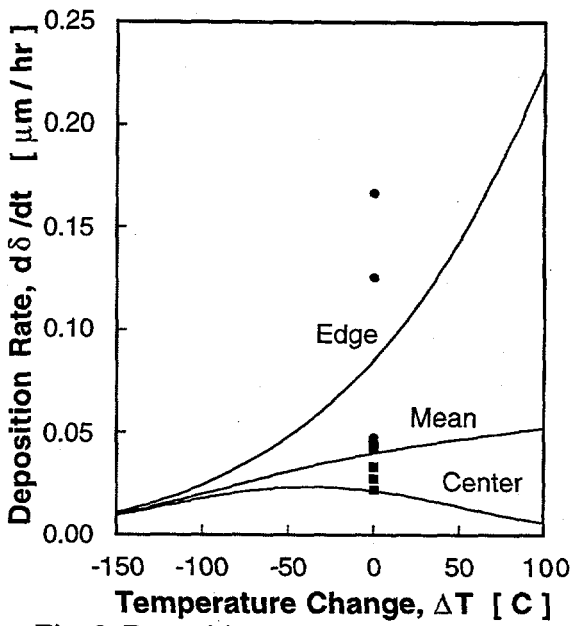

Fig. 8. Deposition rate as a function of relative temperature. ΔT=0 corresponds to the present deposition conditions. Circles represent measurements made at the outside surface of a part; squares represent measurements at the center of a part. Curves show the model predictions for the thickness profile at the edge, mean, and center of the part.

- Deposition uniformity (defined as the ratio of the deposition rate at the center of the preform to that at the edge) is strongly dependent on process temperature, fiber size, and preform thickness. Figure 9 shows the predicted and measured deposition uniformity as a function of relative temperature (as defined above) for preform thicknesses differing by a factor of two. The curves shown are actually composites of several calculations for different operating pressures. The predictions virtually overlap each other for a given preform thickness because, under the present operating conditions, Knudsen diffusion dominates transport within the preform (i.e., the mean-free path of the gas molecules is very large compared with the typical pore size, so that reactant molecules have many more collisions with the walls than with each other.) Thus, our model indicates that decreasing reactor pressure will have no effect on the uniformity, although the deposition rate will drop. Similarly, increasing the pressure is predicted to have no effect on deposition uniformity until the Knudsen number (Kn = mean free path/pore size) becomes on the order of one or smaller, at which point slower diffusion rates will begin to reduce the uniformity.

The model also shows that deposition uniformity decreases with increasing deposition rate and with the square of the part thickness. For example, to increase preform thicknesses by a factor of two (from $w^* = 1$ to $w^* = 2$, where w^* is non-dimensional) while obtaining the same uniformity requires a deposition rate that is a factor of four lower. From Figure 9, this corresponds to lowering the deposition temperature by about 100 °C. Thus, we predict that every factor of two increase in preform thickness will require a factor of four increase in coating time.

- The model predicts that deposition rates can be increased in DLC's current process by increasing the pressure, while reduced deposition temperatures will improve uniformity and increase the center-line deposition rate. These observations are illustrated in Figure 10, where the single data point represents current operating conditions (P^* is a non-dimensional pressure). The plot shows that optimum conditions correspond to a decrease in the operating temperature of 50-75 °C and a factor of four increase in pressure. Under these conditions, it should be possible to increase the center-line deposition rate by a factor of two with a corresponding increase in the uniformity of a factor of three. We note, however, that the onset of homogeneous particle formation or undesirable changes in coating composition and/or microstructure may limit how much of an improvement actually results from these changes.

Task 3. Implementation of strategies for process design, optimization, and operation

Task 3 is scheduled to begin in FY97. In this task, strategies identified as a result of the process modeling performed in FY96 will be tested using reactor facilities at DLC. Results of these experiments will be used to refine the model and identify other factors (such as the onset of particulate nucleation) not accounted for in the model that may limit its applicability.

Task 4. Development of process control sensors

The development of sensors that can monitor the BN deposition process and enable feedback control have the potential to provide major improvements in reactor throughput and product reproducibility. One approach to designing these sensors is to determine whether there are gas-phase species whose concentrations can be related to the deposition rate. The HTFR experiments described above (Task 1), in addition to providing kinetic data, identified several reaction products that can potentially be correlated with the deposition rate. As shown in Reaction 2, both Cl_2BNH_2 and HCl are gas-phase products of the reaction between BCl_3 and NH_3. During FY96, we were able to detect all four species in Reaction 2 via mass spectrometery. Another compound, $ClB(NH_2)_2$, was also detected, although in much smaller amounts. Thus, one possible strategy is to monitor the concentrations of the major boron-containing compounds and use their disappearance as a measure of the BN deposition rate. We detected these species at temperatures as low as 250 °C, suggesting that an *in situ* measurement may not be necessary, but that sampling of the gases downstream of the reactor may be possible. These concepts will be pursued in detail in FY97.

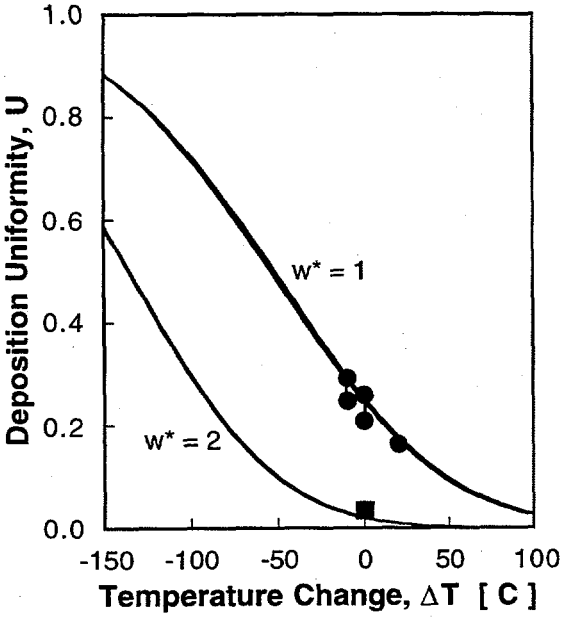

Fig. 9. Deposition uniformity (ratio of center-line to outer surface deposition rates) as a function of relative deposition temperature (defined as in Fig. 3) for two parts varying by a factor of two in thickness. Solid lines: model predictions. Circles and squares: measured BN coating thickness for two part sizes.

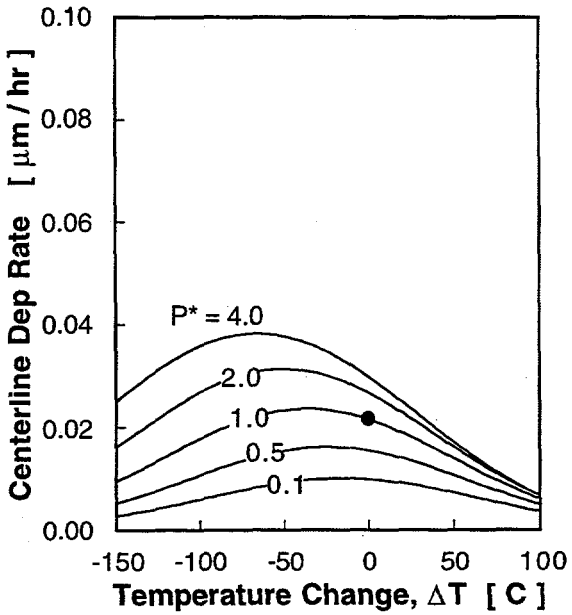

Fig. 10. Center-line deposition rate as a function of relative deposition temperature for a range of operating pressures where P*=1.0 corresponds to the current operating pressure. Curves: model predictions. Circle: current operating condition.

PUBLICATIONS

M. D. Allendorf, C. F. Melius, P. Ho, and M. R. Zachariah, "Theoretical Study of the Thermochemistry of Molecules in the Si-O-H System,"*J. Phys. Chem.*, **99**, 15285 (1995).

M. T. Schulberg, M. D. Allendorf, and D. A. Outka, "The Adsorption of Hydrogen Chloride on Polycrystalline β-Silicon Carbide," *Surf. Sci.*, **341**, 262 (1995).

M. D. Allendorf and T. H. Osterheld, "Chemical Reactions in the CVD of Boron Nitride From BCl_3 and NH_3," *Thirteenth Int. Symp. Chem. Vapor Dep.*, The Electrochemical Society (Pennington, NJ), **96-5**, 16 (1996).

M. T. Schulberg, M. D. Allendorf, and D. A. Outka "The Interaction of HCl with Polycrystalline β-Silicon Carbide," *Covalent Ceramics III: Science and Technology of Non-Oxides*, Materials Research Society, **410**, 471 (1996).

M. D. Allendorf, C. F. Melius, T. H. Osterheld, "A Model of the Gas-Phase Chemistry of Boron Nitride CVD from BCl_3 and NH_3," *Covalent Ceramics III: Science and Technology of Non-Oxides*, Materials Research Society, **410**, 459 (1996).

T. M. Besmann, M. D. Allendorf, McD. Robinson, R. K. Ulrich, Eds., *Proceedings of the Thirteenth Int. Conf. on Chemical Vapor Deposition* ,The Electrochemical Society (Pennington, NH), **96-5**, (1996).

PRESENTATIONS

M. D. Allendorf, T. H. Osterheld, and C. F. Melius, "Gas-Phase Chemistry in the CVD of Boron Nitride: Reactions of BCl_3 and NH_3," MRS Meeting, Boston, Massachusetts, December 1995.

M. T. Schulberg, M. D. Allendorf, and D. A. Outka, "The Interaction of HCl with Polycrystalline β-SiC: Evidence for a Site-Blocking Mechanism for HCl Inhibition of SiC CVD," MRS Meeting, Boston, Massachusetts, December 1995.

M. D. Allendorf, "Thermochemistry and Kinetics of Gas-Phase Reactions in the CVD of Ceramic Materials," Stanford University, February 7, 1996.

M. D. Allendorf, "Kinetics of Gas-Phase and Surface Reactions in the CVD of Ceramic Materials," National Institute of Standards and Technology, Washington, D. C., April 10, 1996.

M. D. Allendorf and T. H. Osterheld, "Chemical Reactions in the CVD of Boron Nitride from BCl_3," *Thirteenth Int. Conf. on Chemical Vapor Deposition*, Electrochemical Society Spring Meeting, Los Angeles, California, May, 1996.

M. D. Allendorf, S. Griffiths, R. Nilson, N. Yang, "Materials Processing by Design: Process Simulation for Advanced Ceramics Production," annual review, DOE/Advanced Industrial Materials Program, Oak Ridge, Tennessee, June 1996.

INDUSTRIAL INPUT AND TECHNOLOGY TRANSFER

Libbey-Owens-Ford Co. (LOF) of Toledo, OH, and Sandia National Laboratories in Livermore, CA, signed a CRADA effective August 21, 1996, whose goals are to obtain chemical-kinetic data and design computer models needed to develop new manufacturing processes for the deposition of energy efficient coatings on float-glass. These results will be used to identify new sensor technologies for on-line control of float-glass coating equipment. LOF is one of the world's largest manufacturers of float glass, which is used for windows in residential and commercial construction and for automobile windshields. The CRADA is expected to last three years, with total funding of $1.06 million. LOF is providing a 120% match of DOE funds, including both direct funds to Sandia and in-kind contributions.

COST SHARING

In kind cost sharing in the amount of $84 K was provided by DuPont Lanxide Composites for support of measurements on BN-coated ceramic preforms.

ESTIMATED ENERGY SAVINGS

The availability of low-cost, fiber-reinforced composites will have a major impact on both energy consumption and pollutant production in energy-intensive industries. For example, it is estimated that widespread use of ceramic composites will result in energy savings of up to 0.52 Quads/year in high-pressure heat exchangers, 0.1 Quads/year in hot-gas cleaning systems, and 0.5 Quads/year in radiant burners (such as those used in the metals and glass industries). Similarly, total emissions from gas turbines used in power generation systems can be reduced by as much as 75-90% (all figures courtesy of the DOE/Continuous Fiber Ceramic Composites Program). These energy savings and emission reductions can be achieved primarily through process operation at higher temperatures, where fuel combustion is more efficient.

SYNTHESIS AND PROCESSING OF COMPOSITES BY REACTIVE METAL PENETRATION

Ronald E. Loehman and Kevin G. Ewsuk
Sandia National Laboratories
Albuquerque, New Mexico 87185

Antoni P. Tomsia
Pask Research and Engineering
Berkeley, California 94720

William G. Fahrenholtz
University of New Mexico
Albuquerque, NM 87106

INTRODUCTION

Achieving better performance in commercial products and processes often is dependent on availability of new and improved materials. Ceramic-metal composites have advantages over more conventional materials because of their high stiffness-to-weight ratios, good fracture toughness, and because their electrical and thermal properties can be varied through control of their compositions and microstructures. However, ceramic composites will be more widely used only when their costs are competitive with other materials and when designers have more confidence in their reliability. Over the past four years reactive metal penetration has been shown to be a promising technique for making ceramic and metal-matrix composites to near-net-shape with control of both composition and microstructure. It appears that, with sufficient development, reactive metal penetration could be an economical process for manufacturing many of the advanced ceramic composites that are needed for light-weight structural and wear applications for transportation and energy conversion devices. Near-net-shape fabrication of parts is a significant advantage because costly and energy intensive grinding and machining operations are substantially reduced, and the waste generated from such finishing operations is minimized. The most promising compositions to date consist of Al and Al_2O_3; thus, these composites should be of particular interest to the aluminum industry.

The goals of this ceramic-metal composite research and development program are:
1) to identify compositions favorable for making composites by reactive metal penetration;
2) to understand the mechanism(s) by which these composites are formed;
3) to control and optimize the process so that composites and composite coatings can be made economically; and
4) to apply to R&D results to problems of interest to the aluminum industry.

TECHNICAL PROGRESS - FY 1996

1. Materials Synthesis

Metal-ceramic composites offer significant improvements in fracture toughness over conventional ceramic parts. We measured the toughness of two different Al_2O_3-Al-Si composites formed by reactive metal penetration (RMP). A fracture toughness of 10.5 MPa $m^{1/2}$ was measured for a composite prepared by reacting Al with porous mullite, whereas a toughness of 8.4 MPa $m^{1/2}$ was measured for Al reacted with porous kaolin.

As part of our evaluation of other ceramic-metal composite systems, we have developed processes for forming composites by reactive hot pressing of Mo-Al-mullite mixtures. Composites containing alumina and either $MoSi_2$, $Mo(Si,Al)_2$, or $Mo(Si,Al)_2$-Mo_3Al_8 were fabricated. Preliminary investigations have focused on the properties and phase equilibria in the Mo-Si-Al system. Although no one has reported on the effects of Al additions to $MoSi_2$, it is considered that ductility increases as the Al content of the Mo-Si-Al compound increases. Processing parameters were optimized to form $MoSi_2$, $Mo(Si,Al)_2$, and Mo_3Al_8, and samples were prepared for subsequent property evaluations.

Task 1. Evaluate Reactions and Mechanisms of Composite Formation in the Al/Mullite System:

We have continued our experiments to understand the mechanism for the reactive metal penetration process. Work this past year has concentrated mainly on TEM studies of reactively-formed composites done in collaboration with Professor Ping Lu of New Mexico Tech. Microstructures obtained for different stages in the reaction suggest a refinement of the hypothesized mechanism described in earlier reports.

The analyses suggest a reaction mechanism for reactive metal penetration involving molten metal penetration of the ceramic preform grain boundaries followed by Al reaction with the individual grains of the ceramic preform. For reaction at 1100°C Si is produced at the reaction front by the overall redox reaction. The rate-limiting step seems to be the dissolution of Si in the advancing molten Al front and its transport out of the developing composite.

By evaluating reactions to understand the mechanisms of composite formation by reactive metal penetration, we are establishing guidelines to control composite formation, and to control the structure and properties of composites formed by reactive metal penetration. These guidelines will form the foundation of a commercially viable process for manufacturing ceramic-metal composites with tailored properties.

Task 2. Evaluate Other Ceramic-metal Systems:

In previous work we made several compositions in other systems than the familiar Al_2O_3/Al materials by reacting mixtures of metal and ceramic powders. Recently, we prepared large monolithic parts of several of these compositions by reactive hot pressing. Reactions 1-5 show the precursor chemistry and the reaction products of the hot pressed speciments. XRD samples were prepared from hot pressed parts by pulverizing a small portion of each sample. The XRD results showed that Reactions 1-7 all produced the desired reaction products. Table 1 gives the precursors, predicted reaction products, and predicted densities for Reactions 1-5. The density, Vickers hardness, and Young's modulus were measured for each of the compositions and the measured values are given in Table 2. The data show the $Al_2O_3/MoSi_2$ composite stands out because of its high Young's modulus and hardness. This composition and the Al_2O_3/Ti composite were chosen for further study.

Reaction Equations

$3\ Mo + 8\ Al + 3\ Al_6Si_2O1_3 \rightarrow 13\ Al_2O_3 + 3\ MoSi_2$ (1)
$4\ Al + 3\ TiO_2 \rightarrow 2\ Al_2O_3 + 3\ Ti$ (2)
$7\ Al + 3\ TIO_2 \rightarrow 2\ Al_2O_3 + Al_2O_3 + 3\ TiAl$ (3)
$2\ Al + 3\ NiO \rightarrow 2\ Al_2O_3 + 3\ Ni$ (4)
$2\ Al + 3\ CuO \rightarrow 2\ Al_2O_3 + 3\ Cu$ (5)

Precursors	Products	Composite Al_2O_3 Content (Vol. %)	Composite Metal/Intermetallic Content (Vol. %)	Predicted Density (g/cm^3)
Mo, Al, Mullite	Al_2O_3, $MoSi_2$	82	18	4.39
Al, TiO_2	Al_2O_3, Ti	62	38	4.15
Al, TiO_2	Al_2O_3, TiAl	47	53	3.90
Al, NiO	Al_2O_3, Ni	56	44	6.12
Al, CuO	Al_2O_3, Cu	55	45	6.23

Table 1. Predicted compositions and densities for Reactions 1-5.

Composite	Measured Density (g/cm^3)	Relative Density	Vickers Hardness (GPa)	Young's Modulus (GPa)
Al_2O_3, $MoSi_2$	4.39	100%	13.8	382
Al_2O_3, Ti	4.12	98%	11.5	262
Al_2O_3, TiAl	3.82	98%	7.4	268
Al_2O_3, Ni	5.81	95%	9.3	292
Al_2O_3, Cu	5.38	86%	8.9	243

Table 2. Density, Vickers Hardness, and Young's Modulus of Al_2O_3-Metal and Intermetallic Composites.

Samples of the $Al_2O_3/MoSi_2$ and the Al_2O_3/Ti composites were prepared for four-point bend testing. As shown in Figure 1, the measured strength of the $Al_2O_3/MoSi_2$ specimen was 450 MPa. This strength is higher than that of the best Al_2O_3/Al composite tested to date, a 30 volume percent Al composite that had a strength of 410 MPa. The Al_2O_3/Ti composite had a much lower bend strength of only 140 MPa. It may be possible to increase the strength of the Al_2O_3/Ti material significantly by removing the last bit of porosity or by post-reaction heat treatment to toughen the metal. In light of these preliminary results, an in-depth study of the $Al_2O_3/MoSi_2$ system is under way.

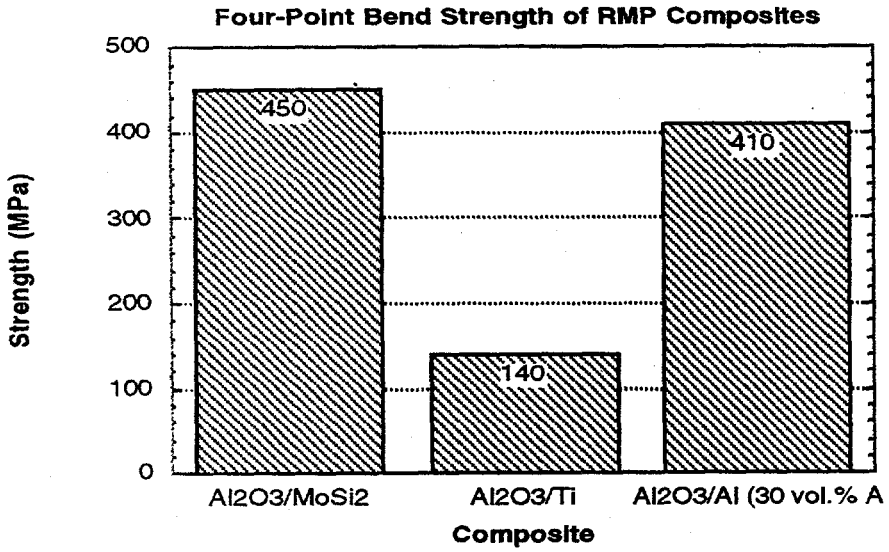

Fig. 1. Four-point bend strength of $Al2O_3/MoSi_2$, Al_2O_3/Ti, and Al_2O_3/Al composites.

As stated above, $MoSi_2$-Al_2O_3 composites can be made by hot pressing mixtures of Al, Mo, and mullite. Processing of these composites is complicated by reaction between Al and $MoSi_2$ that forms $Mo(Si,Al)_2$ and Si. Although no detailed studies have been reported, there is some indication from the research literature that addition of Al to $MoSi_2$ improves ductility, which should make $Mo(Si,Al)_2$ more ductile than $MoSi_2$. Because neither the reactivity of Al with $MoSi_2$ nor the phase equilibrium relations in the Mo-Si-Al system are well understood, we investigated both issues before attempting to optimize composite formation. First, in collaboration with Professor Arturo Bronson of the University of Texas at El Paso we constructed a proposed Mo-Si-Al phase diagram. The composition of the ternary $Mo(Si,Al)_2$ phase and the solid solution ranges of $MoSi_2$ and Mo_3Al_8 were examined using electron probe microanalysis, x-ray diffraction, and thermal analysis of reacted powder mixtures. Knowledge of the phase relations is important for composite formation in order to avoid undesirable phases such as Si during hot pressing. Formation of Si can be prevented by choosing precursors so that products fall within the $MoSi_2$-$Mo(Si,Al)_2$ or $Mo(Si,Al)_2$-Mo_3Al_8 phase fields. The ternary $Mo(Si,Al)_2$ phase was found to have a composition close to $Mo(Si_{0.93}Al_{1.43})$ with narrow two-phase fields extending to $MoSi_2$ and Mo_3Al_8.

In addition to the phase studies, an Al-$MoSi_2$ diffusion couple, shown in Figure 2, was examined by electron microprobe. Results · · that a reaction layer of $Mo(Si_{0.93}Al_{1.43})$ and Si develops between Al and $MoSi_2$ after heating to 900°C. Some of the Si reaction product appears to diffuse out of the reaction zone and into the surrounding Al. This behavior is consistent with the phase relations we determined.

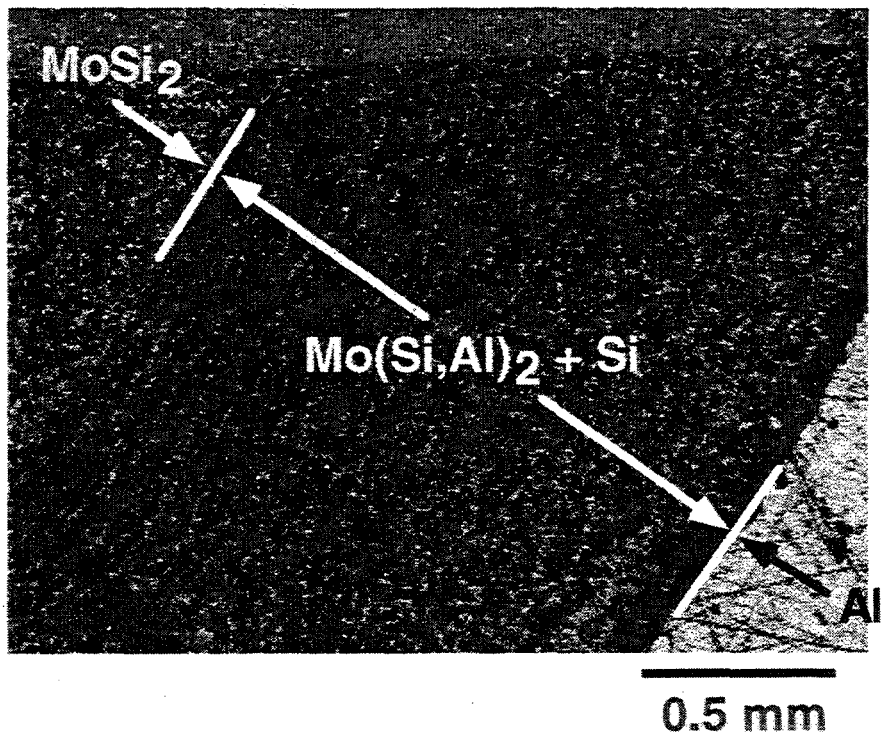

Fig. 2. Al-$MoSi_2$ diffusion couple after heat treatment at 900 °C for 30 minutes.

Using those phase relations, we prepared three different precursor powder mixtures according to the following composite forming reactions:

$$8\ Al + 3\ Mo + 3\ Al_6Si_2O_{13} \rightarrow 13\ Al_2O_3 + 3\ MoSi_2 \quad (6)$$

$$17.3\ Al + 6.5\ Mo + 3\ Al_6Si_2O_{13} \rightarrow 13\ Al_2O_3 + 6.5\ Mo(Si_{0.93}Al_{1.43}) \quad (7)$$

$$25.3\ Al + 9.5\ Mo + 3\ Al_6Si_2O_{13} \rightarrow 13\ Al_2O_3 + 6.5\ Mo(Si_{0.93}Al_{1.43}) + Mo_3Al_8 \quad (8)$$

In addition, hot pressing conditions were developed to form composites according to Reactions 7 and 8. Composite formation by Reaction 6 has already been verified. Because mechanical property data for $Mo(Si_{0.93}Al_{1.43})$ and Mo_3Al_8 are not readily available, we are preparing phase-pure specimens of each to examine density, bend strength, modulus, and fracture toughness. The properties of the individual compounds and the composites will be studied once a sufficient number of samples are prepared.

The discovery that reactive synthesis of ceramic-metal composites is possible in a variety of compositions widens the available range of properties that can be achieved. Use of kaolin as the raw material for ceramic-metal composites may have an enormous impact on the commercialization of such materials because it is a low-cost raw material that is available in nearly unlimited quantities. Combined with the ease of conversion from preform to ceramic-metal composite, the low raw material and processing costs suggest that Al/Al_2O_3 composites will be cost-competitive with traditional materials while offering superior strength and fracture toughness. Composites incorporating $MoSi_2$ made by RMP may offer advantages in increased strength and toughness at high

temperatures. In addition, the mechanism of formation provides some real process efficiencies because the Mo added to the preform internally getters the Si formed by the redox reaction.

2. Evaluation of Ceramic-Metal Composite Microstructure and Properties

Al_2O_3/Al composites prepared by reactive metal penetration (RMP) have an unusually high combination of mechanical strength and fracture toughness. Generally, Al-containing metal-ceramic composites are limited to applications with temperatures below the 660°C melting point of aluminum. The compositional flexibility of the RMP process suggests that higher temperature composites can be made by combining alumina with refractory metals or structural intermetallics if the appropriate precursor system is used. Recently, specimens in several of these more refractory compositional systems were prepared for testing of physical and mechanical properties. The composites we investigated were $Al_2O_3/MoSi_2$, Al_2O_3/Ti, Al_2O_3/TiAl, Al_2O_3/Ni, and Al_2O_3/Cu. Young's modulus, Vickers' hardness, and density were measured for specimens of each composition and four-point bend strengths were measured for the $Al_2O_3/MoSi_2$ and Al_2O_3/Ti materials. Several compositions show promise for structural applications. In particular, $MoSi_2/Al_2O_3$ composites prepared by reaction of Mo, Al, and mullite are intriguing due to their combined high strength (450 MPa) and Young's modulus (381 GPa).

This past year we made a significant effort to obtain reliable properties data for our conventional reactively-formed Al-alumina composites. As reported last year, the average strength of a composite containing ~40 volume percent aluminum was ~250 MPa. That number was only a preliminary estimate because it was based on 4-point bend tests of only 5 samples and at least 30 identical samples must be evaluated under the same conditions to obtain reasonable values for material reliability.

Large numbers of samples were prepared by reacting aluminum with porous (~60% dense) mullite preforms at 1500°C under UHP argon. Under these conditions, aluminum physically infiltrates the pores of the preform and then reacts with the mullite matrix to produce an alumina-aluminum-silicon composite. Unlike reactive penetration of dense preforms, when a porous preform is used a significant amount of silicon is retained in the microstructure as discrete silicon crystals. These composites contain ~45 volume percent alumina and at least 40 volume percent aluminum. Because some of the silicon is replaced by aluminum during reaction the composites contain a maximum of 15 volume percent silicon.

An average strength of 327 MPa with a standard deviation of 49 MPa was measured for 31 composite bars. For the unreacted mullite ceramic bars, a strength of 225 MPa with a standard deviation of 32 MPa was determined. The 4-point bend strength of RMP composites with metal contents ranging from 0 to 40 volume percent Al is shown in Figure 3. Strength does not decrease with increasing metal content as might be expected from a simple rule-of mixture analysis using the 70 MPa yield strength of aluminum. The strength of the composite is higher than expected due to the strength of the alumina skeleton and to the complex, interpenetrating microstructure of the composite.

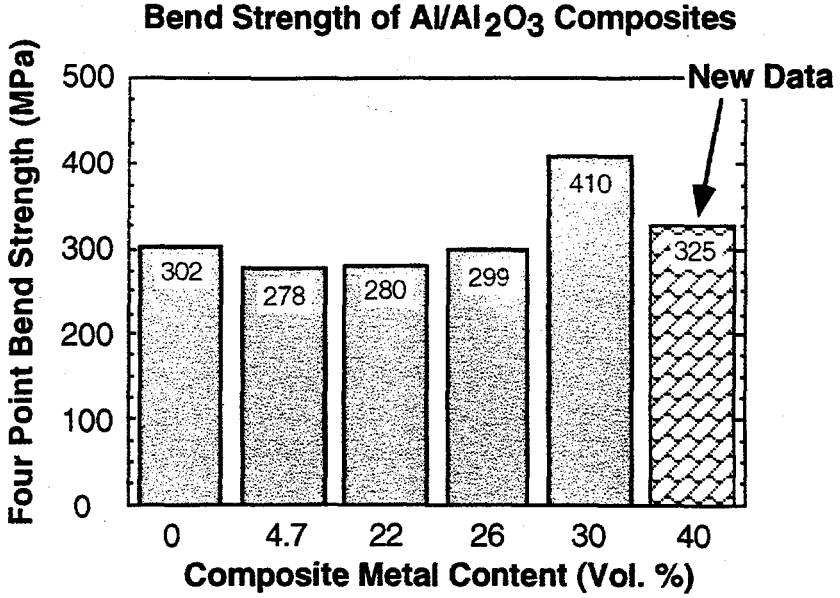

Fig. 3. Strength of RMP composites as a function of metal content.

The reliability, as measured by the Weibull modulus, had a value of about 11 for both the RMP composite and for the mullite ceramic. A reliability plot is given in Figure 4. The data show that the strength of the composite is greater than the ceramic precursor, but the reliability, which is related to the slope and intercept of the probability plot, is the same for the two materials. A Weibull modulus of 11 is fairly high for brittle ceramics such as mullite, but is rather low for a high-toughness composite. An increase in Weibull modulus indicates an increase in flaw tolerance. In the present case, the similarity of the Weibull moduli suggests that sample preparation may be the determining factor. Presently, a series of samples are being prepared for a reliability study in which different post-machining surface treatments will be used in an attempt to increase the reliability of the composites.

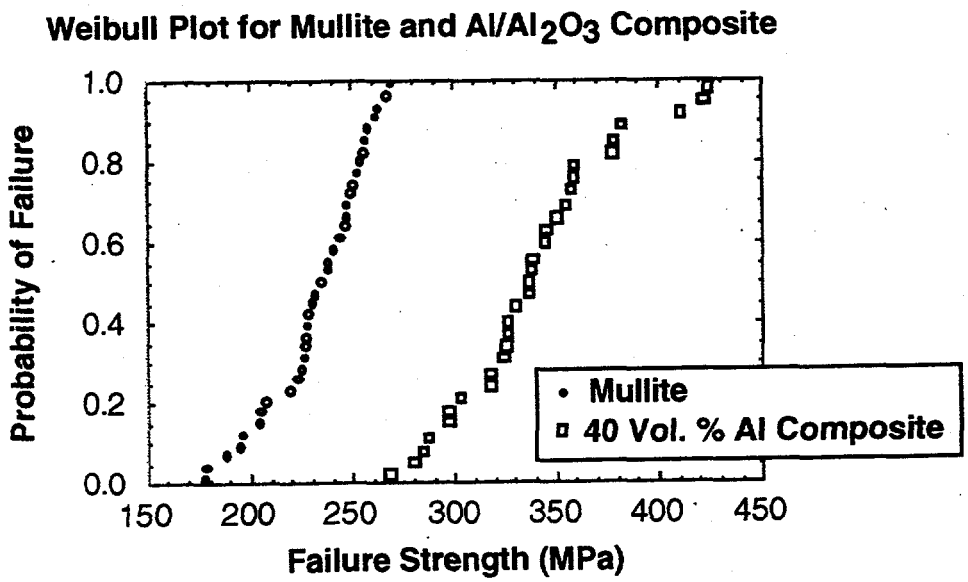

Fig. 4. Reliability of mullite and the 55 vol.% metal composite.

Material	Al Content (volume percent)	Thermal Conductivity (W/m K)
RMP 1	15	43
RMP 2	30	62
RMP 3	40	92
Alumina	0	35
DIMOX™	5	36
C[4]	30	80
Aluminum	100	250

Table 3. Thermal conductivity data for RMP composites, alumina, aluminum, and two Al/Al_2O_3 composites.

Thermal conductivity is an important property for composite applications ranging from brake rotors to electronic packages. One processing objective for composites is to combine the strength and stiffness of ceramics with the high thermal conductivity of metals. Thermal conductivity as a function of metal content was measured for 3 different RMP composite compositions. The thermal conductivity of RMP composites containing 15, 30, and 40 volume percent aluminum is reported in Table 3. Thermal conductivity ranged from 43 W/m K for a composite containing 15 volume percent metal to 92 W/m K for a composite with higher metal content. For comparison, reported values of thermal conductivity for alumina, aluminum, a DuPont/Lanxide DIMOX™ composite, and a C[4] composite containing 30 volume percent aluminum are also given in Table 3.

The fracture toughness of two Al_2O_3-Al-Si composites was determined on short rod specimens. The composites were prepared by the combined physical infiltration and RMP of porous mullite and porous kaolin preforms. Porosity and composition data for both preforms are given in Table 4. As shown in Table 5, both composites contain ~38 volume percent Al. Figure 5 shows the toughness of these composites as compared to previously studied Al_2O_3-Al composites and to data for a dense mullite preform. The composite prepared from porous mullite has a toughness of 10.5 MPa $m^{1/2}$, whereas the toughness of the composite prepared from porous kaolin is 8.4 MPa $m^{1/2}$. The lower toughness of the composite made from kaolin is likely due to its higher Si content (18 volume percent), as compared to the mullite-derived composite (11 volume percent Si). The higher Si content in the composite results from the higher silica to alumina ratio of kaolin as compared to mullite preforms.

The properties we have obtained show that ceramic-metal composites made by RMP are in the range desired for many applications. The trend in values of the Weibull modulus suggests that we are learning how to process these materials more reliably, which will achieve more consistent properties. This consistency is the result of increased understanding of reaction mechanisms we have developed under Task 1. Greater reproducibility and reliability can be expected for RMP composites based on this work.

	Porous Kaolin	Porous Mullite
Porosity (vol. %)	40	38
Material	46	72
RMP 1	54	28

Table 4. Composition and porosity for porous kaolin and porous mullite preforms.

	Kaolin Composite	Mullite Composite
Al (vol. %)	38	38
Al_2O_3 (vol. %)	44	51
Si (vol. %)	18	11

Table 5. Compositions of Al_2O_3-Al-Si composites prepared by physical infiltration and RMP of porous kaolin and mullite ceramic preforms.

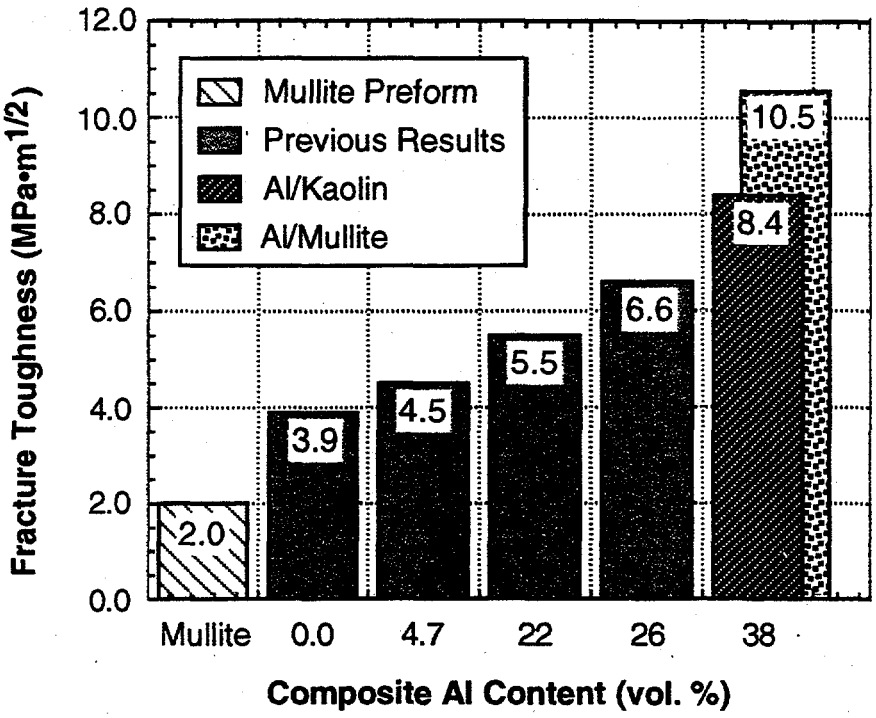

Fig. 5. Fracture toughness of Al_2O_3-Al and Al_2O_3-Al-Si composites as compared to a dense mullite preform.

3. Protective Coatings on Metals (Summary of SRI Results)

Results during the first year of this project indicated that coatings based on a broad range of fillers mixed into low-cost preceramic binders can be applied to metals, adhere well, and are very corrosion resistant. The concept is based on the use of a mixture of preceramic polymers, ceramic powders, and metal powders. Such a formulation, if heated above 450°C, will yield ceramic or metal/ceramic composite coatings, some with near zero shrinkage. At lower temperatures, an inorganic-organic hybrid material (90% and above is inorganic) coating is formed from the highly cured polymer and the filling powders. When applied to aluminum, steel, and other metals, these coatings are very adherent, withstand wear resistance, and allow the use of thinner coatings than with conventional, corrosion resistant paints. In addition, the coatings are resistant to HCl and long-term, salt spray testing. More detailed information on these results are available in the annual report SRI wrote on their subcontract work.

PUBLICATIONS AND PRESENTATIONS

Journals

Ronald E. Loehman, Kevin Ewsuk, and Antoni P. Tomsia, "Synthesis of Al_2O_3-Al Composites by Reactive Metal Penetration," *J. Amer. Ceram. Soc.* **79**[1] 27-32 (1996).

E. Saiz, A. P. Tomsia, R. E. Loehman, and K. G. Ewsuk, "Effects of Composition and Atmosphere on Reactive Metal Penetration Of Aluminum in Mullite, " *Journal of the European Ceramic Society*, **16** 275-280 (1996).

W.G. Fahrenholtz, K.G. Ewsuk, R.E. Loehman, and A.P. Tomsia, "Formation of Structural Intermetallics by Reactive Metal Penetration of Ti and Ni Oxides and Aluminates," *Metall. Mater. Trans,* **27A** [8] (1996).

W. G. Fahrenholtz, K. G. Ewsuk, R. E. Loehman, "Near-Net Shape Processing of Metal-Ceramic Composites by Reactive Metal Penetration," *J. Am. Cer. Soc.* **79**[9] 2497-99 (1996).

Kevin G. Ewsuk, S. Jill Glass, Ronald E. Loehman, Antoni P. Tomsia, and William G. Fahrenholtz, "Microstructure and Properties of Al_2O_3-Al Composites Formed by In-Situ Reaction of Aluminum and Mullite," *Metall. Mater. Trans. A*, **27A**[8] (1996).

Graduate Student Theses

B. P. Hansen, "Wetting and Penetration of Mullite by Reactive Metals," M.S. Thesis, University of Texas at El Paso, El Paso Texas (1996).

Y. Tu, "Microstructure and Infiltration Mechanism Studies of Composites Made by Reactive Metal Infiltration," M.S. Thesis, New Mexico Institute of Mining and Technology (1996).

Presentations

A.P.Tomsia, E.Saiz and R.E. Loehman, "Reactive formation of Al/Al_2O_3 Composites", International Symposium on Synergistic Synthesis of Inorganic Materials, organized by Max Planck Institute. Schloss Ringberg, Germany, March 17-22, 1996.

K.G. Ewsuk, S.J. Glass, and W.G. Fahrenholtz, "Properties, Toughness, and Reliability of Ceramic-Metal Composites Formed By Reactive Metal Penetration," presented at the 98th Annual Meeting of the American Ceramic Society, Indianapolis, IN, April 14-17, 1996.

B.B. Lakshman, W.G. Fahrenholtz, K.G. Ewsuk, and R.E. Loehman, "Formation and Microstructures of Mg-Ceramic Composites," presented at the 98th Annual Meeting of the American Ceramic Society, Indianapolis, IN, April 14-17, 1996.

B.P. Hansen, W.G. Fahrenholtz, R.E. Loehman, and K.G. Ewsuk, "Wetting and Penetration of Mullite by Mg-Al Alloys," presented at the 98th Annual Meeting of the American Ceramic Society, Indianapolis, IN, April 14-17, 1996.

W.G. Fahrenholtz, K.G. Ewsuk, and R.E. Loehman, "Mechanical Behavior of Alumina-Metal and Intermetallic Composites," presented at the 98th Annual Meeting of the American Ceramic Society, Indianapolis, IN, April 14-17, 1996.

A.P. Tomsia and E. Saiz "Metal Ceramic Interfaces in Reactive Formation of Composites," (invited) presented at the 98th Annual Meeting of the American Ceramic Society, Indianapolis, IN, April 14-17, 1996.

R. E. Loehman, B. B. Lakshman, and A. P. Tomsia, "Joining Ceramics with Reactive Metals," (invited) presented at the 98th Annual Meeting of the American Ceramic Society, Indianapolis, IN, April 14-17, 1996.

K. G. Ewsuk and R. E. Loehman, "Forming Al_2O_3-Al Composites by Reacting Aluminum with Aluminosilicate Ceramics," (invited) presented at the Materials Science Seminar, University of Texas El Paso, El Paso, TX, April 29, 1996

K. G. Ewsuk and R. E. Loehman, "Forming Al_2O_3-Al Composites by Reactive Wetting, Penetration, and Reaction of Aluminum with Aluminosilicate Ceramics," (invited) presented at the Materials Science Seminar, Alcoa, Pittsburgh, PA, May 6, 1996

K. G. Ewsuk, R. E. Loehman, W. G. Fahrenholtz, and A. P. Tomsia "Forming Controlled Composition and Property Ceramic-Metal Composites by Reactive Processing", presented at Ceramic Microstructures 96, Berkeley, CA, June 24-27, 1996

R. E. Loehman, K. G. Ewsuk, W. G. Fahrenholtz, and A. P. Tomsia "Ceramic-Metal Composites by *in-situ* Reaction", presented at Ceramic Microstructures 96, Berkeley, CA, June 24-27, 1996

K. G. Ewsuk, R. E. Loehman, W. G. Fahrenholtz, and A. P. Tomsia, "Synthesis and Processing of Composites by Reactive Metal Penetration," presented at the Advanced Industrial Materials (AIM) Program Annual Progress Review for FY95, Oak Ridge National Laboratories, Oak Ridge, TN (June 24-26 1996).

W. G. Fahrenholtz, K. G. Ewsuk, R. E. Loehman, and A. P. Tomsia, "Controlled Composition Al_2O_3/Al Composites formed by Reactive Metal Penetration," presented at the Advanced Industrial Materials (AIM) Program Annual Progress Review for FY95, Oak Ridge National Laboratories, Oak Ridge, TN (June 24-26 1996).

Ronald E. Loehman, Kevin G. Ewsuk, William F. Fahrenholtz, Bala B. Lakshman, and Antoni P. Tomsia, "Reaction Mechanisms and Microstructures of Ceramic-Metal Composites made by Reactive Metal Penetration", Ceramic Microstructures 96, Berkeley, CA, June 24-27, 1996.

Ronald E. Loehman, Kevin G. Ewsuk, William Fahrenholtz, and Bala Lakshman "Interfaces in Reactively-formed Ceramic-Metal Composites," International Workshop on Ceramic Interfaces, Karunda, Australia, July 10-13, 1996.

Ronald E. Loehman, Kevin G. Ewsuk, William F. Fahrenholtz, and Bala B. Lakshman, "Ceramic-Metal Composite Formation by Reactive Metal Penetration," Ceramic and Metal Matrix Composites CMMC96, San Sebastian, Spain, Sept. 9-12, 1996.

HONORS AND AWARDS

None this reporting period

PATENTS/DISCLOSURES

In February, 1996 three Technical Advance (TA) disclosures were filed with Sandia National Laboratories in order to initiate the patent application process. The titles of the TA's were "Method for Forming Low-Cost Metal-Ceramic Composites," "Rapid Method for Forming Metal-Ceramic Composites," and "Method for Forming Ceramic-Metal Composites with Controlled Composition and Properties."

LICENSES

None this reporting period

INDUSTRIAL INPUT, TECHNOLOGY TRANSFER, AND OTHER INTERACTION

Collaboration with other researchers

We are continuing our collaboration with A.P. Tomsia of Lawrence Berkeley Laboratory. Dr. Tomsia is the co-discoverer of reactive metal penetration and has contributed significantly in the past to its understanding and development. Dr. Eduardo Saiz is a visiting scientist working with Dr. Tomsia on the project and supported by LBL. Dr. Tomsia's participation is supported by internal funds from LBL.

Professor Ping Lu of New Mexico Institute of Mining and Technology is supported on a subcontract to the project to provide TEM analysis of reaction zones and other structural information on reaction mechanisms. Bala Lakshman is a graduate student at the University of New Mexico who is doing a Master's thesis on reactive metal penetration under the direction of Dr. Ronald Loehman. Professor Raj Bordia of the University of Washington has provided a graduate student to work on the project during the past three summers at the Advanced Materials Laboratory and throughout the rest of the year at the U. of WA. Brian Hansen, one of Professor Art Bronson's graduate students at UT (El Paso) worked on the project as a co-op student and obtained his MS thesis this FY.

Dr. Sylvia Johnson and Dr. Yigal Blum worked on a subcontract to the project to evaluate oxidation- and corrosion-resistant coatings on steel and Al. The coatings are made by full or partial pyrolysis of mixtures of organo-metallic polymers, metal powders and ceramic additives, as described above.

Kevin Ewsuk and Ron Loehman visited the ALCOA Technical Center in Pittsburgh on May 6, 1996 and give a presentation on the results obtained from the OIT-sponsored composites program. During this meeting ALCOA contact Doug Weirauch discussed his company's interest in Al wetting and reaction with various ceramics for applications to Al processing and to ceramic joining. ALCOA is interested in tapping into the fundamental understanding of Al-ceramic interactions that we have developed from this research.

We also are pursuing a CRADA among Sandia, the Reynolds Metals Company, and A.P. Green, Inc. Our contact at Reynolds is Doug Stewart and at A.P. Green it is Orville Hunter. Reynolds hopes to apply our understanding of aluminum wetting and reaction to the problem of refractory corrosion in aluminum refining. A.P. Green is a major supplier of refractories to the aluminum industry and any insight we develop on improving the lifetime of aluminum refractories will be of considerable benefit to them.

POLYMERS
AND
BIOBASED MATERIALS

CONDUCTING POLYMERS: SYNTHESIS AND INDUSTRIAL APPLICATIONS

S. Gottesfeld

Electronic and Electrochemical Materials and Devices, MST-11
Los Alamos National Laboratory
Los Alamos, New Mexico 87545

INTRODUCTION

The Conducting Polymer project funded by the AIM Program has developed new methods for the synthesis of conducting polymers and evaluated new industrial applications for these materials which will result in significant reductions in energy usage or industrial waste. The applications specifically addressed during FY 1996 included two ongoing efforts on membranes for gas separation and on electrochemical capacitors and a third new application: electrochemical reactors (ECRs) based on polymeric electrolytes.

As a gas separation membrane, conducting polymers offer high selectivity and the potential to chemically or electrically adapt the membrane for specific gas combinations. Potential energy savings in the US. for this application are estimated at 1 to 3 quads/yr.

As an active material in electrochemical capacitors, electronically conducting polymers have the potential of storing large amounts of electric energy in low cost materials. Potential energy savings estimated at 1 quad/yr. would result from introduction of electrochemical capacitors as energy storage devices in power trains of electric and hybrid vehicles, once such vehicles reach 20% of the total transportation market in the US .

In the chlor-alkali industry, electrochemical reactors based on polymer electrolyte membranes consume around 1% of the total electric power in the US. A new activity, started in FY 1996, is devoted to energy efficient ECRs. In the case of the chlor-alkali industry, energy savings as high as 50% seem possible with the novel ECR technology demonstrated by us in 1996.

TECHNICAL PROGRESS - FY 1996

Summary

1. Conducting Polymer Membranes for Gas Separation

We have had during FY-1996 significant achievements in the field of gas separation with membranes of conducting polymers. This chapter of our R&D work for the AIM program has been brought to a point of successful conclusion awaiting now industrial implementation. The first support for this work was provided to LANL by the AIM Program in 1992. Initial efforts at LANL focused on the preparation of membranes of good mechanical quality from concentrated solutions of higher molecular weight polyaniline, and on the fine tuning of the nano-porosity and tortuosity of polyaniline membranes by optimized acid doping. Dense membranes of polyaniline of improved

mechanical quality (typically 25 μm thick) have been demonstrated by us to achieve record high selectivities in gas separations of industrial interest of potential for energy savings, e.g., oxygen from air, methane from carbon dioxide and hydrogen from methane.

As these efforts have advanced during the last three years with continuous support from the AIM program, other resources have been identified and added thanks to the results demonstrated and the special equipment the AIM program assisted in acquiring. This equipment includes an advanced automated gas permeation testing system, and a semi-industrial unit for hollow fiber spinning which the AIM program assisted in shipping and installing at LANL.

For compelling demonstration of the industrial viability of this novel materials application, we still had to demonstrate, however: (a) significantly enhanced throughput in the gas separation process, and (b) fabrication of conducting polymer hollow fibers which are the basis for manufacturing of industrial gas separation units. With combined support from the AIM program and from other resources, Ben Mattes at LANL has recently achieved two very significant milestones towards these targets:

(1) Asymmetric membranes of polyaniline with porous base and apparent skin thickness of 2 μm (Fig 1a), prepared recently by a proprietary process developed at LANL, demonstrated a permeant throughput enhancement by factor 50-80 compared with uniformly dense membranes of the same conducting polymer material (Fig 1b). Very significantly, as seen from Fig 1b, selectivity in pair gas separations was maintained within factor 2, or better, with such an asymmetric membrane of polyaniline, in spite of the very thin selective layer which enables the great enhancement in throughput.

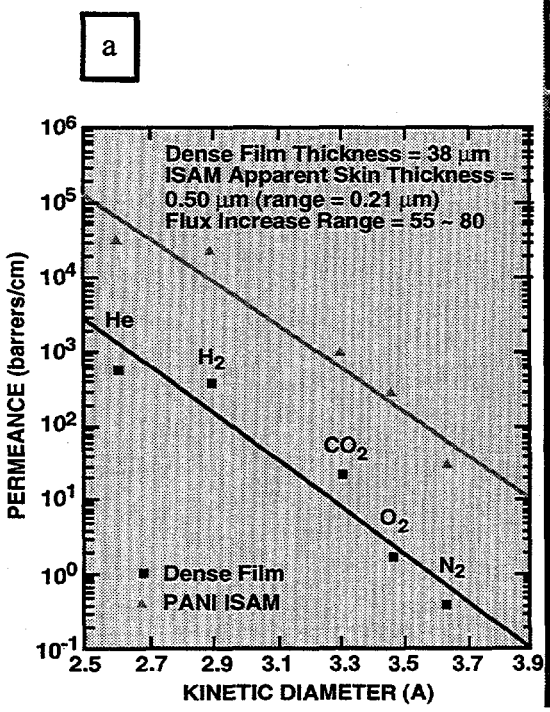

Figure 1a. Permeance throughput of asymmetric membranes of polyaniline

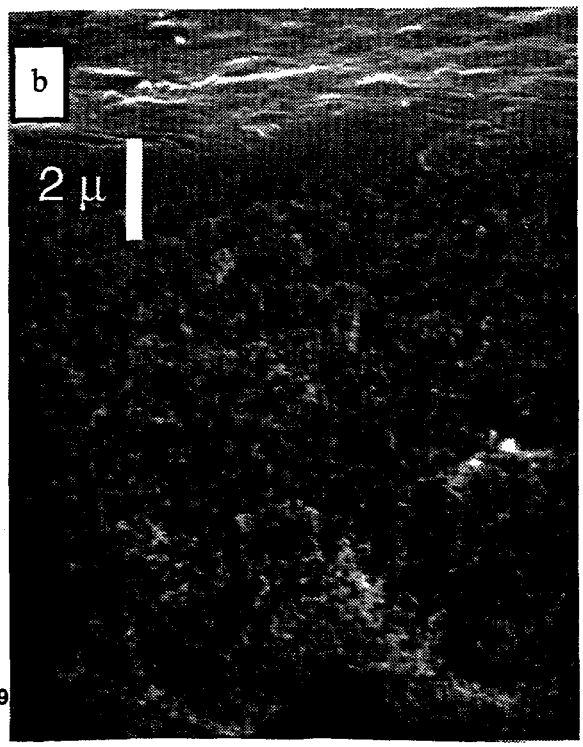

Figure 1b. Thin selective layer (2 μm) on asymmetric membranes

2) Spinning of hollow fibers (Fig 2a) of polyaniline at semi-industrial scale has been demonstrated for the first time ever using the hollow fiber spinner installed at LANL. This has required development of novel formulation and processing, resulting in initial products which have good potential for industrial gas separation processes.

The continued investment of the AIM program in this field of materials science and technology at LANL has thus resulted in significant technical achievements. Industrial interest has developed following these achievements. We are working now with two major US industries to transfer the technology and establish LANL/industry collaborations for the continued development of this novel gas separation technology.

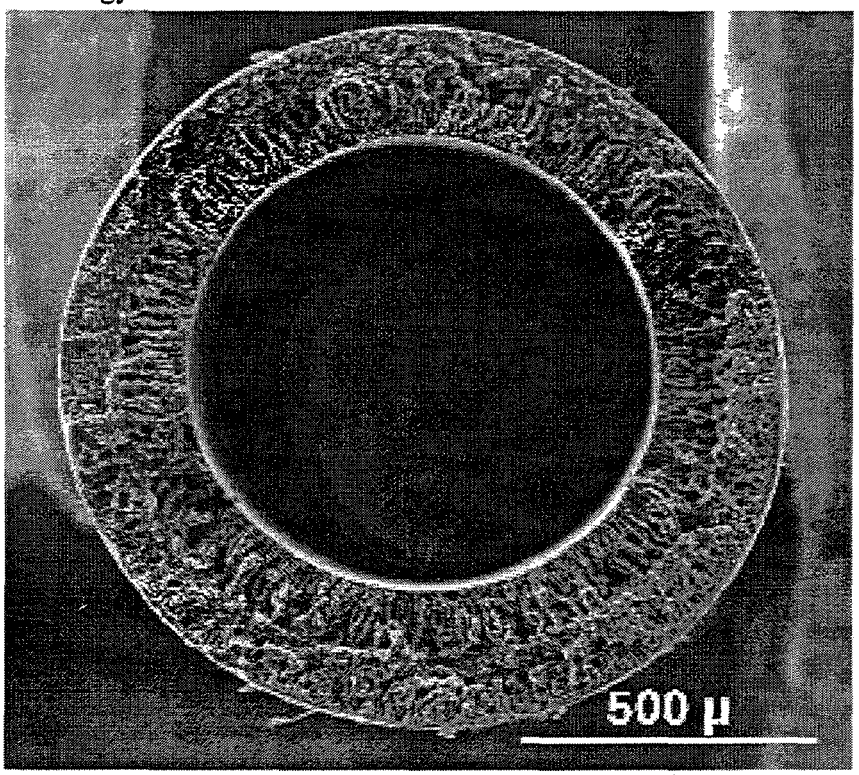

Fig. 2. Hollow fibers of polyaniline

2. Electrochemical Capacitors (Ultracapacitors) Based on Conducting Polymer (CP) Films

The activity in this component of our AIM-sponsored project was significantly reduced during FY-1996, because of lack of sufficient fit to the OIT mission. The fruit of this component of our activity, conducting polymer based ultracapacitors for peak power and/or energy storage applications, would be utilized by the electronics and/or automotive industries, rather than by any of the US industries identified by OIT for focused effort. Consequently, we have started in FY-96 a new effort that builds

on our expertise with (ionically) conducting polymers and electrochemical cells based on such membranes, devoted to significant energy savings in some industrial chemical processes. The project has already been endorsed by a major US chemical industry as basis for a CRADA agreement devoted to further development of this process. Our new effort is described in the next section.

Polymer Electrolyte Electrochemical Reactors (ECRs) of Lowered Energy Consumption -- a new effort started late in 1996.

Figure 3 demonstrates the basic idea of an advanced, polymer membrane based ECR, which we plan to develop in our near-future activity within the AIM program. The figure shows on the left the conventional configuration of an ECR used in the chlor-alkali industry, generating chlorine and caustic soda by electrolysis of sodium chloride brine. The cell employs a cation conducting polymeric membrane (CCM) which enables effective separation of the two cell compartment while providing high (cationic) conductivity. The products at the cathode are concentrated solution of caustic soda and hydrogen gas, and at the anode chlorine gas. The cell voltage required for significant electrolysis current density (typically 300 A/ft^2) is 3.2-3.3 V, as stated in figure 3a. The cell voltage directly reflects the electric energy consumption for the production of a given mass of chlorine (or caustic) product. Lowering of the cell voltage is a very important target in the case of this particular industrial process because the chlor-alkali consumes 1-2% of the total electric energy produced in the United States.

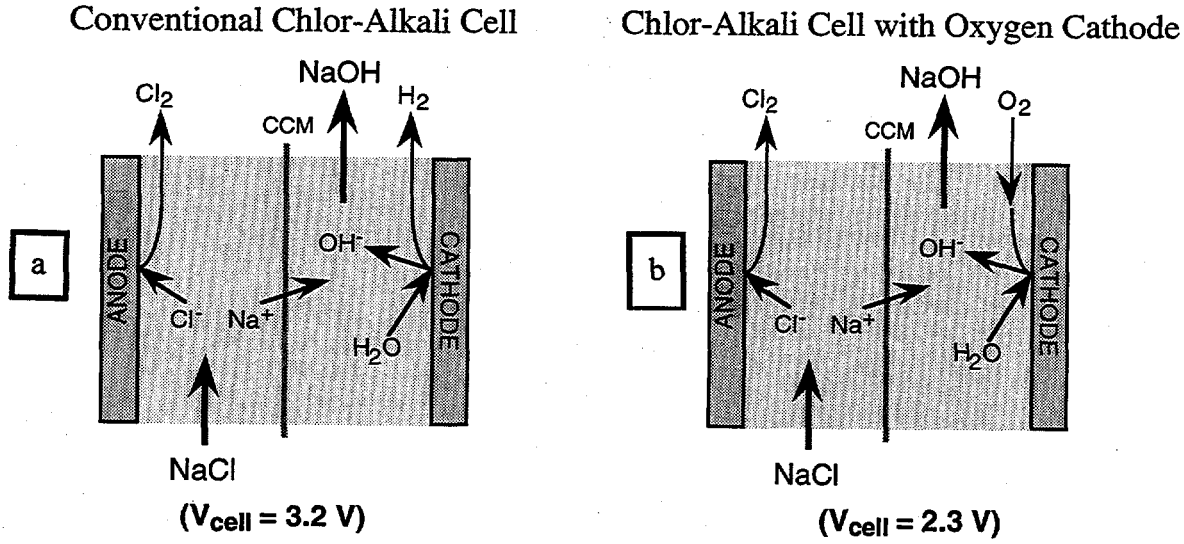

Fig. 3. Scheme for reducing energy consumption in a chlor-alkali ECR, using an effective oxygen cathode and a cation conducting polymeric membrane (CCM) as basis for effective membrane/electrode assembly

It has been recognized some time ago, that, if the hydrogen evolving cathode were replaced by an oxygen reducing cathode, the voltage of the cell could be reduced, in principle, by about 0.9V. The change of the cathodic process by introduction of oxygen as cathode reactant and the corresponding expected lowering in cell voltage are schematically depicted in figure 3b. However, to achieve the

expected savings in cell voltage as a result of introduction of oxygen as "cathode depolarizer", a very effective oxygen electrode is required. Furthermore, the cell configuration has to be such that a gas (oxygen) supplied cathode could operate side-by-side with a liquid (brine) filled cell compartment. Both of these targets have not been easy to achieve and the result has been that chlor-alkali cells with an oxygen cathode have not yet been implemented. This is in spite of the fact that efforts to prove feasibility of the concept continue to date, particularly in Japan.

We have developed in recent years at LANL an advanced oxygen/air electrode technology, originally devoted to application in polymer electrolyte fuel cells. Adaptation of this technology for ECRs, for chlor-alkali reactors as well as ECRs in other applications such as salt-splitting (salt waste minimization) and organic impurity destruction in water supply streams, seemed possible. We have built a small scale cell to demonstrate the concept, and the result has been very promising: At the industrial rate of production of 300 A/ft^2, the cell voltage was as low as 1.7V. This amounts to a savings in electric power consumption per pound of chlorine close to 50% (!) compared with present day chlor-alkali cells, a very significant achievement considering the 1-2% of total electric energy production in the US going to "fuel" this industrial process. The very low cell voltage is strong indication for the superiority of our oxygen electrode and membrane/electrode assembly technologies, as developed originally for our polymer electrolyte fuel cell project.

There is quite a lot that needs to be done in order to further validate the significance of these initial findings, including careful measurements of current efficiencies, optimization of the cation conducting polymeric membrane, including it's nature and thickness, tests of long-term stable performance, scale up of the reactor, and more. One very important element of this new project has been the immediate industrial interest expressed. A major US industry in the field of chlor-alkali production already expressed interest in working with us on this project based on a CRADA. We are thus looking forward to an exciting new chapter of work for the AIM program.

MILESTONES

A major milestone satisfied this year was in our chapter of work on conducting polymer membranes for gas separation. The milestone: "*Achieve enhanced throughput by full order of magnitude vs. dense membranes of polyaniline while maintaining selectivity in key gas separations*", was satisfied by preparation and demonstration of integrally skinned membranes (ISAMs) of polyaniline with a porous polyaniline base and a thin dense polyaniline skin of thickness 0.5-1.0 micrometer. Such bilayer membranes increased the throughput by factor 50-80 compared with dense membranes previously prepared (see figure 1b), while maintaining fully selectivity in key gas separations, as shown in the following Table for several gas pairs of technological interest

	HF Doped Dense Film	ISAM
He/N_2	1,400	1,000
H_2/N_2	960	760
O_2/N_2	6	10

Table 1: Selectivities in several gas separations measured with dense polyaniline membranes and with ISAMs of polyaniline with throughputs enhancements of 50-80.

PUBLICATIONS

X. Ren, J. Davey, S, Gottesfeld, J. Ferraris and D. Belanger "Ultracapacitors based on Conducting Polymer Active Materials," *International Seminar on Double Layer Capacitors and similar Energy Storage Devices Proceedings* (1995).

Xiaoming Ren, S. Gottesfeld and J.P. Ferraris, "Ultracapacitors using P- and N- dopable Poly(3-Arylthiophene)s", in *Electrochemical Capacitors, Proc.* **95-29**,138-161 (1996).

S.Gottesfeld, "Membrane/Electrode Assemblies: From Fuel Cells to Electrochemical Reactors," *10th nternational Forum on Electrolysis in the Chemical Industry* (1996).

PRESENTATIONS

S. Gottesfeld, "Membrane/Electrode Assemblies: From Fuel Cells to Electrochemical Reactors," the 10th International Forum on Electrolysis in the Chemical Industry, Clearwater, Florida, Nov. 1996.

PATENTS/DISCLOSURES

"Electrochemical Supercapacitors, A. Rudge, J. Ferraris and S.Gottesfeld, US Patent No. 5,527,640, June 18, 1996.

"Highly Efficient Electrochemical Reactor for the Generation of Chlorine and Alkali," Pallav Tatapudi, Mahlon Wilson and Shimshon Gottesfeld, June 12, 1996.

INDUSTRIAL INPUT AND TECHNOLOGY TRANSFER

Electrochemical Capacitors

This chapter of our work has now been moved to another DOE program (DOE/OTT), with resumption of interest at OTT in the potential of this technology for power systems in transportation applications. As our activity in this area for OIT was coming to an end during FY-1996, interest was

expressed by a small business, Federal Fabrics and Fibers (FFF) located in Andover, MA, in collaboration on a new concept of cell and stack components for electrochemical capacitors based on conducting polymer active materials. They were awarded a first phase SBIR during FY-1996, while we were still working on this subject under the AIM program. The SBIR is devoted to a collaboration with LANL on this technical subject. We will continue this collaboration with FFF as this activity becomes now a separate project under DOE/OTT.

Conducting Polymer Membranes for Gas Separation

Industrial interest has clearly developed following our recent achievements. We are working now with two major US industries to transfer the technology and establish LANL/industry collaborations for the continued development of this novel gas separation technology.

Energy Efficient Electrochemical Reactors (ECRs)

This is the new chapter of activity in our work for the AIM program. We started this work during FY-1996. Our initial reports on the performance of advanced (small scale) electrochemical reactors for electrochemical oxidations has attracted the attention of a major US company involved in the chlor-alkali industry. This industry is now having intensive discussions with us re. a CRADA agreement on the continued joint development of this advanced concept of ECRs which has a great potential for energy savings, for application in the chlor-alkali industry.

ESTIMATED ENERGY SAVINGS

The chlor-alkali industry is one of the two largest industrial consumers of electric power in the US. It is estimated that between 1-2% of the total electric power produced in the US is consumed in the production of chlorine and caustic soda. The concept of advanced electrochemical reactor for the chlor alkali industry demonstrated by us in 1996 has the potential to achieve savings in energy as high as 50% per ton of chlorine fabricated. The potential overall is thus to save 0.5 -1.0% of the total electric power generated in the US if the industry were to replace all the existing reactors by reactors based on the advanced concept. Lowering the capital costs associated with retrofitting could bring about retrofitting of a significant fraction of existing chlor-alkali plants to save operation costs. This may lead to major savings in energy, i.e., a significant fraction of 1.0% of the total electric power generated in the US.

POLYMERIZATION AND PROCESSING OF POLYMERS IN MAGNETIC FIELDS

Brian C. Benicewicz, Mark E. Smith and Elliot P. Douglas

Polymers and Coatings Group
MST-7, MS E549
Los Alamos National Laboratory
Los Alamos, NM 87545

INTRODUCTION

Liquid crystalline thermosets (LCT's) have become recognized over the past few years as an important class of materials. Numerous reports from our laboratory and others have described their synthesis and phase behavior.[1-10] In particular, we have described important effects due to the orientation of the rodlike molecules in a liquid crystalline phase. We have found that curing rates are enhanced compared to reaction in an isotropic phase,[3] and that the glass transition of the fully cured material can be significantly higher than the final cure temperature.[4]

For structural applications, orientation of LCT's will allow maximum improvement in mechanical properties. A few studies have described use of magnetic fields to orient LCT's.[8,9] However, no measurements were made of the tensile properties of materials processed in magnetic fields. We have conducted experiments which describe the tensile modulus dependence of an LCT over the complete range of magnetic field strengths from 0 to 18 Tesla. Our work has focused on the system composed of the diglycidyl ether of dihydroxy-α-methylstilbene (DGE-DHAMS) cured with sulfanilamide (SAA).

TECHNICAL PROGRESS - FY 1996

Summary

In this report we provide the description of the tensile modulus dependence of a liquid crystalline thermoset on the magnetic field strength over the range 0-18 Tesla. This work has been performed on a bis-epoxy monomer, diglycidyl ether of dihydroxy-α-methylstilbene cured with sulfanilamide. Curing was performed in magnetic fields with sample sizes large enough to permit tensile testing of "dogbone" tensile specimens. Orientation in magnetic fields leads to an increase of almost three times the modulus compared to the unoriented sample. These values are much greater than can be obtained with conventional thermoset polymers. The coefficient of thermal expansion and x-ray diffraction of oriented samples show high degrees of anisotropy, indicating significant chain anisotropy, indicating significant chain alignment in the magnetic field. We have also used a previously developed kinetic model to predict qualitative trends in the orientation kinetics.

1. Kinetic Analysis

We have previously described a model for the orientation kinetics. We have since used this model to qualitatively describe trends in the orientation behavior of reacting systems. The results of the calculation can be used to help define the processing parameters for magnetic field processing.

Figures 1-4 show various results of the calculation. As a reminder, $\varnothing$ is the angle that the rod makes with respect to the magnetic field. Thus, when $\varnothing=0$ the rod is perfectly aligned with the field. Figures 1 and 2 illustrate the advantage of using a low viscosity thermoset system compared to a high viscosity polymer, assuming a viscosity that is constant with time. For the thermoset system the orientation is complete very quickly, while for the polymer the increase in orientation is only a few degrees over the same time scale. Of course, the polymer will achieve complete orientation after either a longer time at the same field strength or in the same time at a higher field strength. However, from a processing point of view both of those options are likely to be impractical.

Figures 3 and 4 illustrate the effect of an exponentially increasing viscosity. In Figure 3 the orientation is allowed to begin at time zero. In this case full orientation is obtained only at the highest field strengths. At lower field strengths the orientation process is halted because the viscosity becomes essentially infinite. This infinite viscosity corresponds to the gel point in the cure, beyond which the epoxy network is formed and molecular level motions are prevented. Figure 4 show the case where the orientation process does not begin until sometime after the cure starts. This situation corresponds to the fact that the epoxy monomer used in this work is initially isotropic at the cure temperature and becomes liquid crystalline during the cure. In this case the orientation obtained before the gel point is minimal, because there is not enough time for full orientation to occur before the material reaches the gel point. Again, higher field strengths will result in full orientation, but longer times in the field do not help because of the gel effect. Thus, in defining process parameters for thermoset systems using magnetic fields one must be aware that there is a limit on the amount of time in the field that is useful.

2. Mechanical Properties

We have found experimentally that the molecules are oriented in the direction of the magnetic field, and that the thermal expansion exhibits a pronounced anisotropy. The results of the thermal expansion measurements are shown in Figure 5. The difference in thermal expansion parallel and perpendicular to the field is due to a difference in the density of primary covalent bonds in each of the two directions. Since the molecules are aligned parallel to the field, the density of bonds is much greater in that direction than they would be in an unaligned sample. Since chemical bonds have a low coefficient of thermal expansion the thermal expansion is reduced. There is a similar increase in the thermal expansion perpendicular to the field direction due to the decreased density of bonds in that direction. Note however, that the volumetric expansion is approximately independent of field strength; the decrease in expansion parallel to the field is balanced by the increase perpendicular to the field.

Measurements of the tensile modulus of oriented samples have also been performed. Figure 6 shows the variation of tensile modulus with field strength. The general trend of this data is similar to that

of the thermal expansion data. There is a rapid increase in modulus at low field strength, followed by a leveling off at approximately 9 Tesla. Most noteworthy is the modulus value obtained at the highest field strengths, almost 1200 kpsi. This value for a tensile modulus is extremely high for an unfilled epoxy, and demonstrates the potential for developing materials with unique properties through magnetic field processing.

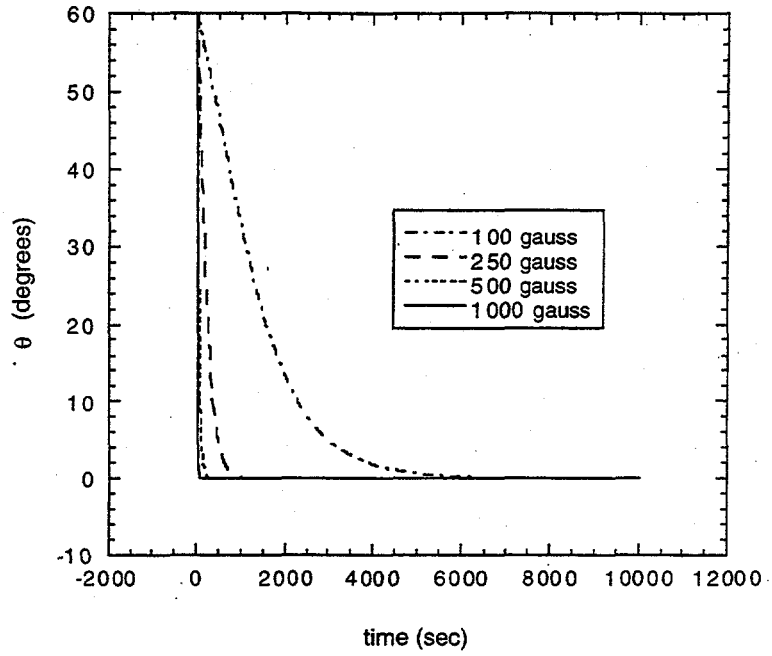

Fig. 1. Calculations of the orientation kinetics of a rod in a magnetic field for the case of constant viscosity with time. The rod initially makes an angle of 60° with the magnetic field, and the viscosity equals 1 poise.

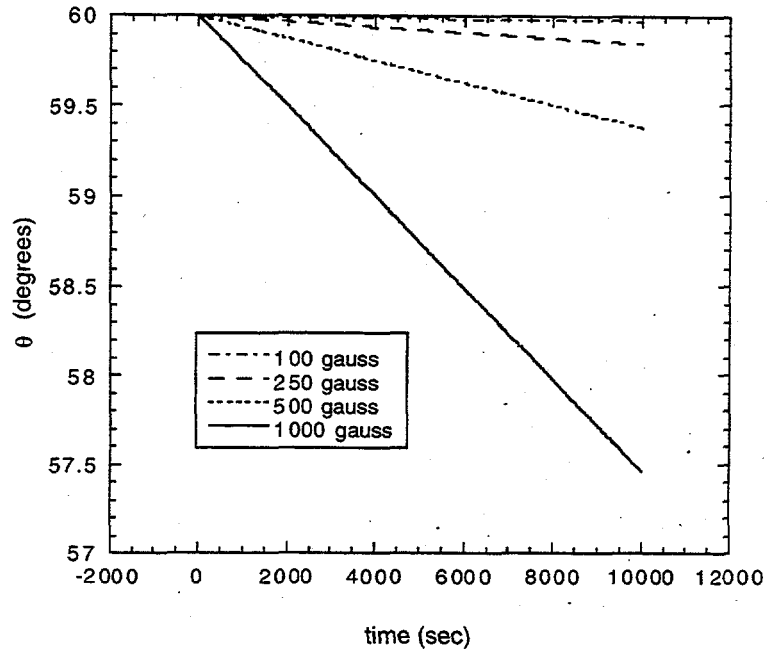

Fig. 2. Calculations of the orientation kinetics of a rod in a magnetic field for the case of constant viscosity with time. The rod initially makes an angle of 60° with the magnetic field, and the viscosity equals 10,000 poise. Note the difference in the y-axis scale compared to Figure 1.

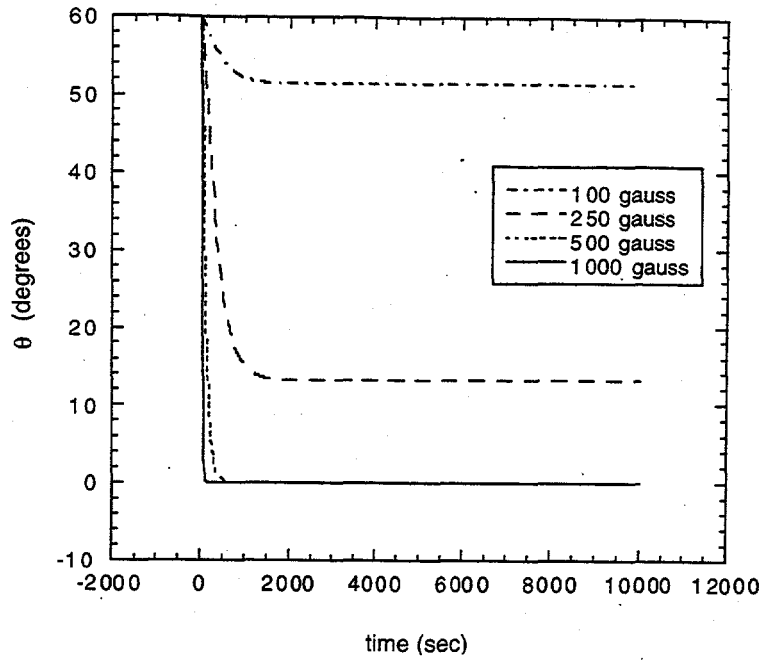

Fig. 3. Calculations of the orientation kinetics of a rod in a magnetic field for the case of exponentially increasing viscosity with time. The rod initially makes an angle of 60° with the magnetic field, the viscosity at t = 0 is approximately 1 poise, and the orientation begins at time t = 0.

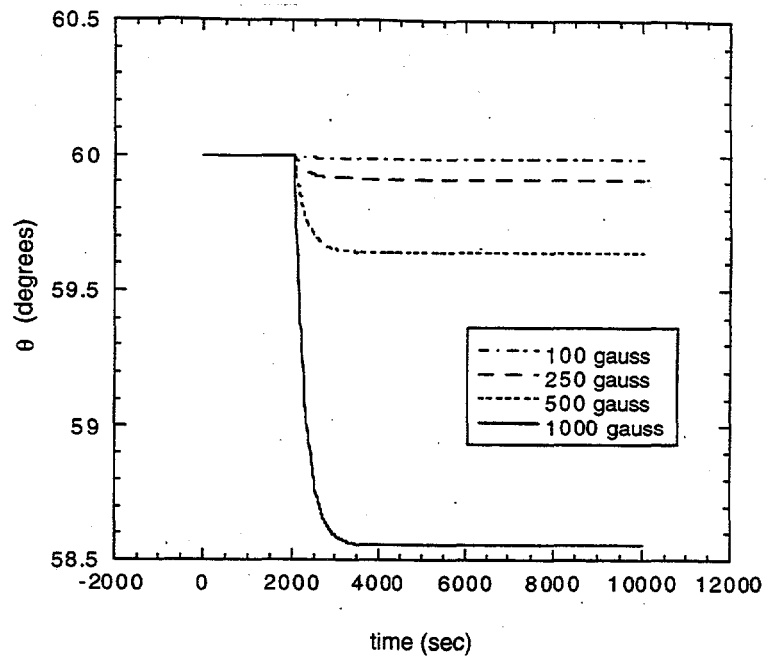

Fig. 4. Calculations of the orientation kinetics of a rod in a magnetic field for the case of exponentially increasing viscosity with time. The rod initially makes an angle of 60° with the magnetic field, the viscosity at t = 0 is approximately 1 poise, and the orientation begins at time t = 34 minutes. Note the difference in the y-axis scale compared to Figure 3.

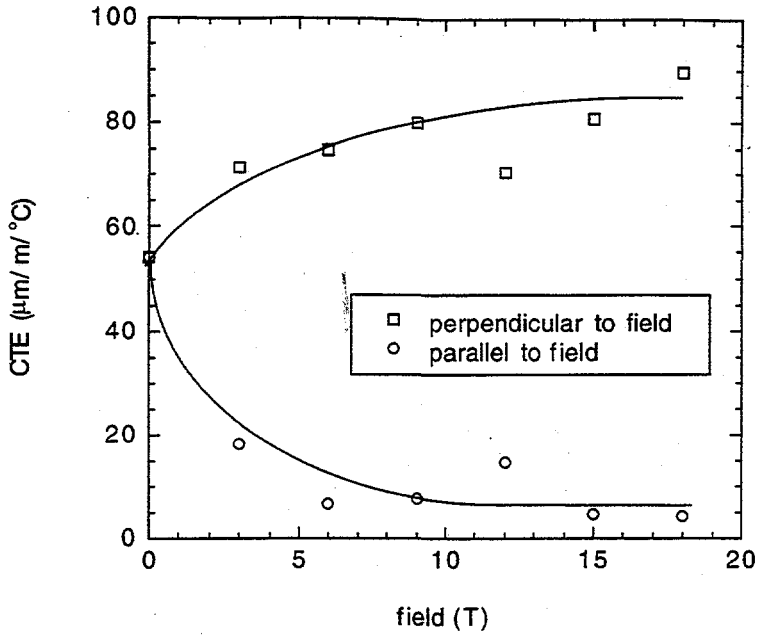

Fig. 5. Coefficients of thermal expansion measured perpendicular and parallel to the field direction as a function of field strength.

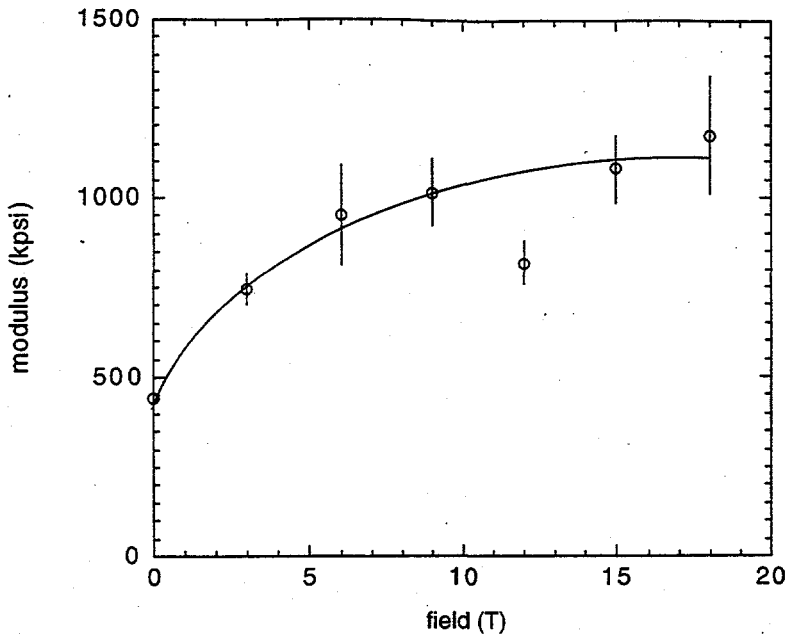

Fig. 6. Tensile modulus measure parallel to the field direction as a function of field strength.

REFERENCES

1. A.E. Hoyt, B.C. Benicewicz, J. Polym. Sci., Part A: Polym. Chem., 1990, 28, 3403.

2. A.E. Hoyt, B.C. Benicewicz, J. Polym. Sci., Part A: Polym. Chem., 1990, 28, 3417.

3. E.P. Douglas, D.A. Langlois, and B.C. Benicewicz, Chem. Mater., 1994, 6, 1925.

4. D.A. Langlois, M.E. Smith, B.C. Benicewicz, and E.P. Douglas, Polym. Mater. Sci. Eng., 1996, 74, 135.

5. M.H. Litt, W. Whang, K. Yen, and X. Qian, J. Polym. Sci., Part A: Polym. Chem., 1993, 31, 183.

6. A.P. Melissaris, M.H. Litt, Macromolecules, 1994, 27, 883.

7. A.P. Melissaris, M.H. Litt, Macromolecules, 1994, 27, 888.

8. A.P. Melissaris, M.H. Litt, Macromolecules, 1994, 27, 2675.

9. G.G. Barclay, S.G. McNamee, C.K. Ober, K.I. Papathomas, and D.W. Wang, J. Polym. Sci., Part A: Polym. Chem., 1992, 30, 1845.

10. G.G. Barclay, C.K. Ober, K.I. Papathomas, and D.W. Wang, Macromolecules, 1992, 25, 2947.

PUBLICATIONS

Properties of Liquid Crystal Thermosets and Their Nanocomposites, D.A. Langlois, M.E. Smith, B.C. Benicewicz, R.P. Hjelm and E.P. Douglas, *Applications of High Temperature Polymers*, CRC Press, Boca Raton, FL, **1997**, 79-96.

Effect of High Magnetic Fields on Orientation and Properties of Liquid Crystal Thermosets, M.E. Smith, B.C. Benicewicz, E.P. Douglas, J.D. Earls, and R.D. Priester, Jr., *Polym. Prepr.* **1996**, *37(1)*, 50-51.

Phase Behavior of Liquid Crystalline Thermosets, D.A. Langlois, M.E. Smith, B.C. Benicewicz, and E.P. Douglas, *Polym. Mat. Sci. Eng.* **1996**, *74*, 135-136.

PRESENTATIONS

M.E. Smith, E.P. Douglas, B.C. Benicewicz, J.D. Earls, and R.D. Priester, Jr., *High Modulus Liquid Crystalline Thermosetting Resins Through Novel Processing Techniques*, Materials Research Society Meeting, San Francisco, CA, 4/96.

B.C. Benicewicz, M.E. Smith, and E.P. Douglas, *Recent Developments in Liquid Crystalline Thermosets*, ACS Meeting ACS Industrial and Engineering Award Symposium, New Orleans, LA, 3/96, invited.

D.A. Langlois, M.E. Smith, B.C. Benicewicz, and E.P. Douglas, *Phase Behavior of Liquid Crystalline Thermosets*, ACS Meeting Polym. Mat. Sci. Eng. Div., New Orleans, LA, 3/96.

M.E. Smith, B.C. Benicewicz, E.P. Douglas, J.D. Earls, and R.D. Priester, Jr., *Effect of High Magnetic Fields on Orientation and Properties of Liquid Crystalline Thermosets*, ACS Meeting Polym. Div., New Orleans, LA, 3/96.

HONORS AND AWARDS

Los Alamos National Laboratory "Excellence in Industrial Partnerships Award", 1996

PATENTS/DISCLOSURES

None

LICENSES

None

INDUSTRIAL INPUT and TECHNOLOGY TRANSFER

Current work on this program is being done under the auspices of a CRADA, originally signed in February, 1994, and renewed in January 1996. The industrial partner is supplying the materials for magnetic field processing and working closely with us on measurements of the effectiveness of the magnetic field processing. Quarterly meetings are held at either Los Alamos National Laboratory or Dow Chemical Company, Freeport, TX.

ESTIMATED ENERGY SAVINGS

This project has the potential for significant energy savings through the introduction of processing techniques to create high strength, light weight structural materials. Additional energy savings could result from the use of self-reinforcing liquid crystalline polymers in manufacturing processes and faster cure times. The faster cycle time per part translates to less energy used on a per part basis during the manufacturing process. Liquid crystalline polymers do not require the use of reinforcements or fillers, resulting in less wear on manufacturing equipment, elimination of compounding as a processing step, and more efficient recycling of materials.

NEW MATERIALS
AND
PROCESSES

ADVANCED INDUSTRIAL MATERIALS (AIM) FELLOWSHIP PROGRAM

Deborah Duncan McCleary

Science/Engineering Education Division
Oak Ridge Institute for Science and Education
Oak Ridge, TN 37830

INTRODUCTION

The Advanced Industrial Materials (AIM) Program administers a Graduate Fellowship Program focused toward helping students who are currently under represented in the nation's pool of scientists and engineers, enter and complete advanced degree programs.

The objectives of the program are to: 1) establish and maintain cooperative linkages between DOE and professors at universities with graduate programs leading toward degrees or with degree options in Materials Science, Materials Engineering, Metallurgical Engineering, and Ceramic Engineering, the disciplines most closely related to the AIM Program at Oak Ridge National Laboratory (ORNL); 2) strengthen the capabilities and increase the level of participation of currently under represented groups in master's degree programs, and 3) offer graduate students an opportunity for practical research experience related to their thesis topic through the three-month research assignment or practicum at ORNL.

The program is administered by the Oak Ridge Institute for Science and Education (ORISE). The following abstracts summarize the activities of two of the participants.

SECTION 1.
INTERFACIAL REACTIONS AND GRAIN GROWTH IN FERROELECTRIC $SrBi_2Ta_2O$ (SBT) THIN FILMS ON Si SUBSTRATES

B.D. Dickerson, X. Zhang, and S.B. Desu

Materials Science and Engineering Department
Virginia Polytechnic Institute and State University
213 Holden Hall, Blacksburg, VA 24061-0237

E.A. Kenik
Metals and Ceramics Division
Oak Ridge National Laboratory
Oak Ridge, TN 37831-6376

Seven "vision industries" use 80% of all U.S. industrial energy.[1] To conserve energy, these industries have requested DOE-sponsored research to develop (among other things) cheaper sensitive thermal imaging of high temperature processes.[2] In response to this need, ferroelectric thin film research could help develop simplified pyroelectric infrared cameras that operate at room temperature.

Much of the cost of traditional infrared cameras based on narrow-bandgap photoelectric semiconductors comes from the cryogenic cooling systems required to achieve high detectivity. Detectivity is inversely proportional to noise. Generation-recombination noise in photoelectric detectors increases roughly exponentially with temperature, but thermal noise in pyroelectric detectors increases only linearly with temperature. Therefore "thermal detectors perform far better at room temperature than 8-14 μm photon detectors."[3] Although potentially more affordable, uncooled pyroelectric cameras are less sensitive than cryogenic photoelectric cameras.

One way to improve the sensitivity to cost ratio is to deposit ferroelectric pixels with good electrical properties directly on mass-produced, image-processing chips. "Good" properties include a strong temperature dependence of the remanent polarization, P_r, or the relative dielectric constant, ϵ_r, for sensitive operation in pyroelectric or dielectric mode, respectively, below or above the Curie temperature, T_{curie}, which is 320°C for SBT.[4] As a ferroelectric material is heated, P_r decreases and ϵ_r increases up to T_{curie}, beyond which P_r vanishes and ϵ_r decreases. When incident infrared radiation is chopped, small oscillations in pixel temperature produce pyroelectric or dielectric alternating currents. The sensitivity of ferroelectric thermal detectors depends strongly on pixel microstructure,[5]since Ps and Er increase with grain size during annealing.[4] To manufacture SBT pixels on Si chips, acceptable SBT grain growth must be achieved at the lowest possible oxygen annealing temperature, to avoid damaging the Si chip below. Therefore current technical progress describes how grain size, reaction layer thickness, and electrical properties develop during the annealing of SBT pixels deposited on Si.

SBT films were deposited from metal organic precursors directly on p-type Si and on Pt-coated Si wafers. Film and interface cross-sections were characterized by SEM, TEM and EDAX, to find out

how grain size and interface thickness increased with annealing temperature. The dielectric constants of Pt/SBT/Pt and Pt/SBT/Si/Pt structures were compared to begin correlating electrical properties with microstructural features.

The lowest annealing temperature that produced grains as long as 100 nm was 700°C. Annealing at higher temperatures did not increase grain size, but it did increase film density by removing voids, and it also increased the thickness and roughness of a reaction layer between the SBT film and the Si substrate, which was tentatively indentified as amorphous SiO_2. After annealing at 750°C in O_2 for 1 hour, the reaction layer was 8 +-4 nm thick, which may partially explain why SBT films on Si had only 1/3 of the capacitance of SBT films on Pt. Despite reaction layer growth, the net capacitance of SBT on Si continued to increase towards the properties of SBT on Pt with higher annealing temperatures and longer annealing times.

Although far from ideal, these results demonstrate that depositing SBT directly on Si may be feasible after futher improvements. With a better undrstanding of how the cross-sectional microstructure of SBT on Pt or Si develops with annealing temperature, the deposition of SBT can be tailored more efficiently towards better electrical properties.

References

1. C.A. Sorrell, Manager, AIM Program, *Compilation of Project Summaries and Significant Accomplishments FY 1995*, ORNL, Oak Ridge, TN, April, 1996, p. 3.

2. Panel discussion, AIM Program Annual Meeting, Oak Ridge, TN, June 24-26, 1996.

3. Paul W. Kruse, "A Comparison of the limits to the performance of thermal and photon dectector imaging arrays," *Infrared Physics & Technology*, Vol. 36, 1995, p. 880.

4. Tze-Chiun Chen, *Structure and Properties Interrelationships of* $SrBi_2(Ta_{1-x}Nb_x)_2O_9$, Ph.D. in MSE, Virginia Polytechnic Institute and State University, Blacksburg, VA, December, 1995, p. 40, 125 and 126.

SECTION 2.
PHASE TRANSFORMATION STUDIES IN MECHANICALLY ALLOYED Fe-Zn AND Fe-Zn-Si INTERMETALLICS

A. Jordan,* O.N.C. Uwakweh,* and P.J. Maziasz**

*Materials Science and Engineering Department
University of Cincinnati
498 Rhodes Hall, Cincinnati, OH 45221-0012

**Metals and Ceramics Division
Oak Ridge National Laboratory
P.O. Box 2008, Oak Ridge, TN 37831

The initial stage of this study, which was completed in FY 1995, entailed an extensive analysis characterizing the structural evolution of the Fe-Zn intermetallic system. The primary interest in these Fe-Zn phases stems from the fact that they form an excellent coating for the corrosion protection of steel (i.e., automobile body panels). The Fe-Zn coating generally forms up to four intermetallic phases depending on the particular industrial application used, (i.e., galvanization, galvannealing, etc.). These intermetallics are designed as Γ, Γ_1, δ andζ individual phases and has been observed to appear in the same order above the steel substrate. However, during industrial application, the coating formed generally results in a non-equilibrium structure since the solidification of Zn occurs simultaneously with reaction to the steel substrate. Because the coating formed is usually very thin, direct identification of the various intermetallic phases can be extremely difficult and in turn, can make phase characterization practically impossible. Since the different coating applications are non-equilibrium in nature, it becomes necessary to employ a non-equilibrium method for producing homogenous alloys in the solid-state to reflect the structural changes occurring in a true coating. This was accomplished though the use of a high energy/non-equilibrium technique known as ball-milling which allowed us to monitor the evolution process of the alloys as they transformed from a metastable to stable equilibrium state. In FY 1996, this study was expanded to evaluate the presence of Si in the Fe-Zn system and its influence in the overall coating. The addition of silicon in steel gives rise to an increased coating. However, the mechanisms leading to the coating anomaly are still not fully understood. For this reason, mechanical alloying through ball-milling of pure elemental powders was used to study the structural changes occurring in the sandelin region (i.e., 0.12 wt % Si). Through the identification of invariant reactions (i.e., eutectic, etc.), we were able to explore the Sandelin phenomenon and also determine the various fields or boundaries associated with the Fe-Zn-Si ternary system.

SECTION 3.
OPTIMIZATION OF A 550/690-MPa HIGH-PERFORMANCE BRIDGE STEEL

by A.B. Magee,* J.H. Gross,* R.D. Stout and B. Radhakrishnan**

*Lehigh University Center for Advanced Technology for Large Structural System (ATLSS)

**Oak Ridge National Laboratory
P.O. Box 2008, Bldg. 4500S, MS-6140
Oak Ridge, TN 37821

This project to develop a high-performance bridge steel was intended to avoid susceptibility of the steel to weld heat-affected-zone cracking and therefore minimize the requirement for preheat and to increase its fracture toughness at service temperatures. Previous studies by the Lehigh University Center for Advanced Technology for Large Structural Systems have suggested that a Cu-Ni steel with the following composition was an excellent candidate for such a bridge steel.

C	Mn	P	S	Si	Cu	Ni	Cr	Mo	V	Cb
0.070	1.50	0.009	0.005	0.25	1.00	0.75	0.50	0.50	0.06	0.010

To confirm that observation, 227-kg heats of the candidate steel were melted and processed to 25- and 50-mm-thick plate by various thermomechanical practices, and the weldability and mechanical properties determined. To evaluate the feasibiity of reduced alloy content, two 227-kg heats of a lower hardenability steel were melted with C reduced to 0.06, Mn to 1.25, and Mo to 0.25 and similarly processed and tested.

The results indicate that the steels were not susceptible to hydrogen-induced weld-heat-affected-zone cracking when welded without preheat. Jominy end-quench tests of the higher-hardenability steel indicate that a minimum yield-strength of 690 MPa should be readily attainable in thicknesses through 50 mm and marginally at 100 mm. Mechanical-property tests of conventionally quenched and tempered plates confirmed these yield-strength observations and showed that a transition temperature lower than -85C was typical for plates through 50 mm. In addition, a yield strength of 690 MPa can be obtained upon accelerated cooling after rolling. The toughness of the steel readily met AASHTO specifications for Zone 3 in all conditions and thicknesses, and may be sufficiently tough so that the critical crack size will minimize fatigue-crack-extension problems.

The results of the Jominy tests on the lower-alloy lower-hardenability steel indicate that a yield strength of 690 MPa could be achieved only through 12-mm think plate, marginally at 25 mm and a yield strength of 80 ksi through 100 mm. Mcehanical-property tests confirmed these observations and showed that the toughness was excellent for 12-mm plate but diminished as the plate-thickness increased.

A production heat of the candidate steel should be melted and tested in plates through 100 mm to confirm the excellent combination of strength and toughness that was obtained in laboratory heats studies of the interaction between carbon and various alloying additions is recommended to optimize the composition of a 70W steel.

PUBLICATIONS

Journals

O.N.C. Uwakweh, A. Jordan and Z. Liu, "Mechanical Alloying Induced Metastability in Fe-Zn Cubic Phases" submitted to *Journal of Alloys and Compounds*, May (1996).

O.N.C. Uwakweh, A. Jordan and Z. Liu, "Mechanical Alloying Induced Metastability & Fe-Local sites in Fe-Zn Gamma Phase" submitted to *Journal of Scripta Metallurgica*, August (1996).

O.N.C. Uwakweh, A. Jordan and P.J. Maziasz " The Study of Metastable to Stable Equilibrium Transformation of Mechanically Alloyed Fe-Zn-Si Materials" submitted to *Metallurgical and Materials Transactions*, September (1996).

O.N.C. Uwakweh, A. Jordan and Z. Liu, "Mössbauer effect Study of Phase Transformations & Transition State in Mechanically Alloyed Fe-Zn Cubic System" submitted to *Journal of Applied Physics* , September (1996).

O. Uwakweh and A. Jordan "Application of Metastable Transformation of Mechanically Alloyed Fe-Zn-Si in Equilibrium Phase Studies" submitted to *Journal of Phase Equilibria,* November (1996).

Other Publications

B.D. Dickerson, M. Nagata, H.D. Nam, Y.S. Song and S.B. Desu, "Spectroscopic Ellipsometry Characterization of $La_2Ti_2O_7$ Thin Films," Materials Research Society Symposium Proceedings, Vol. 361, (MRS, 1994), pp. 197-202.

PRESENTATIONS

Oral Presentations

B.D. Dickerson, E.A. Kenik, X. Zhang and S.B. Desu, "Crystallization of Modified $SrBi_2Ta_2O_9$ (SBT) Thin Films," Summary of summer research presentation to Microscopy and Microanalytical Sciences Group, and Report to Metals and Ceramics Division, Oak Ridge National Laboratory, July 29, 1996.

A. Jordan, "Study of Fe-Zn and Fe-Zn-Si Intermetallics" presented at the Annual Meeting of the AIM Program, sponsored by the Advanced Industrial Materials Program, held in Oak Ridge, TN on June 25-26, 1996.

Poster Sessions

1. A. Jordan, "The Study of Fe-Zn Intermetallics" presented at the Annual Meeting of the AIM Program, sponsored by the Advanced Industrial Materials Program, held in Washington, DC on June 14-16, 1995.

2. A. Jordan, "Study of Fe-Zn and Fe-Zn-Si Intermetallics" presented at the Annual Meeting of the AIM Program, sponsored by the Advanced Industrial Materials Program, held in Oak Ridge, TN on June 25-26, 1996.

HONORS AND AWARDS

B.D. Dickerson - Advanced Industrial Materials Program MS Scholarship, 1995-1997, administered by Oak Ridge Institute for Science and Education, sponsored by DOE.

B.D. Dickerson - Cunningham Ph.D. Fellowship, 1997-2000, administered by the Graduate School, Virginia Polytechnic Institute and State University.

ADVANCED MICROWAVE PROCESSING CONCEPTS

R. J. Lauf, A. D. McMillan and F. L. Paulauskas

Metals and Ceramics Division
Oak Ridge National Laboratory
Oak Ridge, Tennessee 37831-6087

INTRODUCTION

The purpose of this work is to explore the feasibility of several advanced microwave processing concepts to develop new energy-efficient materials and processes. The project includes two tasks: (1) commercialization of the variable-frequency microwave furnace; and (2) microwave curing of polymeric materials.

The variable frequency microwave furnace, whose initial conception and design was funded by the AIM Materials Program, allows us, for the first time, to conduct microwave processing studies over a wide frequency range. This novel design uses a high-power traveling wave tube (TWT) originally developed for electronic warfare. By using this microwave source, one can not only select individual microwave frequencies for particular experiments, but also achieve uniform power densities over a large area by the superposition of many different frequencies.

Microwave curing of various thermoset resins will be studied because it holds the potential of in-situ curing of continuous-fiber composites for strong, lightweight components or in-situ curing of adhesives, including metal-to-metal. Microwave heating can shorten curing times, provided issues of scaleup, uniformity, and thermal management can be adequately addressed.

TECHNICAL PROGRESS - FY 1996

1. Thermosetting Adhesives Studies

Structural adhesives often require long cure times which translate into elevated per part costs. In order to make the use of adhesives for primary structures a reality in high production rate consumer goods industries, technologies for reducing the cure time of the adhesive must be developed. Adhesive bonding through the application of variable frequency microwave radiation has been evaluated as an alternative curing method for joining composite materials, metals, or metals to ceramics or composites. The studies showed that the required cure time of a thermosetting epoxy adhesive is substantially reduced by the used of VFM when compared to conventional (thermal) curing methods. Variable frequency microwave processing appeared to yield a slight reduction in the required adhesive cure time when compared to processing by the application of single frequency microwave radiation. In contrast to the single frequency processing, the variable frequency methodology does not readily produce localized overheating (burnt or brown spots) in the adhesive or the composite. This makes handling and location of the sample in the microwave oven less critical for producing high quality bonds and allows for a more homogeneous distribution of the cure

energy. Variable frequency microwave processing is a valuable alternative method for rapidly curing thermoset adhesives at low input power levels.

The first system evaluated was comprised of glass slides adhesively bonded using VFM with a center frequency of 5.03 GHz over a range of input powers and frequency sweep ranges. In the high power range, the experimental data indicates that the power varies as the negative power of the cure time, while for the lower input power region, the input power is inversely proportional to the exposure or cure time. With the variable frequency, much less input power was required to achieve curing.

Cure times below fifteen minutes, which correspond to input powers in the region of 200 watts produced samples with a significant volume fraction of bubbles in the as-cured adhesive. It should be noted that 200 watts is the maximum input power available in this specific microwave system. It is likely that the density of energy deposition into these samples occurred too rapidly resulting in excessive heating of the adhesive prior to sufficient crosslinking to prevent the outflow of the adhesive or generation of exothermic bubbles. As a result, there exists an upper threshold of energy for curing this adhesive with this technology. As the input power was decreased the time required for complete crosslinking was increased. At sufficiently low power inputs, crosslinking would not be promoted. For this material system, the lower threshold is below 125 watts. Therefore, for this adhesive/substrate material combination, VFM system, and processing conditions, the effective curing range of the adhesives is between 125 and 200 watts and the complete cure can be achieved in as little as fifteen minutes. It should be noted that the upper and lower power threshold for the variable frequency processing were much lower than for the single frequency processing. This indicates, that from an energy standpoint, variable frequency processing may be much more efficient for this type of operation.

The second system evaluated was a glass fiber reinforced isocyanurate composite. The composite was adhesively bonded under the same conditions as the glass slides. The data revealed that the effective curing range of the adhesive is between 150 and 200 watts. Additionally, the optimal cure time was fifteen minutes, which is longer than the twelve minutes required by the single frequency radiation. However, this may be related to the lower power level available in the variable furnace used in this work; perhaps the higher power level is needed to heat the substrate.

Mechanical evaluation revealed that the samples processed in the VFM for 12-14 minutes had strengths and total elongations far below those of conventionally processed samples or the microwave samples cured for longer periods of time at lower energies. Post failure analysis revealed that these samples contained bubbles characteristic of a material that underwent too high of an energy deposition during curing. This same phenomenon has been previously noted where the same adhesive was thermally cured at too high of a temperature. The samples processed by lower input energies for longer periods of time had ultimate strengths almost exactly identical to those of thermally cured samples. The total elongation (i.e., ductility, lack of stiffness) of the samples microwaved between 22 and 30 minutes was slightly greater than that of thermally cured samples. Thus equivalent failure strengths and increased ductility was noted at cure times that were between ½ and ⅔ those required for conventional curing. The increased ductility for variable frequency processed samples was not as extensive as that noted for single frequency processed samples. Further studies are required in this area to find an explanation for this observation.

Some conclusions drawn from this work are that the resultant energy deposition profile is more uniform for variable frequency microwave systems than for fixed frequency microwave systems. As a result, VFM curing is independent of sample placement in the oven while fixed frequency curing is highly position sensitive. Contrary to fixed systems, samples cured in VFM furnaces are processed with less generation of localized hot spots which result in better quality bonds. Also, the VFM technology represents a valuable alternative method for rapidly curing thermoset adhesives at low input power levels. For the substrates and adhesive used in this project, surprisingly low levels of input power were required for processing. Additionally, the application of microwave processing for joining substrates using epoxy-based adhesives significantly reduces the curing time to only a third to a quarter of the conventional cure time.

Future work may involve processing refractories via variable frequency microwaves. We have been approached by a university professor who is interested in evaluating the efficacy of the VFM methodology.

2. Microwave Furnace Development

Lambda is now actively commercializing the VFMF. As a direct result of ORNL's work on adhesive curing via variable frequency microwave irradiation, a unit was delivered to a major electronics manufacturer and additional units are pending.

PRESENTATIONS

A.D. McMillan and F.L. Paulauskas, "Processing Thermosetting Prepreg Laminates by Variable Frequency Microwave Heating," Spring Materials Research Society Meeting, San Francisco, California, April 8-12, 1996; published in the proceedings.

F.L. Paulauskas, A.D. McMillan, and C.D. Warren, "Adhesive Bonding via Exposure to Variable Frequency Microwave Radiation,"Spring Materials Research Society Meeting, San Francisco, California, April 8-12, 1996; published in the proceedings.

PATENTS/DISCLOSURES

"Process for Manufacturing Multilayer Capacitors," R.J. Lauf, et al., U.S. Patent No. 5,481,428.

"Apparatus and Method for Microwave Processing of Materials,"A.C. Johnson, R.J. Lauf, et al., U.S. Patent No. 5,521,360.

LICENSES

Lambda Technologies, Incorporated

ADVANCED POWDER PROCESSING

M.A. Janney

Metals and Ceramics Division
Oak Ridge National Laboratory
P.O. Box 2008
Oak Ridge, Tennessee 37831

INTRODUCTION

Gelcasting is an advanced powder forming process. It is most commonly used to form ceramic or metal powders into complex, near-net shapes. Turbine rotors, gears, nozzles, and crucibles have been successfully gelcast in silicon nitride, alumina, nickel-based superalloy, and several steels. Gelcasting can also be used to make blanks that can be green machined to near-net shape and then high fired. Green machining has been successfully applied to both ceramic and metal gelcast blanks.

Recently, we have used gelcasting to make tooling for metal casting applications. Most of the work has centered on H13 tool steel. We have demonstrated an ability to gelcast and sinter H13 to near net shape for metal casting tooling. Also, blanks of H13 have been cast, green machined into complex shape, and fired. Issues associated with forming, binder burnout, and sintering are addressed.

TECHNICAL PROGRESS - FY 1996

Summary

Gelcasting is a process for forming ceramic and metal powders into complex shapes. It was originally developed for ceramic powders (1-5). It is a generic process that has been used to produce complex-shaped ceramic parts from over a dozen different ceramic compositions ranging from alumina-based refractories to high-performance silicon nitride. Gelcasting can also be used to make green body blanks that are strong enough to be machined in the green state. A particular application of gelcasting to H13 tool steel for application to metal casting molds is presented.

The gelcasting process is based on a synthesis of ideas borrowed from traditional ceramics and from polymer chemistry. A process flow sheet is given in Figure 1. Gelcasting technology depends on the use of an organic monomer solution that can be polymerized to form a strong, crosslinked polymer-solvent gel. The preferred solvent is water (2-5); however, organic solvent systems have been developed as well (1,4). The balance of this paper will assume water as the solvent. The aqueous monomer solution provides a low-viscosity vehicle that is combined with ceramic powder and appropriate dispersants to form a highly fluid slurry. Methacrylamide (MAM) is the preferred monomer and methylene bisacrylamide (MBAM) and poly(ethylene glycol) dimethacrylate (PEG-DMA) are the preferred crosslinkers. Ammonium persulfate (APS) is the free radical initiator used most often; tetramethylethylene diamine (TEMED) is frequently added to catalyze the breakdown of APS in solution and, therefore, to accelerate the polymerization and crosslinking reactions. The

slurry can be easily poured into molds to form complex shapes. The monomer solution in the slurry polymerizes and crosslinks to form a polymer-water gel that permanently immobilizes the ceramic particles in the shape defined by the mold. Because the crosslinked polymer-solvent gel contains only about 15 wt % polymer, the solvent (which constitutes about 85 wt% of the liquid vehicle) can readily be removed from the gelled part by a drying step. Once dried, the crosslinked polymer can be removed using standard thermal pyrolysis (binder burnout) procedures. There is only about 2-4 wt % polymer in the dried body (based on the weight of ceramic powder), which is similar to polymer contents found in dry pressed bodies. Furthermore, there are pore channels in the dried body (which are opened during the drying stage) for the pyrolysis products to migrate through to the surface. This prevents pressure buildup and consequent bloating or cracking of the body during binder burnout. Subsequent high firing to sinter and densify the part follows procedures typical to the particular ceramic composition.

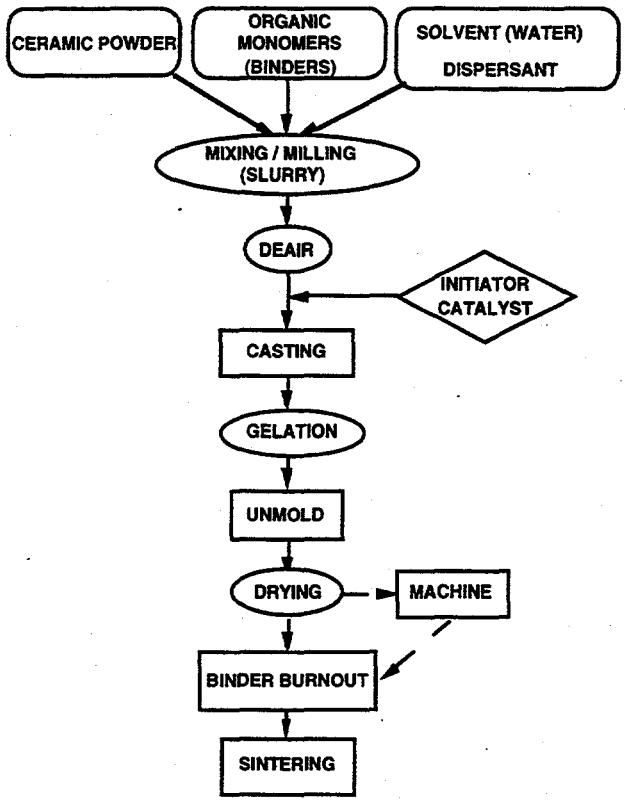

Fig. 1. Gelcasting flowchart.

Gelcasting depends on the formation of a crosslinked polymer-aqueous solution gel as the setting mechanism. Unlike systems that depend on a particular inorganic chemistry (e.g., ethyl silicate- or phosphate-bonded refractories, or sol-gel bonded ceramics), the gelcasting gel system is totally organic. Because of this, the process can be used to cast parts from any ceramic powder. Ceramics that have been gelcast include alumina, fused quartz, zirconia, silicon, silicon carbide, silicon nitride, sialon, and ferrites.

Applying gelcasting to the forming of metal powders should be a straightforward endeavor. However, there are significant differences between the physical characteristics of ceramic powders and steel powders. These differences can affect how the powder suspensions behave during gelcasting. Ceramic powders such as alumina, silicon nitride and silicon carbide tend to be finer (average diameter of 0.2 to 5 μm) and have a lower density (density from 2 to 6 g/cm^3) than do steel powders (average diameter of 20 to 100 μm, density between 7 and 9 g/cm^3). There are advantages and disadvantages for the steel powders that result from these physical property differences. One advantage is that coarser steel powders are easier to disperse than the finer ceramic powders; therefore, achieving a high solids loading in the gelcast suspension should be easier with the steel powder. A second advantage is that the pore channels in the gelled body are larger with the steel powder; therefore, drying should proceed at a faster rate and capillary stresses generated during drying should be lower. One disadvantage is that the larger diameter and higher density steel powder tends to settle out of suspension leading to problems of segregation and dilatant flow. A second disadvantage is that the body forces acting on the part are higher for the steel part because of its higher density. Problems in warping and handling may result, especially in the gelled state. The challenge is to develop a gelcasting system that addresses these concerns.

1. Gelcasting Process Development

H13 tool steel powder (Homogenous Metals, Inc., Clayville, NY) was used in this investigation. It was supplied as a -100 mesh argon gas atomized powder. A deairing paddle-type mixer (Whip-Mix, Inc., Louisville, KY) was used to blend the steel powder with the aqueous premix solution to make the gelcasting suspension. The particle size distribution of the steel powder is shown in Figure 2. The steel powder was much larger in diameter than the typical ceramic powders used for gelcasting in the past. It also exhibited features uncommon to ceramic powders such as hollow cavities in many of the larger particles and flakes of poorly atomized material (Figure 3).

The gelcasting premix used is summarized in Table 1. A higher concentration of gel former (monomer and crosslinker) was used for casting the steel powder than is typically used for gelcasting ceramics (20 wt % vs the standard 15 wt %). Also, the ratio of monomer to crosslinker was changed from 6:1 to 3:1. Both changes were made to produce a stiffer and stronger gel that would help to support the denser gelled steel parts. In addition, a proprietary suspending agent was used in the steel powder premix to prevent settling of the large, high-density steel particles.

H13 steel parts were cast from suspensions having 57 vol % (91.2 wt %) solids. The suspensions were fluid enough that they could be poured into molds. Vibratory assist was used to help mold filling. A typical batch formula is given in Table 2. The suspensions were successfully cast in aluminum and polyethylene molds. Parts were typically cured at 55°C for 30 min. After curing, the parts were cooled to ambient temperature and stripped from the molds. Parts were dried in air for about one day before binder burnout.

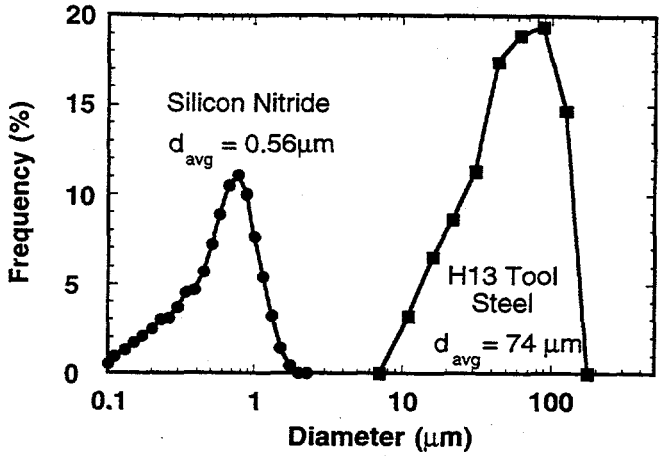

Fig. 2. H13 tool steel powder was more than two orders of magnitude larger than the ceramic powders normally used in gelcasting.

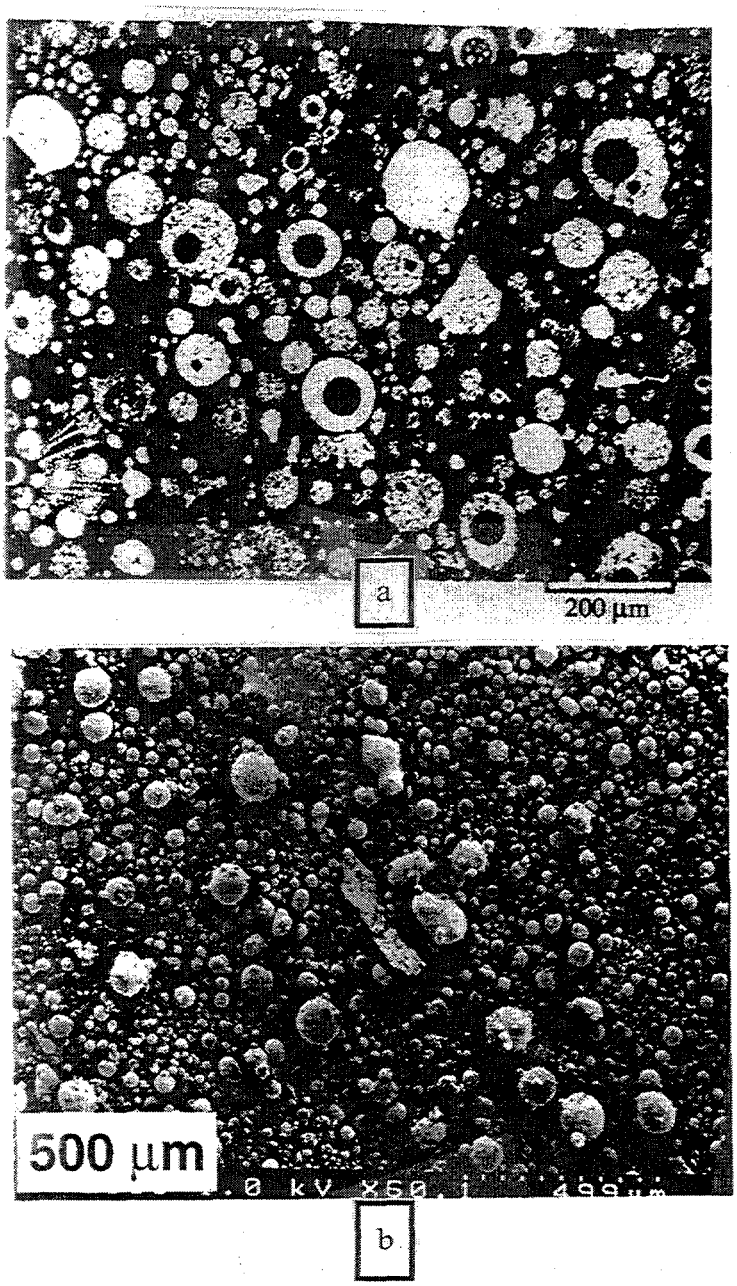

Fig. 3. Micrographs of H13 steel powder. Fig. 3a is polished section, reflected light. Fig. 3b is SEM.

Component	Ceramic		Tool Steel	
Monomer	MAM[a]	12.9 wt %	MAM	15 wt %
Crosslinker	MBAM[b]	2.1 wt %	MBAM	3 wt %
Solvent	Water	85 wt %	Water	80 wt %
Total premix		100 wt %	100 wt %	
Monomer to crosslinker ratio	6:1		3:1	

[a]Methacrylamide (Aldrich Chemical Co., Milwaukee)
[b]N,N' - methylene bisacrylamide (Aldrich)
Table 1. Premix Compositions for Gelcasting Ceramic and Steel

Component	Weight	Density	Volume
	(g)	(g/cm^3)	(ml)
Tool steel powder	900.0	7.80	115.4
10% APS in water	0.5	1.0	0.5
20 wt%, 3:1 MAM-MBAM in water	86.5	1.0	86.5
Total liquid			87.0
Total system volume			202.4
Solids loading, %			57.0
Weight % solids	0.91		
Density of slurry (g/cm^3)		4.88	
Total processing volume (slurry)		202.4	

Table 2. Batch Sheet for Gelcast H13 Tool Steel

Samples were placed on dense alumina setters for binder burnout and high firing to aid in supporting the parts. Binder burnout was conducted in an air-fired furnace (static conditions) at 1°C per min to temperatures between 200 and 350°C followed by a one hour hold at the highest temperature. After binder burnout, the parts were fragile owing to the coarse nature of the powder. High firing was accomplished in Ar-4%H_2. Parts were heated at 5°C per min to 1000°C, held at 1000°C for 2 hours to reduce oxides then heated at 5°C per min to between 1350 and 1420°C, and held at the sintering temperature for 1 hour.

Results And Discussion

A basic concern for the success of gelcasting the steel powder was binder removal. All work to date with ceramics had used an oxidizing binder burnout step to remove the polymer from the dry gelcast parts. It was not clear how such a thermal treatment would affect the steel powder particles. Therefore, simultaneous thermogravimetric analysis and differential thermal analysis (TGA/DTA, Thermal Analyst 2100, TA Instruments, Inc., Newark, Del.) of a gelcast H13 steel part was conducted, Figure 4. The analysis was conducted at two different heating rates (1 and 10°C per min) to two different peak temperatures (350°C and 500°C). The results showed that most of the binder could be removed from the part using the slower heating rate followed by a 1h hold at 350°C. The powder was partially oxidized after this treatment as evidenced by a slight blue tinge of the part.

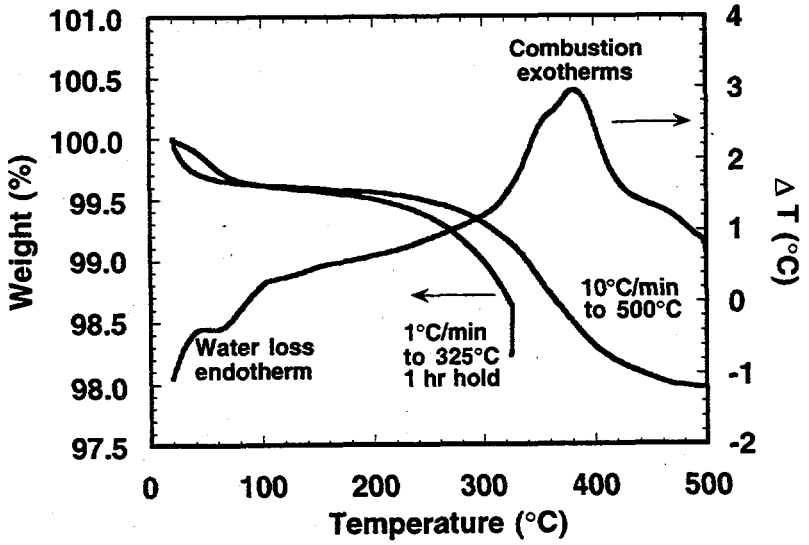

Fig. 4. Binder burnout in gelcast H13 depended on the heating rate.

An extensive study was conducted to determine how the binder burnout conditions affected the sintering of the powder and the sintered properties. Baseline properties were determined on the starting H13 powder using loose stack sintering. The powder was placed in an alumina crucible and tapped to increase its density. The green density of this powder was about 60 vol %. We determined that the best sintering conditions for this powder were achieved by firing in a tungsten element furnace (Model 901, R.D. Brew, Inc., Concord, N.H.) at 1415°C in Ar - 4% H_2. The part made from as-received powder sintered to 91.6% theoretical density (7.15 g/cm^3), contained 0.32 wt % carbon and 0.002 wt % oxygen (as determined by combustion analysis), and had a hardness of 69 R_A.

Gelcasting tends to introduce carbon into a system. For most ceramic applications, the carbon is eliminated by burning out the binder in an oxidizing atmosphere at temperatures as high as 600°C. Occasionally, the additional carbon provided by the gelcast polymer is desirable, such as with silicon carbide or boron carbide. In these cases, burnout is conducted in a neutral or reducing atmosphere. Under those conditions, the gelcast binder leaves a carbon residue equal to about 15% of the initial weight of binder in the gelcast part. Between the extremes of removing all the carbon and leaving as large a carbon remnant as possible is a continuum of residual carbon contents. For the H13 study we chose to investigate this continuum and find out if an appropriate amount of carbon could be retained in the steel even if binder removal was conducted in an oxidizing atmosphere.

furnace (Model 901, R.D. Brew, Inc., Concord, N.H.) at 1415°C in Ar - 4% H_2. The part made from as-received powder sintered to 91.6% theoretical density (7.15 g/cm^3), contained 0.32 wt % carbon and 0.002 wt % oxygen (as determined by combustion analysis), and had a hardness of 69 R_A. Gelcasting tends to introduce carbon into a system. For most ceramic applications, the carbon is eliminated by burning out the binder in an oxidizing atmosphere at temperatures as high as 600°C. Occasionally, the additional carbon provided by the gelcast polymer is desirable, such as with silicon carbide or boron carbide. In these cases, burnout is conducted in a neutral or reducing atmosphere. Under those conditions, the gelcast binder leaves a carbon residue equal to about 15% of the initial weight of binder in the gelcast part. Between the extremes of removing all the carbon and leaving as large a carbon remnant as possible is a continuum of residual carbon contents. For the H13 study we chose to investigate this continuum and find out if an appropriate amount of carbon could be retained in the steel even if binder removal was conducted in an oxidizing atmosphere.

We conducted a series of binder burnout trials. Samples were heated at 1°C per min to temperatures between 200 and 350°C in air, followed by sintering at 1415°C. The results of those tests are summarized in Figure 5. The properties of the fired H13 parts were relatively constant for burnout temperatures between 200 and 250°C, with the highest density being achieved at 250°C. Above 250°C, the hardness, density, and carbon content all fell rapidly, and the oxygen content rose rapidly. These experiments demonstrate that H13 can be processed in a water-based gelcasting system with binder burnout in air and still produce materials having acceptable properties. Typical microstructures are given in Figure 6. The samples clearly shows remnants of the hollow starting particles. The density of the starting powder (as determined by water displacement pycnometry) was 7.4 g g/cm^3, or about 95% of theoretical. The as-sintered parts had a maximum density of about 91% of theoretical. This implies that nearly fully dense material could be achieved in this system if a fully dense starting powder were used.

3. Conclusions

Gelcasting was successfully applied to H13 tool steel. All slurry processing was conducted in water-based suspensions and binder removal was accomplished in air at temperatures between 200 and 350°C. Sintered properties such as density, hardness, carbon content, and oxygen content were comparable for H13 that was gelcast and H13 that was sintered starting from a tapped powder stack.

References

1. Janney, M. A., "Method for Molding Ceramic Powders," U. S. Pat. No. 4,894,194, Jan. 16, 1990.
2. Young, A. C., O. O. Omatete, M. A. Janney, and P. A. Menchhofer, "Gelcasting of Alumina," J. Am. Ceram. Soc., Vol.74, No.3, pp.612-18, (1991).
3. Janney, M. A. and O. O. Omatete, "Method for Molding Ceramic Powders Using a Water-Based Gelcasting," U. S. Pat. No. 5,028,362, July 2, 1991.
4. Omatete, O. O., M. A. Janney, and R. A. Strehlow, "Gelcasting - A New Ceramic Forming Process," Am. Ceram. Soc. Bull., Vol.70, No.10, pp.1641-49, (1991).
5. Janney, M. A. and O. O. Omatete, "Method for Molding Ceramic Powders Using a Water-Based Gelcasting Process," U. S. Pat. No. 5,145,908, Sept. 8, 1992.

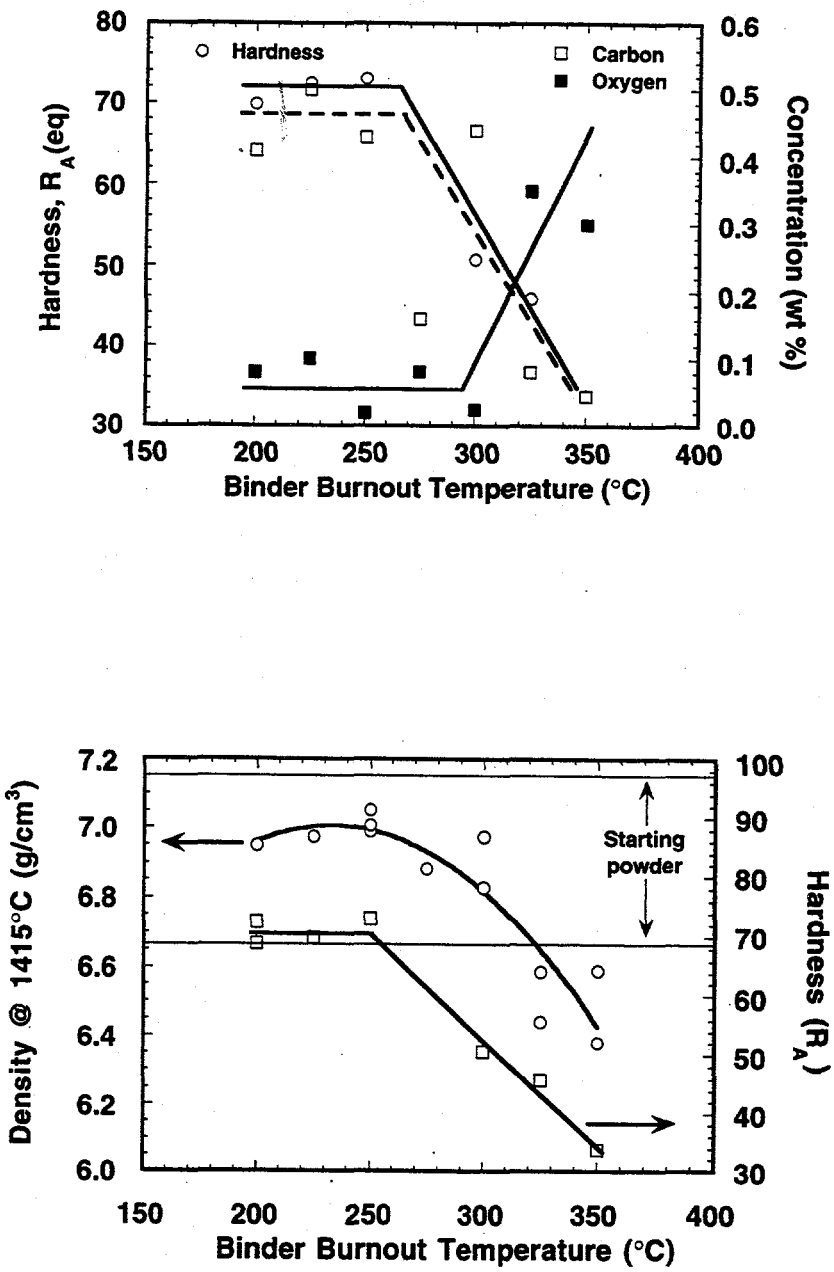

Fig. 5. Sintered density, hardness, carbon and oxygen content were affected by burnout temperature. temperature.

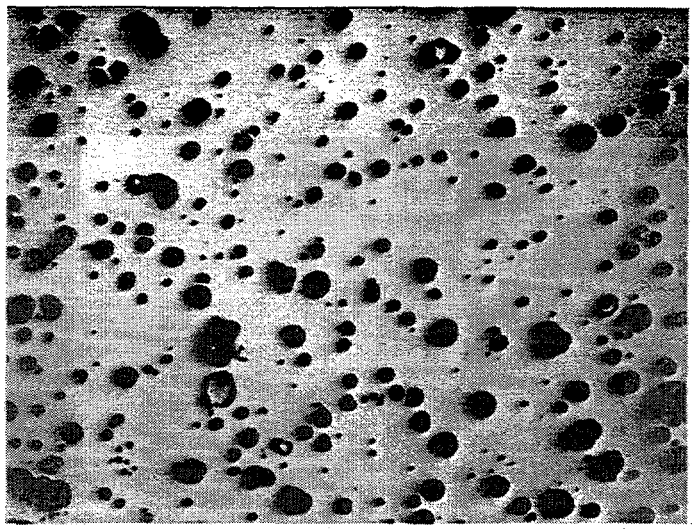

Fig. 6. H13 micrograph, polished section, reflected light. Taped powder/sintered 1415 °C, R_A70.

MILESTONES

None

PUBLICATIONS

Journals

M. A. Janney, W. Ren, G. H. Kirby, S. D. Nunn, and S. Viswanathan, "Gelcast Tooling: Net Shape Casting and Green Machining," to be published in *Materials and Manufacturing Processes*, 1997.

Other Publications

M.A. Janney, W. Ren, and S. Viswanathan, "Gelcasting H13 Tool Steel," to be published in *Advances in Powder Metallurgy and Particulate Materials, 1996*, Metals Powder Industries Federation, Princeton, NJ, 1996.

R. Raman, M. A. Janney, and S. Sastri, "An Innovative Processing Approach to Fabricating Fully Dense, Near-Net-Shape Advanced Material Parts," to be published in *Advances in Powder Metallurgy and Particulate Materials, 1996*, Metals Powder Industries Federation, Princeton, NJ, 1996.

PRESENTATIONS

Oral Presentations

M.A. Janney, W. Ren, and S. Viswanathan, "Gelcasting H13 Tool Steel," International Conference on Powder Metallurgy and Particulate Materials, Washington, DC, June 1996.

R. Raman, M. A. Janney, and S. Sastri, "An Innovative Processing Approach to Fabricating Fully Dense, Near-Net-Shape Advanced Material Parts," International Conference on Powder Metallurgy and Particulate Materials, Washington, DC, June 1996.

M.A. Janney, "Gelcasting Metal Powders," Powder Injection Molding 1996, Pennsylvania State University, State College, PA, August 1996.

HONORS AND AWARDS

None

PATENTS/DISCLOSURES

None

LICENSES

None

INDUSTRIAL INPUT and TECHNOLOGY TRANSFER

We have evaluated gelcasting of metal powders for a manufacturer of surgical-grade steel components with very encouraging results.

A cooperative research and development (CRADA) with OSRAM has continued.

ESTIMATED ENERGY SAVINGS

Development of gelcast steels and machining dies in the green state would limit stack rework and improve the overall energy balance in producing dies.

CONTROL TECHNOLOGY FOR SURFACE TREATMENT OF MATERIALS USING INDUCTION HARDENING

J. Bruce Kelley and Russell D. Skocypec

Sandia National Laboratories
P.O. Box 5800
Albuquerque, New Mexico 87185-0828

INTRODUCTION

In the industrial and automotive industries, induction case hardening is widely used to provide enhanced strength, wear resistance, and toughness in components made from medium and high carbon steels. The process uses significantly less energy than competing batch process, is environmentally benign, and is a very flexible in-line manufacturing process. As such, it can directly contribute to improved component reliability, manufacturing agility, and the manufacture of high-performance lightweight parts.

However, induction hardening is not as widely used as it could be. Input material and unexplained process variations produce significant variation in product case depth and quality. This necessitates frequent inspection of product quality by destructive examination, creates higher than desired scrap rates, and causes de-rating of load stress sensitive components. In addition, process and tooling development are experience-based activities, accomplished by trial and error. This inhibits the use of induction hardening for new applications, and the resultant increase in energy efficiency in the industrial sectors.

In FY96, a Cooperative Research and Development Agreement (CRADA) under the auspices of the Technology Transfer Initiative (TTI) and the Partnership for a New Generation of Vehicles (PNGV) was completed. A multidisciplinary team from Sandia National Labs and Delphi Saginaw Steering Systems investigated the induction hardening by conducting research in the areas of process characterization, computational modeling, materials characterization, and high speed data acquisition and controller development. The goal was to demonstrate the feasibility of closed-loop control for a specific material, geometry, and process. Delphi Steering estimated annual savings of $2-3 million dollars per year due to reduced scrap losses, inspection costs, and machine down time if reliable closed-loop control could be achieved. Development of computational process simulation tools was also desired in order to decrease product development lead times and enable optimized component processing. Success was demonstrated in the areas of closed-loop control, computational modeling, and material-process interactions. A factor of five improvement in process precision was demonstrated and is now operational on the factory floor, processing all Saturn intermediate axle shafts. This accomplishment provides the basis for necessary advancements of the technology to have broad industrial impact.

The goal of this FY96 project for the Office of Industrial Technology (OIT) is to support the establishment of an induction hardening consortium consisting of Delphi Saginaw Steering Systems/General Motors, Ford, and Chrysler Corporation; and their first-tier suppliers as appropriate. This project will further develop the closed-loop control technology and broaden the range of materials and components to which it can be applied. The project has an advisory board consisting of representatives of the heat treating, steel, casting, and forging industries through appropriate professional societies or trade associations. This participation will provide guidance to ensure that the technology developed is broadly applicable and will have maximum industrial impact.

Induction heating and hardening is a cross-cutting technology applicable to a number of the OIT Industries of the future as discussed in our annual report last year (1). The potential energy savings compared to competing technologies makes broader application of this technology of great importance to the heat treating, steel, forging, casting, paper and pulp, and aluminum industries. As reported previously (2), direct energy savings of 630 trillion BTUs, and total energy savings of about 1 quadrillion BTUs, are possible over 20 years in the heat treating industry alone. The forging and steel industries have identified significant additional energy savings opportunities for induction heating technology if uniform and reliable heating can be achieved. The ability to tailor the properties of components is becoming increasingly important.

Induction heating is one of the most widely used, cost effective technologies for tailoring the properties of cast and wrought components. The issue in these applications is to avoid overheating edges and corners while heating the bulk of the material uniformly. The ability to model the induction heating process completely is critical to achieving success.

TECHNICAL PROGRESS - FY 1996

Summary

Efforts this year were aimed at getting the follow-on consortium established and developed support for this consortium through a number of professional and trade societies. A Joint Work Statement (JWS) was developed, reviewed, and approved by each of the participating companies. A poster was displayed at the Advanced Industrial Materials (AIM) conference held June 24-26, in Oak Ridge. Discussions about the induction project were held with representatives of the Forging Industry Association (FIA), the Steel Founders Society (SFS), and the North American Die Casting Association (NADCA), as well as with a number of interested industrial companies. Additional discussions have been held with representatives of the American Iron and Steel Institute (AISI) and ASM International (ASMI). Support for the project in the form of willingness to serve on an advisory board for the project has been received form the Forging Industry Association, ASM International, and AISI. The CRADA was established in November, and a kick-off meeting was held November 12, 1996.

MILESTONES

Establish Consortium to Further Develop Process Control and Process Modeling Technology
This milestone was accomplished with the signing of the CRADA.

PUBLICATIONS

J. Bruce Kelley and Russell D. Skocypec, "Control Technology for Surface Treatment of Materials Using Induction Hardening," Sandia National Laboratories, EEW-2359-7, Annual Report, 1995.

J.B. Kelley and D.R. Adkins, "Cost and Energy Savings Analysis for Induction Hardening Processes," Internal Sandia Memo, September, 1995.

PRESENTATIONS

None

HONORS AND AWARDS

Sandia National Laboratories Award for Excellence
1. Lockheed-Martin Corporation NOVA Award for Excellence in Teamwork

PATENTS/DISCLOSURES

None

LICENSES

None

INDUSTRIAL INPUT and TECHNOLOGY TRANSFER

A CRADA was established with Chrysler, Ford, and Delphi Saginaw Steering Systems. Discussions were held with and input was received from representatives of the Forging Industry Association (FIA), the Steel Founders Society (SFS), and the North American Die Casting Association (NADCA), as well as with a number of interested industrial companies. Additional discussions have been held with representatives of the American Iron and Steel Institute (AISI) and ASM International (ASMI). Support for the project in the form of willingness to serve on an advisory board for the project has been received form the Forging Industry Association, ASM International, and AISI.

ESTIMATED ENERGY SAVINGS

Based on energy estimates supplied by ASM International and used to develop, "Vision 2020, The Heat Treating Industry of the Future," direct energy savings of 630 trillion BTUs, and total energy savings of about 1 quadrillion BTUs, are possible over 20 years in the heat treating industry alone if half the parts currently carburized can be converted to induction hardening. This estimate is documented in Reference 2.

DEVELOPMENT OF IMPROVED REFRACTORIES

A. A. Wereszczak, M. K. Ferber, K. C. Liu

Metals and Ceramics Division
Oak Ridge National Laboratory
P. O. Box 2008
Oak Ridge, Tennessee 37831

R.E. Moore

University of Missouri-Rolla
1870 Miner Circle, 222 McNutt Hall
Rolla, MO 65409-0330

INTRODUCTION

The goal of the proposed project is to provide expertise and facilities for the high temperature mechanical properties characterization of refractory materials which are of interest to the U.S. D.O.E.'s Office of Industrial Technologies' Advanced Industrial Materials Project. Initially the project would establish dedicated refractory testing facilities which would be capable of generating representative engineering creep and high temperature modulus of elasticity (MOE) data to a temperature of 3300°F (1815°C) in ambient air. The generated engineering creep and MOE data would serve R&D requirements of refractories-manufacturers and its glass-manufacturer end-users and designers. The relevance of this effort to the refractory and glass-making industries would be ensured by coordinating our research activities through a membership with Alfred University's Center for Glass Research (CGR) Satellite Center at the University of Missouri-Rolla (UMR), an NSF Center.

Valid engineering creep and high temperature MOE data currently do not exist for almost all commercial refractories. Refractory end-users such as glass-manufacturers require such data for efficient and economical design of their various glass-melting furnace superstructures (e.g., furnace crowns). Refractories in glass production furnaces may be subjected to extreme temperatures as high as 3200°F (1760°C). With the simultaneous imposition of mechanical and thermal stresses, creep deformation of the refractory material will assuredly occur as a consequence. Designers must ensure that the structural integrity is maintained, so these high temperature deformations must be considered for successful glass furnace superstructure design. These criteria can only be satisfied with the utilization of representative engineering creep and high temperature MOE data for the refractory materials that are chosen for the design of the refractory superstructures.

The proposed refractory high temperature testing facilities will be equipped with the necessary instrumentation to accurately control and monitor refractory creep and high temperature MOE tests. A minimum of two test frames, one solely dedicated to compression creep testing and another capable of either creep or high temperature MOE measurements, will be used for this task. Each of these testing stations will be comprised of a testing frame, a computer and appropriate software for

test control and data acquisition, a furnace and load train capable of achieving and maintaining loads and temperatures to 3300°F, and a high temperature extensometer to monitor strain as a function of time or stress. High temperature test conditions will be selected that mimic those of refractory service (determined through consultation with CGR-UMR members). Success of this subtask will be demonstrated when representative engineering creep and high temperature MOE data become available to those scientists, engineers, and technicians, and academicians requiring it for use in materials development and structural design.

TECHNICAL PROGRESS - FY 1996

Summary

High temperature mechanical testing frames that can be used for compressive creep and dynamic loading testing of refractories were designed, and hardware for the frames' construction was procured. This project was initiated 1 July 1996, so only three months were available for productive work in FY96.

MILESTONES

The acquisition of hardware and components for setting up a high temperature dynamic compressive testing machine to determine the moduli of refractories was completed. [Deadline: 30Sep96]

The acquisition of hardware and components for setting up a high temperature static compressive creep testing machine to determine the creep parameters of refractories was completed. [Deadline: 30Sep96]

PRESENTATIONS

"Development of Improved Refractories," A. A. Wereszczak (presenter), K. C. Liu, M. K. Ferber, and C. R. Brinkman, Advanced Industrial Materials (AIM) Program Annual Meeting, Oak Ridge, Tennessee, June 24, 1996, [poster presentation].

INDUSTRIAL INPUT and TECHNOLOGY TRANSFER

Members of the Center for Glass Research Satellite Refractory Center at the University of Missouri at Rolla will suggest during FY97 which candidate refractory materials will be tested as part of this subtask. There is no technology transfer issues at this time.

ESTIMATED ENERGY SAVINGS

A quantifiable amount of savings is unknown at this time.

METALS PROCESSING LABORATORY USER CENTER (MPLUS)

Gail Mackiewicz-Ludtka and H. Wayne Hayden

Metals and Ceramics Division
Oak Ridge National Laboratory
P.O. Box 2008
Oak Ridge, TN 37831

INTRODUCTION

The Metals Processing Laboratory User (MPLUS) Center was officially designated as a DOE User Facility in February, 1996. It's primary purpose is to assist researchers in key U.S. industries, universities, and federal laboratories in improving energy efficiency and enhancing U.S. competitiveness in the world market. The MPLUS Center provides users the unique opportunity to address technology-related issues to solve metals-processing problems from a fully integrated approach (Figure 1). DOE facilitates the process and catalyzes industrial interactions that enables technical synergy and financial leveraging to take place between the industrial sector identifying and prioritizing their technological needs, and MPLUS, which provides access to the technical expertise and specialized facilities to address these needs.

MPLUS is designed to provide U.S. industries with access to the specialized technical expertise and equipment needed to solve metals-processing issues that limit the development and implementation of emerging metals-processing technologies. As originated, MPLUS includes the following four primary user centers: Metals Processing, Metals Joining, Metals Characterization, and Metals Process Modeling. These centers are devoted to assisting U.S. industries in adjusting to rapid changes in the marketplace and in improving products and processes. This approach optimizes the complementary strengths of industry and government. Tremendous industrial response, has resulted in MPLUS expanding to meet the ever-growing technical needs and requests initiated by U.S. industry. Figure 2 illustrates some of the interactions possible with MPLUS.

TECHNICAL PROGRESS - FY 1996

Summary

From the official inception of MPLUS as a DOE designated User Center on February 9, 1996, MPLUS has grown continuously, always initiated by industrial needs and requests, from representing the Engineering and Materials Section within the Metals & Ceramics Division, to include other User Centers within ORNL (e.g., the High Temperature Materials Laboratory (HTML), and the Computational Center for Industrial Innovativeness (CCII)), and even beyond. MPLUS has provided industry (based upon its need and request) with access to unique capabilities and technologies.

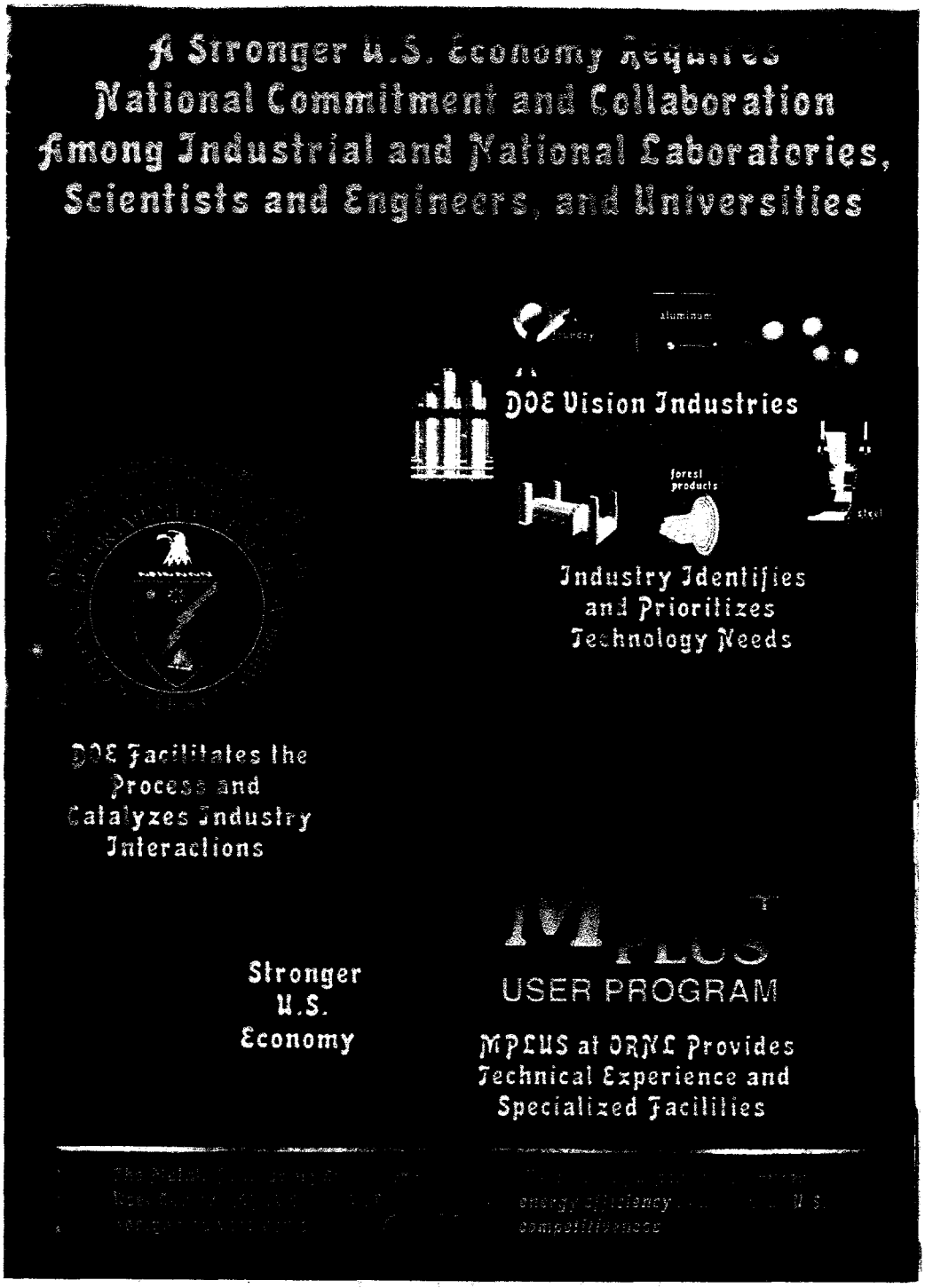

Fig. 1. The MPLUS Center provides users the unique opportunity to address technology-related issues to solve metals-processing problems from a fully integrated approach.

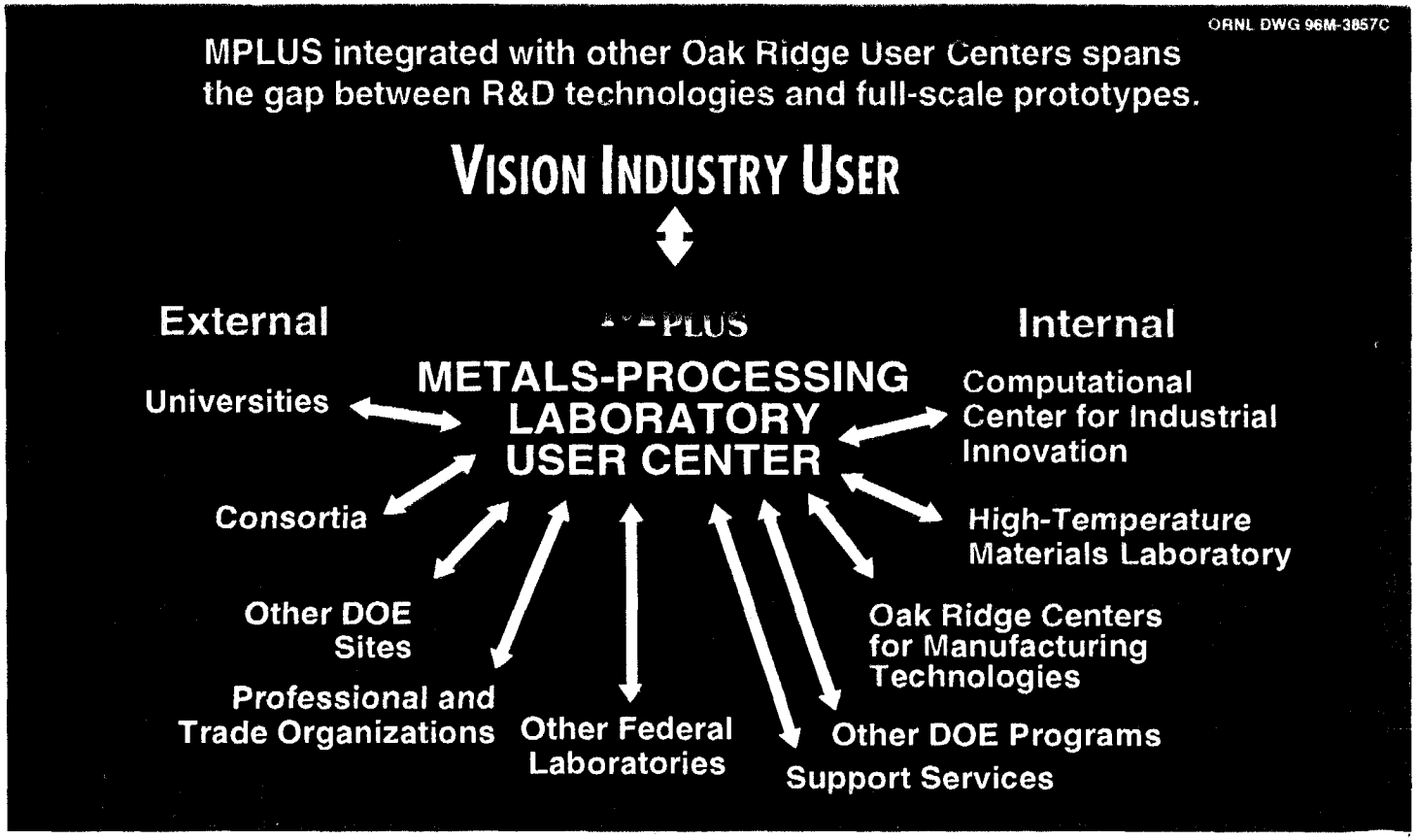

Fig. 2. MPLUS integrated with other user centers and facilities provides the opportunity to technologically and financially leverage resources between the national laboratories and the industrial sector.

In fact, it is becoming clear, with the growing response and needs being identified via MPLUS, that MPLUS may in fact be a vehicle to unite other National Laboratory User Facilities to provide industry with a mechanism to access these National Resources as a "Virtual Laboratory."

As of September 30, 1996, a total of 31 MPLUS Proposals were received from 27 companies and universities representing 17 states (Figure 3). Of these 32 proposals, 22 were reviewed, 18 were approved, and the others were either still under development, or were being modified. Two (2) projects were completed, and 12 User Companies had already utilized the MPLUS facilities.

MILESTONES

Designated as a DOE User Facility	February 1996
Developed Program Methodology and Database	March 1996
Developed User Brochure	April 1996
User Information on Internet	June 1996
Initiated 15 Vision Industry Proposals	June 1996
1st Draft of Business Management Plan	July 1996
Evaluated Future Needs	August 1996

PUBLICATIONS

Metals Processing Laboratory User Center Report, ORNL/M-4466

"MPLUS Center Welcomes First Industrial User," The M&C Pipeline, published by the Metals and Ceramics Division, Vol. 5, No. 2, p. 10 (March/April 1996).

MPLUS User Program Brochure: April, 1996.

Internet Information/ Web Pages: May, 1996.
(URL: http://www.ms.ornl.gov/emfacility/mplus/mplus.htm)

Oak Ridge User Facilities Pamphlet, Summer 1996, pp. 16 -17.

PRESENTATIONS

Poster Session:
"Metals Processing Laboratory User Center," Oak Ridge National Laboratory User Center, for Poster Session at the Advanced Industrial Materials (AIM) Program Annual Meeting in Pollard Auditorium, Oak Ridge, TN, June 24 -26, 1996.

Informal Oral Presentations:

"Metals Processing Laboratory Users Center (MPLUS) Update," for Program Managers Meeting (July 25, 1996).

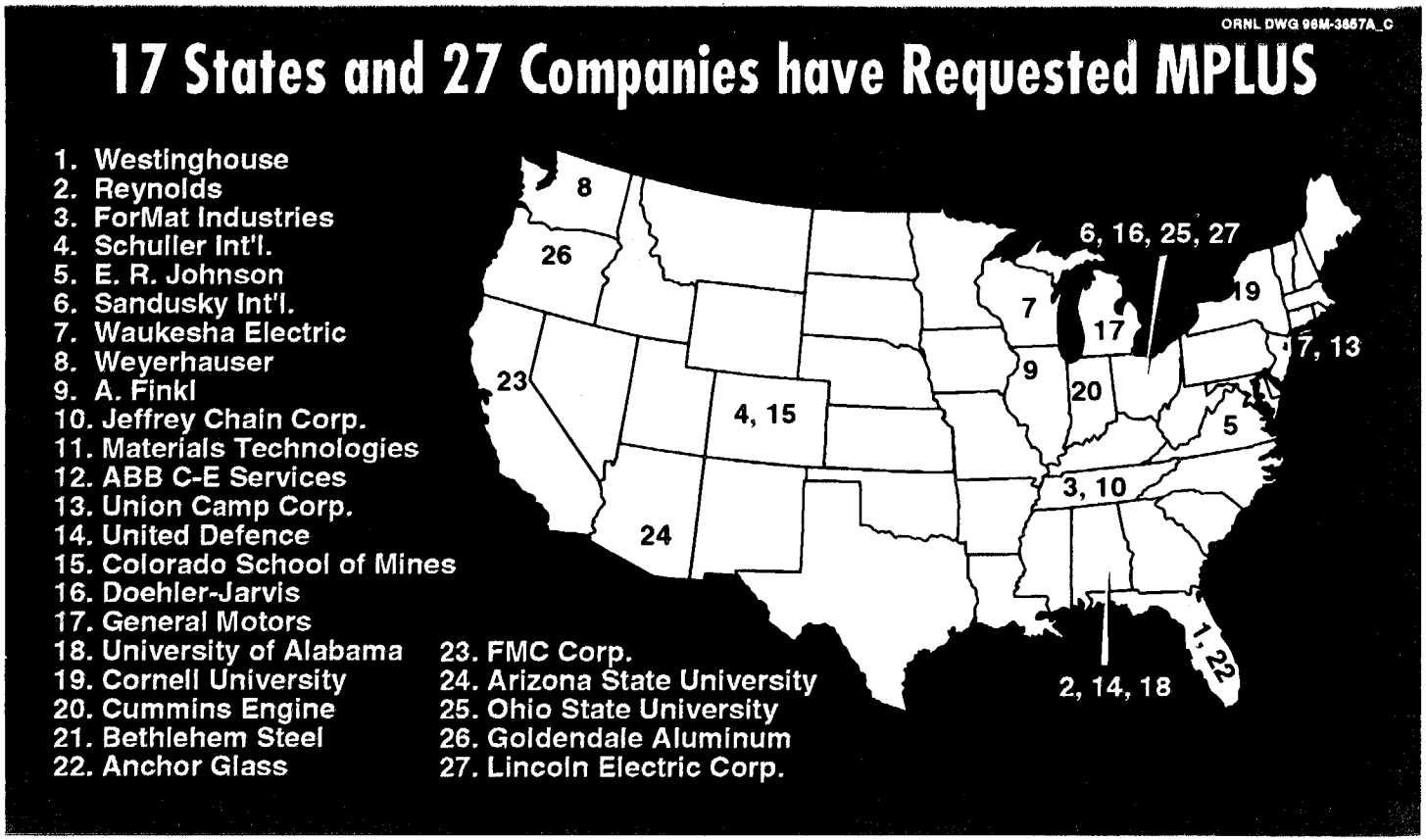

Fig. 3. As of September 30, 1996, a total of 31 MPLUS Proposals were received from 27 companies and universities representing 17 states.

"Overview of the Metals Processing Laboratory Users Center (MPLUS)," for the Directors and staff members of 10 State Energy Offices, as well as representatives from the Southern States Energy Board, the Harmony Project from Charleston, S.C., and the DOE Atlanta Regional Support Office (November 20, 1996).

"Metals Processing Laboratory Users Center (MPLUS)" for DOE/OIT: W. Parks and C.A. Sorrell, (December 5, 1996).

HONORS AND AWARDS

November, 1996: The President's Award for Continuous Improvement; for the MPLUS User Center- Metals Processing Users Project.

LICENSES

None

INDUSTRIAL INPUT and TECHNOLOGY TRANSFER

As of September 30, 1996, a total of 31 MPLUS Proposals were received from 27 companies and universities representing 17 states. Of these 32 proposals, 22 were reviewed, 18 were approved, and the others were either still under development, or were being modified. Two (2) projects were completed, and 12 User Companies had already utilized the MPLUS facilities.

ESTIMATED ENERGY SAVINGS

Each individual MPLUS project has energy efficiency aspects..

MICROWAVE JOINING OF SiC

R. Silberglitt, I. Ahmad and Y.L. Tian

FM Technologies, Inc.
10529-B Braddock Road
Fairfax, VA 22032

W.M. Black
George Mason University
4400 University Drive
Fairfax, VA 22030

J.D. Katz
Los Alamos National Laboratory
PoSt Office Box 1663, Mail Stop G771
Los Alamos, NM 87545

INTRODUCTION

The purpose of this work is to optimize the properties of SiC-SiC joints made using microwave energy. The current focus is on identification of the most effective joining methods for scale-up to large tube assemblies, including joining using SiC produced in situ from chemical precursors. During FY 1996, a new microwave applicator was designed, fabricated and tested that provides the capability for vacuum baking of the specimens and insulation and for processing under inert environment. This applicator was used to join continuous fiber-reinforced (CFCC) SiC/SiC composites using a polymer precursor to form a SiC interlayer in situ.

TECHNICAL PROGRESS - FY 1996

1. Joining of Reaction Bonded SiC Tubes

During the previous fiscal year, reaction bonded SiC tubes were joined at several different joining temperatures, and evaluation of test bars machined from sectioned joined specimens demonstrated that in the joining temperature range of 1420-1515°C the joined specimens had fracture toughness equal to or greater than the as-received material. In order to provide further data for the optimization of the joining temperature within this range, tubes of reaction bonded SiC with outer diameter of 3.49 cm (1.375"), inner diameter of 2.54 cm (1") and length of 2.54 cm (1") were joined at two different joining temperatures: 1440°C ± 5°C and 1490°C ± 10°C. These tubes were provided by Coors Ceramics of Golden, CO and were identical to and from the same lot as those used for the previous evaluations. A stainless steel 2' x 2' x 2' multimode applicator was used in these experiments and the specimens were placed inside a cylindrical enclosure consisting of high temperature alumina insulation with a thin lining of SiC to provide hybrid (microwave plus radiant)

heating. In each case the joining temperature was maintained for approximately 30 minutes. The microwave power input was 4 kW for the ramp and 2.8 kW during the soak. The joined specimens were sent to Los Alamos National Laboratory for mechanical evaluation.

2. Joining of CFCC SiC/SiC Composites Using a Metallic Braze

Microwave joining experiments were performed on continuous fiber-reinforced SiC/SiC composites using a TE_{103} single mode applicator. The specimens were 2.54 cm (1") diameter disks 3 mm (approximately 1/8") thick that were manufactured by DuPont Lanxide Composites, Inc. of Newark, DE. A 2 mil thick brazing foil of Cusin-1 ABA™ manufactured by WESGO, Inc. of Belmont, CA was used as the interlayer material. The specimens were held in place with mullite push rods and maintained at approximately 900°C for 30 minutes in a 95% N_2, 5% H_2 environment, using 600-800 Watts of input power. (The liquidus temperature of the brazing alloy is 806°C.) The joined specimen was removed from the applicator and sectioned. The region near the outer edge of the specimen came apart during cutting, but the remainder of the sectioned specimen remained intact and appeared to have a homogeneous metallic interlayer. An optical micrograph of the sectioned joint at a magnification of 200 X is shown in Figure 1. It appears from this micrograph that the braze alloy wet the ceramic composite and spread into the pores in the SiC matrix.

Fig. 1. Optical micrograph of SiC/SiC composite joint (200 X).

3. Joining of CFCC SiC/SiC Composites Using Polymer Precursor

A new multimode applicator to be used with the existing 6 kW 2.45 GHz microwave source was designed, fabricated and tested. This applicator is approximately 16" in diameter and 16" long. It is capable of evacuation and backfilling to establish any required environment for production of SiC

or other interlayers from chemical reactions in situ. The applicator includes flanges with provision for Rf gaskets and O-rings, waveguide connection, pumping ports, and observation/diagnostic ports. Top and bottom design includes fittings to allow application of pressure using a hydraulic press. The applicator, which was constructed from 6061 T6 aluminum, was assembled from components that had been fabricated both in-house and by vendors and then tested for minimum reflected power with a microwave transparent window capable of sustaining a vacuum in the range of 10^{-3} torr. Prior to inserting the specimens to be joined, the following procedure was used to remove moisture present in the insulation material to be used, including the hybrid heating enclosure.

The insulation stack was assembled inside the cavity in an identical configuration as that for the joining experiment. The cavity was then closed and the vacuum pump turned on. A very slow rate of pressure reduction indicated the presence of moisture and perhaps other volatiles to be baked off. Thus the vacuum valve was closed and microwave power was turned on. The temperature of the hybrid heating enclosure was brought to approximately 1000°C and this temperature was maintained for one and one half hour. This was to ensure that sufficient heat would be conducted to the adjacent insulation to thoroughly bake the insulation and free it of any moisture. During the heating period the vacuum valve was opened briefly and moisture was observed condensing on the transparent tube between the vacuum pump and the cavity. This process was repeated several times until no moisture was observed on the transparent tube. At this stage the microwave power was turned off and the vacuum valve was left open to allow continuous pumping of the cavity to establish a vacuum of $6x10^{-3}$ torr.

The SiC/SiC composite specimens were 1.27 cm (½") x 1.27 cm (½") plates 3 mm thick that were cut from a larger plate manufactured by DuPont Lanxide, Inc. of Newark, DE. The specimens were prepared for joining by grinding the surfaces to be joined on a 240 and then a 600 grit diamond wheel. A polymer precursor was used in order to form SiC in situ at the joint interface. The precursor was Allylhydridopolycarbosilane (AHPCS), which was supplied by Starfire Systems, Inc. of Watervliet, NY. The precursor was mixed with a fine SiC powder to form a viscous paste that was applied to both of the surfaces to be joined. The composite specimens with the paste were then placed together so as to sandwich the precursor.

Prior to inserting the specimens, the cavity was back-filled with argon. The cavity was then opened briefly in order to allow insertion of the specimens inside the hybrid heating enclosure. The system was configured to allow monitoring of the surface temperature at the joining interface with a two-color optical pyrometer. The system was then closed, the vacuum valve opened and the cavity pumped to a pressure of approximately $1x10^{-2}$ torr. The cavity was then back-filled with argon and the microwave source was turned on. The specimen temperature was monitored with the pyrometer through a vacuum port that included a metal screen to prevent microwave leakage, and also through a hole in the hybrid heating enclosure that was lined up with the joint interface. The specimens were initially heated slowly and held at low temperature to allow cross-linking of the polymer. The following heating cycle was used: ambient temperature to 700°C in one hour 15 minutes and then 700°C to 1100°C in 15 minutes. The specimens were held at 1100°C for 30 minutes and then the

microwave power was turned off and the specimens were allowed to cool naturally. Upon cooling the specimens were removed and observed to be joined. The joint was then sectioned, polished and examined using a scanning electron microscope (SEM). The following conclusions were drawn from the SEMs.

*The joint contained some bonded regions with no visible interface and some bonded regions with a continuously filled interface;

*At the joint interface the SiC produced by decomposition of the AHPCS precursor formed a two-phase mixture with the SiC powder added to the precursor;

*The joint contained some regions with remnant porosity; however in these regions the porosity at the interface was similar to porosity elsewhere in the specimen, except that there was substantial pore filling by the two-phase SiC mixture formed during the microwave joining process.

Figure 2 is a typical SEM of a bonded region with full filling (no remnant porosity). The joint is vertical and in the center of the figure. Figure 3 is a typical SEM of a bonded region with partially filled remnant porosity. Again the joint is vertical and in the center of the figure. Note the large pores in the SiC-SiC specimens away from the interface in Figure 3. Figure 4 is a higher magnification view of the two-phase SiC mixture filling the pores at the interface, which is again in the center of the figure.

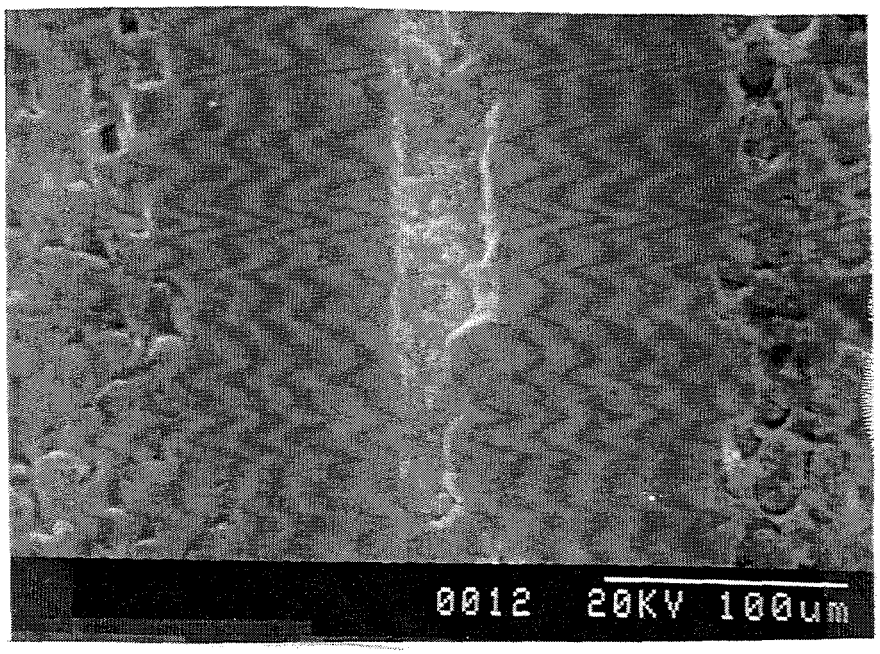

Fig. 2. SEM micrograph of SiC/SiC composite joint.

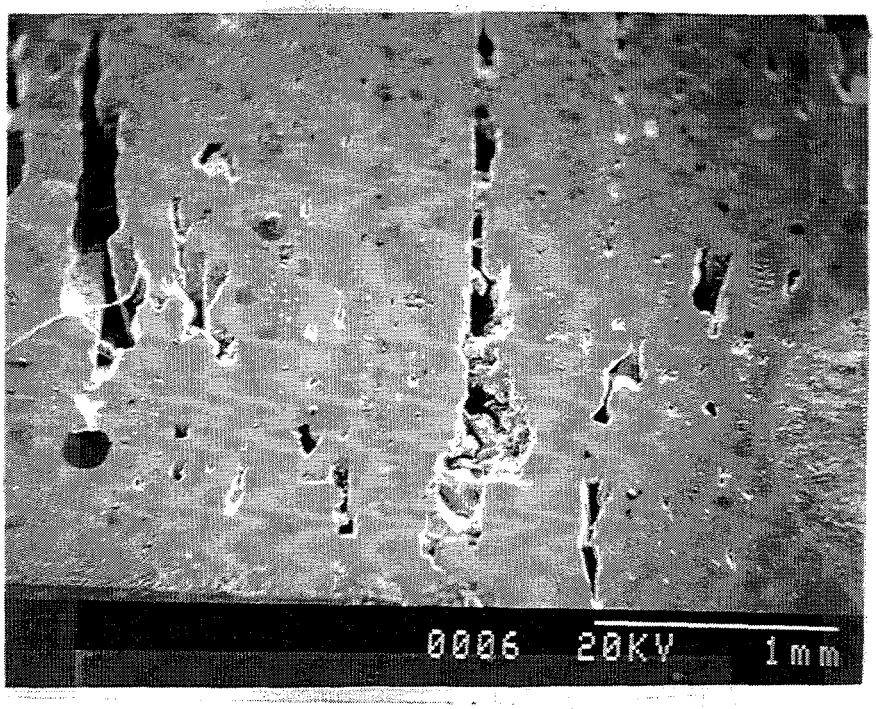

Fig. 3. SEM micrograph of SiC/SiC composite joint.

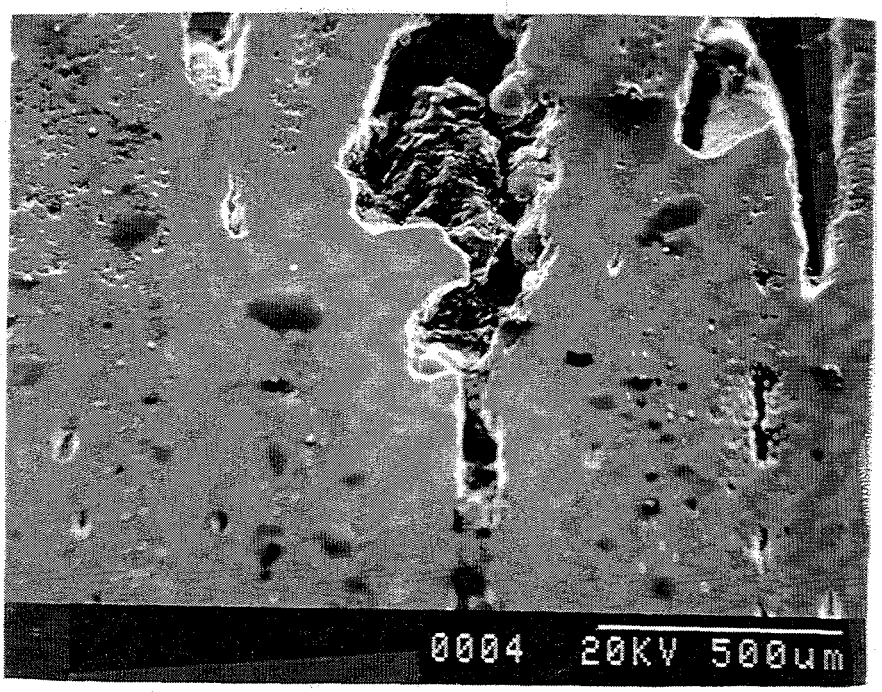

Fig. 4. SEM micrograph of SiC/SiC composite joint.

MILESTONES

1. Design, fabrication and testing of a multimode microwave applicator capable of evacuation and back-filling to provide inert atmosphere for microwave joining experiments on large specimens such as tubes up to 10 cm (~ 4") outer diameter (May 1996).

2. Joining of continuous fiber-reinforced (CFCC) SiC/SiC composites using microwave-assisted decomposition of polymer precursor in an inert environment to form a SiC interlayer in situ (June 1996).

PUBLICATIONS

None.

PRESENTATIONS

R. Silberglitt, I. Ahmad, Y. L. Tian, W. M. Black and J. D. Katz, "Microwave Joining of SiC," poster presented at the Advanced Industrial Materials Annual Review Meeting, Oak Ridge, TN, June 24-26, 1996.

HONORS AND AWARDS

None.

PATENTS/DISCLOSURES

None.

LICENSES

None.

INDUSTRIAL INPUT and TECHNOLOGY TRANSFER

During FY 1996, discussions were initiated with Stone & Webster concerning potential use of microwave joining in the fabrication of components for the high pressure heat exchange system (HiPHES) for ethylene production that is being developed under a cooperative agreement with the DOE Office of Industrial Technologies (OIT). A work scope has been developed and a contract is under negotiation for microwave joining of tube sections supplied by Stone & Webster that will be tested at ORNL under environmental conditions that simulate the HiPHES service environment.

Discussions were also initiated with several members of the Project Teams participating in the OIT-sponsored CFCC Program, and a presentation of the results of the microwave joining experiments on CFCC SiC/SiC composites was planned for the CFCC Review Meeting and BES/CFCC Workshop on Joining in San Diego, CA on October 16-18, 1996.

ESTIMATED ENERGY SAVINGS

Natural gas savings are estimated at $172,892 per year due to 4-7% higher efficiency of SiC radiant burner tubes. Use of SiC tube heat exchanger in externally fired combined cycle coal power plants is projected to produce a 20% increase in thermal efficiency, together with a 20% reduction in CO_2 emissions and a 90% reduction in SO_x emissions. Energy savings through the reduction of feedstock consumption and decoke fuel and steam requirements with an advanced ethylene production process using HiPHES are projected by Stone & Webster at 63.9 trillion BTUs per year.

NEW METHOD FOR SYNTHESIS OF METAL CARBIDES, NITRIDES AND CARBONITRIDES

R. Koc, J. S. Folmer, S. K. Kodambaka

Department of Mechanical Engineering and
Energy Processes
Southern Illinois University
Carbondale, IL 62999

P. F. Becher
Metals and Ceramics Division
Oak Ridge National Laboratory
P.O. Box 2008
Oak Ridge, TN 37831-6068

INTRODUCTION

The purpose of this work is to develop a novel synthesis method using a carbothermic reduction reaction of carbon coated precursors for producing high purity, submicron, non-agglomerated powders of metal carbide, metal nitride and metal boride systems. We also want to demonstrate the advantages of the process and provide information on the applicability of the process for synthesizing related advanced ceramic powders (e.g. SiC, WC, TiN, TiB_2, Si_3N_4). During the FY96 of the project, steps are taken to investigate the reaction mechanisms and phase evolution during the formation of TiC from carbon coated titania precursors and to produce submicron TiC powders with desired stoichiometries. Depending on the carbon content in the coated titania precursor, TiC powder was produced with different stoichiometries (different amount of oxygen and free carbon). The synthesized submicron TiC powders with desired stoichiometries have been supplied to ORNL (Dr. P.F. Becher), 3M Ceramic Technology Center (Dr. V. Nehring and Dr. Charles Shaklee), and Greenleaf (Dr. E. Randich) for evaluation.

TECHNICAL PROGRESS - FY 1996

Summary

Kinetics and phase evolution of TiC formation process by carbothermal reduction of carbon coated titania (TiO_2) powder were investigated using TGA, XRD, and chemical analysis. The TiC synthesis in the present work proceeded via forming titanium oxycarbide (TiC_xO_y) followed by its purification toward titanium carbide (TiC). The formation of TiC_xO_y was achieved via two routes. The uniformly coated pyrolytic carbon on fine titania particles formed the first TiC_xO_y phase at a temperature of 1000°C. The additional TiC_xO_y formed from Ti_3O_5 as temperature increased. The activation energy of the additional TiC_xO_y formation process was calculated to be 278.1 kJ/mole. The resultant TiC powders prepared at 1550°C for four hours in flowing argon showed fine particle size (0.08-0.2 m), oxygen content of 0.6 wt%, lattice parameter of 4.332 Angstrom, uniform particle shape, and loose agglomeration between particles.

Background

Hard metals based on titanium carbide are finding increasing application as materials capable in quality to the conventional hard-metal grades containing the strategic metal tungsten [1]. For advanced applications, the titanium carbide powders with a homogeneous chemical composition, fine particle size, a narrow particle size distribution, and a loose agglomeration are required. Methods that have been developed to synthesize TiC powders include the direct carbonization of titanium metal (combustion synthesis) [2] or titanium hydride [3], the gaseous pyrolysis of titanium halide such as $TiCl_4$ in a carbon containing atmospheres, and the carbothermal reduction of TiO_2 with carbon in controlled atmospheres at high temperatures [5,6]. Metallic titanium as a starting material is relatively expensive, and furthermore, the oxygen contained in the metal can hardly be reduced, so that the product is generally characterized by a high oxygen content[5]. Titanium chloride as a precursor is of importance in the field of chemical vapor deposition, but it is very expensive.

An inexpensive method of producing titanium carbide that has been applied commercially[6] involves the carbothermal reaction between titania (TiO_2) and carbon particles:

$$TiO_2(S) + 3C(s) = TiC(s) + 2CO(g) \quad \text{---------- (1)}$$

The actual TiC production by carbothermal process is achieved at much higher temperatures than thermodynamic onset temperature of reaction (1) (1289°C when partial pressure of CO gas is 1 atm [7]) because of kinetic barriers such as limited contact area between reactants and uneven distribution of carbon in the reactants. These limitations and higher temperature processing result in a grain growth, particle coalescence, non-uniform particle shape, considerable quantities of unreacted oxides of titanium and carbon in the final product. For example, in the commercial production of TiC[6], reactants are fired at 1900° to 2300°C in an inert atmosphere while sintered lumps of titanium carbide forms. This then requires crushing using jaw crushers and fine-milling thereafter.

The process developed in this project avoids the expense of the first two methods while surmounting the inability of the third (carbothermal reduction of TiO_2) to make a suitable product. It minimizes kinetic barriers by improving the way that carbon is introduced to the reactants. The process consists of two steps[8]. The first step is the coating of TiO_2 powders with carbon by decomposing a hydrocarbon gas (C_3H_6) at temperatures of 400°-600°C. The second stage involves the formation of TiC powders by promoting the carbothermal reduction of the carbon-coated TiO_2 particles in an inert atmosphere at temperatures of 1200°-1550°C. This way of increasing contact area between reactants (reduction of kinetic barrier) would result in a more complete reaction and a purer product at a temperature closer to the thermodynamic onset point. The complete separation of the TiO_2 particles by coated carbon and the low temperature processing would result in products with less particle agglomeration and uniform shape.

MILESTONES

1. Characterization of Carbon Coated Titania Precursor

Figure 1 shows bright field TEM micrograph of the carbon coated titania precursor. As shown in the figure, a very uniform circumferential carbon coating (bright area due to low atomic weight of carbon) on titania particle surfaces is apparent. This shows the effectiveness of the carbon coating process (on titania surfaces) by the pyrolysis of C_3H_6 gas. XRD pattern of the carbon-coated titania precursor is shown in Figure 2 (bottom trace). In the figure, the absence of crystalline carbon phases implies that the deposited carbon in Figure 1 has an amorphous (pyrolytic) structure.

Figure 3 shows TGA trace (heated at 4°C/min in argon) for the carbon coated titania precursor (32.6 wt% carbon). For comparison, the result for the carbon black (Monarch 880, Cabot, Waltham, MA)/titania powder mixture with the same carbon content is also shown. In the light of reaction (1), the weight loss of the system indicates the degree of reaction progressed. In Figure 4, the significant weight loss of the carbon/titania mixture started at about 1100°C while carbon coated titania precursor showed similar weight loss at about 900°C. The difference in weight loss behavior demonstrates the higher reactivity of the carbon-coated titania precursor as compared to the conventional carbon/titania mixture.

2. Phase Evolution

XRD patterns from samples passed through the isothermal TGA analysis at various temperatures are shown in Figure 4. At 1000°C, the system consists of rutile, anatase, and TiC_xO_y phases (As will be shown later using oxygen content and lattice parameter in Figure 6, initial formation is not pure TiC, it is in fact a solid solution of TiC and TiO with the virtual formula of TiC_xO_y). At 1100°C, Ti_3O_5 phase appears with increased TiC_xO_y peak intensities. At 1150°C, trace amount of Ti_3O_5 is identified with further grown TiC_xO_y . Above 1200°C, only TiC_xO_y phase is formed with no other phases.

At 1100°C, the remained TiO_2 lowers its oxidation states to Ti_3O_5. The trace amount of Ti_3O_5 with increased TiC_xO_y at 1150°C indicates the growth of TiC_xO_y at the expense of Ti_3O_5. The TiC_xO_y formation by the latter mechanism is named as the second stage formation of TiC_xO_y in this work.

The growth of TiC_xO_y from Ti_3O_5 implies that Ti_3O_5 is the lowest oxide phase before forming TiC_xO_y in the second stage. This is inconsistent with other works reporting Ti_2O_3 [5,7] or TiO [10] as the lowest oxide of the system while consistent with the observation of Ouensanga [11], who observed Ti_3O_5 from the carbon titania mixture compressed under a pressure of about 8 tons/cm^2. The presence of TiO was not detected by XRD while its presence was concluded by chemical calculation [10]. Comparing the result of this work with Berger [5] and Koc[7] who observed Ti_2O_3 as the lowest oxide before forming TiC_xO_y the titania source with higher reactivity (such as the precursor used in this work) would be capable of forming TiC_xO_y before it fully lowers its oxidation state to Ti_2O_3.

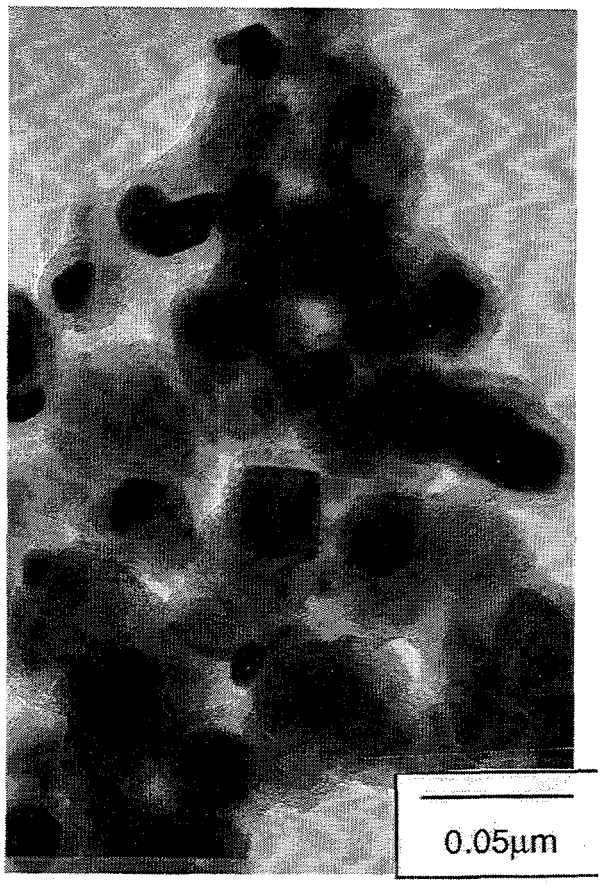

Fig. 1. TEM micrograph of carbon-coated titania precursor.

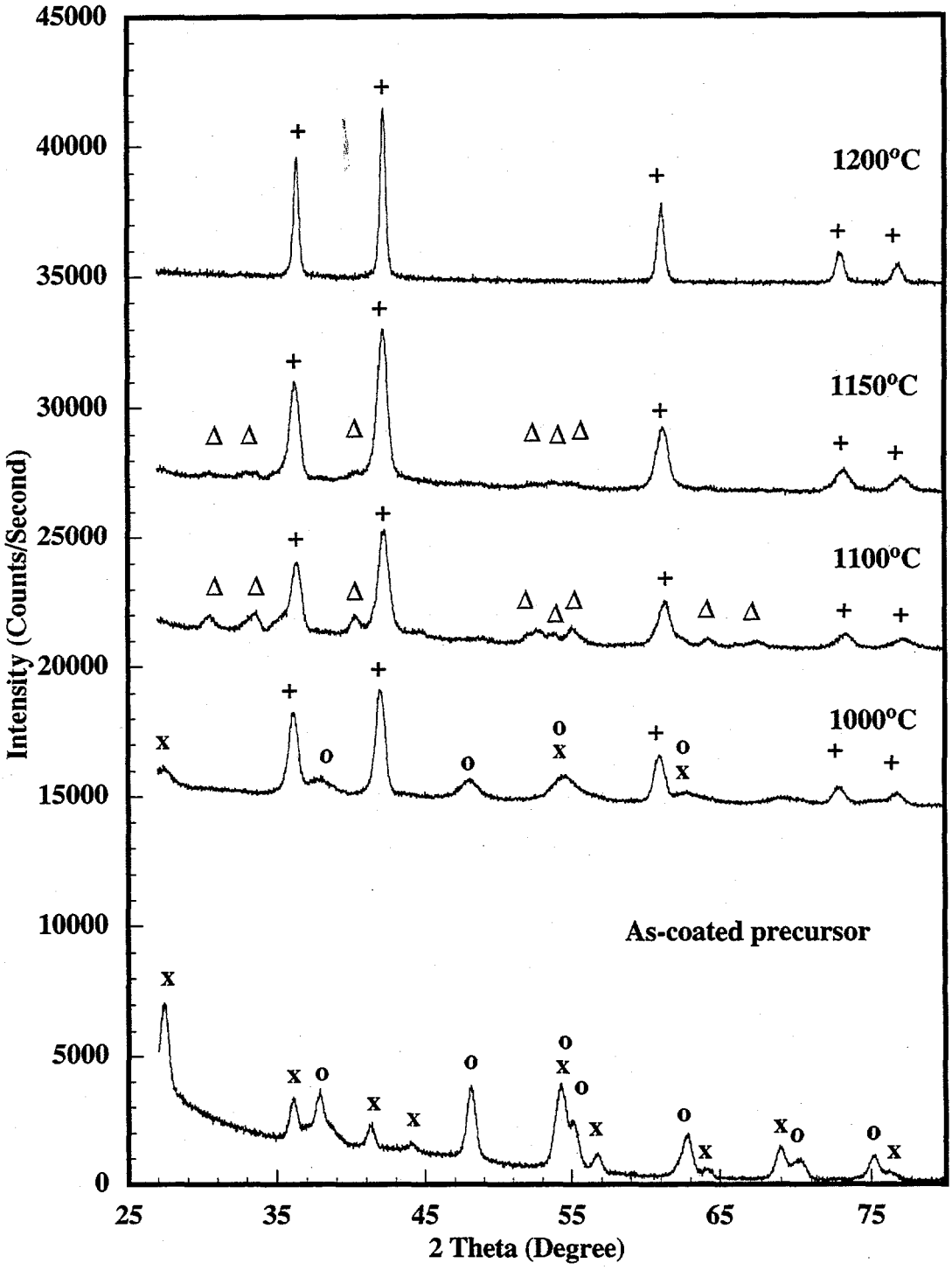

Fig. 2. XRD results of reaction products from carbon coated Degussa P-25 titania samples passed through TGA analysis (heat treatment for two hours at various temperatures). x = Rutile Titania; o = Anatase Titania; + = TiC_xO_y ; $\Delta = Ti_3O_5$

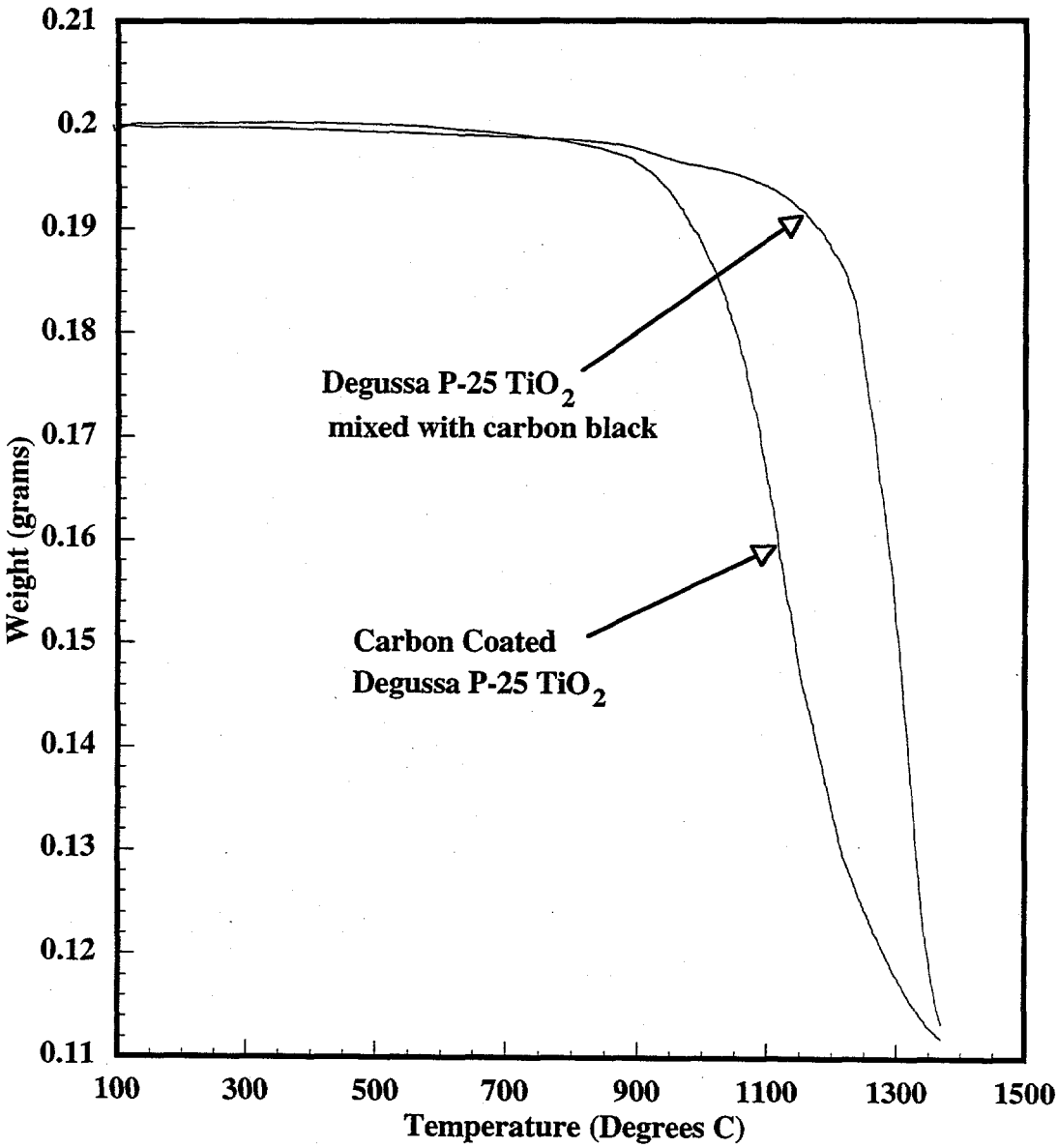

Fig. 3. TGA traces of carbon-coated titania precursor and carbon/titania mixture heated at 4 °C/min.

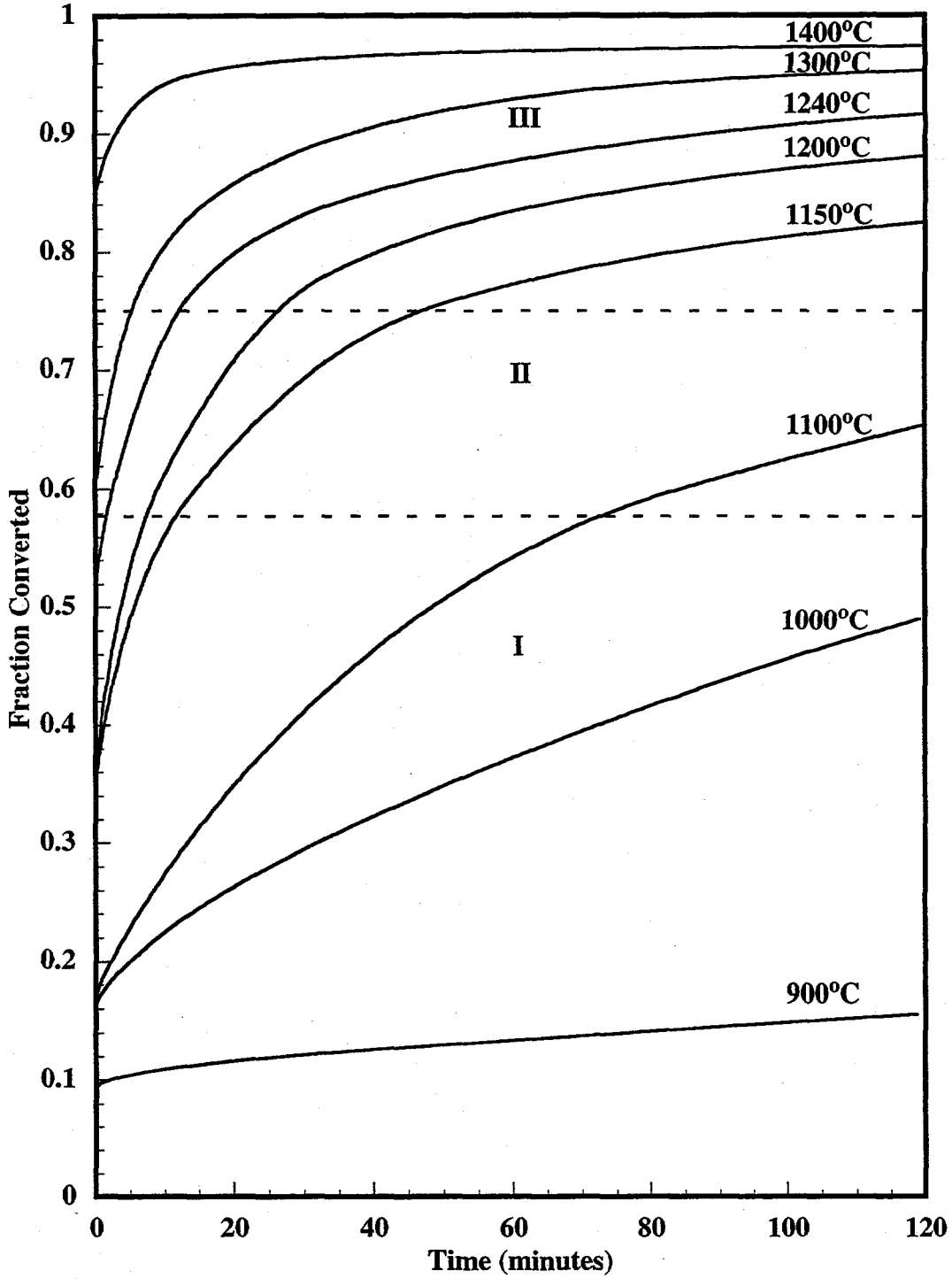

Fig. 4. Isothermal TGA traces at various temperatures.

3. Isothermal TGA Results

Figure 4 shows the isothermal TGA traces at various temperatures. The fraction of conversion, ( ), is based on the relation,

= wt.% loss/ Theoretical wt.% loss

where the theoretical loss limit is 48.33 wt% based on reaction (1). In the figure, the higher the soaking temperature, the more fraction of reaction occurs before reaching the firing temperature, resulting in the higher initial ( ) values.

In Figure 5, roughly linear -time relationship is observed at a range between ~0.58 and ~0.75 (marked as stage II). Based upon this observation, three stages are categorized in the figure (stage I through III). Combining with XRD results, 1000°C-TGA trace shows that the formation of TiC_xO_y from the intermediate phases accompanies with considerable weight loss. In 1100°C-TGA trace, the first stage TiC_xO_y formation would continue until the point where apparent change in trend is observed, implying the start of a different reaction mechanism (stage II).

Considering the observation of Ti_3O_5 after 1100°C-TGA trace, the linear -time relationship appearing after value of ~0.58 in the TGA trace, would be associated with TiO_2 reduction process. After 1100°C-TGA trace, no appreciable TiO_2 phases are observed, implying that the conversion to Ti_3O_5 is completed. Further weight loss of stage II via 1150°C-TGA trace showed trace amount of Ti_3O_5 with enhanced TiC_xO_y peak intensities. This indicates that stage II is also associated with the conversion of Ti_3O_5 to TiC_xO_y while no significant change in reaction rate is noticed. The weight loss during stage III would mainly be associated with the purification of TiC_xO_y phase since no other phases are observed from 1200°C and above.

4. Reaction Mechanism and Activation Energy

The first stage formation of TiC_xO_y phase (stage I) results in value of ~0.55 while the second stage TiC_xO_y formation (stage II) results in value of ~0.18. This indicates that the first stage formation is the major formation process. The trend of stage I in Figure 4 showed a diffusion controlled process.

The best description of stage II using a linear -time relation implies that this process may be a reaction rate controlled process. Such a linear relation was also observed during the carbothermal reduction of silica [12] where a gas phase (SiO) assisted reaction was recognized. While stage II is basically a reduction process, the solid state diffusion of reducing agent carbon would not result in such a linear relation. The reducing ability of carbon monoxide via equilibrium of CO_2 gas would be a plausible mechanism for such a linear relation:

$3TiO_2(s) + CO(g) = Ti_3O_5 + CO_2(g)$ ---------- (2)
and

$Ti_3O_5(S) + 8CO(g) = 3TiC_xO_y(s) + 5CO_2(g)$ ---------- (3)

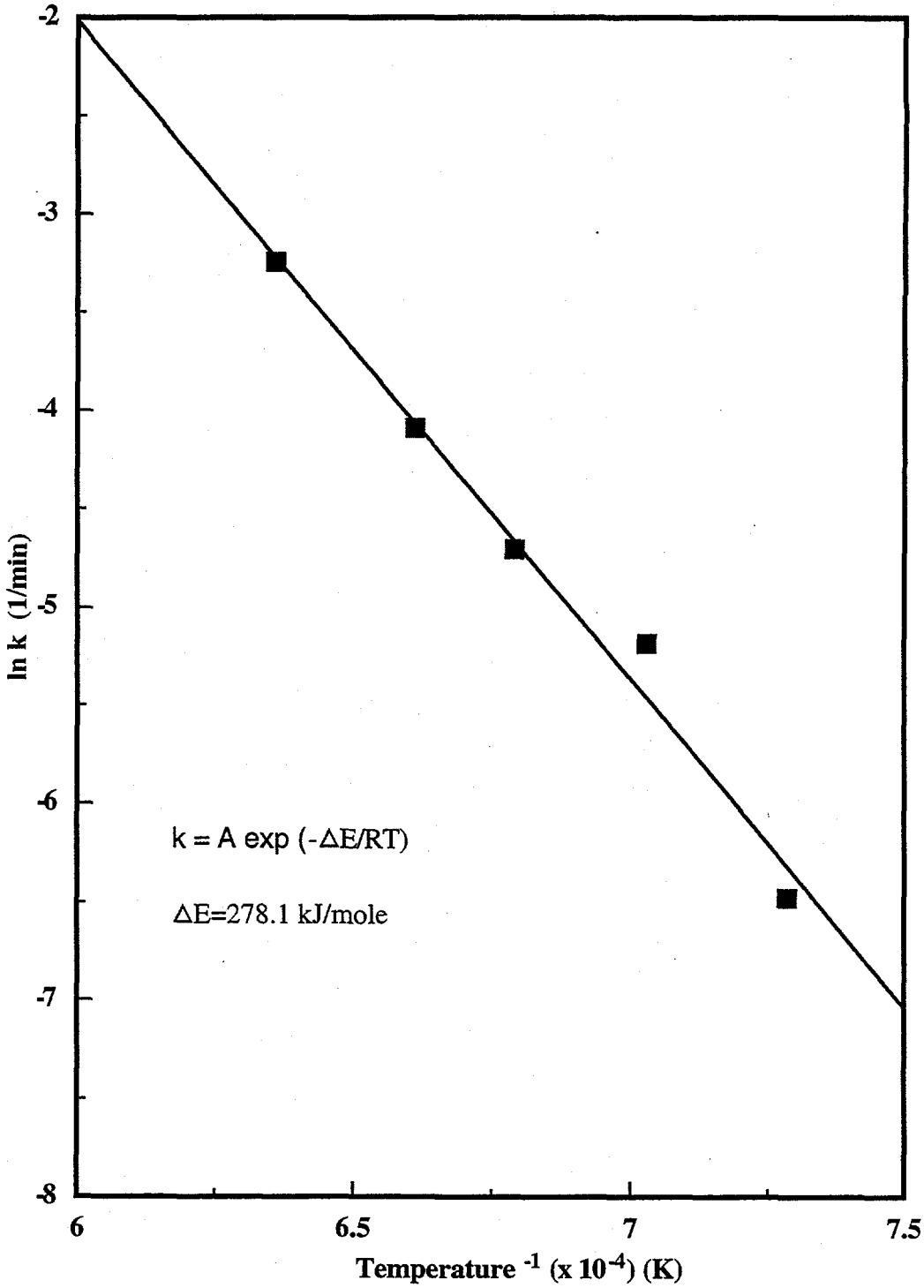

Fig. 5. Arrhenius plot for Stage II in Fig. 4.

where the equilibrium CO_2/CO ratio is also maintained via reaction

$CO_2(g) + C(s) = 2CO(g)$ ---------- (4)

In reaction (3), reaction coefficients are balanced for the case where x=l and y=0. If the CO_2/CO ratio is governed by reaction (4), TiO_2 and Ti_3O_5 reduction by CO gas is thermodynamically favorable (The Gibbs free energy change of reactions (2)-(4) is the same as their overall reaction, reaction (1)).

The decay of the reaction rate from stage III as compared to stage II may imply the change of reaction mechanism from a reaction controlled process (stage II) to a diffusion controlled one (stage III), or reflect decreasing total surface area of Ti_3O_5 as the content of Ti_3O_5 is depleted. The latter reason appeals in this work since trace amount of Ti_3O_5 is still observed after passing through 1150°C-TGA trace. Similar change of reaction rate was also observed in the synthesis of SiC [12] where no significant purification of SiC is noticed. Hence, it is hard to correlate the trend (shape) of weight loss occurring at the final stage of the total reaction (stage III) with the mechanism of TiC_xO_y purification (The purification starts from stage III). Further work is required to uncover the detailed purification mechanism of TiC_xO_y.

The reaction rate constant of the diffusion controlled process (stage I) was not calculated due to the unavailability of initial stage isothermal data. However, the linear slope of stage II allowed to obtain reaction rate constant k and the result is plotted in terms of $ln\ k$ versus $1/T$ in Figure 5. The slope in the figure corresponds to an Arrehenius relation,

$k = A \exp(- E/RT)$

where E is activation energy, A is preexponential constant, and RT is with its usual meaning. The activation energy of stage II is calculated to be 278.1 kJ/mole.

5. Properties of TiC Product Powder

The lattice parameter of the TiC powder produced was calculated as a function of reaction temperature and is plotted in Figure 6. The change in oxygen content as a function of reaction temperature is also included in the figure. As it can be seen in the figure, the lattice parameter increases with reaction temperature while oxygen content decreases. The calculated lattice parameter of TiC produced at 1550°C for four hours under 1LPM argon gas was found to be 4.332 Angstroms as compared to 4.331 Angstroms for commercially available TiC powder (H.C. Stark Vacuum Grade A). Since oxygen and nitrogen are common impurities in TiC and are known to lower the lattice parameter of TiC [13], the observed low lattice parameters of the reaction products with high oxygen content (at 1300°-1400°C) would be due to the fact that TiC (a_o = 4.3316 or 4.328 Angstrom [13]) formed a solid solution with TiO (a_o=4.180 Angstrom [13]). Figure 6 implies that TiC_xO_y (instead of pure TiC) forms at a lower temperature and then it is purified toward TiC at a higher temperature. Table I provides the summary of the comparison between commercially available TiC (High Vacuum Grade A. H.C. Stark) powder with the TiC powders produced using the developed process.

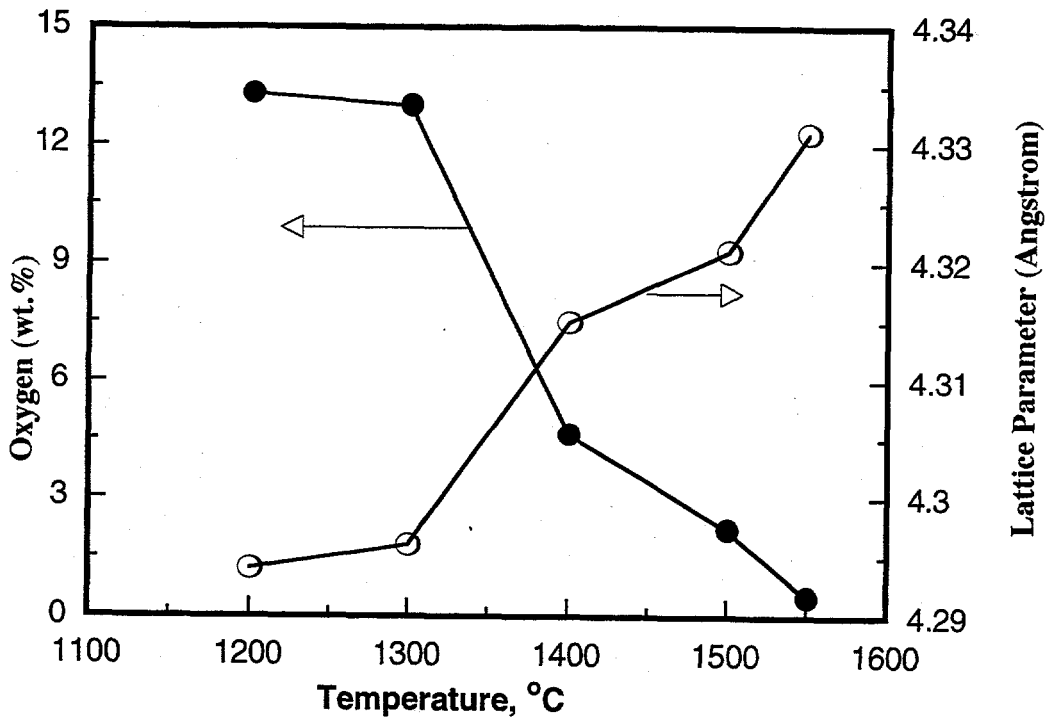

Fig. 6. Change in oxygen content and lattice parameter of TiC powder product as a function of production temperature. Two hours of reaction period at each temperature except for data at 1550°C for four hours in flowing argon.

	Synthesized at 1550°C for 2 hrs.	Synthesized at 1550°C for 4 hrs.	Synthesized at 1550°C for 6 hrs.	H.C. Starck High Vacuum Grade A
Particle Size, μm, from TEM	0.05 - 0.15	0.08 - 0.2	0.1 - 0.3	1 - 1.5
Surface Area, BET, m^2/g	32	21	16	2 - 3.5
Total Carbon, wt%, LECO C200	22.3	22.2	22.1	20 - 21
Total Oxygen, wt%, LECO RO416DR	1.24	0.6	0.48	0.7
Lattice Parameter, a_o, Å calculated	n/a	4.332	n/a	4.331

Table. 1. Properties of the produced TiC powders and comparison with commercially available TiC.

The morphology of the TiC product fired at 1550°C for four hours is shown in Figure 7 (bright field image of TEM). As shown in the figure, the produced TiC powders have fine particle size, narrow particle size distribution (0.08 - 0.2 m), and are loosely agglomerated.

6. Conclusion

The carbothermal synthesis of titanium carbide in the present work proceeded via forming titanium oxycarbide followed by the purification of titanium oxycarbide toward pure titanium carbide. The formation of titanium oxycarbide proceeded by two routes. The uniformly coated pyrolytic carbon on fine titania particles formed TiC_xO_y phase. Then an additional titanium oxycarbide started to form from the Ti_3O_5 phase. Ti_3O_5 was the oxide phase with lowest oxidation states before forming the oxycarbide phase in the additional formation of titanium oxycarbide and the activation energy of the process was 278.1 kJ/mole. The resultant titanium carbide powders prepared at 1550°C for four hours in flowing argon showed fine particle size (0.08-0.2 m), oxygen content of 0.6 wt%, lattice parameter of 4.332 Angstrom, uniform particle shape, and loose agglomeration between particles.

ACKNOWLEDGMENT

This research was sponsored by the U.S. Department of Energy, Office of Industrial Technologies, as part of the Advanced Industrial Materials Program, under contract DE-AC05-84OR21400 with Lockheed Martin Energy Systems, Inc.

REFERENCES

R.A. Andrievskii, S.A. Alekseev, G.T. Dzodziev, A.Zh. Dzneladze, G.C. Travushkin, V.N. Turehin, and A.F. Chertovich, "Physicomechanical Properties of Titanium Carbide with Titanium Nitride Additions", *Soviet Powder Metallurgy and Metal Ceramics,* 19 [9] (1980) 612-615.

D.C. Halverson, K.H. Ewald, and Z.A. Munir, "Influence of Reactant Characteristics on the Microstructures of Combustion Synthesized Titanium Carbide", *J. Mater. Sci.,* (1993) 4583-94.

N. Mihailescu, M. L. De Giorge, C. H. Boulmer-Leborgne and S. Udrea, "Direct Carbide Synthesis by Multipulse Exciter Laser Treatment of Ti Samples in Ambient CH4 Gas at Superatmospheric Pressure", *J. Appl. Phys.,* 75, (1994) 52865294 .

D. D. Harbuck, C. F. Davidson and B. Monte, "Gas Phase Production of TiN and TiC Powders", *J. Metals.,* 38, (1986) 47-50.

L. M. Berger, "Titanium Carbide Synthesis from Titanium Dioxide and Carbon Black", *J. Hard Mater., 3* [11 (1992) 3-15.

R. Divakar, K.Y. Chia, S.M. Kunz, and S.K. Lau, "Carbides", in *Encyclopedia of Chem. Tech.,* Vol., 4, Eds., J.I. Kroschwitz and M. Howe-Grant, J.Wiley and Sons, New York, NY, (I 992), 841-91 1.

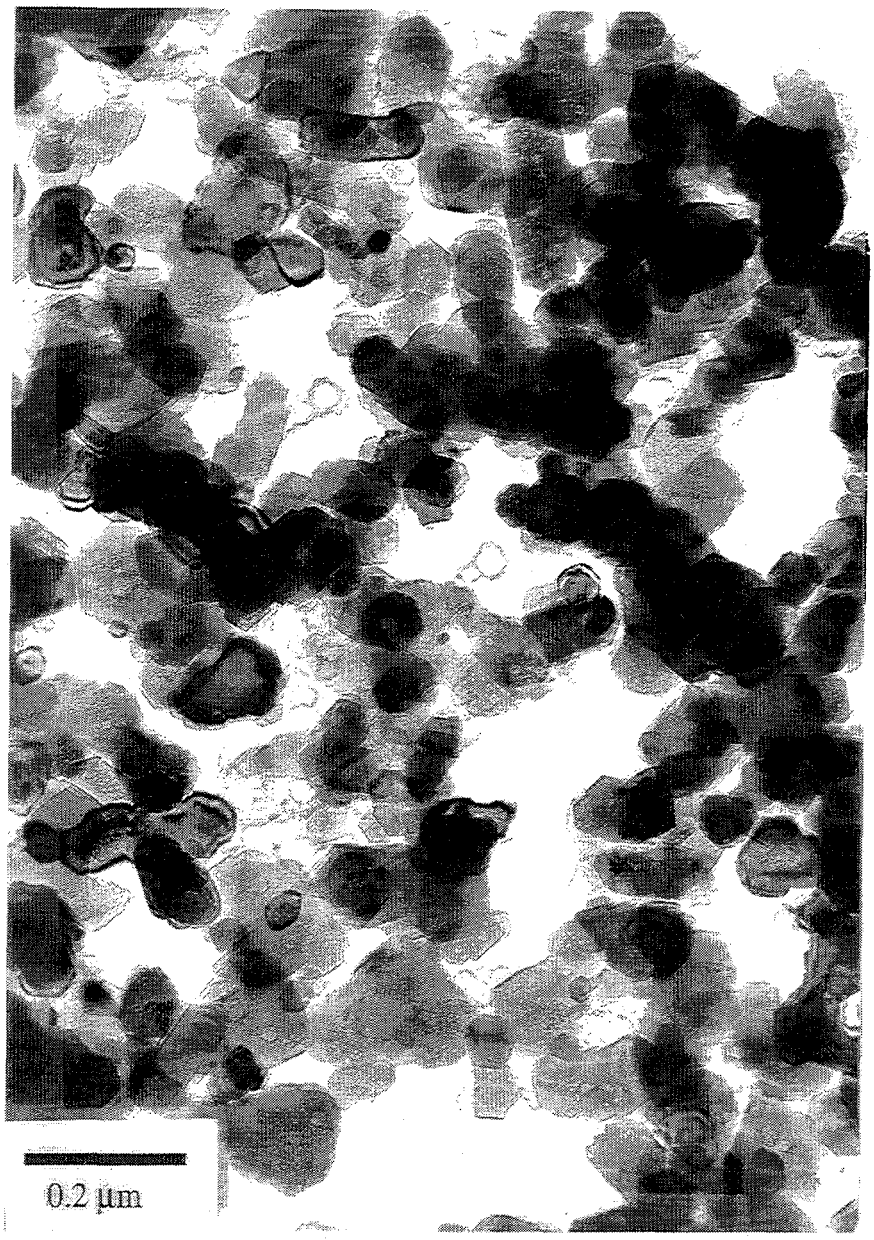

Fig. 7. TEM micrograph of TiC powder product synthesized at 1550 °C for four hours in flowing argon atmosphere.

R. Koc "Kinetics and Phase Evolution during Carbothermal Synthesis of Titanium Carbide from Ultrafine Titania/Carbon Powder Mixture", to be published elsewhere.

R. Koc and G. Glatzmaier, "Process for Synthesizing Titanium Carbide, Titanium Nitride and Carbonitride", *U.S. Patent* No: 5,417,952, 1995.

B.D. Cullity, *Elements of X-ray Diffraction, 2nd Ed.,* pp. 360, Addison-Wesley Publishing Company, Inc., Reading, Massachusetts, 1978.

V.D. Lyubimov, S.I. Alyamovskii, and G.P. Shveikin, "Mechanism of the Reduction of Titanium Oxides by Carbon", *Russian J. Inorg. Chem.*. 26 [9] (198 1) 1243- 47 (198 1); *Zh. Neorg. Khim.,* 26, (1981) 2314-22.

A. Ouensanga, "Thermodynamic Study of the Ti-C-0 System in the Temperature Range 1400-1600K", *J. Less-Common Met.,* 63, (1979) 225-235.

J.G. Lee and I.B. Cutler, "Formation of Silicon Carbide From Rice Hulls", Am. *Ceram. Soc BulL, 54* [2] (1975).

E. K. Storms, *The Refractory Carbides,* Refractory Materials Series, Vol. 2, Academic Press, (I 967) New York, p. 1.

PUBLICATIONS

Journal

R. Koc and J.S. Folmer,"Synthesis of Submicron Titanium Carbide Powders", accepted for publication in the Journal of American Ceramic Society, September 1996.

R. Koc, Kinetics and Phase Evolution During Carbothermal Synthesis of Titanium Carbide from Carbon Coated Titania", accepted for publication in the Journal of European Ceramic Society, November 1996.

R. Koc, Kinetics and Phase Evolution During Carbothermal Synthesis of Journal of Materials Science, August 1996.

R. Koc and J. S. Folmer, Carbothermal Synthesis of Titanium Carbide Using Ultrafine Titania Powders", submitted to the Journal of Materials Science, July 1996.

Other Publications

R. Koc and J.S. Folmer, New Method for Synthesis of Submicron TiC Powders", to appear in the Ceramic Engineering and Science Transactions", 1996.

PRESENTATIONS

R. Koc, J.S. Folmer, S.K. Kodambaka, H. Shin, P. Becher, Synthesis of Submicron Titanium Carbide Powders Using Carbon Coated Titanium Dioxide Precursor ", 3M Ceramic Technology Center, St. Paul, MN, August 28, 1996 (invited).

R. Koc, Synthesis of Submicron Titanium Carbide Powders", Advanced Refractory Technologies Inc., Buffalo, NY, June 5, 1996 (invited).

R. Koc, J.S. Folmer and S.K. Kodambaka, Synthesis of Submicron 1996.

R. Koc and J.S. Folmer, Synthesis of Submicron TiC and TiN Powders", ACS 1996 Annual Meeting & Exposition, Paper No: BP-30-96, Indianapolis, IN April 15, 1996.

HONORS AND AWARDS

R&D 100 for the Development of Method for Making Silicon Carbide Powder, Award Winning Team, Rasit Koc, Greg C. Glatzmaier, Kent Scholl, Mark Anselmo, Jack Sibold (1995).

Federal Laboratory Consortium Award for Technology Transfer, Award Winning Team, Rasit Koc, Greg C. Glatzmaier, Kent Scholl, Mark Anselmo, Jack Sibold (1996).

PATENTS/DISCLOSURES

R. Koc and G. Glatzmaier, Process for Synthesizing Titanium Carbide, Titanium Nitride and Carbonitride," U.S. Patent No: 5,417,952.

R. Koc and S. K. Kodambaka, Process for the Production of Tungsten or Tungsten Monocarbide Powders," Patent application is in process.

LICENSES

ART Inc. has licensed the SiC patent to produce SiC powders.
Greenleaf Inc. is in process of licensing TiC patent.

INDUSTRIAL INPUT AND TECHNOLOGY TRANSFER

Meetings were carried out with staff members from 3M Ceramic Technology Center and ART to explore the use of TiC powders in Al_2O_3 -TiC composites.

ESTIMATED ENERGY SAVINGS

This technology will improve energy efficiency when compared the conventional ones because it does not require high reaction temperatures for production of these powders.

SELECTIVE INORGANIC THIN FILMS

Mark L. F. Phillips, Phillip I. Pohl and C. Jeffrey Brinker

Sandia National Laboratories
Albuquerque, New Mexico 87185

INTRODUCTION

Separating light gases using membranes is a technology area for which there exists opportunities for significant energy savings. Examples of industrial needs for gas separation include hydrogen recovery, natural gas purification, and dehydration. A membrane capable of separating H_2 from other gases at high temperatures could recover hydrogen from refinery waste streams, and facilitate catalytic dehydrogenation and the water gas shift ($CO + H_2O \rightarrow H_2 + CO_2$) reaction. Natural gas purification requires separating CH_4 from mixtures with CO_2, H_2S, H_2O, and higher alkanes. A dehydrating membrane would remove water vapor from gas streams in which water is a byproduct or a contaminant, such as refrigeration systems.

Molecular sieve films offer the possibility of performing separations involving hydrogen, natural gas constituents, and water vapor at elevated temperatures with very high separation factors. It is in applications such as these that we expect inorganic molecular sieve membranes to compete most effectively with current gas separation technologies. Cryogenic separations are very energy intensive. Polymer membranes do not have the thermal stability appropriate for high temperature hydrogen recovery, and tend to swell in the presence of hydrocarbon natural gas constituents. Our goal is to develop a family of microporous oxide films that offer permeability and selectivity exceeding those of polymer membranes, allowing gas membranes to compete with cryogenic and adsorption technologies for large-scale gas separation applications.

The microporous media in these films consist of zeolites and nonaluminosilicate open framework structures such as zinc phosphates. Zeolites are microporous aluminosilicates with pore diameters in the 3-7 Å range; they are already used in bulk form for gas separations and dehydration. The zinc phosphates (ZnPOs) have pore diameters that are generally smaller than those of zeolites; the range of sizes currently available is ideal for dehydration and hydrogen recovery. These phases are also stable at higher temperatures (up to 700 °C) than those generally tolerated by typical alkali zeolites. Many of the ZnPO phases and all of the ZnPO films described here were synthesized for the first time in the course of this project. We have also begun to study shape-selective molecular sieve membranes for separating arenes, and are initiating a CRADA with Amoco Chemical Co. to determine the feasibility of using membranes containing shape-selective zeolites to enrich *p*-xylene from mixtures of xylene isomers.

In addition to investigating inorganic films as gas membranes, we have used these films as selective media for surface plasmon resonance (SPR)-based chemical sensors in collaboration with with the University of Washington. The SPR technique yields real time information about the dielectric constant in the vicinity of the sensing film; this can be altered by adsorption of minute quantities of analyte. In order to improve the detection sensitivity of SPR sensors, we have developed a phase

detection system that uses an optical heterodyne design to measure the phase from the SPR sensor. This system offers detection sensitivity exceeding that of more conventional configurations by an order of magnitude.

TECHNICAL PROGRESS - FY 1996

Summary

Selectivity is controlled in polymer membranes by differences in gas solubility and diffusivity. In contrast, zeolitic phases can separate gases via molecular sieving. Gas molecules smaller than the critical pore diameter are allowed to permeate; larger molecules are completely rejected. A zeolite film with a pore diameter of 4.1 Å (such as Linde Type A) would thus effectively separate methane (kinetic diameter = 3.8 Å) from propane (kinetic diameter = 4.3 Å) or higher alkanes (Figure 1).

The molecular sieve membranes described in this report consist of films of microporous phases deposited on porous supports, such as α-Al_2O_3 or ZnO wafers, and α-Al_2O_3 tubes (Figure 2). The latter are one-directional gas filter membranes in which pore size becomes progressively smaller toward the tube interior, terminating with a layer of 40 Å γ-Al_2O_3 (Figure 3). The films must completely cover the substrate in order to demonstrate any selectivity based on molecular sieving, and the films must be thermally durable enough to withstand operating temperatures and/or calcination. In particular, the film must survive the thermal expansion mismatch between itself and the substrate without cracking or peeling. In our membranes this is accomplished by incorporating an amorphous phase that acts as a binder or "caulk". The limited porosity of the amorphous phase reduces nonselective gas flow between zeolite crystals, while its flexibility mitigates the thermal expansion mismatch between the film and the substrate. We have used a number of different binders for this purpose, including sol-gel silicas, alone or combined with colloidal aluminas, organic-inorganic hybrid gels, and silicones.

In FY96 we investigated methods of film deposition and caulking with Linde Type A and MFI-type zeolites. We have studied permeation of light gases through the resulting membranes. In addition, we synthesized films of new and known zinc phosphates (ZnPOs), and identified numerous new ZnPO phases. In the course of this work we prepared the first ZnPO films with molecular sieving behavior, and the first organic-templated ZnPO in which the template can be removed without altering the host framework.

1. Zeolite A Films

In FY95 we demonstrated the synthesis of supported membranes consisting of pure LTA from the action of aqueous NaOH on kaolinite films deposited on porous alumina discs. We also collected gas permeation data from both unconverted clay films and from zeolite films. Permeation results from kaolinite and metakaolinite films revealed gas separation that is characteristic of Knudsen diffusion and surface flow; this showed that these precursor films can be prepared without macroscopic cracks or holes. However, the films cracked upon conversion to LTA. In FY96 we studied the effects of precursor film thickness and substrate porosity on cracking susceptibility. We found that reducing the thickness of the kaolinite film can eliminate macroscopic cracking, but that

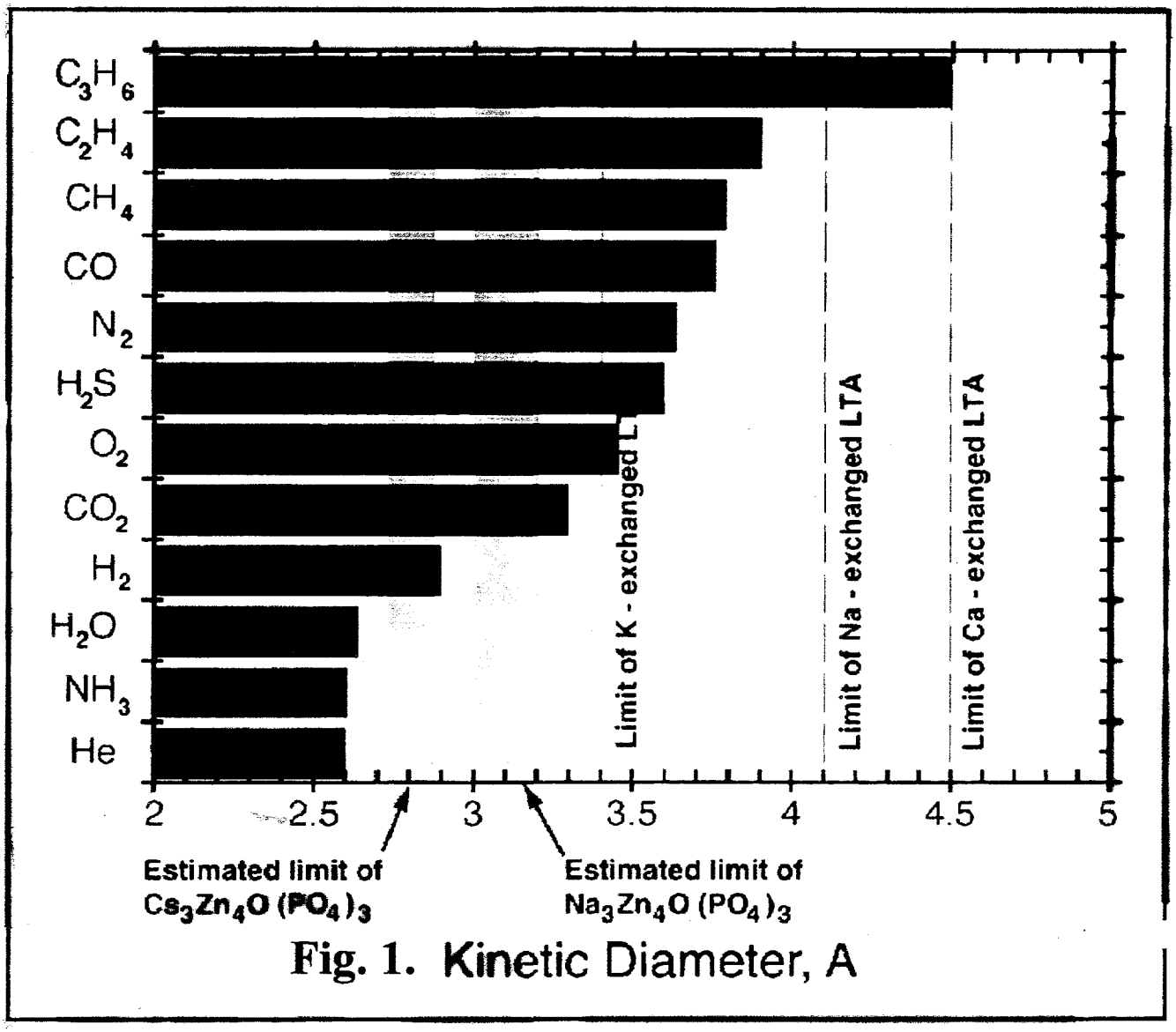

Fig. 1. Kinetic Diameter, A

Fig. 1. Zeolite film with a pore diameter of 4.1 Å (such as Linde Type A) would thus effectively separate methane (kinetic diameter = 3.8 Å) from propane (kinetic diameter = 4.3 Å) or higher alkanes.

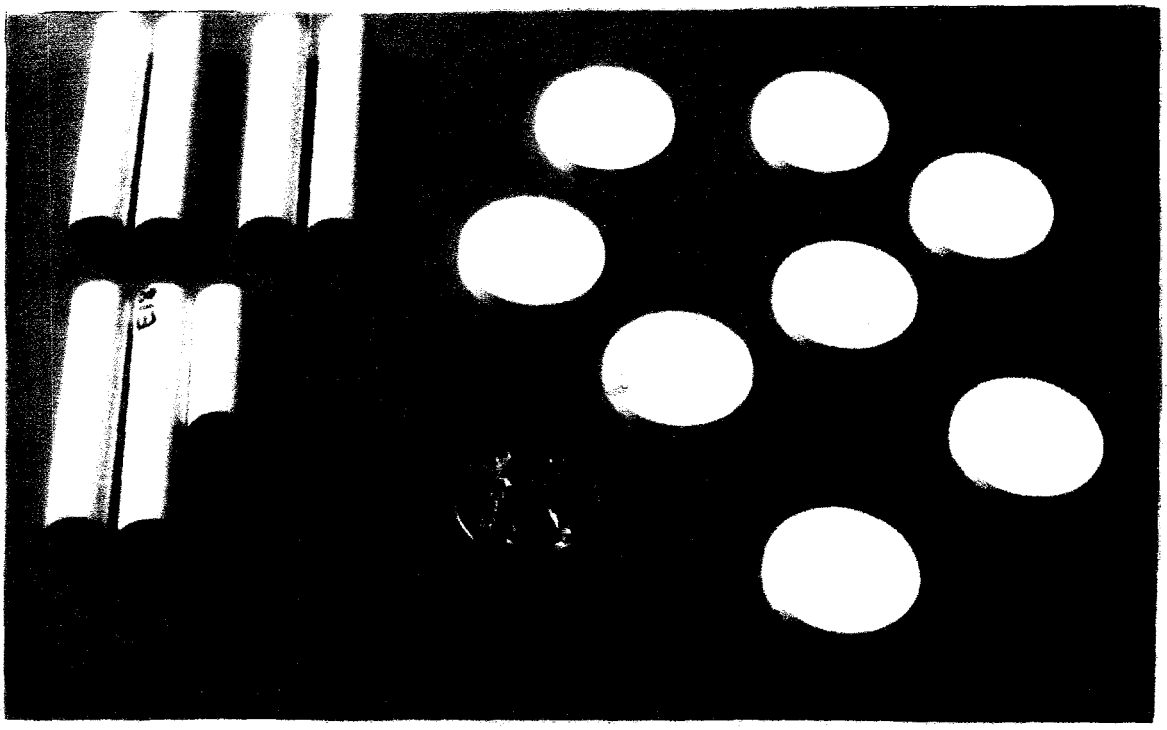

Fig. 2. Films of microporous phases deposited on porous supports, such as α-Al_2O_3 or ZnO wafers, and α-Al_2O_3 tubes.

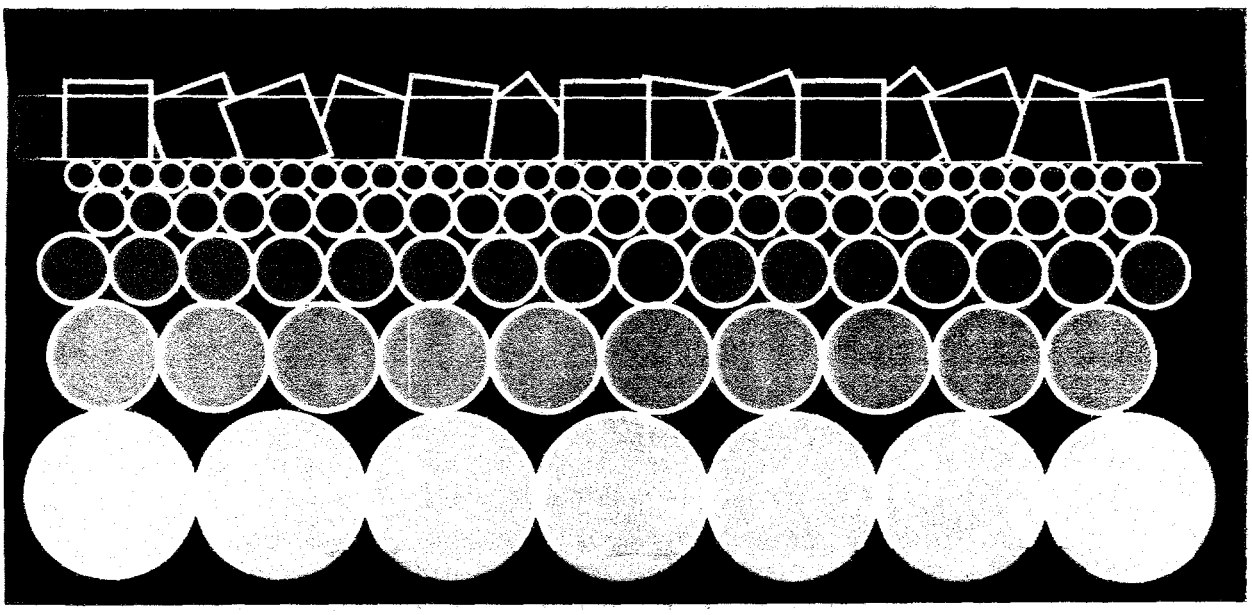

Fig. 3. One-directional gas filter membranes in which pore size becomes progressively smaller toward the tube interior, terminating with a layer of 40 Å γ-Al_2O_3.

leakage still occurs through microscopic intercrystalline gaps. We then studied the effects of "caulking" the LTA film surface to fill in the intercrystalline voids. Caulking materials tested included silicone polymers, nonporous silica sols, colloidal boehmite suspensions, organic-inorganic silica-based sols, kaolinite (with subsequent conversion to LTA), and LTA mother liquor.

The silica sol approach involves coating the films with silica sols (partially hydrolyzed solutions of tetraethyl orthosilicate [TEOS] in ethanol), then heat treating the membrane to render the films impermeable. We found that the intercrystalline gaps in the LTA films are too large (> ca. 0.1 μm) to be adequately caulked using these sols. We have since investigated regrowing the film crystallites in LTA mother liquor, and precaulking with boehmite (α-AlOOH) prior to SiO_2 film deposition to reduce intercrystalline voids prior to treatment with silica sol. In the mother liquor approach, the LTA film is immersed in an aqueous solution of $(CH_3)_4NOH$, Al_2O_3, SiO_2, and NaOH that precipitates colloidal LTA upon heating. In the precaulking approach, a boehmite sol is deposited onto the LTA film to reduce the intercrystalline surface porosity to ca. 40 Å, which is fine enough to be caulked by the silica sol.

Both the kaolinite retreatment and mother liquor methods yielded growth of additional crystallites on the surfaces of the films, rather than expansion of the original crystallites. Therefore, these processes alone have not reduced intercrystalline gaps to sizes that TEOS silica sols can effectively caulk. We have synthesized LTA films sequentially caulked with colloidal boehmite and SiO_2 sol, and will report gas permeation data from these films in FY97.

It has been reported that the selectivities of silicone rubber films for light gases and water/alcohol mixtures can be altered by incorporating zeolite crystallites.[1] We performed a series of similar experiments to determine if a silicone rubber film can improve the selectivity of a pre-deposited LTA film via caulking. We found that a coating of RTV silicone adhesive was sufficient to eliminate measurable gas permeability of an Al_2O_3 disk. With a sufficiently thin application, it may be possible to fill cracks and pinholes in a Zeolite A film with this caulk without obstructing the crystallite pores. To test this, we first measured the thickness of several dip-coated silicone films vs. concentration of dissolved silicone in toluene, and found complete coverage on Si substrates with silicone concentrations of 5 weight percent and greater after a single coating. We then coated these films onto porous alumina disks and measured gas permeabilities of the films. The silicone inhibited viscous flow at coating concentrations in excess of 10%, but allowed some permeation of CO_2 and CH_4, probably due to solution/diffusion. With sufficiently thick application the silicone rubber can indeed stop gas flow through the membrane, though the required thickness is ca. 20 times that of the LTA film. We have concluded that the permeability of RTV silicone adhesive is probably too great to be used as a caulk.

We investigated deposition of thin LTA films from suspensions of colloidal LTA and metallic Al films as an alternative to kaolinite films in order to control intercrystalline porosity. Colloidal LTA was prepared according to [2], and centrifuged onto alumina wafers. This yielded continuous thin films similar in appearance to those made from kaolinite, with similar macroscopic porosity. To test the possibility of synthesizing LTA films from thin Al films, Al coupons were soaked in sodium silicate solutions with Na_2O/SiO_2 ratios of 1 and 2, and held at 100 °C for several days. This process yielded spongy masses of boehmite at a Na_2O/SiO_2 ratio of 1, and a mixture of boehmite and faujasite in the more alkaline solution. No syntheses were made using Al thin films.

2. Clathrasils

Certain organic bases, such as pyridine, are capable of templating microporous all-silica zeolite analogues known as clathrasils. If thin films of these phases could be made from a nonporous silica sol and a vapor phase template, the presence of residual silica as a binder would render an ideal molecular sieve membrane. Synthesis conditions and crystallographic data are available for one of these phases, Dodecasil 3-C.[3] This provides an opportunity for modeling gas transport through this structure prior to film synthesis. Our permeation calculations show that molecular transport is possible only through 5-and 6-ring windows in this clathrasil, and that the internal pores are accessible to He and smaller gases. In principle, such membranes could be used for dehydration, but we are investigating zinc phosphate membranes for this application instead.

3. Zinc Phosphates

In recent years a number of phosphate-based molecular sieve phases have been identified. The most well-known of these are the $AlPO_4$ structures, which are neutral porous frameworks templated by organic bases. Anionic frameworks such as zinc phosphates and beryllophosphates (and arsenates) have been identified as well. These phases are not as thermally stable as the AlPOs, probably because of lower cation-oxygen bond order, and generally have not heretofore survived dehydration or template removal. Unlike the AlPOs, however, microporous zinc phosphates (ZnPOs) can be made using inorganic templates, which may not have to be removed in order for these phases to function as molecular sieves. In addition, ZnPOs are much easier to synthesize as thin films than are the AlPOs.

3.1 Thin film synthesis

In FY94, we reported that certain ZnPOs thought to be microporous could be readily synthesized as films from metallic zinc-coated substrates. In FY96 we showed via computer modeling of gas permeation that the zinc oxide phosphates $M_3Zn_4O(PO_4)_3$ (M = Na, Li) should admit He and H_2, but reject larger gas molecules.[4] In addition, these pores are interconnected in three dimensions, so that gas permeation through the lattice should be both rapid and independent of crystallographic orientation of the film (Figure 4). The phases containing smaller cations generally possess larger kinetic diameters. For example, $Na_3Zn_4O(PO_4)_3$ should accomodate H_2, but not CO_2; while $CsZn_2OPO_4$ should reject H_2, but still be permeable to He, H_2O and NH_3. This prediction is partially corroborated by the observation that these phases can reversibly absorb and desorb both NH_3 and H_2O (kinetic diameters ca. 2.6 Å) without structural change. A $Na_3Zn_4O(PO_4)_3$ membrane could therefore be used for H_2 recovery, while a $CsZn_2OPO_4$ membrane could be used for gas dehydration.

We have devised routes to $K_3Zn_4O(PO_4)_3$ and $CsZn_2OPO_4$ films from ZnO wafers (prepared by cold pressing ZnO powder, then sintering) and Zn metal films (Figure 5). The K phase is particularly useful, since it is readily ion exchanged to yield the more permeable Na and Li phases. We have also found that the ZnO wafers are gas permeable, allowing viscous flow, and are thus useful as membrane substrates. Early results from gas-flow experiments with $CsZn_2OPO_4$ films made from ZnO wafers show significant permeabilities only to He, which is consistent with molecular sieving.

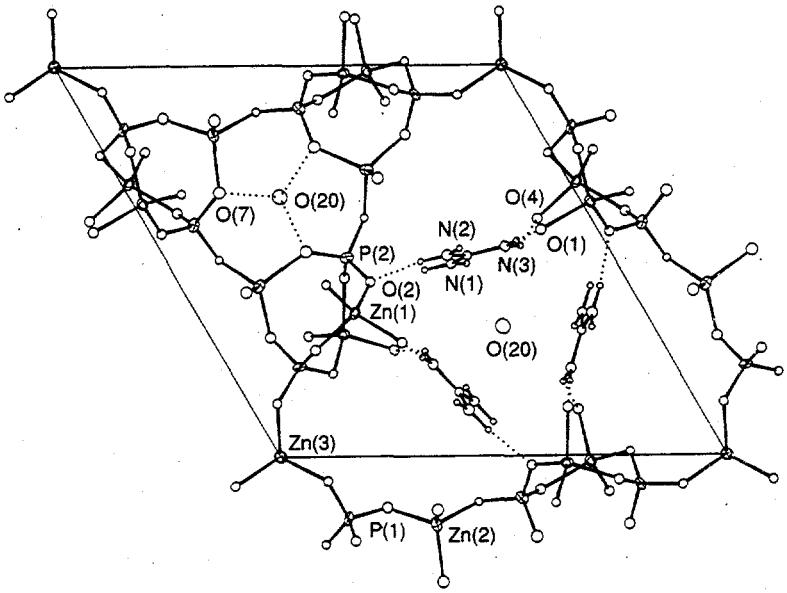

Fig. 4. Pores interconnected in three dimensions, so that gas permeation through the lattice should be both rapid and independent of crystallographic orientation of the film.

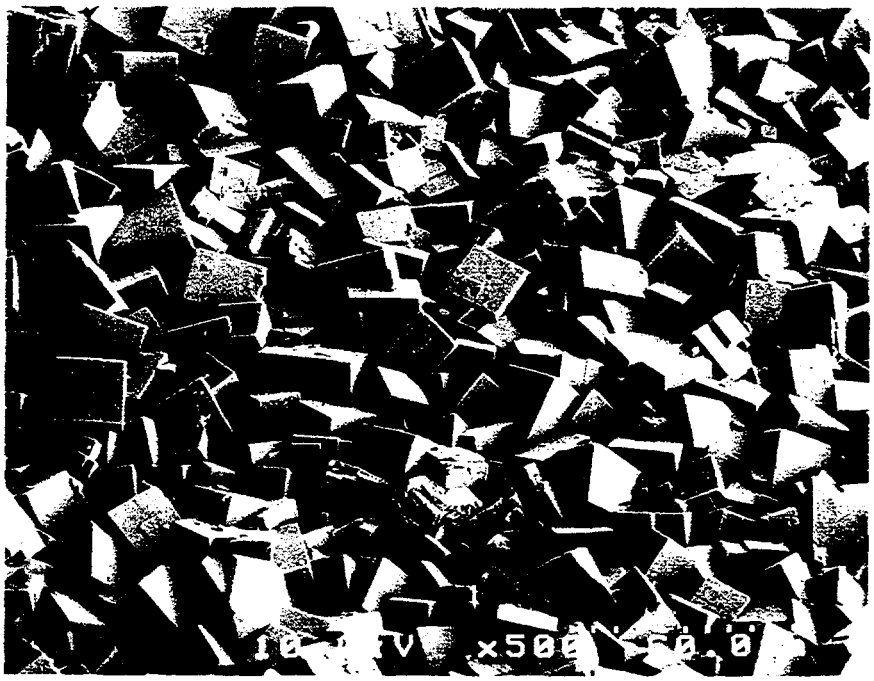

Fig. 5. Routes to $K_3Zn_4O(PO_4)_3$ and $CsZn_2OPO_4$ films from ZnO wafers (prepared by cold pressing ZnO powder, then sintering) and Zn metal films.

While the films can be made leak-free, they are still fairly thick (ca. 20 μm), and thus do not yield high gas flow rates.

To render these process compatible with conventional tubular gas membranes, a method for depositing Zn metal or ZnO film on the inside of an alumina tube must eventually be found. We were able to deposit continuous, 600Å thick ZnO coatings onto flat SiO_2 substrates by dip-coating the substrates in a solution of zinc acetate in alcohol, then baking the films at 600 °C. These ZnO nutrient films were etched off in the highly alkaline solutions used to produce ZnPO films in early attempts. We are investigating methods for making thicker ZnO films, as well as electroplating and dip-coating metallic Zn onto the substrates. The ZnO film technique discovered in this program may have impact on other DOE technologies as well, such as replacing indium tin oxide in conducting screens, producing conductive antireflective coatings for solar cells, and in DOE Defense Programs-relevant applications such as varistor and lightning arrestor connect films.

3.2 New zinc phosphate phases

In addition to the inorganic ZnPOs described above, we are investigating organic ZnPOs as molecular sieves. Because organic cations are larger than alkali metal cations, it is possible to produce larger-pore structures using organic templates. Given the relative facility of preparing ZnPO films, we view this approach as an alternative route to molecular sieve films with pores in the 3-5 Å range. However, all zinc phosphates stable with respect to dehydration or ion exchange have, to date, been inorganic zinc oxide phosphates. The goal of this project element is thus to identify large-pore ZnPOs that are stable enough to survive template removal without structural collapse.

It is possible that Zn-O-Zn bonds, such as those present in the Zn_4O groups in the $M_3Zn_4O(PO_4)_3$ phases, may be responsible for their exceptional thermal stability. Extra ZnO units are generally absent from organic zinc phosphates, and these cannot be dehydrated or have template removed without structure collapse. However, all of the templates used in organic ZnPOs reported to date have been too weakly basic to stabilize the excess zinc oxide. Therefore, we have investigated ZnPO synthesis using template species that are basic enough to dissolve ZnO, and contain a high nitrogen/carbon ratio to facilitate post-synthesis template removal via calcination in oxygen.

We have partially surveyed the aqueous phase space of ZnO and P_2O_5 with guanidine, methylamine, and hydrazine. Two new phases have been identified in the $MeNH_2 \bullet ZnO \bullet P_2O_5 \bullet H_2O$ system. Heating the first phase in oxygen at 350 °C results in complete removal of both water and template, leaving the ZnPO framework undisturbed; this is the first example of an organic microporous zinc phosphate that survives template removal. The second phase is too delicate to allow removal of methylamine but can be reversibly dehydrated, and loses 25% of its weight in water between 25 and 100 °C. This material is being prepared in quantity for testing as an air conditioning dessicant by Engelhard Corporation.

The guanidine $\bullet$ ZnO $\bullet$ P_2O_5 $\bullet$ H_2O phase space has yielded a new family of guanidine zinc phosphates, with six new phases discovered so far. Crystallographic structure solutions have been obtained for four of these phases by Prof. W. T. A. Harrison at the Universty of Western Australia, and were submitted for publication in FY96. One phase in particular, $(CN_3H_6)_3 \bullet Zn_7(H_2O)_4(PO_4)_6$

• H_3O, contains the unusual structural feature of three guanidinium ions acting in concert to template an 18-membered ring. Rings of this size have never been identified in zeolites, and only recently in aluminophosphates [5], and this is the first example of cooperative templation in metal oxide frameworks (Figure 6). Two of the other three structures that have been solved contain unusual structural features as well. The phase $(CN_3H_6)_2$ • $Zn(HPO_4)_2$ has the lowest framework density (number of tetrahedral atoms per unit volume) of any crystalline microporous material identified to date. $(CN_3H_6)_6$ • $Zn_2(OH)(PO_4)_3$ • H_2O adopts a one-dimensional chain structure involving three PO_4 groups triply-bridging pairs of distorted ZnO_4 tetrahedra. This feature has been seen in long-chain metal phosphonates, but this phase appears to be the first simple phosphate to adopt this polymeric configuration.

We have not yet demonstrated template removal with retention of structure in the guanoZnPOs, but are currently attempting to stabilize the framework by including alkali metal cations to increase the Zn/P ratio.

Impact:

The petroleum and natural gas refining industries would benefit significantly from high permeability molecular sieve films capable of separating light, fixed gases, particularly if the membranes can be used at high temperatures. The alkali metal zinc phosphates that we have synthesized as membranes are stable up to 700 °C, which is compatible with hydrogen recovery. With sufficiently high permeability and low unit area cost, energy savings of several quad/yr could be achieved when all feasible applications of inorganic membranes are considered.[6]

4. Shape selective membranes - xylene separation

We are studying with Amoco Chemical Co. the use of microporous inorganic membranes to separate *p*-xylene from mixtures of the isomers. The *para* isomer is the precursor to terephthalic acid, which is principally used in poly (ethylene terephthalate) plastics. Because of this, *p*-xylene is a high-tonnage commodity, and a significant component of chemical industry production. Conventional technology for separating the isomers requires successive recrystallizations of the mixture at cryogenic temperatures, which is very energy intensive. The membranes will be used to enrich the mixture in *p*-xylene prior to crystallization, which will allow warmer temperatures and fewer crystallization steps to be used.

The composition of the "equilibrium mixture" of xylenes that results from toluene alkylation or disproportionation reactions is approximately 2 meta : 1 ortho : 1 para (i.e., 25% p-xylene). In *p*-xylene production, a feedstock containing an "equilibrium" mixture of xylenes is fed into a series of crystallizers operating at -90 °C. The solid phase is enriched in the *para* isomer. The remainder is reisomerized (at ca. 500 °C) and returned to the first crystallizer unit. Our goal is to use shape-selective membranes to replace the first crystallizer, which is the most energy consumptive unit in the process.

It is known that the diffusivity of *p*-xylene through the zeolite phase ZSM-5 (MFI structure type) is ca. 10,000 times that of ortho- or meta-xylene, due to smaller kinetic diameter of the para

isomer.[7] This enhanced diffusivity favors synthesis of *p*-xylene in toluene alkylation and disproportionation reactions, and xylene isomerization, with the appropriately modified ZSM-5 catalysts. MFI/sol-gel films might thus be used to separate *p*-xylene from a product stream consisting of a mixture of isomers; in addition, such a membrane could be packed with catalyst, separating *p*-xylene as it is formed.

Three general methods for synthesizing MFI-type molecular sieve films have been explored. The first involves suspending the zeolite in a silica sol, then dip coating the substrate with the suspension. We used this method to make selective films with several zeolites, including ZSM-5, that have been used as discriminating elements in acoustic wave sensors.[8] An advantage of this "slurry" method is that it can be used with any desired molecular sieve that can be prepared with a sufficiently fine particle size (typically less than 1 μm). We have also demonstrated a second method in which a nonpermeable sol-gel film is added to a zeolite film that has been previously deposited on a porous support. The sol-gel phase acts to caulk intercrystalline gaps, and to promote adhesion to the substrate. In a third method, the zeolitic phase is hydrothermally nucleated and crystallized from sol-gel derived nutrients pre-deposited on a substrate.[9] Each of these methods will be used to synthesize composite MFI/sol-gel membranes for testing in a bench-scale xylene separation module.

In FY97, we will write a computer code that will allow us to predict relative permeation rates of xylene isomers through several zeolitic phases with a variety of compositions. Amoco will also begin to test xylene permeation through Sandia-synthesized membranes consisting of high-silica zeolites such as ZSM-5 and silicalite.

Impact:

If these membranes eliminate the first crystallization step in *p*-xylene production worldwide, approximately 0.070 quad/yr will be saved, principally in the form of decreased natural gas consumption.

5. Surface plasmon resonance

In 1996 we continued to develop surface plasmon resonance (SPR) as an analytical technique that would take advantage of the chemical selectivity of membranes developed in this program to enhance sensor sensitivity and specificity. The SPR transduction principle is widely used as an analytical tool for measuring small changes in the optical refractive index (RI) of chemical and biological samples. Using an optical sensor based on this principles makes it is possible to obtain real-time information about the monitored sample. The basic mechanism of the SPR experiment is described in the FY94 and FY95 annual reports.

The SPR phenomenon can be detected by using one of several methods. The most commonly researched and commercialized techniques are based on the analysis of the reflection coefficient from the sensor using either angle modulation or wavelength modulation. One area of SPR detection that has received little attention to date is the study and measurement of the phase of the reflected light. The motivation at the onset of this work was to develop an SPR phase modulation system, and determine if this type of configuration offers any significant advantages over the existing techniques.

Two phase detection techniques were modeled and experimentally realized. The first technique was a polarization interference method. Although this method does not strictly measure phase, the simplicity of design and use may be very useful in many applications; more research is required to develop this technique to its potential. The second technique incorporated an optical heterodyne design to measure the phase from the SPR sensor. For a given sensor configuration, and index of refaction samples near water, the sensitivity was measured at 8.9×10^{-6} RI/degree phase with a dynamic range of 1.2×10^{-2} RI. This is one order of magniture more sensitive than that available from either angle or wavelength modulation detection. The sensitivity and dynamic range of the sensor is highly dependent upon the sensor configuration, and in particular, the sensing film thickness. All techniques and measurements are reported in detail in a M.S. thesis by Spencer Nelson, University of Washington.

Impact:

SPR sensors with appropriately selective films will have a significant impact on the markets for real-time industrial process monitoring and biomedical sensing. If these sensors can be used as *in situ* waste stream and environmental monitors, this technology will save millions of dollars in analytical costs.

REFERENCES

1. *a.* te Hennepe, H. J. C.; Bargeman, D.; Mulder, M. H. V.; Smolders, C. A. *J. Membr. Sci.* **1987**, *35,* 39-55. *b.* Jia, M.; Peinemann, K.-V.; Behling, R.-D. *J. Membr. Sci.* **1991**, *57,* 289-296.

2. Schoeman, B. J.; Sterte, J.; Otterstedt, J.-E. *Zeolites* **1994**, *14,* 208-216.

3. Marquart, T. A. Ph.D. Dissertation, University of Illinois-Urbana, 1994.

4. The synthesis of bulk $M_3Zn_4O(PO_4)_3$ phases was first reported in Harrison, W. T. A.; Broach, R. W.; Bedard, R. A.; Gier, T. E.; Bu, X.; Stucky, G. D. *Chem. Mater.* **1996**, *8*, 691-700. The MZn_2OPO_4 phases were first synthesized in FY94 as part of this project.

5. Freyhardt, C. C.; Tsapatsis, M.; Lobo, R. F.; Balkus, K. J.; Davis, M. E. *Nature* **1996**, *381*, 295-298.

6. Fain, D. E. *MRS Bulletin* April 1994, p. 40.

7. *a.* Chen, N. Y.; Kaeding, W. W.; Dwyer, F. G. *J. Amer. Chem. Soc.* **1979**, *101*, 6783. *b.* Young, L. B.; Butter, S. A.; Kaeding, W. W. *J. Catal.* **1982**, *70,* 418.

8. Bein, T; Brown, K.; Frye, G. C.; Brinker, C. J. *J. Am. Chem. Soc.* **1989**, *111*, 7640.

9. Dong, J.; Dou, T.; Zhao, X.; Gao, L. *J. Chem. Soc., Chem. Commun.* **1992**, 1056-8.

PUBLICATIONS

B. G. Karle, C. J. Brinker, and M. L. F. Phillips, "Zeolite Membranes from Kaolin," *Mat. Res. Soc. Symp. Proc.* **1996**, *431*, in press.

W. T. A. Harrison and M. L. F. Phillips, "Template Cooperation Effect Leading to 18-Ring Cavities in the Open-Framework Guanidine Zincophosphate $(CN_3H_6)_3 \bullet Zn_7(H_2O)_4(PO_4)_6 \bullet H_3O$," *Chem. Comm.* **1996**, 2771-2772.

W. T. A. Harrison and M. L. F. Phillips, "Crystal Structures of Novel Guanidinium Zinc Phosphates," *Chem. Mater.* submitted for publication, 1996.

S. G. Nelson,"Surface Plasmon Resonance Sensing Based on Phase Detection," Master's thesis, University of Washington, 1996.

S. G. Nelson, K.S. Johnston, and S. S. Yee, "High Sensitivity Surface Plasmon Resonace Sensor Based on Phase Detection," *Sensors and Actuators B* **1996**, *35*, 1-6.

PRESENTATIONS

B. G. Karle, C. J. Brinker, and M. L. F. Phillips, "Zeolite Membranes from Kaolin," Materials Research Society, San Francisco, CA, April 8-12, 1996.

A. V. Chavez, M. L. F. Phillips, and W. T. A. Harrison, "Microporous Zinc Phosphates with Nitrogen-Rich Templates," The Eighth Annual Joint Meeting of the New Mexico Secions of the Americal Ceramic Society and the Materials Research Society, Albuquerque, NM, Oct. 28, 1996.

M. L. F. Phillips, L. A. Weisenbach, T. V. Bohuszewicz, P. I. Pohl, and C. J. Brinker, "Selective Inorganic Thin Films," AIM Program Annual Review, Oak Ridge, TN, June 24-26, 1996.

S. G. Nelson, K.S. Johnston, and S. S. Yee, "High Sensitivity Surface Plasmon Resonance Sensor Based on Phase Detection," The Sixth International Meeting on Chemical Sensors, National Institute of Standards and Technology ,Gaithersburg, MD, July 22-25, 1996.

HONORS AND AWARDS

Alejandra V. Chavez was awarded second prize in the Student Poster competition at the NMACerS/NMMRS Meeting for her poster titled, "Microporous Zinc Phosphates with Nitrogen-Rich Templates."

PATENTS: None during this reporting period.

PATENT DISCLOSURES

M. Phillips, "A Thermally Stable Zinc Phosphate Molecular Sieve," SD-5962.

M. Phillips, "A New Method for Preparing Zinc Oxide Thin Films from Solution," SD-5963.

LICENSES: None during this reporting period.

INDUSTRIAL INPUT AND TECHNOLOGY TRANSFER

As part of the CRADA in negotiation, Amoco Chemical Co. will provide crystallographic data for and samples of zeolites of interest for xylene separation. We will use the structure data to model relative permeation rates of xylene isomers in mixtures, and synthesize membranes from the zeolite samples. Amoco will then measure selectivity of composite zeolite-sol gel membranes invented at Sandia to determine feasibility of scale-up to a pilot plant.

HIGHLIGHTS

We have fabricated molecular sieve membranes by depositing films of microporous cesium zinc oxide phosphate onto porous zinc oxide wafers. These membranes are permeable to helium, but not to hydrogen or to the other light, fixed gases tested. We have also synthesized an organic zinc phosphate phase that survives removal of template and water without altering the structure of the ZnPO framework. This is the first ZnPO phase for which nondestructive template removal has been demonstrated. Films of this phase were successfully grown onto ZnO wafers.

We are negotiating a CRADA with Amoco Chemical Co. to study the feasibility of using shape selective molecular sieve membranes to enrich *p*-xylene from mixtures of the isomers. In FY97, we will write a computer code that will allow us to predict relative permeation rates of xylene isomers through several zeolitic phases with a variety of compositions. We will also synthesize shape-selective membranes using zeolitic phases identified by Amoco as having promise for arene separations. Amoco will measure xylene permeation through these Sandia-synthesized membranes.

PROJECT INVESTIGATORS

In FY96 this project involved participants from Sandia National Laboratories, Albuquerque, NM 87185; the Center for Micro-Engineered Materials, University of New Mexico, Albuquerque, NM 87131; the Dept. of Electrical Engineering, University of Washington, Seattle, WA 98195, and the Dept. of Chemistry, University of Western Australia, Nedlands, WA 6907, Australia.

NAME	PROJECT ROLE
Dr. Mark L. F. Phillips, SNL	Principal investigator, film synthesis
Dr. Phillip I. Pohl, SNL	Permeation modeling
Dr. C. Jeffrey Brinker, SNL	Sol-gel film development
Alejandra V. Chavez, UNM	Zinc phosphate synthesis
Bhushan G. Karle, UNM	Membrane synthesis
Prof. Sinclair Yee, UW	Surface plasmon resonance
Spencer Nelson, UW	Surface plasmon resonance
Prof. William T. A. Harrison, UWA	Crystallography

INTERNAL DISTRIBUTION

1-2. Central Research Library
3. Document Reference Section
4-5. Laboratory Records Department
6. Laboratory Records, ORNL RC
7. ORNL Patent Section
8. D. J. Alexander
9. L. F. Allard
10. P. Angelini
11. B. R. Appleton
12. G. Aramayo
13. R. L. Beatty
14. P. F. Becher
15. R. F. Beckmeyer
16. T. M. Besmann
17. E. E. Bloom
18. C. A. Blue
19. R. A. Bradley
20. C. R. Brinkman
21. G. M. Caton
22. K. M. Cooley
23. R. H. Cooper, Jr.
24. D. F. Craig
25. S. A. David
26. R. B. Dinwiddie, Jr.
27. J. R. DiStefano
28. D. S. Easton
29. M. K. Ferber
30. A. T. Fisher
31. E. P. George
32. G. M. Goodwin
33. H. W. Hayden, Jr.
34. L. L. Horton
35. C. R. Hubbard
36. T. Huxford
37. M. A. Janney
38. D. R. Johnson
39. R. R. Judkins
40. M. A. Karnitz
41. J. R. Keiser
42. E. A. Kenik
43. H. D. Kimrey, Jr.
44. W. LaBarge
45. R.J. Lauf
46. C.T. Liu
47. K.C. Liu
48. Gail M. Ludtka
49. Gerald M. Ludtka
50. H.F. Longmire
51. P.J. Maziasz
52. A.D. McMillan
53. K.L. More
54. T.A. Nolan
55. A.F. Pasto
56. F.L. Paulauskas
57. S.J. Pawel
58. E.A. Payzant
59. K.P. Plucknett
60. B. Radhakrishnan
61. M.L. Santella
62. A.C. Schaffhauser
63. J.H. Schneibel
64. V.K. Sikka
65. S. Simunovic
66. P.S. Sklad
67. S. Spooner
68. R.D. Stout
69. R. Subramanian
70. R.W. Swindeman
71. B. Taljat
72. J.R. Theis
73. R.L. Thomas
74. T.N. Tiegs
75. S. Viswanathan
76. J.M. Vitek
77. M.A. Wall
78. X.L. Wang
79. S.B. Waters
80. A. Wereszczak
81. T. Zacharia
82. H.W. Foglesong (Consultant)
83. E.L. Menger (Consultant)
84. J.G. Simon (Consultant)
85. K.E. Spear (Consultant)

EXTERNAL DISTRIBUTION

86-87. ABB CE Services, Combustion Engineering, Inc., 911 West Main Street, Chattanooga, TN 37402

Domenic Canonico
Mark LeBel

88. AFFCO, 6th & Jefferson, P.O. Box 1071, Anaconda, MT 59711

Jim Liebetrau

89. ASM International, 9639 Kinsman Road, Materials Park, Ohio 44073-0002

Edward Langer

90. Advanced Refractory Technologies, Incorporated, 699 Hertel Avenue, Buffalo, NY 14207

Keith A. Blakely

91. Alabama Pine Pulp Company, Inc., Po. O. Box 100, Perdue Hill, AL 36470

Sunil Chandnani

92-93. Alfred University, Center for Advanced Ceramic Technology, Alfred, NY 14802

Richard M. Spriggs
Harrie J. Stevens

94. Allegheny Ludlum Steel Corporation, Research Center, Alabama & Pacific Avenue, Brackenridge, PA 15014

Gerald L. Houze, Jr.

95. Allied-Signal Aeorspace Corporation, Ceramic Components Division, Dept. 26000 TOR 1/5-1, 2525 West 190th Street, Torrance, CA 90504

Maxine L. Savitz, General Manager

96. Allied-Signal, Incorporated, Ceramics Program, P.O. Box 1021R, Morristown, NJ 07960

Clifford P. Ballard

97. Alloy Engineering and Casting Company, 1700 West Washington Street, Champaign, IL 61821

James R. Lytle

98. Aluminum Association, 900 19th Street, NW, Washington, DC 20006

John Greene

99. Aluminum Company of America, Government Marketing, 1615 "M" Street, NW, Washington, DC 20036

Pam Patrick

100-101. Amoco Research Center, P.O. box 3011, Naperville, IL 60566-7011

N. Calamur
M. Carrera

102. Andritz Sprout Bauer, Sherman Street, Muncy, PA 17756

Ronald L. Musselman

103. Applied Materials Inc., Santa Clara, CA 95054

T. H. Osterheld

104. Army Materials Technology Laboratory, Watertown, MA 37919

Robert N. Katz

105. Army Research Office, P.O. Box 12211, Research Triangle Park, NC 27709

Andrew C. Crowson

106. Babcock & Wilcox, 2302 Parklake Drive, NE, Suite 300, Atlanta, GA 30345

Robert Larsen

107-109. Babcock & Wilcox, 20 S. Van Buren Avenue, P.O. Box 351, Barberton, OH 44203-0351

Joan Barna
John Clement
J. William Smith

110. Battelle, 505 King Avenue, Columbus, OH 43201-2693

Jeffrey Colwell

111. Battelle Pacific Northwest Laboratories, Department of Materials Science, P.O. Box 999, Richland, WA 99352

Gary L. McVay, K2-45

112. Bethlehem Steel Corporation, Homer Research Laboratories, Bethlehem, PA 18016

Charles R. Beechan

113.-114. Bethlehem Steel Corporation, P.O. Box 248, Chesterton, IN 46304

Dan Ellwood
Anthony Simola

115-116. Black & Decker, Incorporated, 701 East Joppa Road, TW 460, Towson, MD 21286

Nick Achterberg
Stephen R. Crosby

117-119. Boeing Aerospace, Material Lobby, Renton, WA 98124-2499

K. Y. Blohowiak, Building 7-20, Mail Stop 73-09
Thomas S. Luhman, Building 7-20, Mail Stop 73-09
M. S. Strasik, Building 7-20, Mail Stop 73-09

120-121. Bowater, Inc., 5020 Highway 11, South, Calhoun, TN 37309

John E. Griffey
LeRoy Hershey

122. Carpenter Technology Corporation, 92 Burning Tree Lane, Reading, PA 19607

Robert L. Caton

123-124. Carpenter Technology Corporation, 101 West Bern Street, P.O. Box 14662, Reading, PA 19612-4662

Bradford A. Dulmaine
Nicholas Fiore

125. Caterpillar, Incorporated, Engineering and Research Materials, Technical Center, Building E, P.O. Box 1875, Peoria, IL 61656-1875

Michael H. Haselkorn

126. Ceracon, 1101 North Market Street, Suite 9, Sacramento, CA 95834

Henry S. Meeks

127. Ceradyne, Incorporated, 3169 Redhill Avenue, Costa Mesa, CA 92626

Joel P. Moskowitz

128-130. Ceramatec, Incorporated, 2425 South 900 West, Salt Lake City, UT 84119

Raymond Cutler
Ronald S. Gordon
David W. Richerson

131. Champion International Corporation, W. Nyack Road, W. Nyack, NY 10994

Dave Bennett

132. Columbia Falls Alumina Col, 2000 Aluminum Dr., Columbia Falls, MT 59912

David Wilkening

133-134. Corning Corporation, Sullivan Park FR-02-5, Corning, NY 14831

Thomas P. DeAngelis
Frank E. Murphy, Jr.

135-136. Cummins Engine Company, Incorporated, P.O. Box 3005, Columbus, IN 47202-3005

Magan J. Patel, Mail Code 50183
James W. Patten, Mail Code 50183

137. Delta M Corporation, 525 Warehouse Road, Oak Ridge, TN 37830

Reginald W. McCulloch

138. William Dennis, 225 Linden Court, Sewickley, Pennsylvania, 15143

139-140. Dow Chemical Company, Incorporated, 1776 Building, Midland, MI 48674

David A. Dalman
Richard D. Varjian

141. Dynamet Technology, Incorporated, 8 "A" Street, Burlington, MA 01803

Walter Bergler

142. Eaton Corporation, Corporate Research & Development, Milwaukee, Center, 4201 North 27th Street, Milwaukee, WI 53216

John W. Kroll

143-144. Electric Power Research Institute, Nuclear Plant Corrosion Control, 3412 Hillview Avenue, Palo Alto, CA 94303

Ben Banerjee
Mohamad M. Behravesh

145. Electric Power Research Institute, 2000 L Street, Suite 805, Washington, DC 20036

W. Eugene Eckhart

146. Engineering Materials Tech. Laboratories, GE Aircraft Engines, Technology Implementation, Mail Drop H-85, 1 Newman Way, Cincinnati, OH 45215-6301

Dr. Lyman A. Johnson

147. Energetics, Incorporated, 7164 Gateway Drive, Columbia, MD 21046

Aziz Azimi

148. EXXON R&D Labs, P.O. Box 2226, Baton Rouge, LA 70821

R. C. Schucker

149-151. FM Technologies, Incorporated, Patriot Square, 10529-B Braddock Road, Fairfax, VA , 22032

Zi. Ahmad
Richard S. Silberglitt
Y. L. Tian

152. FMC Corporation, Materials Engineering, P.O. Box 8, Princeton, NJ 08543

Mr. Anatoly Nemzer, Manager

153. Ford Motor Company, 35500 Plymouth Road, Box 13, Lovonia, MI 48150

Mark G. Shapona

154-157. Ford Motor Company, P.O. Box 2053, Dearborn, MI 48121-2053

John E. Allison, Mail Drop 3182
William E. Dowling, Jr., Room S2065
Gorton M. Greene
Kenneth Hass, Room S3028

158. Ford Motor Company, P.O. Box 1899, Room 354, Dearborn, MI 48121

Vello Arrak

159. Forging Industry Association, 25 Prospect Avenue West, suite 300, Cleveland, Ohio 44115

George Mochnal

160. Foster Wheeler Development Corporation, 12 Peach Tree Hill Road, Livingston, NJ 07039

Jeffrey L. Blough

161. General Electric Company, Research & Development, Met Building, Room 263, P.O. Box 8, Schenectady, NY 12301

Alan I. Taub

162-163. General Electric Company, One Newmann Way, Cincinnati, OH 45215

Ram Darolia, Mail Drop M-89
James Williams, Mail Drop H-85

164. General Motors Corporation, 1660 L Street N.W., Suite 400, Washington, DC 20036

Bo Campbell

165-168. General Motors Corporation, AC Rochester, 1300 North Dort Highway, Flint, MI 48556

R. F. Beckmeyer
Lawrence A. Carol
W. LaBarge
Carl E. Miller

169-174. General Motors Corporation, 30500 Mound Road, Warren, MI 48090-9055

M. S. Rashid
Edward F. Ryntz
James G. Schroth
Michael M. Shea
Susan Smyth
Charles S. Tuesday

175-179. General Motors Corporation, Saginaw Division, 3900 Holland Road, Saginaw, MI, 48601-9494

Steven L. Avery
Randy P. Bal
Madhu S. Chatterjee
James Fargo
David H. Hitz

180. General Motors Powertrain Division, 895 Joslyn Road, Pontiac, MI 48340-2920

Robert Wiltse

181-184. General Motors Powertrain Division, 1629 North Washington Avenue, Saginaw, MI, 48605-5073

Ron Cafferty
Paul N. Crepeau
Mark E. Hoover
Dennis Meyers

185. General Motors Tech Center, Composite Section Manufacturing Building, A/MD-24, 30300 Mound Road, Warren, MI 48090-9040

I. E. Poston

186-190. George Mason University, 4400 University Drive, Fairfax, VA 22030

W. M. Black
R. F. Cozzens
H. S. Sa'adaldin
T. H. Shan
T. L. Tian

191-196. Georgia Institute of Technology, School of Materials Engineering, 778 Atlantic Drive, Atlanta, GA 30332-0245

Steve Antolovich
W. Brent Carter
Joe K. Cochran, Jr.
S. Lee
Thomas L. Starr
S. R. Stock

197. Georgia-Pacific Corp., 133 Peachtree Street, N.E., 11th Floor, Atlanta, GA 30303

Karl T. Morency

198. Dr. Norman A. Gjostein, 544 Claremont, Dearborn, MI 48124

199. Glass Industry Consulting, P.O. box 6730, Laguna Niguel, California, 92607

Phillip Ross

200-202. Golden Technologies Company, Incorporated, Research & Development, 17750 West 32nd Avenue, Golden, CO 80401

Rick Kleiner
Dean Rulis
Jack Sibold

203. T. M. Grace Company, Incorporated, 2517 S. Harmon Street, Appleton, WI 54915

Thomas Grace

204. Herty Foundation Development, P.O. Box 7798, Savannah, GA 31418

James Anderson

205. Hoskins Manufacturing Company, 10776 Hall Road, Hamburg, MI 48139

Forrest Hall

206-208. Hughes Research Laboratories, 3011 Malibu Canyon Road, Malibu, CA 90265

Jesse Matossian
John McLendon
Robert Schumacher

209. IBIS Associates, Inc., 55 William Sreet, Suite 200, Wellesley, MA 02181

Dr. John V. Busch

210-212. Idaho National Engineering Laboratory, EG&G Idaho, P.O. Box 1625, Idaho Falls, ID 83415-2218

Elmer Fleischman
D. Kunerth
E. S. Peterson

213-217. Institute of Paper Science & Technology, Inc., 500 10th Street, N.W., Atlanta, GA 30318

Jefferey A. Colwell
Maclin S. Hall
Robert H. Horton
Thomas McDonough
David Orloff

218. International Paper, P. O. Box 160707, Mobile, AL 36616

Russell S. Andrews

219. International Paper, Paper Mill Road 36610, P. O. Box 2787, Mobile, AL 36652-2787

Subhash Pati

220-226. Iowa State University, Ames Laboratory, 126 Metals Development Building, Ames, IA 50011

L. Carson
L. S. Chumbley
D. C. Jiles
H. Mahmood
K. L. Pauwels
P. P. Pulvirenti
R. Bruce Thompson

227. James River Corporation, P.O. Box 2218, Richmond, VA 23217

Ronald Estridge

228-229. James River Corporation, 1915 Marathon Avenue, P. O. Box 899, Neenah, WI 54957-0899

Dave Clay
Bill Steed

230. John Hopkins University, Center for Nondestructive Evaluation, Maryland Hall 107, Baltimore, MD 21218

Robert E. Green, Jr.

231-232. Johnson Controls, Inc., 507 East Michigan Street, P.O. Box 423, Milwaukee, WI 53201

Carl F. Klein
Bryan L. McKinney

233. Kaiser Aluminum & Chemical Corporation, P.O. Box 870, Pleasanton, CA 94566

S. C. Carniglia

234-235. Kvaerner Pulping, 8008 Corporate Center Drive, Charlotte, NC 28226

Joe Barsin
Bo O. Oscarsson

236. Lawrence Berkeley Laboratory, 1 Cyclotron Road, Mail Stop 90-2024, Berkeley, CA 94720

Arlon J. Hunt

237-238. Lawrence Livermore National Laboratory, P.O. Box 808, Livermore, CA 94550

M. Fluss, Mail Stop L-326
Jeffery Wadsworth, Mail Stop L-353

239-240. Lehigh University, Center for Advanced Technology for Large Structural Systems (ATLSS), 117 Atlss Drive, Bethlehem, PA 18015-3094

J. H. Gross
A. B. Magee

241-262. Los Alamos National Laboratory, P.O. Box 1663, Los Alamos, NM 87545

P. G. Apen, D453
T. A. Archleta, MST-7,E549
R. S. Barbero, MST-7. E549
A. H. Bartlett, MST-6, MS K762
B. Benicewicz, MST-7, E549
D. P. Butt, G755
R. G. Castro, G770
David J. Devlin, E549
Elliott P. Douglas, E549
Frank D. Gac, G756
Shimshon Gottesfeld, D429
P. J. Hay, B268
K. J. Hollis, G770
J. D. Katz, G771
H. H. Kung, K765
R. Leipens, E549
R. LeSar, K765
John J. Petrovic, G771
A. Redondo, D429
K. N. Siebien, MST-7, MS E549
M. E. Smith, MST-7, E549
Gerald J. Vogt, G771

263-264. MTCI, 5570 Sterrett Place, Suite 20, Columbia, MD 21044

Amal Mansour
Momtaz Mansour

265. MacMillan Bloedel Packaging, Inc., Hwy 10, P. O. Box 336, Pine Hill, AL 36769

Wallace Baxter

266. Mercury Marine, W6250n West Pioneer, Fond-du-Lac, Wisconsin 54935

Ray Donahue

267. National Aeronautics & Space Administration, Materials & Structures Division, Code RM, 600 Independence Avenue, S.W., Washington, DC 20546

Samuel L. Venneri

268. National Aeronautics & Space Administration, Lewis Research Center, 21000 Brookpart Road, MS: 49-1, Cleveland, OH 44135

Joe Stevens

269. National Forge Company, Irvine, PA 16329

Ashok Khare

270-272. National Institute of Standards and Technology (NIST), Gaithersburg, MD 20899

Edwin R. Fuller, Jr., Ceramics Division, Room, A256, Building 223
Richard E. Ricker, Depart. of Commerce, Materials Bldg., Room B254
Lyle Schwartz, Director

273-274. National Materials Advisory Board, HA-262, National Research Council, 2101 Constitutional Avenue, NW, Washington, D.C. 20418

Mr. Thomas E. Munns, Senior Program Officer
Dr. Robert Schafrik, Director

275-279. National Renewable Energy Laboratory, 1617 Cole Boulevard, Golden, CO 80401-3393

Helena L. Chum
Robert J. Evans
Gregory Glatzmaier
Neil Kelley
Stephen S. Kelley

280-281. National Science Foundation, Metallurgy Section, 1800 "G" Street, N.W., Washington, DC 20550

Bruce A. MacDonald
Robert Reynik

282. Naval Research Laboratory, Building 43, Room 212, Code 6000, 4555 Overlook Avenue, SW, Washington, DC 20735-5341

Bhakta B. Rath

283. North Carolina A&T State University, Department of Mechanical Engineering, Greensboro, NC 27411

V. S. Avva

284-285. North Carolina State University, Department of Materials Science and Engineering, Box 7907, Raleigh, NC 27695-7907

Carl C. Koch
Nkadi Sukidi

286. Norton Company, Goddard Road, Northboro, MA 01532-1545

Normand D. Corbin

287. Oak Ridge Institute for Science and Education, Badger Avenue, Oak Ridge, TN 37830

Deborah McCleary

288. Parsons and Whittemore, Inc., Atlanta Office, P. O. Box 637, Clarkston, GA 30021

Adam Melton

289. Parsons and Whittemore, Inc., Monroeville Office, P. O. Box 65, Perdue Hill, AL 36470

Adam Melton

290. Pask Research and Engineering, Berkeley, California 94720

Antoni P. Tomsia

291-292. Precision Castparts Corporation, 4600 SE Harney Drive, Portland, OR 97206-0898

David A. Chang
Larry J. Watland

293. Pulp and Paper Research Institute of Canada, Vancouver Laboratory, 3800 Westbrook Mall, Vancouver, B.C. V6S 2L9

Doug L. Singbeil

294. Rapid Technologies, Incorporated, P.O. Box 368, 170 Werz. Ind. Blvd., Newnan, GA 30264

Ed Dailey

295. Rennsselaer Polytechnic Institute, School of Engineering, Materials Engineering Department, 8th Street, Troy, NY 12180-3590

N. S. Stoloff

296. Reynolds Metal Company, P.O. Box 1200, Shefield, AL 35660

Nolan E. Richards

297-303. Sandia National Laboratories, Division 8361, P.O. Box 969, 7011 East Avenue, Livermore, CA 94551-0969

Mark D. Allendorf
S. M. Ferko
S. Griffiths
Donald R. Hardesty
A. McDaniel
R. Nilson
N. Yang

304-314. Sandia National Laboratory, 1515 Eubank, S.E., Albuquerque, NM 87185-5800

C. S. Ashley, Division 1846, Mail Stop 1405
T. V. Bohuszewicz, Mail Stop 1349
C. J. Brinker, Division 1846, Mail Stop 0607
Gary Carlson, Division 6211, Mail Stop 0710
Bob Eagan, Division 1800
G. Ewsuk, Division 1849, Mail Stop 0609
Kay Hays, Mail Stop 1709
R. E. Loehman, Division 1808, Mail Stop 1349
Mark L. F. Phillips, Divison 1846, Mail Stop 0607
P. I. Pohl, Division 6626, Mail Stop 0720
Alan P. Sylwester, Division 6203, Mail Stop 0749

315. Sandia National Laboratory, University of New Mexico, Advanced Materials Laboratory 1708, 1001 University Boulevard, SE, Suite 100, Albuquerque, NM 87106

W. G. Fahrenholtz

316. Sandusky International, 615 W. Market Street, Box 5012, Sandusky, OH 44871-8012

Dan Scott

317. Sandvik Steel Co., P. O. Box 1220, Scranton, PA 18501-1220

Jim Noble

318-320. Southern Illinois University, Dept. of Mechanical Engineering and Energy Process, Carbondale, IL 62999

J. S. Folmer
R. Koc
S. K. Kodambaka

321-322. Stone Container Corporation, 8170 South Madison Street, Burr Ridge, IL 60521

Max Moskal
Chuck Timko

323. TRW, Incorporated, 23555 Euclid Avenue, Cleveland, OH 44117

A. L. Bement, Jr.

324. Tampella Power Corporation, 2300 Windy Ridge Parkway, Suite 1125, Atlanta, GA 30339

Markku Isoniemi

325. Technology Forging Division, Associate Professor, 244 Worchester Street, North Grafton, MA 01536

Dr. Timothy Howson

326. Tennessee Technological University, Center for Manufacturing Res. & Tech. Util. College of Engineering, P.O. Box 5014, Cookeville, TN 38505

Joseph T. Scardina

327-328. The Carborundum Company, P.O. Box 187, Keasbey, NJ 08832

Craig L. Dillman
Stanley Gursky

329. The Carborundum Company, P.O. Box 832, Niagara Falls, NY 14302

Monika O. Ten Eyck

330. The Timken Company, 1835 Dueber Avenue, S.W., Canton, OH 44706-2798

Robert L. Leibensperger

331-335. The Pennsylvania State University, Department of Materials Science and Engineering, Metals Science and Engineering Program, 221 Steidle Building, University Park, PA 16802

John Hellman
Paul R. Howell
George L. Messing
William A. Pratt
Richard E. Tressler

336-337. The University of Tennessee, Department of Materials Science & Engineering, Knoxville, TN 37996-2200

C. R. Brooks
Ben F. Oliver

338. Thermo-Chem, Incorporated, 5570 Sterrett Place, Suite 210, Columbia, MD 21044

David A. Scearce

339. Thermo Electron Technologies, 85 First Avenue, Waltham, MA 02254

Peter Reagan

340-341. U.S. Air Force, Wright Patterson AFB, Dayton, OH 45433-6533

Dennis M. Dimiduk, WRDC Material Laboratory
Allan Katz, AFWAL/MLLM Material Laboratory

342-379. U.S. Department of Energy/Headquarters, 1000 Independence Avenue, SW, Washington, DC 20585

David Boron, EE-23, 5F-059/FORS
Rolf Butters, EE-24, 6H-034/FORS
B. Cranford, EE-21, 5F-043/FORS
Sidney Diamond, EE-34, 5G-064/FORS
Sara Dillich, EE-22, 5F-059/FORS
Russell Eaton, III, EE-22, 6A-116/FORS
James J. Eberhardt, EE-33
Doug Faulkner, EE-21, 5F-059/FORS
T. D. Foust, EE-21, 5F-043/FORS
Ehr-Ping Huang Fu, EE-22, 6A-116/ FORS
Marvin E. Gunn, Jr., EE-14, 6H-034/FORS
Deborah A. Haught, EE-32
M. P. Hoffman, GC-62, 5F-043/FORS
Ramesh Jain, EE-22, 6A-116/FORS
Gobind Jagtiani, EE-22, 6A-116/FORS
Theodore Johnson, EE-21, 5F-043/FORS
Douglas E. Kaempf, EE-234, 5F-043/FORS
Hank Kenchington, EE-21, 6B-025/FORS
Toni Marechaux, EE-32,
John N. Mundy, ER-131,
William P. Parks, Jr., EE-23, 5F-035/FORS
James E. Quinn, EE-20,
Marsha L. Quinn, EE-24, 6H-034/FORS
Scott L. Richlen, EE-21, 5F-035/FORS

U.S. Department of Energy/Headquarters, 1000 Independence Avenue, SW, Washington, DC 20585 (continued)

V. T. Robinson, HR-422, 100 H ST
Charlie Russomanno, EE-22, 6A-116/FORS
Peter H. Salmon-Cox, EE-23, 5F-059/FORS
Robert B. Schulz, EE-34, 5F-064/FORS
Kurt Sisson, EE-21, 6B-025/FORS
M. A. Smith, EE-21, 5F-035/FORS
Charles A. Sorrell, EE-232, 5F-059/FORS
Louis Sousa, EE-20, 6B-025/FORS
Denise F. Swink, EE-20, 6B-052/FORS
B. G. Volintine, EE-22, 5F-059/FORS
Daniel E. Wiley, EE-21, 5F-059/FORS
F. W. Wilkins, EE-21, 5G-067/FORS
Stanley M. Wolf, EM-54, 413/TREV
Harvey Wong, EE-21, 5F-059/FORS

380-384. U.S. Department of Energy, 19901 Germantown Road, Germantown, MD 20585

Fred Glaser, FE-72, GTN
Robert J. Gottschall, ER-13, J-322/GTN
Helen Kerch, ER-13, J-322/GTN
F. W. Wiffen, ER-52, G-258/GTN

385. U.S. Department of Energy/Albuquerque, P.O. Box 5400, Albuquerque, NM 87115

D. Morton

386. U.S. Department of Energy/Oak Ridge, Building 4500N, Mail Stop 6269, P.O. Box 2008, Oak Ridge, TN 37831-6269

Mary Rawlins

387. U.S. Department of Energy/Idaho, 785 Dow Place, Idaho Falls, ID 83402

Joanne Malmo

388. U.S. Department of the Interior Bureau of Mines, 2401 "E" Street, NW, Washington, DC 20241

Garrett R. Hyde

389. Union Camp Corporation, Research and Development Division, P. O. Box 3301, Princeton, NJ 08543-3301

Dave Crowe

390-391. United Defense, Steel Products Div., 2101 West 10th St., Box 1030, Anniston, AL 36202

John Orth
Nectar L. Ramirez

392. United Technologies Research Center, East Hartford, CT 06108

Vincent C. Nardone

393. University of Alabama, Metal Casting Technology Center, P.O. Box 6374, Tuscaloosa, AL 35487

Thomas S. Piwonka

394. University of Cincinnati, Department of Materials Science & Engineering, 498 Rhodes Hall, Cincinnati, OH 45221-0012

A. Jordan

395-396. University of Maine, 5737 Jenness Hall, Orono, ME 04469-5737

Joseph Genco
Marquita Hill

397. University of Missouri School of Mines & Met., Ceramic Engineering, 120 Fulton Hall, Rolla, MO 65401-0249

Robert E. Moore

398. University of New Mexico, Albuquerque, New Mexico 87106

William Fahrenholtz

399. University of Pennsylvania, Department of Mechanical Engineering, 111 Towne Building, 220 South 33rd Street, Philadelphia, PA 19104-6315

David Pope

400. University of Utah, Electrical Engineering Department, Salt Lake City, UT 84112

M. Iskander

401. Vander Linden & Associates, 5 Brassie Way, Littleton, CO 80123

Carl R. Vander Linden

402. Varian Associates, Palo Alto, CA 94304

M. T. Schulberg

403-405. Virginia Polytechnic Institute and State University, Materials Science & Engineering Dept, 213 Holden Hall, Blacksburg, VA 24061-0237

B. D. Dickerson
S. B. Desu
X. Zhang

406. James Wessel, 127 West View Lane, Oak Ridge, Tennessee 37830

407. Westinghouse R&D, 1310 Beulah Road, Pittsburgh, PA 15235

Garth Clarke

408-409. Westvaco, Laurel Technical Center, 11101 Johns Hopkins Road, Laurel, MD 20723-6006

Lad Falat
W. B. A. (Sandy) Sharp

410. Weyerhaeuser Paper Company, Columbus Pulp and Paper Complex, P. O. Box 1830, Columbus, MS 39703-1830

Joe May (cc/Jim Noles)

411-415. Weyerhaeuser Paper Company, Research and Development, WTC 2H22, Tacoma, WA 98477

Dick Ericson
Margaret Gorog
Peter Gorog
Denny Hunter
Dick Shenk

416. Wright State University, Department of Mechanical and Matmerials Engineering, Dayton Ohio 45435

Dr. Harry A. Lipsitt

417. Worcester Polytechnic Institute, Department of Mechanical Engineering, 100 Institute RJ, Worcester, MA 01609

Robert N. Katz

418. 9208 Burning Tree Road, Bethesda, MD 20817

Samuel Goldberg

419-420. 14390 W. 30th Avenue, Golden, CO 80401

Richard Kleiner
David G. Wirth

421. 3M Industrial & Electronic Sector, Research Laboratory, Building 201-4N-01, 3M Center, St Paul, MN 55144-1000

Ross H. Plovnick

422-423. Department of Energy, Office of Scientific and Technical Information, Office of Information Services, P.O. Box 62, Oak Ridge, TN 37831

For distribution by microfiche as shown in DOE/OSTI-4500, Distribution Category UC-310 [Industrial Programs (General)]